Late Quaternary dune activity in the Thar Desert and its implications for palaeoenvironmental reconstructions: an insight from optically stimulated luminescence dating

Aayush Srivastava

Supervisors: Prof David S.G. Thomas and Dr Julie A. Durcan

Hertford College

Thesis submitted for the degree of

Doctor of Philosophy



University of Oxford

Trinity Term 2019

Abstract

Sand dunes in the Thar Desert, owing to their location in the Indian summer monsoonal (ISM) regime, are rich archives of past geomorphological and palaeoenvironmental changes. However, existing dune records are not robust enough to allow their assessment and integration with a growing multiproxy framework of palaeoenvironmental change. Therefore, with an aim to *investigate the timing of dune activity in the Thar*, three research questions are answered in this thesis: (i) what are the key phases of dune activity; (ii) what is the effect of anthropogenic influences on the landscape; and (iii) how can dune chronologies be interpreted most effectively to reconstruct late Quaternary environmental changes? To answer these, systematic sampling of multiple dunes was carried out in the dunefields in the central and northern Thar, and luminescence dating was used to provide a detailed chronological framework.

Results demonstrate that the Thar dunes are >58 ka old, with preserved accumulation phases throughout the Holocene at ~11.6-8.5, 4-3, 2-1, 0.6-0.2 and 0.07 ka. First records of modern net accumulation are presented, with rates varying between 2-5 m/year, attributable to anthropogenic disturbances. Dune accumulation intensity methodology, in conjunction with available highly-resolved marine and terrestrial datasets, is used to infer palaeoenvironmental changes in the Thar. Whilst the strengthening of the ISM has been evidently shown to have a significant influence on widespread dune accumulation in the early Holocene, equivocal relationships between both lake levels/dune accumulation and monsoon variability during later Holocene suggest a complex interplay of regional and more local drivers like sediment supply, lowered sea levels etc. The study concludes with emphasis on the importance of recognising external and local controls on dune systems, and demonstrates that diverse responses to same environmental stimuli should be expected in palaeoenvironmental reconstructions.

Acknowledgements

I express my sincere gratitude to my supervisors Dave and Julie for their guidance, expertise, and never-ending encouragement throughout the course of my D.Phil. I am grateful to the Clarendon Fund scholarship without which I would not have been able to carry out this invigorating research. I thank the Fell Fund for providing funding for fieldwork and laboratory analyses. I am also grateful to the Quaternary Research Association, the International Association of Geomorphologists, the International Society for Aeolian Research, the European Geosciences Union, the International Union for Quaternary Research, the British Society for Geomorphology and Hertford College, whose support enabled my participation at various conferences in the UK and internationally.

A due mention of gratitude to numerous residents of the villages in the Thar for allowing access to their lands and excavators ensuring smooth fieldwork. Thanks to everyone in the OLD Lab for their helpful and instructive discussions on everything related to OSL and beyond, especially Szilvi, Catherine, Kaja, Hong and Mona. A big thanks also to Matt and Giles for kindly agreeing to be my examiners.

On a personal note, thanks to all fantastic friends in Oxford, especially Vishal and Madhav, who have been instrumental in contributing towards maintaining a good work-life balance. A big cheer to Avinash for planning several holidays and giving remote access to his laptops, and to Nupur for being just a message away always. To Aman, Spriha and Sreedip for the much needed good vibes and laughs.

A huge thank you to my family- Manjula, Rajendra, Rishika, Mili, Rachit, Aarna and Kaashvi for their constant love, support, and encouragement along the way.

Finally, to Sneha, when distant and close, for everything.

Contents

Abbreviations and Units x

Glossary xi

Chapter 1: Research Context 1

1.1. Motivation 2

1.2. The Thar Desert dunes 6

1.3. History of human settlement in the Thar 12

1.4. Indian Summer Monsoon and its variability 19

1.5. Dunes as geoproxies of past changes 30

1.6. Thesis aim and research questions 35

1.7. Thesis structure 37

1.8. Conclusions 38

Chapter 2: Previous luminescence dating based investigations 40

2.1. Introduction 41

2.2. Generating dune accumulation chronologies 41

2.6.1. Basic principles of luminescence dating 42

2.6.2. Quartz OSL dating 44

2.3. Previously published chronologies from the Thar dunes 46

2.4. Review of previously published Thar dune chronologies 51

2.8.1. Fieldwork strategies 51

2.8.2. Use of Multiple Aliquot Additive Dose methods for D_e calculations 53

2.8.3. Lack of fading correction of IRSL ages 55

2.5. Conclusions 56

Chapter 3: Materials and methods 58

3.1 Introduction 59

3.2. Study areas 59

3.2.1. Jodhpur dunefield 62

3.2.2. Bikaner dunefield 64

3.2.3. Suratgarh region 65

3.2.4. Sampling strategy 66

3.2.4. Dating strategy 67

3.3. Laboratory methods: equivalent dose determination 69

3.3.1. Sample preparation 71

3.3.2. Luminescence signal measurement 72

3.3.3. Single grain assessment of luminescence signals 73

3.3.4. Combined dose recovery and pre-heat plateau tests 75
3.3.5. Dose recovery tests 79
3.3.6. The post-IR SAR protocol used in the study 80
3.3.7. Analyses of luminescence signals 81
3.4. Environmental dose rate determination 92
3.4.1. Internal dose rate 93
3.4.2. External dose rate 94
3.4.3. Total environmental dose rate 96
3.5. OSL ages 101
3.6. Conclusions 101

Chapter 4: Holocene dune activity in the Thar Desert, India (Paper 1) 103
Abstract 104
4.1. Introduction 105
4.2. Study Site and methods 107
4.2.1. Site selection and sampling 108
4.2.2. Sedimentological analyses 109
4.2.3. Luminescence dating 109
4.3. Results 118
4.3.1. Sedimentology 118
4.3.2. Luminescence dating 118
4.4. Discussion 122
4.4.1. Holocene dune activity in the region 122
4.4.2. Implications for the timing and evolution of parabolic dunes 127
4.5. Conclusions 130

Chapter 5: Analysis of late Quaternary linear dune development in the Thar Desert, India. (Paper 2) 132
Abstract 133
5.1. Introduction 134
5.2. Study sites and methods 137
5.2.1. Study sites 137
5.2.2. Sedimentological analyses 140
5.2.3. Sediment preparation for luminescence dating 140
5.2.4. Equivalent dose determination 141
5.2.5. Dose rate determination 142
5.3. Results 142
5.3.1. Sedimentology 142
5.3.2. Luminescence dating 146

5.4. Discussion 154
5.5. Conclusions 159

Chapter 6: Holocene palaeoenvironmental changes in the Thar Desert: an integrated assessment incorporating new insights from aeolian systems (Paper 3) 162
Abstract 163
6.1. Introduction 164
6.2. Accumulation Intensity modelling 167
6.2.1 Data included in *AI* analysis 169
6.2.2 A new *AI* record for the Thar Desert 174
6.3. Drivers of Thar landscape change during the Holocene 177
6.3.1 Early Holocene (~11.7 - ~8.2 ka) 177
6.3.2 Middle Holocene (~8 - ~4.2 ka) 182
6.3.3 Late Holocene (~4.2 ka - ~present) 185
6.4. Conclusions 188

Chapter 7: Implications and conclusions 191
7.1. Introduction 192
7.2. Addressing thesis research questions 193
7.2.1. RQ1. When did dune accumulation occur during the late Quaternary in response to drivers of landscape change? 193
7.2.2. RQ2. Given the large and dense population that the Thar hosts, what is the effect of anthropogenic pressure on dune activity? 195
7.2.3. RQ3. What do dune records reveal about the late Quaternary geomorphological and palaeoenvironmental changes in the Thar? 197
7.3. Future work and considerations 201
7.4. Overall conclusions 206

References 210

Appendices 258
Appendix A: Contribution of authors 259
Appendix B: Sedimentological analyses 260
Appendix C: Measurement of radionuclide concentrations 268
Appendix D: Calculation of the environmental dose rate 269
Appendix E: Paper 1 (Chapter 4) as included in journal *Earth Surface Processes and Landforms*. 274
Appendix F: Paper 2 (Chapter 5) as included in journal *Geomorphology*. 286
Appendix G: Supplementary Information for Paper 3 (Chapter 6). 295

Abbreviations and Units

a	annum (one year)
AI	Accumulation Intensity
C	Carbon
CAM	Central Age Model
$\dot{D}$	Total environmental dose rate
D_α	Alpha dose rate
D_β	Beta dose rate
D_γ	Gamma dose rate
$\dot{D}_{cosmic}$	Cosmic dose rate
D_e	Equivalent dose
DRAC	Dose Rate and Age Calculator
DRC	Dose Response Curve
DRT	Dose Recovery Test
Gy	Gray
HCL	Hydrochloric acid
HF	Hydrofluoric acid
H_2O_2	Hydrogen peroxide
H_2SiF_6	Fluorosilicic acid
IR	Infra-red
IRSL	Infra-red stimulated luminescence
ISM	Indian Summer Monsoon
K	Potassium
ka	kilo annum (one thousand years)
µm	Microns
LED	Light emitting diode
L_x	Natural luminescence signal
L_x / T_x	Sensitivity corrected signal
MAAD	Multiple aliquot additive dose
OSL	Optically stimulated luminescence
ppm	part per million
σ_d	over-dispersion
PH	Pre-heat
SAR	Single aliquot regenerative
Th	Thorium
TL	Thermo-luminescence
T_x	Test dose luminescence signal
U	Uranium

Glossary

Aliquot: sub-sample whose luminescence signal is to be measured; may contain variable number of grains, depending upon the grain size and disc area used.

Alpha (α) particle: a type of radiation emitted from atoms when they undergo radioactive decay; comprises two neutrons and protons; can travel up to 20 μm.

Anomalous fading: the phenomenon that makes a luminescence signal anomalously unstable compared with theoretical predictions; affects feldspars; underestimates determined luminescence ages.

Beta (β) particle: a type of radiation emitted from atoms when they undergo radioactive decay; comprises an electron; can travel up to 2 mm.

Bleaching: the exposure of a sample either to daylight or artificial light which removes the trapped electron population.

Cosmic rays: a high energy, penetrating extra-terrestrial radiation made up of charged particles; can be deflected by the Earth's magnetic field.

Environmental dose rate ($\dot{D}$): the total radiation dose to which a sample has been exposed in a given period of time; expressed as a rate ($Gy.a^{-1}$ or $Gy.ka^{-1}$).

Dose response curve: a plot of an increase in a luminescence signal as a function of the absorbed radiation dose.

Equivalent dose (D_e): the laboratory estimate of the radiation dose that the sample received during burial/last exposure to hear or light.

Fast ratio: an objective measure to test the dominance of the fast component in the initial part of a quartz OSL signal.

Gamma (γ) ray: a type of radiation emitted from atoms when they undergo radioactive decay; type of electromagnetic radiation that can travel up to 300mm.

Gray (**Gy**): SI unit used for absorbed radiation dose; 1 Gy is equivalent to 1 joule of energy deposited in 1 kilogramme of sample.

Incomplete bleaching: a term used when sediments have not received sufficient exposure to daylight before deposition to reset the trapped electron population.

Indian Summer Monsoon (ISM): the seasonally reversing south-westerly winds which bring rain to the Indian subcontinent and cause upwelling along the continental margins; caused by differential heating of the land and sea.

Infrared Stimulated Luminescence (**IRSL):** the luminescence signal emitted following exposure to infrared radiation (~880 nm); used for dating feldspars.

Isotope: a variant of an element; isotopes (of an element) have the same number of protons but different numbers of neutrons in each atom (e.g. ^{16}O, ^{17}O, and ^{18}O).

Luminescence: the weak light emitted by dosimetric minerals when thermally/ optically stimulated following exposure to ionising radiation; detectable by a PMT.

Optically Stimulated Luminescence (OSL): the light emitted from a sample when it is stimulated by exposure to light.

Overdispersion (σ_d): the measure of the underlying variability in D_e population; usually expressed as a percentage of the D_e.

Photomultiplier tube (PMT): a highly sensitive device that measures luminescence.

Preheat: the heating a sample to remove unstable signals prior to measuring its luminescence; typically, temperatures range between 150°C to 300°C.

Radial plot: a type of graph commonly used to display D_e populations.

Radioactivity: the spontaneous disintegration of atoms by emission of matter and energy, including α and β particles, and γ rays.

Recuperation: the amount of luminescence measured after a zero dose.

Recycling ratio: ratio between the sensitivity corrected luminescence signal from same regenerative doses in two different (typically first and last) SAR cycles.

Single aliquot regenerative dose (**SAR**) **protocol**: a sequence of laboratory operations commonly used to measure D_e; advantageous as it uses a test dose so that any changes in the luminescence sensitivity of the sample are explicitly monitored and corrected.

Test Dose: the radiation dose given to an aliquot to monitor if the aliquot is undergoing changes in its luminescence properties during the SAR cycle.

Thermal transfer: the movement of electrons from one trap to another in a crystal by heating.

Thermoluminescence (TL): the light emitted from a sample when it is stimulated by exposure to heat.

Trap: a site within crystal where electrons can become lodged and remain stored for some period of time; may be formed by chemical impurities or structural defects.

Chapter 1: Research Context

1.1. Motivation

The arid and semi-arid regions account for more than one third of the world's land area (Gilbert, 2011; Wang *et al.*, 2012), and support more than 2 billion people (Middleton *et al.*, 2011). These drylands, being home to the most vulnerable ecosystems and people, are becoming an increasing concern amongst scientists, and consequently the decade 2010-2020 has been declared as United Nations Decade for Deserts and the fight against Desertification (UN, 2010). The investigation of the past climate and environmental changes in these regions can reveal the thresholds, time scales and variability of geomorphic, hydrological and sedimentary processes that shaped them. Such studies further assist in developing plans for future adaptation and mitigation of climate-induced changes in the deserts.

The Thar or Great Indian Desert, a subtropical dryland in South Asia, is one such region that supports a large and dense human population. Covering an area of ~200,000 km^2, the Thar is largely located in the state of Rajasthan in north-west India, bordering the irrigated Indus River Plains in Pakistan to the west, the Punjab Plains in the north and north-east, the Aravalli range in the south-east and the Rann of Kachchh in the south (Figure 1.1). The Luni (~500 km long) is the only river system in the desert, which is dotted by various saltwater lakes including Didwana, Sambhar, Lunkaransar, Bap-Malar etc. Various types of sand dune types have been identified in the region, ranging from parabolic to transverse and star dunes to linear and network dunes (Wasson *et al*., 1983; Kar 1993) (Figure 1.2). The Thar is located in the transitional yet dominant regime of the south-westerly Indian summer monsoon (ISM), and the amount of annual rainfall ranges from 100 mm or less in the west to about 500 mm in the east.

about ~90% of which is received during the southwest monsoon season between July and September.

Previous studies by Goudie *et al*. (1973) and Wasson *et al*. (1984) hypothesised that the Thar experienced expansion and contraction during the late Quaternary, based on the presence of sand dunes in the areas where modern precipitation is several times higher than what will allow dune activity. The location of the Thar in monsoonal regime, which controls wind seasonality, precipitation and vegetation cover, implies that minor perturbations in monsoon dynamics may impact on the geomorphic processes, including aeolian dynamics, in this seasonally semi-arid to arid region. The sand dunes in the Thar are strongly aligned in the dominant direction of SW monsoon winds. The extensive dune systems in the Thar, therefore, provide an opportunity to understand temporal changes in aeolian dynamics in the late Quaternary.

Earlier attempts to quantify dune records and develop a chronology (e.g. Goudie *et al*., 1973; Raghavan and Courty, 1987) were based on radiocarbon dating and proved difficult because of scarcity of dateable material and contamination of carbonate nodules. However, the advent of luminescence dating made way for using widespread buried sand as an important chronometric tool and added a quantitative dimension to the study of palaeo-desert dynamics (Singhvi and Porat, 2008; Lancaster, 2008). The first application of luminescence dating to aeolian sand occurred in the Thar Desert (Singhvi *et al*., 1982), and in the following years various dune sites in the desert were dated (Thomas *et al*., 1999; Kar *et al*., 2004). However, the sampling strategies utilised in these studies were opportunistic and rather relied on the deep trenches exposed during the construction of canals in 1970s and 1980s (discussed later in Chapter 2). The

primary focus of these studies was to establish the antiquity of the desert, rather than using sand dunes as geoproxies of geomorphological and late Quaternary climatic and environmental changes. The International Union for Quaternary Research's Dune Atlas chronologic database (Lancaster *et al*., 2016) reports 146 luminescence ages from the Thar dunes (from both published papers and from unpublished PhD theses). All of these dates, which often represent patchy records spatially and temporally, were determined using older dating protocols and associated with large uncertainties. Singhvi and Kar (2004) and Singhvi and Porat (2008) in their review of previous studies note that the available records only provide a first-level understanding of dune development in the Thar and recommend further investigations. Both instrumental and methodological advances in luminescence dating (e.g. Murray and Wintle, 2000, 2003; Wintle and Murray, 2006; Duller *et al*., 2003, 2008) provide the potential for more robust age calculation.

Additionally, the density of human population in the Thar is high today, at more than 110 people per km^2 (in sharp contrast with other deserts which have population densities below 10 people per km^2; Census of India, 2011) and consequently, the Thar is undergoing intense human pressure (Kar, 2013; Dhir, 2018). The Central Arid Zone Research Institute, India reports that most of the dune systems in the Thar, which occupy 45 - 50 % of the total area of the desert, are semi-stabilised, potentially making them sensitive to both activation through natural processes, and those enhanced by human activities. It, therefore, also becomes necessary to understand the past thresholds, time scales and amplitudes of the variability of geomorphic processes shaping the dunes to

elucidate the amplitudes of the recent effect of humans and make meaningful comparisons (Singhvi and Kar, 2004; Singhvi and Porat, 2008).

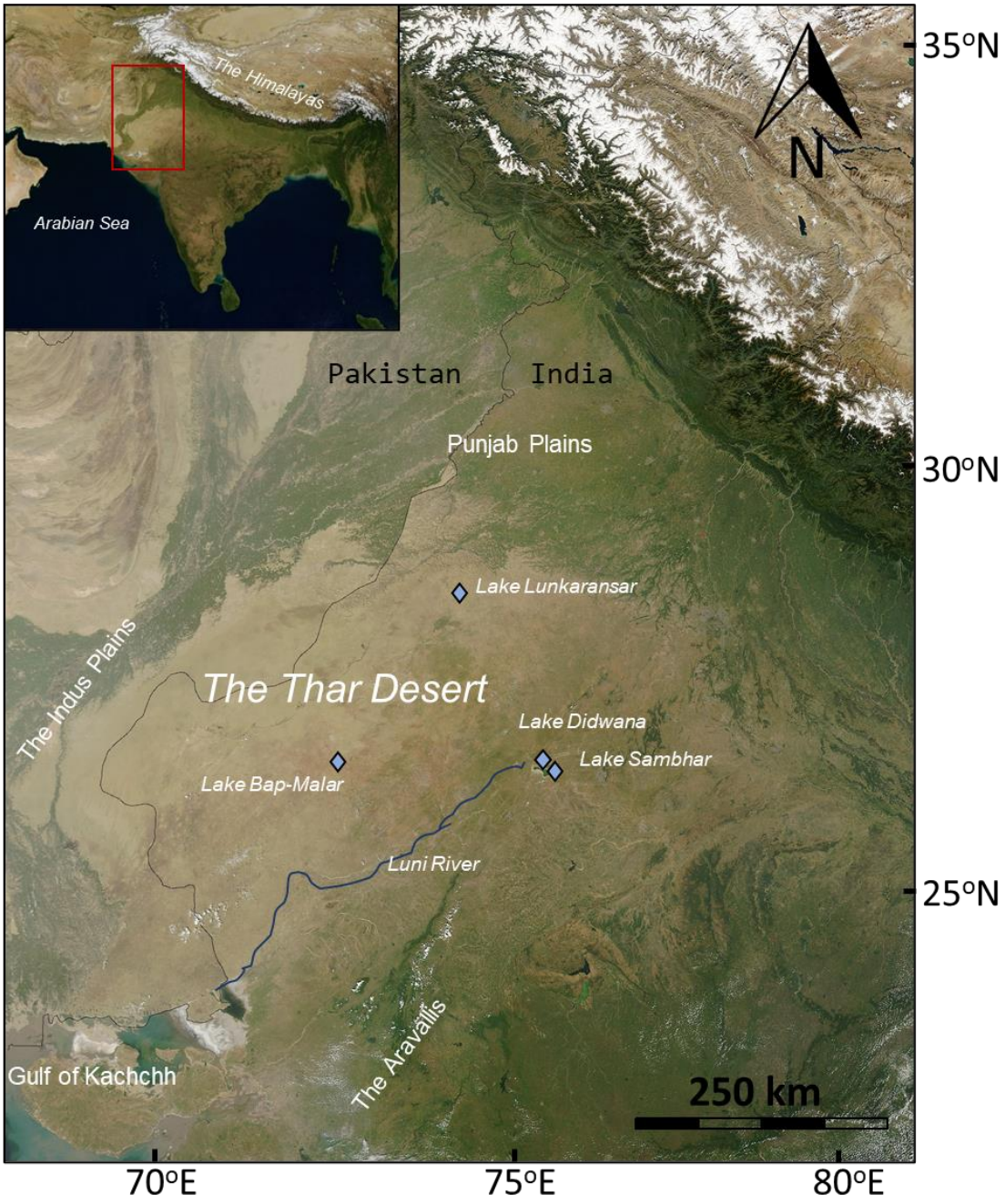


Figure 1.1. The location of the Thar Desert in South Asia. (NASA Blue Marble: Next Generation satellite imagery was obtained from NASA's Earth Observatory).

1.2. The Thar Desert dunes

Several types of sand dunes have been mapped in the Thar by extensive fieldwork in the past (Goudie *et al.*, 1973; Wasson *et al.*, 1983; Kar, 1987; Kar, 1993) and more recently by digital interpretation of remotely sensed images (Moharana *et al.*, 2013) (Figure 1.2). These dunes including parabolic, linear, transverse, barchans etc. vary in dimensions and cover ~60 % of the total landscape in the Thar. The orientation of these dunes suggests a dominant role of the south-westerly ISM winds in their formation. Due to monsoonal rainfall, large expanses of dunes and interdune plains are vegetated, comparable to the landscapes in the south-west Kalahari, inland Australia and the central Argentina (Bullard *et al.*, 1995; Hesse, 2010; Zárate and Tripaldi, 2012).

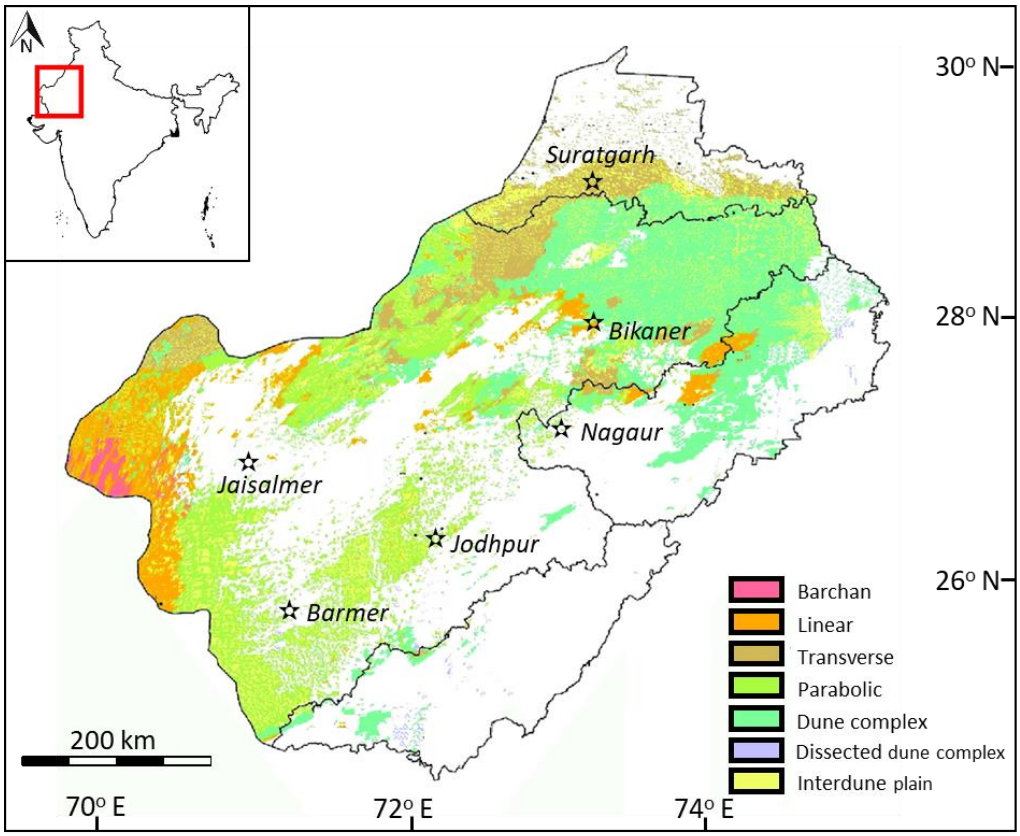


Figure 1.2. Distribution of various dunes types in the Thar Desert (after Moharana *et al*., 2013).

Parabolic dunes

Parabolic dunes typically form in arid or semiarid areas where vegetation is present, such as in the great plains of North America (Halfen *et al.*, 2010; Hanson *et al.* 2009; Hugenholtz *et al.*, 2008), the Australia (Hesse, 2011), and the Arabia (Anton and Vincent, 1986). In the Thar, parabolic dunes are the most abundant dune type, with major dunefields occurring in Barmer, Jaisalmer, Jodhpur and Bikaner districts (Figure 1.2). These parabolic dunes are strongly aligned in the direction of the dominant southwest monsoon winds (Figure 1.3A). These dunes, which have a U-shaped or a V-shaped form, are often linked to adjacent dunes in a fashion that they appear to share arms, creating 'rake-like' formations (Wasson *et al.*, 1983; Figure 1.3A). These can be up to 2500 m long, with interarm spacing ranging between 150 m and 650 m. These 'rake-like' parabolic dunes have rounded nose which can be up to 40 m high and may contain more than 35 % of total dune sand by volume (Kar *et al.*, 2004).

Parabolic dunes can be active, semi-active or inactive, in terms of mobility and accumulation as these dunes show sensitivity to an array of factors in the environment they exist. Vegetation plays a significant role in the formation and development of parabolic dunes. Vegetation retards the sand motion functioning like an anchor and protects the less mobile arms against aeolian processes, thereby allowing the central section to advance downwind to produce the hairpin form (Goudie, 2011). The vital role of vegetation in the formation and development of parabolic dunes has been modelled by Nishimori and Tanaka (2001), Duran *et al.* (2005), Baas and Nield (2007) and Nield and Baas (2008). If vegetation cover increases or wind strength decreases, parabolic dunes may replace barchans (Tsoar and Blumberg, 2002; Wolfe and Hugenholtz, 2009;

Ardon *et al.*, 2009; Reitz *et al.*, 2010). For example, in the Canadian Prairies, over the last few hundreds of years relatively stable parabolic dunes have tended to replace active barchans (Wolfe and Hugenholtz, 2009). Conversely, if parabolic dunes lose their vegetation, they may turn into active transverse dunes (Barchyn and Hugenholtz, 2012). Jerolmack *et al.* (2012) have presented an analysis of the transition between barchanoid ridges and parabolic dunes in the White Sands, New Mexico. Parabolic dunes tend to occur in areas with high groundwater levels. Reduction in groundwater levels due to over-pumping of aquifers or increasing salinity (both affect vegetation growth) can affect parabolic dune reactivation (Langford *et al.*, 2009). Parabolic dunes have been reported to get reactivated by fire in the Brazilian Amazon (Nelson, 1994) and agricultural land use in Hungary (Kiss *et al.*, 2009). The Thar has been experiencing deteriorating vegetation cover conditions and anthropogenic disturbances in the last century (Dhir, 2018), that makes the parabolic dunes in the desert vulnerable to reactivation and geomorphic transformation to a more mobile form.

Linear dunes

Linear dunefields occur in the western Thar and contiguous parts of Pakistan. Smaller dunefields have been mapped near Bikaner (Kumar *et al.*, 1993; Saxena and Singh, 1976) and Jodhpur (Kar, 1997; Verstappen, 1968) (Figure 1.3B). The dunes have been termed as longitudinal in some literature (Kar, 1987; Kar, 1993). The term longitudinal more specifically defines a dune trend within the 15 % of resultant transport direction (Hunter *et al.*, 1983), while the term linear describes the dune morphology rather than implying particular formative processes.

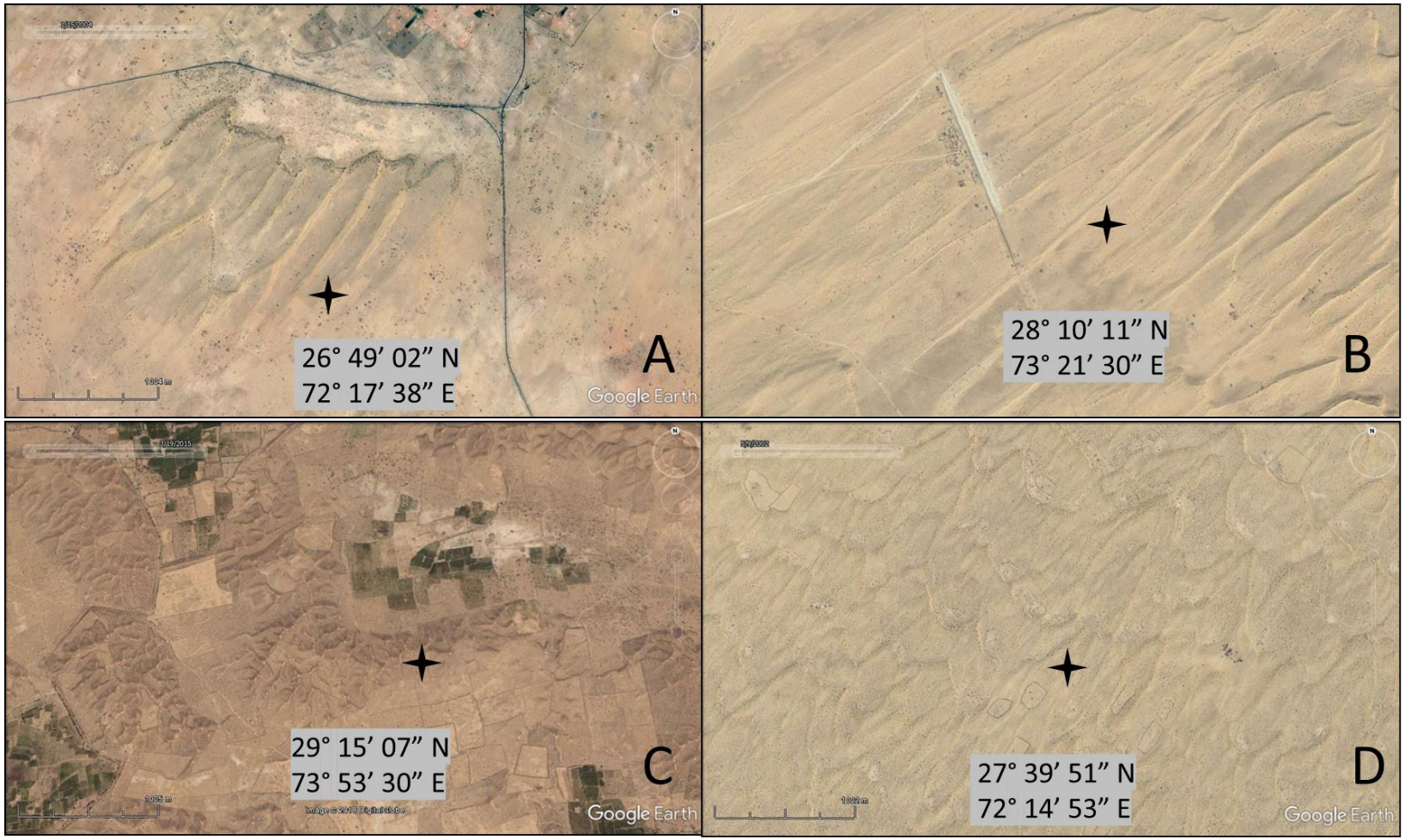


Figure 1.3. Examples of different dune types present in the Thar. (A). Parabolic dunes in the central Thar. (B). Linear dunes in the northern Thar. (C). Dune complex in the north-eastern Thar. (D). Transverse dunes in the western Thar.

The orientation of Thar linear dunes is along the direction of dominant monsoon winds and gradually changes from WSW in the western-most part to SW in the eastern part (Figure 1.3B). These dunes range in height from 5 m to 20 m and <10 km in crest-line length and are covered by varying degree of vegetation. The dune forms vary from Y-junctions to clusters of 5-8 linear dunes joining at acute angles like that of vegetated linear dunes in the north-western Negev (Tsoar and Moller, 1986, Tsoar *et al.*, 2008) and the south-western Kalahari (Bullard *et al.*, 1995; Thomas and Shaw, 1991).

Similar to the linear dunes elsewhere (Telfer *et al.*, 2017), the mechanism of linear dune formation in the Thar remains contested. Verstappen (1968) suggested that the Thar linear dunes originated from progressive elongation parabolic dune arms and the removal of the central curved part of the dunes- a view that was supported in later studies by Singh *et al.* (1982) and Wasson *et al.* (1983). Verstappen's (1968) observations were based on the study of a parabolic-linear dunefield situated to the south of Jodhpur. Wasson *et al.* (1983) made similar observations that some dunes in the northern Thar might have originated from source bordering transverse dunes, with their lee-side getting sand from the nearby Ghaggar-Hakra palaeochannel. Kar (1987) proposed that colonisation of narrow strips of land by barchans under the influence of strong unidirectional wind and their subsequent coalescence that gradually assumed a smoother convex crest resulted in the formation linear dunes, based on his observation in the western Thar. Whilst these theories do not have concrete evidence to prove their veracity, different and diverse opinions do emphasise on the need to conduct further research in this field.

In other deserts, linear dune accumulation chronologies have been frequently and consistently used for palaeoenvironmental reconstructions, owing to the accumulatory nature of linear dunes, making them important geoproxy records (Thomas 1992, Nanson *et al.*, 1992; Munyikwa, 2005, Thomas, 2013; Telfer and Hesse, 2013). However, the Thar linear dunes have received very limited attention as the majority of studies have been conducted on more widespread parabolic dunes (Thomas *et al.*, 1999; Singhvi and Kar, 2004). Therefore, this context provides an opportunity to establish the first linear dunefield chronology from the Thar, and develop those as geoproxies for regional palaeoenvironmental changes.

Other dunes

Besides the two dominant dune types, other forms also occur in the Thar. Transverse dunes of varying heights have been mapped mainly to the west of Bikaner, NW of Jaisalmer, and in parts of Ganganagar and Hanumangarh districts in the north-eastern Thar (Figure 1.3D). The dunes generally occur in 1-5 km long chains with narrow interdune plains in between (Kar, 1993). Barchans are found in the west and south-west of Jaisalmer. These are 15 to 40 m high, coalesced, and occur in long chains within the linear dune field (Kar 1987; 1993). Dune complexes, consisting of several 12-20 m high dune types, have been mapped in the northern part of the desert, where the dunes are so closely spaced and differently oriented that it is difficult to delineate them individually (Figure 1.3C) (Moharana *et al.*, 2013).

1.3. History of human settlement in the Thar

Owing to its location in the transitional zone from the Saharo-Arabian deserts to the Oriental biogeographical zone, the Thar has been considered as an important location in understanding early human occupation in South Asia during the late Quaternary, and therefore has attracted significant research in the past decades (e.g. Misra *et al*., 1963; Allchin *et al*., 1978, Misra *et al*., 1982; Blinkhorn, 2012 and references therein). The human occupation in the Thar was contingent on the availability of the water sources, which in turn was dependent on the dynamism of the fluctuating ISM during the late Quaternary (Zhisheng *et al*., 2011; Cai *et al*., 2015). Several extensive archaeological surveys in the Thar, spanning the last seven decades, have identified a large number of Palaeolithic sites, which have been synthesised and classified into Lower (>1.07 ma to ~ 130 ka), Middle (78 ka to 38 ka) and Upper Palaeolithic (38 ka to early Holocene). The Thar Palaeolithic archaeology is known largely from surface surveys, such as palaeochannels, dune deposits and artefacts (Allchin *et al*., 1978, Misra *et al*., 1982; Raghavan and Courty, 1987; Blinkhorn, 2012). As shown in Figure 1.4, the majority of Lower Palaeolithic sites are located to the south of the Thar in Gujarat while a concentration of sites also occurs in the eastern Thar, as identified by Misra *et al*. (1982) and Allchin *et al*. (1978). Middle Palaeolithic sites are lesser in number and have been identified in the southern and central Thar, while Upper Palaeolithic are the most numerous and widespread and found all across the Thar (Allchin *et al*., 1978; Misra, 1963). However, there remain very few dated and excavated evidence for early human behaviour in the Palaeolithic Thar. 16R and Kataoti, both associated with dune features, are two key sites (Figure 1.4) which have had sediments dated using luminescence dating. Middle Palaeolithic

assemblages from Kataoti feature stone tools date between ~100 and ~60 ka, which overlap a Middle Palaeolithic occupation at 16R bracketed by dates of ~80 and ~40 ka. (Misra and Rajaguru, 1986, Misra and Rajaguru, 1989, Raghavan *et al*., 1989, Blinkhorn *et al*., 2013). Assemblages at both these sites offer important insights into the technological development in the Thar in the context of climatic changes and human expansion. These sites further identify the Thar as a pivotal region to investigate major changes in early human demography and its association with migration between Africa and southern Asia (Blinkhorn *et al*., 2013).

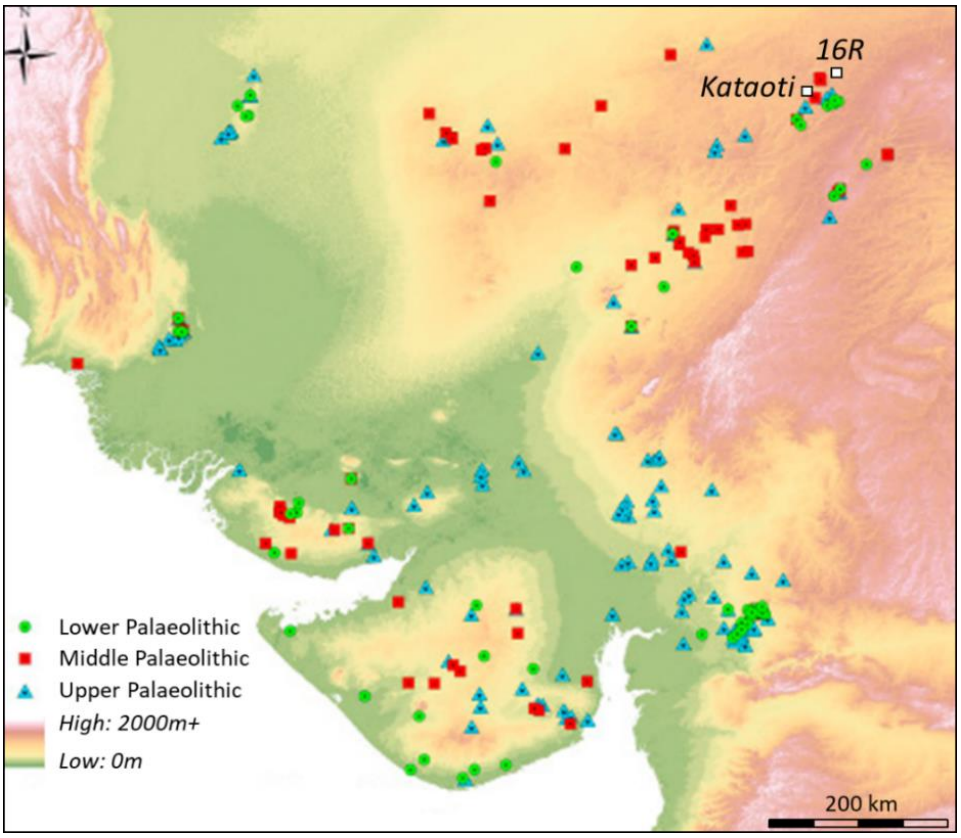


Figure 1.4. Distribution of Palaeolithic sites in the Thar (Blinkhorn, 2012).

In addition, few sites of Mesolithic and Neolithic cultural phase (Holocene blade and microlith focussed industries) have been identified in the Thar (Blinkhorn, 2012 and references therein).

However, the urban phase of the Indus Civilisation, one of the earliest complex societies in the world, which flourished along the vast alluvial plains forming the margins of the Thar between ~4.5 and 3.9 ka, arguably remains the most research and investigated topic of archaeology in the north-western India (e.g. Kenoyer, 1998; Possehl, 2002, Wright, 2010; Petrie *et al*., 2010).

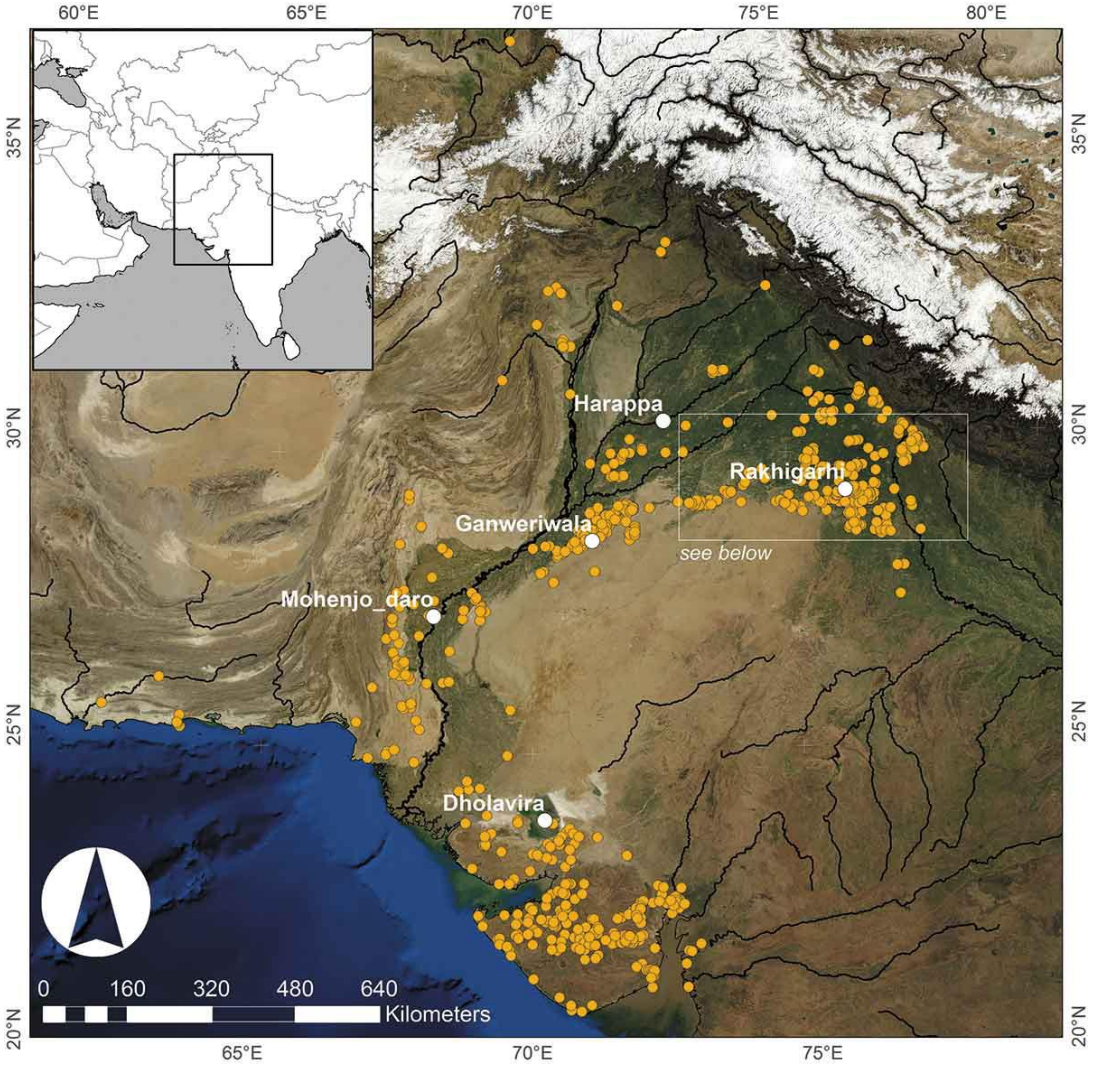


Figure 1.5. Location of the Indus Civilisation's major urban centres and small sites (Parikh and Petrie, 2019). The boxed area shows centres associated with the Ghaggar-Hakra palaeochannel.

Petrie *et al*. (2017) detail a wide range of new evidence covering several aspects of the nature of the Indus Civilisation, particularly the environmental and

climatic context within which urbanism developed, thrived and ultimately declined. There were four or five particularly large Indus settlements, usually described as cities, namely *Mohenjo-daro, Harappa, Rakhigarhi, Dholavira, and possibly Ganweriwala*; Figure 1.5) (Kenoyer, 2008). The excavated evidence suggest that inhabitants of these cities produced and traded distinctive types of material culture including pottery, jewellery, figurines, stamp seals, standardised weights etc (e.g. Wright, 2010; Coningham and Young, 2015).

Ghaggar-Hakra palaeochannel, which forms the northern margin of the Thar, has been described as a key river system for the civilisation (Mughal, 1997; Kenoyer, 1998; Wright, 2010). Hydrological changes in the Ghaggar-Hakra palaeochannel system in the backdrop of mid-Holocene climatic variability has been associated with the decline of Indus urban centres (e.g. Enzel *et al*., 1999; Giosan *et al*., 2012; Petrie *et al*., 2017). As a result, this now-ephemeral channel has been subject of several investigations in a bid to understand the link between fluvial activity and urban demise (e.g. Gangal *et al*., 2010; Maemouku *et al*., 2013; Giosan *et al*., 2012; Singh *et al*., 2016; Durcan *et al*., 2019). Giosan *et al*. (2012) use a combination of high resolution topographic data, geomorphologic analysis and sediment dating to establish a chronology of the evolution of fluvial landforms and suggest that the Ghaggar-Hakra had a monsoon driven perennial flow prior to ~4.5 ka, which became ephemeral thereafter. Durcan *et al*. (2019), based on luminescence dating of fluvial demonstrate that parts of the Ghaggar-Hakra were still flooding after the demise of the Indus urban centres. Nevertheless, as Parikh and Petrie (2019) and Petrie *et al*. (2017) note, there still remains significant geochronological evidence to elucidate link between climate, environment and Indus urban society.

In the last millennium, the available records suggest that during 8th to 14th century, several political, trading and religious centres emerged in the greater Thar, suggesting permanent settlements in the region (Tod, 1832). During the medieval period, many independent dynastic constituencies were established, even in the drier western sub-regions of Jaisalmer and Barmer, which continued to thrive until the colonial rule began in the 19th century. James Tod, a British Colonel who surveyed the region, estimated the number and size of settlements for early 19th century. He documented over 3000 settlements in Jodhpur, ~1200 in Bikaner and ~300 in Jaisalmer districts in western Thar, and attributed it to the construction of smaller canals in the region which brought water from the Indus and its tributaries to the Thar (Tod, 1832). A detailed analysis of medieval human population in the Thar has been compiled by Dhir *et al*. (2018). Since the year 1891, regular census data have been recorded which show that the human population did not display any significant net growth up to year 1921. A collective analysis of historic records showed that at the end of 19th century and early 20th century, the Thar experienced as many as 13 famines, each lasting for 2-4 consecutive years, had a negative impact on population growth (Narain *et al*., 2000). However, from the year 1921 there had been a steady growth, the decadal growth being ~20 % in the decades to year 1951 and ~30 % from then on to census year 2001 (Dhir *et al*., 2018). The population more than doubled between 1921-1961, and rose to another three and half times in the next five decades from 1961 to 2011 (Figure 1.6). An analysis by Dhir *et al*. (2018) shows that decadal growth rate of the Thar has been higher than that of Rajasthan and India for most of the time, ranging between a high of ~40 % in 1971-1981 to ~20 % as reported for the last decade. This acceleration in growth has been attributed to

subcontinent's independence and subsequent mass migration of people, agricultural and irrigational reforms.

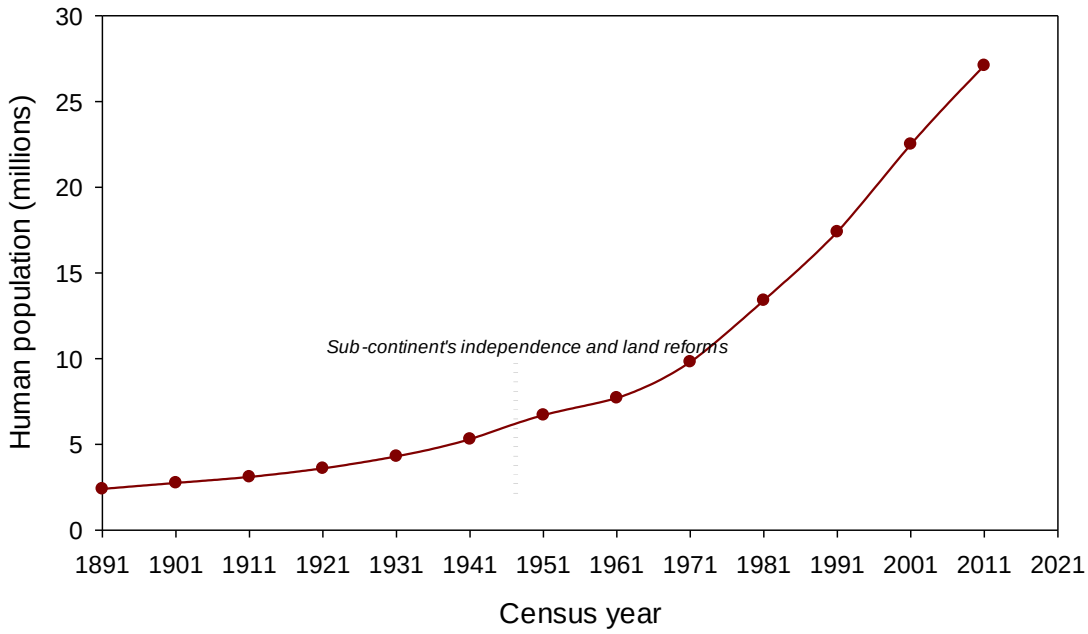


Figure 1.6. Growth of human population over the decades in the Indian side of the Thar (based on data presented in Dhir *et al*., 2018).

At present, the Thar is world's most densely populated desert, with over 110 people living per km^2. Owing to increasing human population and associated irregular use of available land, the Thar landscape is subjected to environmental deterioration. Degradation of community grazing land, loss of root binding plant species, flattening of semi-stabilised dunes, mechanised ploughing etc are increasing the risk of sediment erosion, sand mobility and reactivation of dunes (Kar *et al*., 2004; Kar, 2014; Dhir *et al*., 2018). Figure 1.7 shows an example of a parabolic dunefield in the central Thar which has witnesses flattening of dunes and rapid expansion of agricultural fields in less than 20 years.

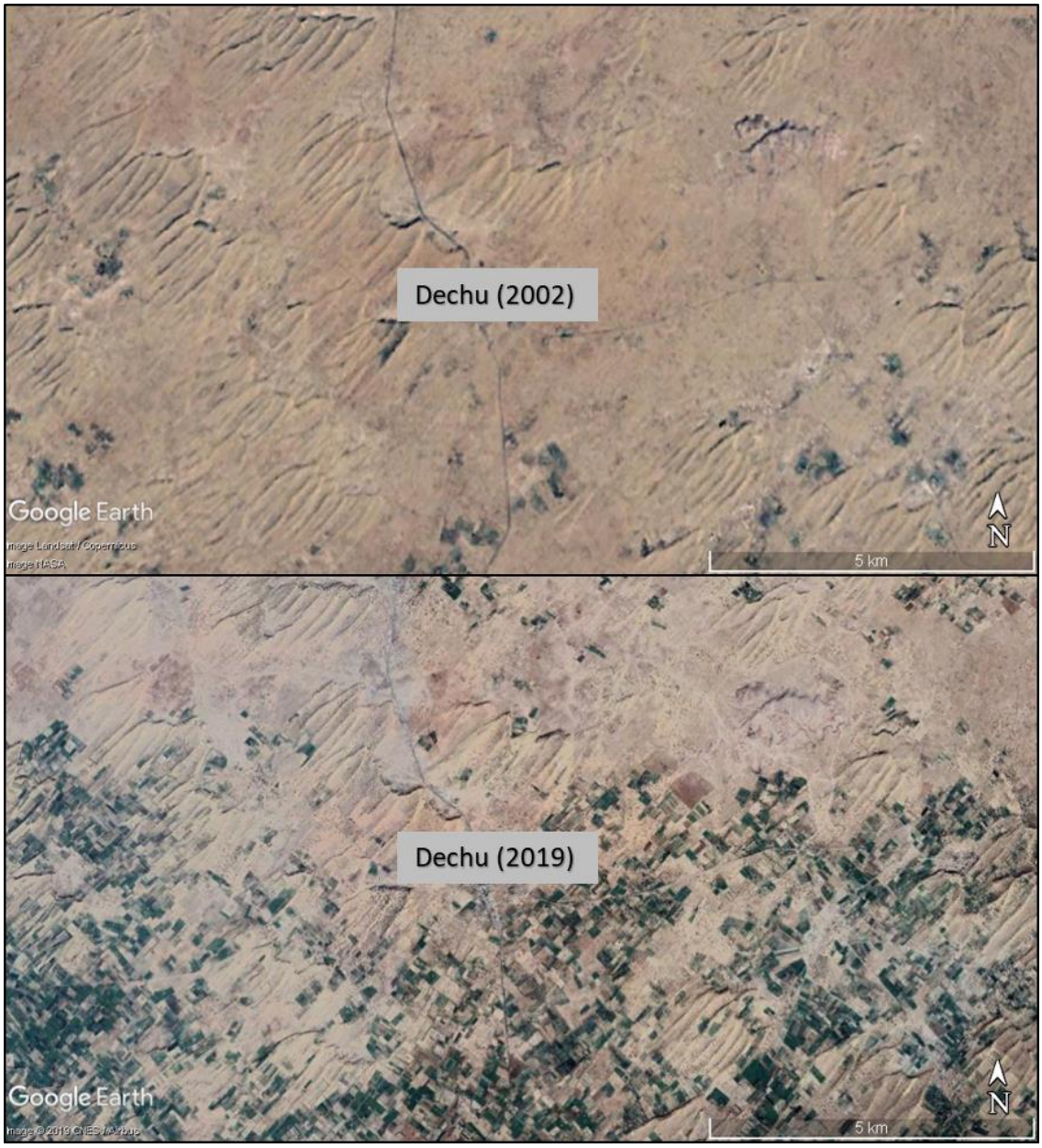


Figure 1.7. An example of expansion of agricultural land into the parabolic dunefield and changing landscape within a span of two decades in the central Thar. The same dunefield has been investigated in Chapter 4 to demonstrate how these parabolic dunes have reactivated in a response to anthropogenic influences.

1.4. Indian Summer Monsoon and its variability

As discussed in Section 1.2, based on the orientation of the sand dunes in the Thar, it is evident that the ISM plays a big role in their development (Figure 1.3). The ISM begins each year in mid-May as a result of heating of the Indian subcontinent and the Tibetan Plateau, which creates a temperature and therefore, surface pressure gradient, between the land and the surrounding ocean which in turn initiates the movement of monsoon jet, which lasts until late September (e.g., Li and Yanai, 1996; Wu *et al*., 2007; Rajagopalan and Molnar, 2013). The strength of the ISM (both wind and precipitation) has been reconstructed using an array of terrestrial records from the Indian subcontinent and beyond, and marine records from the Arabian Sea. In general, the records suggest that during the late Quaternary (especially the Holocene), due to changes in the precessional cycle and summer insolation, the ISM showed great variability. These insolation driven changes have been shown to have resulted in periods of variable precipitation and the onset of enhanced regional aridity in the Indian subcontinent.

Marine records from the Arabian Sea

The Arabian Sea experiences intense upwelling driven by the ISM offshore winds, therefore, variations in proxies for upwelling and wind intensity have often been interpreted to reflect variations in monsoon intensity using marine sediments. Sirocko *et al*. (1993)'s pioneering study, based on oxygen isotopes and carbonates from core 74KL from the upwelling region of the western Arabian Sea (Figure 1.8), showed that the ISM exhibits a direct albeit nonlinear response to the intensity of solar insolation during summers. The observation was further attested by Gupta *et al*. (2003) who presented a continuous Holocene old record of *Globigerina bulloides* from a core from ODP site 723A, off Oman in north-

western Arabian Sea (Figure 1.8). The authors provided a high-resolution centennial-scale monsoon variability throughout the Holocene and revealed a monotonic decrease in *G. bulloides* between 10 and 2 ka, which was used to infer decreasing strength of summer monsoon winds. The authors also identified several intervals of weak summer monsoon that coincided with cold periods documented in the North Atlantic region—including the most recent climate changes from the Medieval Warm Period to the Little Ice Age. Ivanochko *et al*. (2005) used productivity records from another planktic foraminifer (Ba/Al ratios from *Neogloboquadrina dutertrei*) from a core (NIOP-905), off the Somali coast, southwestern Arabian Sea (Figure 1.8) and also implied decreased upwelling from 10 ka to present.

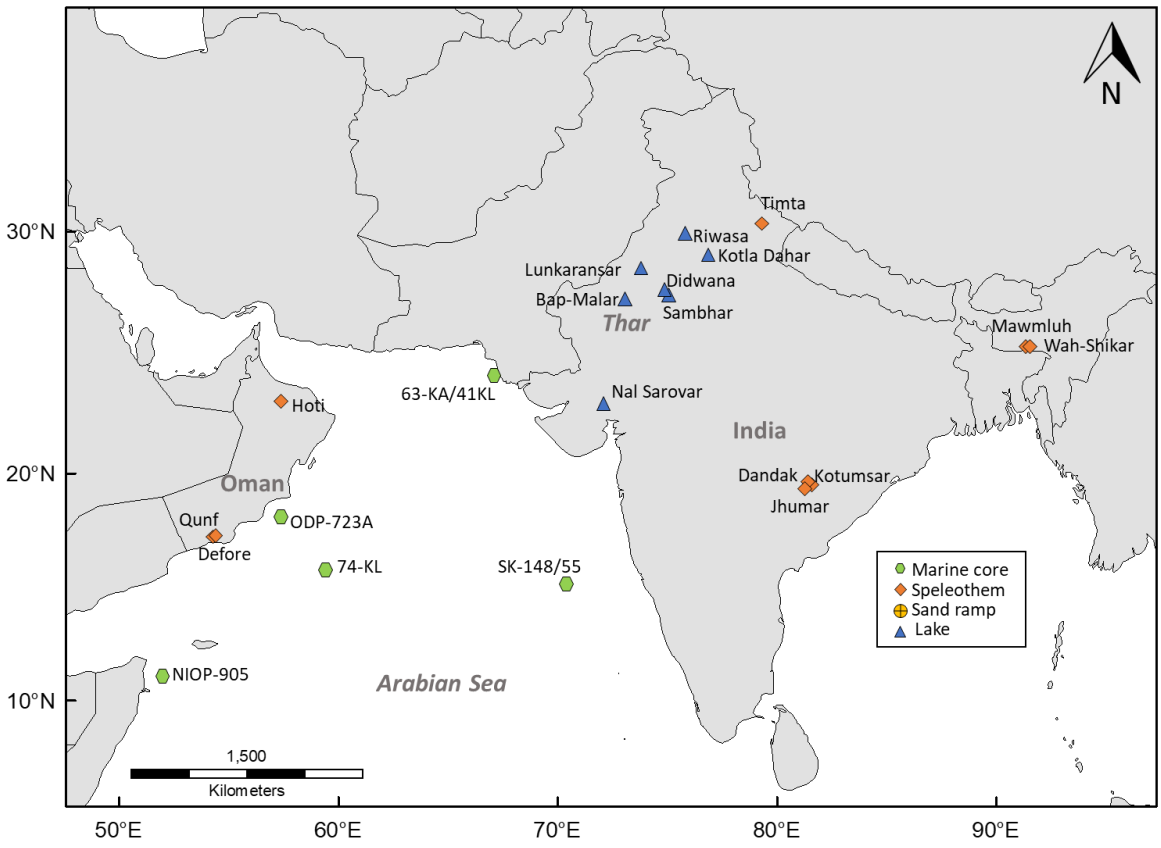


Figure 1.8. The locations of different types of proxy records that have been reconstructed for the past ~12 ka as discussed in the thesis.

Studies by Sarkar *et al*. (2000) (cores 2502G, 2491G, 3268G5 and 3104G) and Thamban *et al*. (2001) (core SK148/55), based on several planktonic foraminifera like *Globorotalia menardii*, *Globigerinoides sacculifer* and *Globigerinoides ruber*, suggested a mid-Holocene arid event around 6.5-5.5 ka, wherein both precipitation and oceanic productivity remained low. During the late Holocene, the ISM conditions again deteriorated around ~3.5 ka. And ~1.6 ka as demonstrated by Thamban *et al*. (2007), Sarkar *et al*. (2000) and Ivanochko *et al*. (2005). However, study by Staubwasser *et al*. (2003), who investigated *Globigerinoides sacculifer* from core 63KA from a site on the continental margin off Pakistan coast and presented a record of freshwater input by the Indus River, shows a mismatch with other Arabian Sea records. The changes in $\delta^{18}O$ values have been explained in the context of mixture caused by spring/winter rainfall and meltwater input from Himalayan glaciers (Staubwasser *et al*., 2003). Recently, Gill *et al*. (2017) reconstructed fields of Arabian Sea summer wind stress curl and ISM rainfall anomalies since early Holocene using sea surface temperature (SST) proxies (Mg/Ca and alkenones) from 27 locations scattered across the equatorial Pacific using a multiproxy reduced dimension methodology. Their calculated positive anomalies in wind stress curl during the early to middle Holocene are consistent with greater early Holocene upwelling records presented by Gupta *et al*. (2003). Figure 1.9 shows the results from aforementioned studies in a wiggle plot. Whilst these are high-resolution indicators of variability ISM strength, the implications may not be directly true to infer palaeoenvironmental changes in the Thar by means of extrapolation, unless integrated with records from within the desert (e.g. Thomas *et al*., 1999).

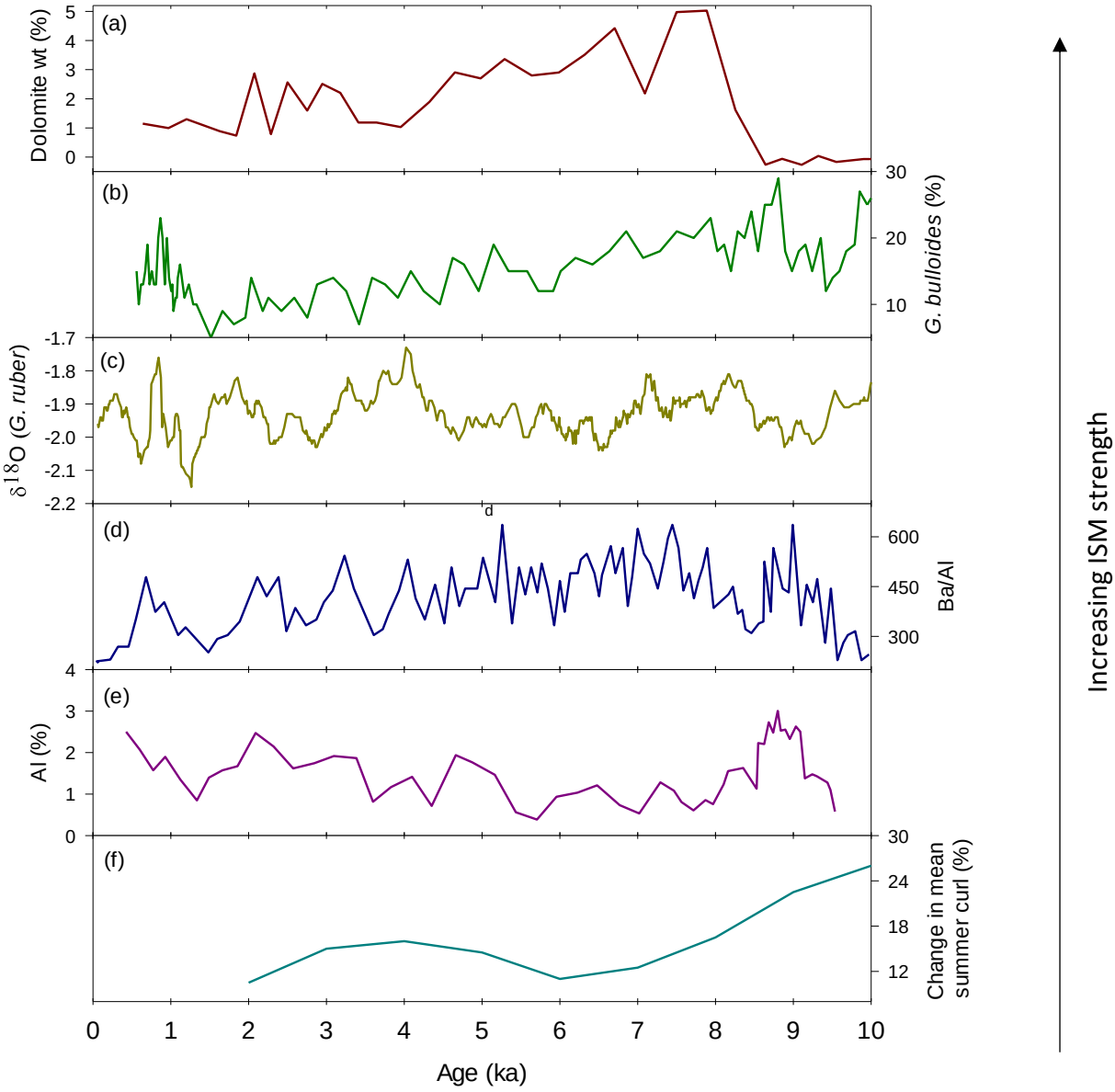


Figure 1.9. Synthesis of Holocene variations in the ISM as records in the Arabian Sea cores. (a) aridity record based on generated dolomite peaks from core 74KL (Sirocko *et al*., 1993). (b) ISM induced upwelling record based on *G. bulloides* % from core 723A (Gupta *et al*., 2003). (c) Precipitation records based on $\delta^{18}O$ values from *G. ruber* from core 63KA (Staubwasser *et al*., 2003). (d) Biological productivity records based on Ba/Al ratio from *N. dutertrei* off from core NIOP-905 (Ivanochko *et al*., 2005). (e) Precipitation records based on Al concentrations derived from *G. ruber*

from core SK148/55 (Thamban *et al*., 2007) (f) wind stress curl change across the western Arabian Sea, based on SST proxies from 27 locations scattered across the region (Gill *et al*., 2017).

Speleothem records from India and the Arabian Peninsula

In last two decades, speleothems have appeared as important archives to reconstruct monsoonal fluctuations, particularly during the late Quaternary (Yadava and Ramesh, 1999; Dixit and Tandon, 2016; Kaushal *et al*., 2018). The high-resolution, high-quality geochemical records from these archives provide valuable information about the changes in larger circulation patterns, seasonality in rainfall, and local changes in temperature and precipitation amount (Kaushal *et al*., 2018 and references therein). However, when compared to Eastern Asia and the Arabian Peninsula, there still remain few speleothem-based monsoonal studies in the Indian subcontinent (Figure 1.8) and most of the ISM speleothem $\delta^{18}O$ records only cover a small period of the Holocene time scale (Figure 1.10). Sinha *et al*. (2005) generated a high-resolution ^{230}Th-dated stalagmite $\delta^{18}O$ records from Timta Cave documenting ISM precipitation variations during the Bølling-Ållerød period (15.2 to 11.7 ka). The authors concluded that ISM precipitation was enhanced during the period compared with the glacial and Younger Dryas, and multidecadal monsoon variability was an important aspect of ISM behaviour at that time. Perhaps, the most detailed studies of speleothem have been from the Mawmluh Cave in Meghalaya, north-east India, after which Meghalayan sub-division of the Holocene has been named (Walker *et al*., 2019). The stable $\delta^{18}O$ records of speleothems from Mawmluh provide information about changes in the ISM strength on decadal to centennial timescales during the past

few millennia (Dutt *et al*., 2015; Berkelhammer *et al*., 2012). Fleitmann *et al*. (2003), based on their stalagmite studies in Qunf Cave, Southern Oman noted an abrupt onset and rapid increase in monsoon precipitation between ~10.3 and 9.6 ka indicating a rapid northward migration of the ITCZ. After ~8 ka, monsoon precipitation decreased gradually in response to changing Northern Hemisphere summer solar insolation, with decadal to multidecadal variations in monsoon precipitation being linked to solar activity. The other speleothem records indicate a rapid increase in ISM precipitation between ~10.6 and 9.7 ka in Southern Oman and ~10.1 and 9.2 ka BP in Northern Oman (Fleitmann *et al*., 2007). Band *et al*. (2018) studied $\delta^{18}O$ ratios from the Kotumsar Cave, Central India and their reconstruction record shows a gradual decline in intensity of ISM from 8.5 to 7.3 ka, followed by increasing trend from 7.3 to 5.6 ka.

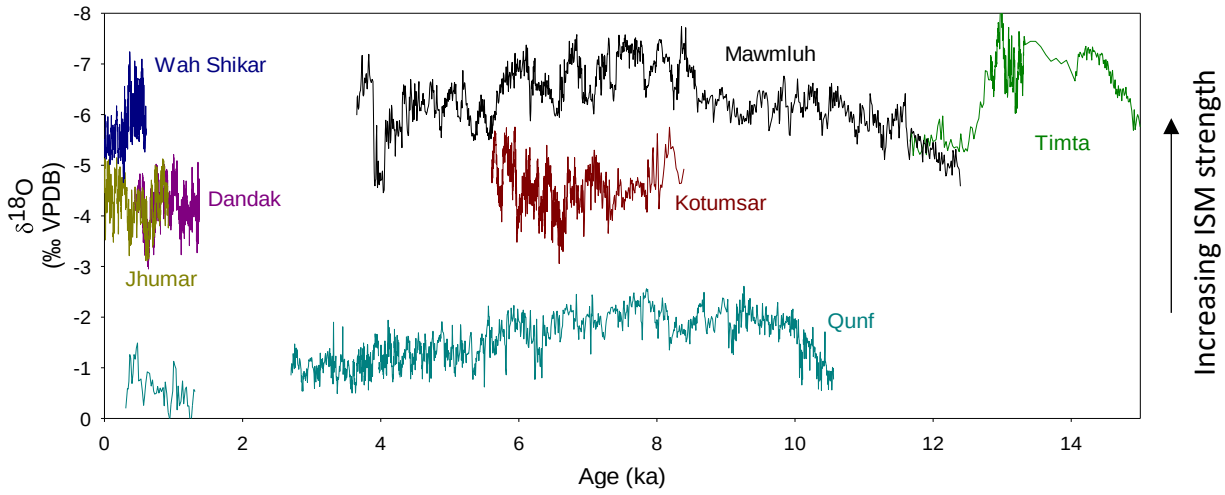


Figure 1.10. Summary of selected ISM stalagmite $\delta^{18}O$ records from Caves Qunf (Fleitmann *et al*., 2003); Mawmluh (Berkelhammer *et al*., 2012); Timta (Sinha *et al*., 2005); Kotumsar (Band *et al*., 2018); Jhumar (Sinha *et al*., 2011a); Dandak (Sinha *et al*., 2006) and Wah Shikar (Gupta *et al*., 2019).

From Dandak and Jhumar Caves in central India, there are now near annually resolved records of the ISM rainfall variations from 600 to 1500 AD (Sinha *et al*., 2007; Sinha *et al*., 2011a; Sinha *et al*., 2011b; Berkelhammer *et al*., 2010). The $\delta^{18}O$ records from these caves show historic accounts of famines and droughts correlating with their reconstruction of weakened monsoon. Recently, Gupta *et al*. (2019) presented a new high-resolution $\delta^{18}O$ based reconstruction of ISM rainfall over the last ~900 years from a stalagmite collected from the Wah Shikhar Cave in north-east India. The authors identified abrupt shifts in the ISM and suggested its profound impact on human societies in the context of agriculture productivity, declining economy, and societal crisis. However, as with the marine productivity records, since there are no speleothem studies from the Thar (or north-western India), the interpretations are extrapolated to infer palaeoenvironmental changes in the desert.

Lacustrine records from the Thar

The seminal palaeoclimate and ecological studies on the lakes of Rajasthan (Sambhar, Didwana and Lunkaransar; Figure 1.8) by Singh *et al.* (1974) drew the attention of Quaternary scientists to the region and initiated a series of systematic palaeoclimate research in the region. A number of other lake sites, and advances in radiocarbon dating since then provided important records of palaeoenvironmental reconstructions, primarily based on palynology, geochemistry, and sedimentology (Prasad and Enzel, 2006).

Wasson *et al*. (1984) reconstructed of the history of salinity and water-level changes in Didwana Lake along the eastern Thar margin (Figure 1.8) using

sediment texture, mineralogy and geochemistry of lake sediments. They suggested that hypersaline conditions prevailed at about the LGM, and between ~13 ka and ~6 ka the lake levels fluctuated widely. The lake dried briefly ~4 ka and since then the lake has been ephemeral with a lowered rate of sedimentation and mildly saline conditions rather like those of today. Enzel *et al*. (1999) analysed the sedimentology, mineralogy, and isotopic composition of the organic material and carbonates from laminated deposits in Lunkaransar Lake (in NE Thar; Figure 1.8). They revealed that the lake levels were very shallow and fluctuated often in the early Holocene, rose abruptly around ~6.3 ka and then the lake completely desiccated ~4.8 ka. The authors noted that this end of 1500-year wet period coincided with a period of intense dune destabilisation in the region. Prasad *et al*. (1997) carried out multiproxy investigations in Nal Sarovar, a shallow lake in the palaeodesert margin of Thar in Gujarat (Figure 1.8) using C/N and $\delta^{13}C$ of organic matter. They deduced two main arid phases between ~7.8–7.2 ka and ~6.1–5.4 ka, and suggested two brief ones around ~4.2 ka and ~3.3 ka. Macdonald (2011) presented a summary of reconstructed lake levels and palaeoprecipitation at Lakes Didwana and Lunkaransar, as well as a relative climate at Lake Nal Sarovar, and noted that these lakes show both similarities and differences when compared to each other (Figure 1.11) like these lakes did not dry up simultaneously, and each showed maximum wetness and aridification at different times during the Holocene.

The geochemical studies from Sambhar, the largest lake in Thar (Figure 1.8) reveal significant departures from the available lacustrine record (Sinha *et al*, 2006). The Sambhar did not desiccate throughout its history unlike the Didwana and Lunkaransar (located further west) which desiccated completely between ~

4 ka and ~3 ka (Figure 1.12). The authors identified an abrupt and brief arid event between ~7.5 and ~6.8 ka, and correlated humid records from Sambhar with monsoonal intensification reconstructed from the Arabian Sea record. Similar fluctuations in lake levels and salinity have also been observed at Didwana, and Lunkaransar from the early to mid-Holocene, and at Bap-Malar albeit with differing onset timings. The records then suggest a re-establishment of the monsoonal circulation in the region from ~6 ka onwards (earlier at Bap-malar, see Figure 1.12). As shown in Figure 1.12, the onset in mid-Holocene humidly is over 1 ka earlier at Bap-Malar than in the other lake basins. This suggests that lake may be influenced more by local factors like groundwater discharge than larger drivers like the ISM (Deotare *et al*., 2004). Also, the lake basins span a large geographic area and, while different hydrological responses to rainfall changes might be a function of basin size, depth and morphology (Bowler, 1986), they may represent real spatial differences in monsoon penetration into the Thar. Furthermore, differences in lake record interpretations can be a function of different proxy records being analysed in individual studies or different interpretations of proxy signals between studies. A similar issue has been raised and discussed in the context of African lake basins by Burrough and Thomas (2009). A final point is that individual studies do not necessarily apply the same dating methods nor have the same interpretive resolutions (Cohen, 2003). At all four discussed lakes, whilst radiocarbon methods were used, the dated material and resolution differ significantly. A new assessment by Misra *et al*. (2019) notes that Sambhar, Didwana and Bap-Malar offer low-resolution records with a multi-millennial scale resolution, which constrain their comparative analyses.

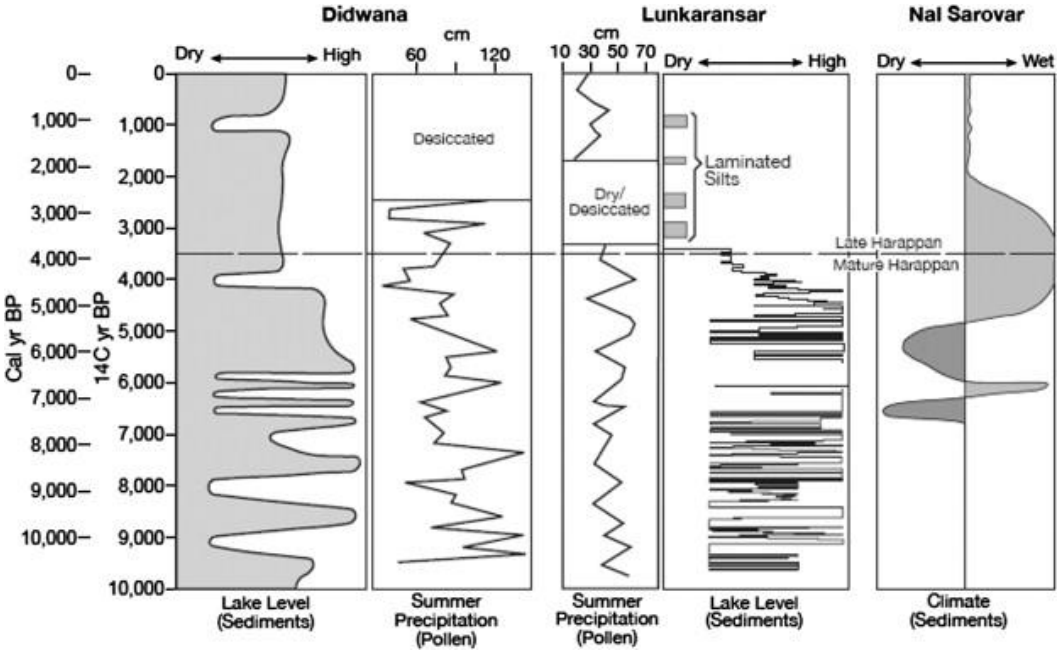


Figure 1.11. Generalised lake level reconstructions of Lakes Didwana, Lunkaransar and Nal Sarovar by Macdonald (2011).

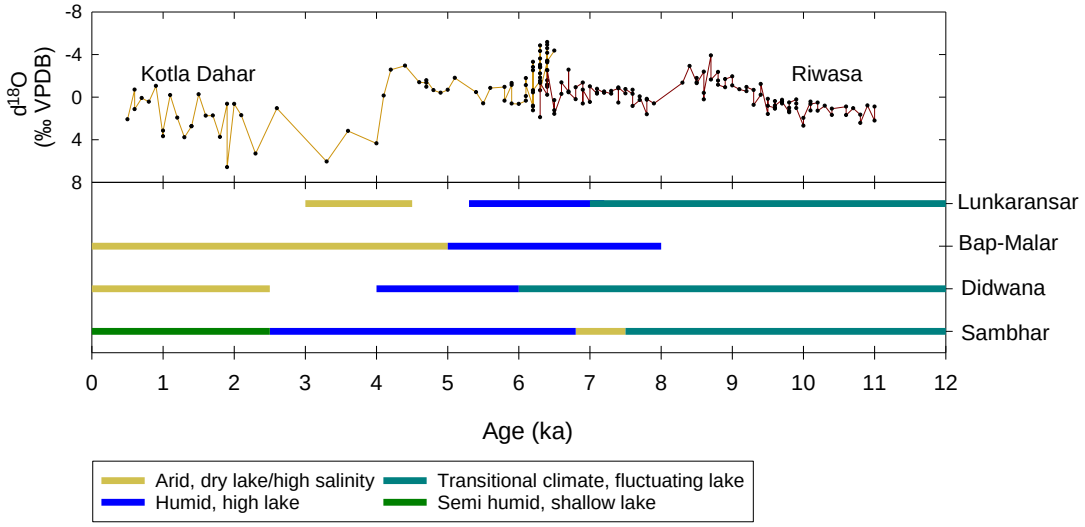


Figure 1.12. Gastropod $\delta^{18}O$ record (‰ VPDB) from palaeolakes Kotla Dahar (Dixit *et al*., 2014a) and Riwasa (Dixit *et al*., 2014b). (h) Schematic representation of Holocene palaeolimnological history of four inland lakes in the Thar (Wasson *et al*., 1984; Deotare *et al*., 1998; Enzel *et al*., 1999; Sinha *et al*., 2006).

More recently, high resolution and robust proxy records have emerged from lakes along the northern margin in Haryana (Figure 1.8) which add to the geomorphic response of the landscape. Dixit *et al*. (2014a) presented an $\delta^{18}O_a$ record of gastropod aragonite from palaeolake Kotla Dahar (Figure 1.12). The authors concluded a relatively deep fresh-water lake conditions between ~6.5 ka and ~5.8 ka, which is consistent with early to middle-Holocene monsoon strengthening records from Oman and the Arabian Sea (Fleitmann *et al*., 2003; Gupta *et al*., 2003), followed by higher evaporation/ precipitation conditions between ~5.8 ka and ~4.2 ka. The authors conducted another $\delta^{18}O$ study from palaeolake Riwasa (Figure 1.12) which provides a history of ISM from ~11 ka to ~6 ka (Dixit *et al*., 2014b). The authors inferred that ISM reached its greatest strength between ~9.4 ka and ~8.3 ka when Lake Riwasa was at a high stand, after which it abruptly desiccated between ~8.3 ka and ~7.9 ka.

In summary, as discussed in different sub-sections here, these are several high resolution records of variability in the ISM and paleoenvironmental changes determined from marine and terrestrial proxies, but due to their limited spatial context, diverse methodologies and different temporal range, the landscape scale response interpretation arising from these geochemical proxies are often conflicting in nature (e.g. Macdonald, 2011, Band *et al*., 2018; Misra *et al*., 2019). Further, their extrapolation to reconstruct late Quaternary environmental changes in the Thar is another concern. As such, dunes which dominate the landscape of the Thar but remain under-utilised, become a valuable alternative as geoproxies.

1.5. Dunes as geoproxies of past changes

A major limit on palaeoenvironmental and palaeoclimate reconstructions in deserts is the scarcity of traditionally dateable material such as organic matter and carbonates that could serve as proxy of past changes (Lancaster, 2008). Even when present, these materials often come with complications. Radiocarbon ages from drylands are often erroneous because of contamination from the incorporation of old and modern carbon and the dating system (mostly in carbonates) not being closed. Other methods such as uranium series disequilibrium dating require pure carbonates that are rarely found in drylands (Singhvi *et al.*, 1996). Due to extreme changes in temperature and lack of organic matter, amino acid racemisation methods are also difficult to apply in deserts (Owen *et al.*, 2007). The use of tephra as time markers has also remained limited in deserts because preservation of tephra layer is rare in dunefields owing to high aeolian activity (Lowe, 2011). As such, widespread desert dunes become a valuable source of information on the past changes (Lancaster, 2008; Singhvi and Porat, 2008).

The development and applications of luminescence dating to sands (Singhvi *et al.*, 1982) and loess (Wintle *et al.*, 1984) have indubitably transformed the analysis of geomorphic and sedimentary environments in deserts and drylands by adding a new dimension of chronometric control to the interpretation of sedimentary records and stratigraphic correlations. Luminescence dating determines the burial age of a sample (see Section 2.2), and hence, from multiple vertical samples phases of dune accumulation can be established (Duller, 2004). Lancaster (2008) notes that the advances in luminescence dating have occurred during a period in which significant conceptual progressions have also been

made in aeolian geomorphology. Prior to the availability of luminescence dating, identification of periods of dune accumulation was based on indirect reference to stratigraphic relationships to deposits or features such as lacustrine deposits or palaeosols. This approach can provide data on the chronology of periods of aeolian deposition but is often marked by a very broad temporal and spatial resolution (e.g. the Sahara; Swezey, 2001).

Dunes, like many other geomorphic features, have complex accumulation histories involving multiple cycles of erosion and subsequent re-deposition that may result in the removal of the onset (Nanson *et al.*, 1992), end phases (Munyikwa, 2005), or the entirety of aeolian events. This results in 'filtering' of signal between initial deposition and the interpretation of the luminescence ages (Bailey and Thomas, 2014). Figure 1.13 shows a schematic view of how the filtering of environmental information leads to the modification or loss of data. The extraction of information about the past from dune sequences, therefore, requires an enhanced understanding of factors including sediment supply, transport capacity of the wind and sediment availability (Preusser, 2009), sediment preservation (Munyikwa, 2005; Stone and Thomas, 2008), dune formation, and migration and stabilisation (Thomas and Burrough, 2012). Luminescence ages from dune sands provide evidence for the timing of past geomorphic activity, i.e. re-working and accumulation of sediment (Thomas and Bailey, 2012). As dry periods are expected to be more active (in both erosion and accumulation) than wetter periods, dated dune sediment ages are most likely to reflect periods of drier and/or windier conditions. A preservation is bias towards extremely large events and towards young events is also more likely to come from the end of dry

and/or windy periods, in the approximate relationship of $1/\sqrt{age}$ (Bailey and Thomas, 2014).

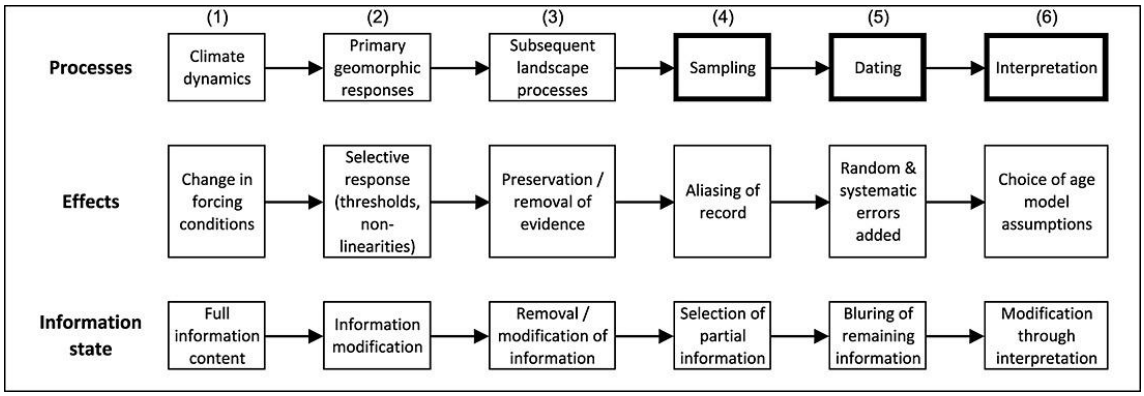


Figure 1.13. An illustration of the 'filtering' process that occurs between past forcing conditions and the luminescence dated record. At each stage information is lost, modified and degraded by natural and investigative processes. Thick-walled boxes refer to the processes that can be controlled (Bailey and Thomas, 2014).

The gaps in the chronological records are equally important and could represent an artefact of sampling or periods of relatively wetter and/or calmer conditions with little dune activity. Confidence in environmental interpretations of gaps increases when the gaps remain open in the face of additional new data, but such interpretations remain provisional in the absence of independent verification (Bailey and Thomas, 2014). Since luminescence ages only reveal a part of sedimentation history, the incorporation of all available evidence including stratigraphic and sedimentological data is important when interpreting chronologies. It allows for recognition of a more complex system and a thorough assessment of the meaning of the dates in terms of dune development (Fitzsimmons and Telfer, 2008; Singhvi and Porat, 2008). Stratigraphic features,

where present, can be used to facilitate environmental interpretation to support assessments of chronologies, especially regarding the presence of accumulation hiatuses and whether sampling resolution is sufficient to capture variability in the observable record. Dune stratigraphy has been exploited to 'target' luminescence sampling of large sets of cross stratification around inferred unit boundaries (Bristow *et al.*, 2005). Intensive sampling and dating of a dune with an exposed and clear stratigraphy may provide an opportunity to identify and explain the issues that hamper dune chronology development: representativeness and reproducibility (Leighton *et al.*, 2014). However, the interpretation of internal features is not straightforward and requires careful intervention. For example, palaeosols, which are indicators of surface stability, can have an uncertain timescale of formation due to bioturbation. As constraining the time of pedogenesis is difficult, periods of hiatus in dune activity cannot easily be linked to regional pedogenesis across the dunefields (Fitzsimmons *et al.*, 2007).

In the context of palaeoclimate reconstructions and interpretations, it has often been suggested that suites of dune accumulation ages cannot simply be attributed to discrete 'arid' phases (Chase, 2009; Chase and Thomas, 2006; Lancaster, 2008). Several studies have shown the importance of the interplay of numerous factors affecting dune development (Chase, 2009; Chase and Thomas, 2006). These factors include moisture (Bray and Stokes, 2004; Lomax *et al.*, 2011; Wiggs *et al.*, 2004), windiness (Chase and Thomas, 2007; Roskin *et al.*, 2011b), sediment supply (Goudie *et al.*, 2000; Preusser, 2009) and human activity (Yang *et al.*, 2012). Within the Thar, dune sediments dated by luminescence have often been interpreted as records that can be attributed to strengthening and

weakening of monsoons and associated aridity (Kar *et al.*, 2001; Singhvi and Kar, 2004).

Recently quantitative approaches have been employed to understand dated dune stratigraphies (e.g. Leighton *et al*., 2014; Bailey and Thomas, 2014). Thomas and Bailey (2017) developed a numerical model to utilise chronometric and sedimentological data from individual dunefields to generate 'Accumulation Intensity' (*AI*) records of dunefield sediment accumulation through time. This methodology has been applied to dune age records from the Asian, southern African and Australian dune systems to allow for the first time both a systematic analysis and comparison of the timing of dune accumulation through the continent's drylands and an assessment of the quality of regional data sets, all in conjunction with other continental and marine records (Thomas and Bailey, 2017; 2019).

1.6. Thesis aim and research questions

Given the context provided in previous sections that the Thar dunes are a rich archive of past geomorphological and environmental change in the desert and there is a huge potential for using them geoproxies of past changes, the aim of this study is *to investigate the timing of dune accumulation in the Thar Desert, India during the late Quaternary, in relation to potential drivers of dune activity*. This thesis addresses this aim through a programme of field and laboratory analyses that address three broad questions:

RQ1. When did dune accumulation occur during the late Quaternary in response to drivers of landscape change?

The identification of different phases of dune accumulation is the first step towards understanding the controls operating on dune development and the palaeoenvironmental conditions which lead to accumulation, and subsequent change in the landscape. To answer this question, first previous studies will be reviewed in the context of field and laboratory strategies, then different dunefields will be investigated (to test temporal and spatial variability in records).

RQ2. Given the large and dense population that the Thar hosts, what is the effect of anthropogenic pressure on dune activity?

Whilst it is known, much like in any other environment, that anthropogenic pressure is altering the landscape in the Thar, the quantification of modern records of dune activity will be attempted (by investigating sensitive parabolic dunes in the central Thar) to aid our current understanding of thresholds and sensitivity of landscape to anthropogenically-induced changes.

RQ3. What do the dune records reveal about the late Quaternary geomorphological and regional palaeoenvironmental changes in the Thar?

Late Quaternary palaeoenvironmental reconstructions in the Thar are currently limited by a paucity of records. Using the information gained by answering research questions 1 and 2, the dune records will be mathematically modelled using existing *AI* methodology and then integrated with other available proxy records from the Thar and beyond. This will shed light on the landscape change and also provide a case study of the palaeoenvironmental utility of the dunes.

To meet the aim and answer these research questions, following research objectives have been designed to :

- Identify key sampling regions to include spatial coverage that embraces geographic variability in the system.
- Conduct systematic sampling of dunes for luminescence dating and sedimentological investigations, including full dune profile sampling.
- Produce a new, robust set of chronologies of dune accumulation in the Thar, using a modern and robust dating protocol.
- Provide an insight into the timing and nature of the development of the two abundant dune types in the Thar.
- Compare dune accumulation records from different regions in the Thar.
- Analyse the both new and already published Thar dune age data set using the numerical Accumulation Intensity (*AI*) analysis approach.
- Establish and further develop the dune records as proxies of desert climate change during late Quaternary and compare that with a growing multiproxy framework of past climate and environmental changes in the region.

1.7. Thesis structure

The thesis has been written by papers conforming to the guidelines by the School of Geography and the Environment, University of Oxford. The paper route involves the inclusion of three papers which have been submitted to a range of peer-reviewed journals. The papers are incorporated as chapters in their thesis adapted form, but a certain degree of unavoidable repetition may be observed in the thesis. These papers, which have been co-authored with supervisors, include a major portion of the results and discussion. Co-author contributions are noted in Appendix A. The thesis is divided into three parts:

Part 1 consists of three chapters. Chapter 1 provides an overview of the research motivation and context, presents the thesis aim and research questions, and ends with structure of the thesis. Chapter 2 discusses generation of luminescence ages summarises the published dune chronologies from the Thar and reviews them in the context of modern advancements in fieldwork and dating techniques. Chapter 3 discusses the geomorphological context of the studied dunefields, adopted sampling strategy, and provides the details of the sampled sections. It also details the laboratory methods used in the determination of the luminescence ages, and presents all the luminescence data that form a key analytical component of the central research of the thesis.

Part 2 presents the geomorphic and palaeoenvironmental research and the interpretations of the results. This part consists of three papers, edited in format to be presented as Chapters 4, 5, and 6. *Paper 1* (published in *Earth Surface Processes and Landforms* in 2019) presents a new record of Holocene dune activity in the central Thar and its implications for the evolution of parabolic

dunes with time. *Paper 2* (published in *Geomorphology* in 2019) the timing and nature of linear dune accumulation in the northern Thar. *Paper 3* (accepted to be published in *Quaternary Science Reviews*) collates existing and new geochronological records, analyses them in a numerical model, and assesses them along with other proxy data sets to evaluate landscape dynamics and change in the Thar.

Part 3 draws the research together to address the research aim and questions. It includes the last Chapter 7 where implications of the new suite of luminescence ages in the context of wider geomorphological and palaeoenvironmental research are discussed.

1.8. Conclusions

The chapter has laid out the research context and introduced the important concepts regarding the Thar aeolian landscape. The distribution of dune types in the Thar is briefed followed by description of two dominant dune types i.e. parabolic and linear dunes. The chapter discusses the history of human settlement in the Thar and the association of dune in investigating archaeology in brief next, followed by the rapid population growth in the last century and its implications for changing landscape. It also introduces the Indian Summer Monsoon (ISM), one of the major drivers of dune development in the Thar, and the various proxies that have been used to reconstruct the ISM variability and their shortcomings. The chapter then discusses the suitability of luminescence dating to date sediments in dryland settings and the interpretation of the luminescence ages.

The chapter ends with the thesis aim, which is investigating the fundamental aspects of dune accumulation in the Thar *during the late Quaternary, in relation to potential drivers of dune activity*, and lists the research questions which are addressed in this thesis and the various objectives pursued to meet the aim. In the final section, the chapter briefs about the thesis structure that comprises papers written conforming to the School of Geography and the Environment's guidelines.

Chapter 2: Previous luminescence dating based investigations

2.1. Introduction

A number of luminescence dating studies focussing on the dune sands of the Thar Desert have been carried out since the first generation of ages from the Thar dune sands in early 1980s (Singhvi *et al.*, 1982). Since then, over a hundred luminescence ages have been determined from dunes in the Thar using a range of luminescence dating techniques including thermoluminescence (TL), infra-red stimulated luminescence (IRSL), and blue/green light stimulated luminescence (BLSL/GLSL) signals. An important part of this thesis is to assess the robustness of previous luminescence studies in order to provide a more appropriate and meaningful way of collecting sampling, selecting dating protocols to generate ages, and interpreting data. Therefore, this chapter introduces the basic principles of luminescence dating and how dune chronologies are generated. The chapter then collates the published dune accumulation records from the Thar and evaluates the published ages in the context of sampling approach and modern dating protocols.

2.2. Generating dune accumulation chronologies

Luminescence dating is the ideal means to directly date periods of aeolian deposition, as it determines the time elapsed since burial of sediment (Duller, 2004). Consequently, several luminescence dating techniques have been applied in a range of aeolian contexts around the world and over 4000 ages have been generated to reconstruct the timing and rate of dune accumulation (Lancaster *et al*., 2016). This thesis uses OSL dating to provide chronometric control for the records of dune accumulation in the Thar Desert. Natural minerals in the environment, such as quartz and feldspars, act as dosimeters, producing

luminescence in response to naturally occurring radioactivity in the environment (e.g. Aitken, 1985; Aitken, 1998; Duller, 2008). This luminescence is produced upon contact with heat (thermoluminescence) or light (optically stimulated luminescence), either in the environment or the laboratory. For dating purposes, it is the magnitude of the luminescence signal, accumulated since the last exposure of sediment to light which is of interest. The equivalent dose (D_e) is the amount of laboratory radiation (in Grays, Gy) required to replicate the natural luminescence signal, and the D_e is the numerator of the age calculation equation. To calculate an age, it is also necessary to measure the rate of radioactivity delivered to the sample from the surrounding sediment matrix, and this is termed the environmental dose rate ($\dot{D}$). A luminescence age is derived using the equation below,

$$\textit{Age (ka)} = \frac{Equivalent\ dose\ (Gray)}{Total\ environmental\ dose\ rate\ (\frac{Gray}{ka})} \qquad \textit{Equation 1}$$

2.6.1. Basic principles of luminescence dating

The physical principles of luminescence dating have been described by Aitken (1985; 1998) and Preusser *et al.* (2008), and unless otherwise stated, the following synopsis has been written with reference to these texts.

The phenomenon of luminescence is related to the interaction of natural radiation with mineral grains, by the activation of and subsequent trapping of electrons at defects within the crystal lattice. Aitken (1990) summarises these luminescence processes using the energy-level diagram in Figure 2.1. In silicate minerals like quartz or feldspars, during both natural and laboratory ionisation or irradiation, anions are removed from their parent nuclei into the conduction band and leave a ‘hole’ in the valence band (Irradiation; Figure 2.1i). Whilst there is sufficient

energy, the excited electrons diffuse in their excited state in the conduction band before recombination occurs. The excited electrons attracted to the defects or traps (T_1, T_2; Figure 2.1ii) are stored as long as there is insufficient energy to re-excite them into the conduction band (Storage). When the crystal is stimulated by light or heat, the electrons in the traps are evicted into the conduction band (Eviction) (Figure 2.1iii). From there, they can recombine with holes at the luminescence centres (L), resulting in the emission of a photon of light. This light is referred to as luminescence and the method is called TL or OSL, depending upon the method of stimulation. The intensity of light emitted by a sample during stimulation is proportional to the number of recombining electrons and therefore proportional to the number of electrons trapped prior to stimulation.

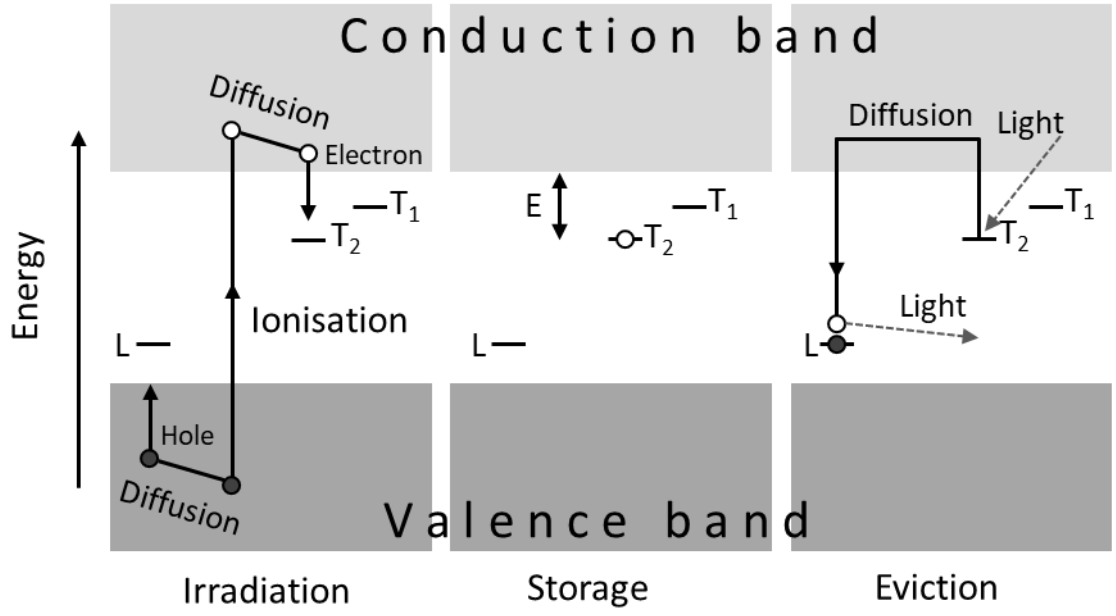


Figure 2.1. Energy level representation of the processes involved during (i) irradiation, (ii) storage and (iii) eviction due to heating or exposure to light. T and L refer to traps and holes respectively (T_2 referring to a deeper trap,

which is more stable over time) and E refers to the depth of trap below the conduction band (redrawn from Aitken, 1990).

2.6.2. Quartz OSL dating

Generally, in geomorphological systems such as deserts, the OSL signal from quartz is preferred for dating (Lancaster, 2008; Singhvi and Porat, 2008) because it bleaches rapidly in nature (e.g. Godfrey-Smith *et al.*, 1988; Duller, 2008), with near complete bleaching of the quartz OSL signal after 100 s exposure to daylight (Figure 2.2). Another advantage of quartz, unlike feldspar, is that it does not suffer from anomalous fading, which hampers the reliability of luminescence dating with feldspars by underestimating the ages (e.g. Visocekas, 1982; Spooner, 1994; Huntley and Lamothe, 2001).

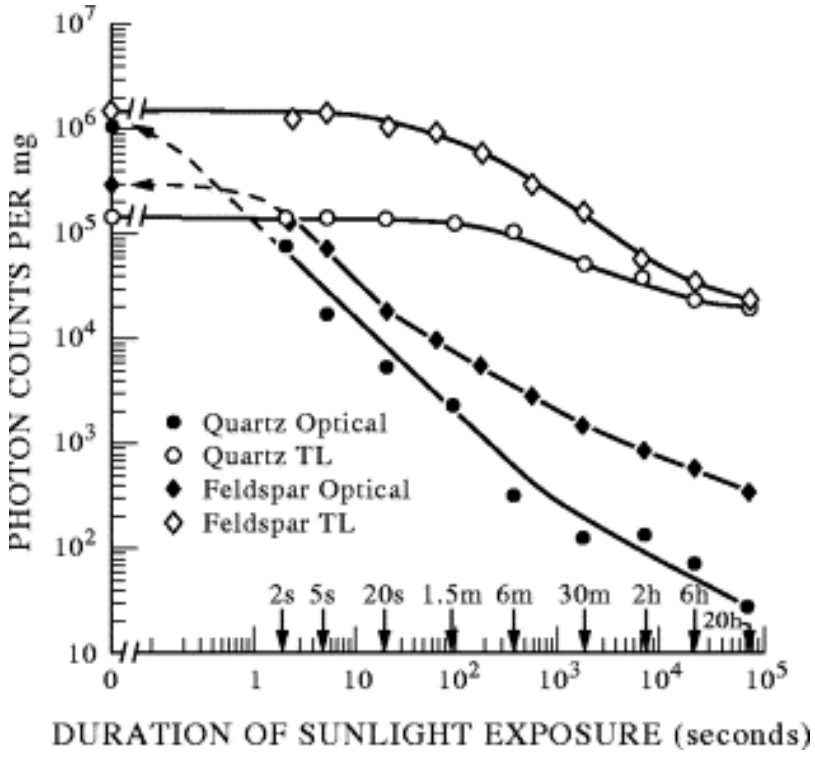


Figure 2.2. Comparison of bleaching rates of natural TL and OSL signals from quartz and feldspars. OSL signals reduce more rapidly and more completely than the TL from the same sample (Godfrey-Smith *et al.*, 1988).

In deserts, like in other geomorphological systems, cycles of erosion, transportation and deposition of sediments is observed over numerous temporal and spatial scales. During deposition, mineral grains present in sediments are exposed to surrounding ionising radiation and electrons are trapped in their crystal defects. The electron populations build up and the luminescence signal is acquired over time, proportional to the radiation exposure (the environmental dose rate) (Figure 2.3a). The luminescence is zeroed by exposure to sunlight with erosion and transportation (Figure 2.3b). With another cycle of burial and exposure to ionizing radiation, free electrons are again stored in charge defects within grains' crystal lattices (Figure 2.3c), and further light exposure of grains to light during erosion and transportation zeroes the luminescence (Figure 2.3d). The grains are buried again, and luminescence is acquired with exposure to ionizing radiation (Figure 2.3e). Following sampling without exposure to light, the natural luminescence signal can be measured, and from this, the luminescence age calculated.

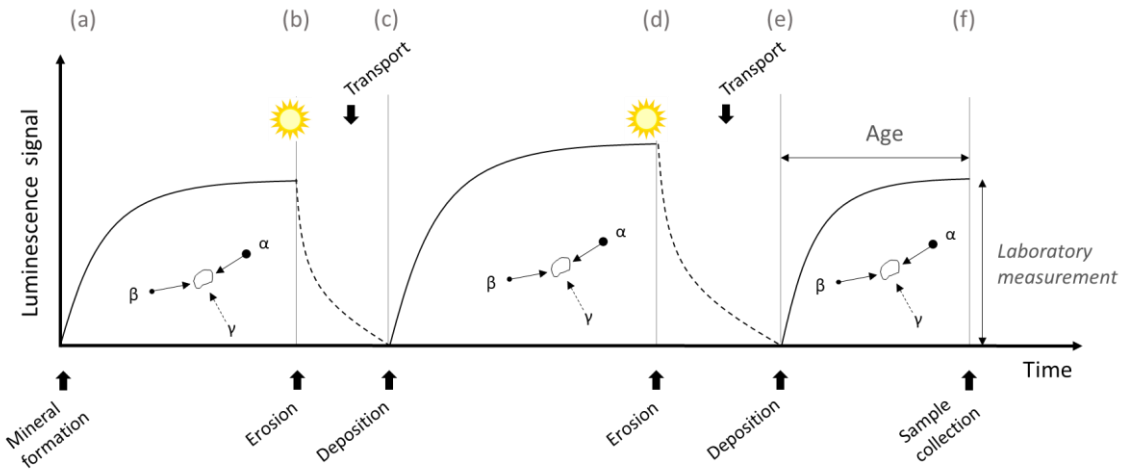


Figure 2.3. Schematic representation of luminescence signal accumulation and resetting in nature.

2.3. Previously published chronologies from the Thar dunes

The Thar Desert witnessed the first application of luminescence dating to sand dunes anywhere in the world 37 years ago by Singhvi *et al*. (1982) who used TL dating to date eight dune samples from archaeological contexts at Amarpura, Langhnaj and Bagor (Figure 2.4). Since then, numerous dune sites in different regions of the desert have been dated using different luminescence dating methods (e.g. Chawla *et al.*, 1992; Singhvi *et al.*, 1994; Kar *et al.*, 1998; Andrews *et al.*, 1998; Thomas *et al.*, 1999, Kar *et al.*, 2001; Juyal *et al.*, 2003; Dhir *et al.*, 2010; Singhvi *et al.*, 2010) (Figure 2.4) (Tables 2.1; 2.2).

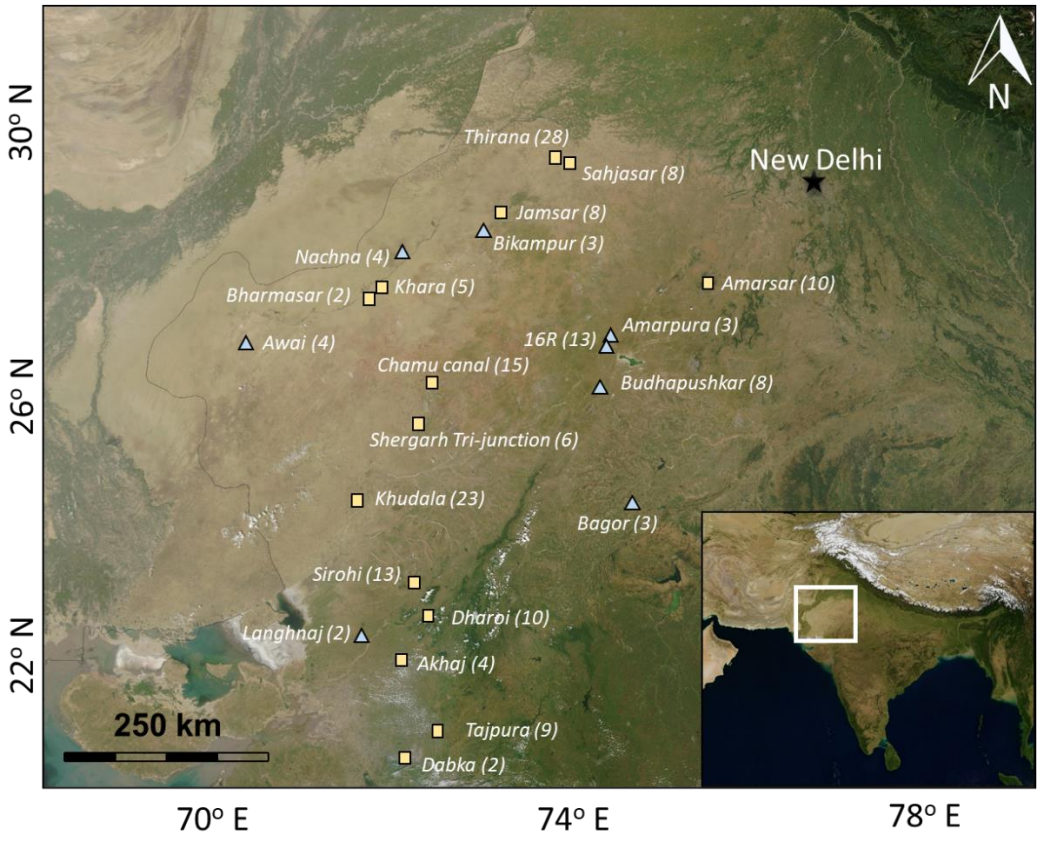


Figure 2.4. All dated dune sites in the Thar (with number of published ages) . Yellow square symbols denote sites listed in Singhvi and Kar (2004) and the INQUA dunes atlas chronologic database (Lancaster *et al.*, 2016). Blue triangle symbols indicate sites reported elsewhere (see Table 2.2).

The two dune sequences that provide the oldest evidence of dune activity in the Thar Desert are in the east-central Thar and include ages of ~187 ka at 16R dune (Singhvi *et al.*, 2010) and ~155 ka at Chamu dune (Dhir *et al.*, 2010). These two dune sites remain the only dated evidence of dune activity beyond 100 ka in the Thar, with accumulation events occurring both before and between ~105-81 ka at Chamu (Figure 2.5; Dhir *et al.*, 2010) and at ~130-109 ka and ~80 ka at 16R dune (Singhvi *et al.*, 2010). Other reported older phases include ~64 and ~60 ka

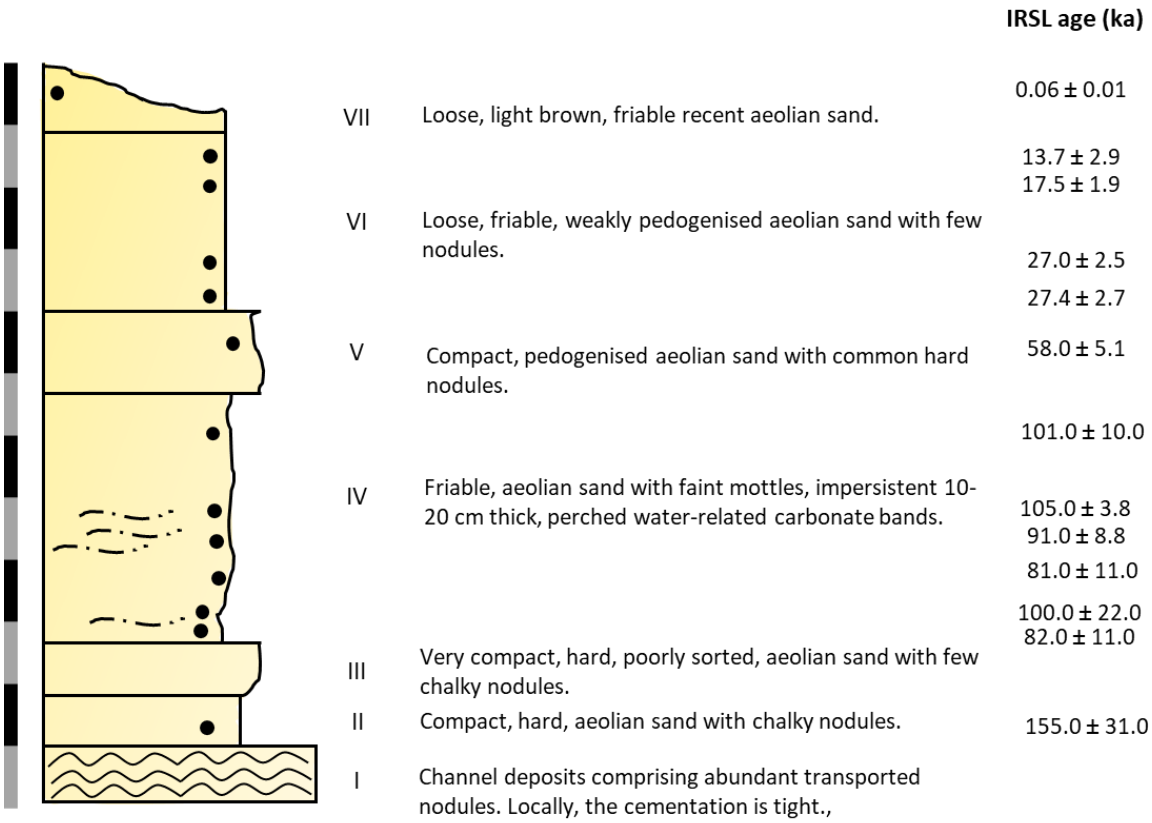


Figure 2.5. Field log and some analytical data of Chamu dune section studied by Dhir *et al.* (2010). Sampling points for dating are represented by solid circles.

at Shergarh Tri-junction (Andrews *et al.*, 1998), ~55 ka and ~43 ka at Shergarh Tri-junction (Andrews *et al.*, 1998), ~58 ka at Chamu (Dhir *et al.*, 2010), ~40 ka

at 16R Dune (Singhvi *et al.*, 2010) (all in the east-central Thar) and ~40-30 ka at Awai (western Thar) (Chawla *et al.*, 1992). After ~30 ka, the majority of evidence of dune activity comes from the southern margin of the Thar, with only one record dating to ~27 ka from Chamu in the central Thar (Dhir *et al.*, 2010) and another dating to ~21 ka at 16R Dune in the eastern Thar (Singhvi *et al.*, 2010). In the southern Thar, dune activity has been recorded at ~25 ka at Dharoi and ~26 ka at Akhaj (Juyal *et al.*, 2003). Post ~18 ka, evidence for dune activity is more widespread in the Thar. In the east and central regions, dune accumulations occurred at between ~17-13 ka at Chamu in the central Thar (Dhir *et al.*, 2010), between ~15-13 ka at Nachna in the west (Chawla *et al.*, 1992), ~13.5-11.5 ka at Bikampur in the north (Chawla *et al.*, 1992) and ~13-11 ka at 16R Dune in the east (Singhvi *et al.*, 2010). Singhvi and Kar (2004) report that the dune accumulation continued till ~7 ka, with less vigour though, which then started to decline between ~7 and ~6 ka. Based on the records from Khara (Kar *et al.*, 1998), Jamsar and Thirana in the northern Thar (Thomas *et al.*, 1999), Kar *et al.* (2004) suggested a phase of 'high aeolian activity' between ~5 and ~3.5 ka. The Thar experienced a lull in dune activity between ~3.7 and ~2 ka according to Singhvi and Kar (2004), after which three phases of dune accumulation were identified – between ~2.1 and 1.9 ka, ~1.8 and ~0.6 ka and the latest phase since ~0.3 ka, all based on a transverse dune site in Khara in the western Thar (Kar *et al.*, 1998). Unlike in the previous phases, the last phase is marked by high human pressure on the sandy landscape. Thomas *et al.* (1999) and Singhvi and Kar (2004) note that existing data sets provide limited opportunity of recent records of dune activity and recommended more intensive field studies and finer chronology to understand the impact of anthropogenic disturbances.

Table 2.1 Luminescence ages from the Thar dunes included in summary by Singhvi and Kar (2004)which were later entered in the INQUA dunes atlas chronologic database (Lancaster *et al.*, 2016). *[Y/N= data available/ not available]*

Sample location	Ages (#)	Dune type	Depth data	Protocol	Luminescence type	Mineral	Fading correction	Age model	Reference
Thirana I	16	parabolic	*Y*	MAAD	TL	Quartz	-	*N*	Thomas *et al.* (1999)
Thirana II	12	parabolic	*N*	MAAD	OSL	Quartz	-	*N*	Singhvi & Kar (2004)
Sahjasar	8	parabolic	*N*	MAAD	BGSL	Quartz	-	*N*	Thomas *et al.* (1999)
Sirohi	13	undifferentiated	*N*	MAAD	IRSL	Feldspars	*N*	*N*	Thomas *et al.* (1999)
Chamu	15	sand sheet	*Y*	MAAD	IRSL	Feldspars	*N*	*N*	Dhir *et al.* (2010)
Shergarh	6	not mentioned	*N*	MAAD	IRSL/OSL/TL	Mixed	*N*	*N*	Andrews *et al.* (1998)
Jamsar	8	linear	*Y*	MAAD	GLSL	Quartz	-	*N*	Thomas *et al.* (1999)
Amarsar I	6	parabolic	*Y*	MAAD	TL	Quartz	-	*N*	Singhvi & Kar (2004)
Amarsar II	4	parabolic	*Y*	MAAD	TL	Quartz	-	*N*	Singhvi & Kar (2004)
Ghughalia	3	not mentioned	*Y*	MAAD	IRSL	Feldspars	*N*	*N*	Thomas *et al.* (1999)
Khara	5	transverse	*N*	MAAD	IRSL	Feldspars	*N*	*N*	Kar *et al.*, (1998)
Bharmasar	2	transverse	*N*	MAAD	IRSL	Feldspars	*N*	*N*	Kar *et al.*, (1998)
Dharoi I	7	obstacle	*Y*	MAAD	BGSL	Quartz	-	*N*	Juyal *et al.* (2003)
Dharoi II	3	obstacle	*Y*	MAAD	BGSL	Quartz	-	*N*	Juyal *et al.* (2003)
Akhaj	4	poorly organised	*Y*	MAAD	BGSL	Quartz	-	*N*	Juyal *et al.* (2003)
Tajpura I	4	obstacle	*Y*	MAAD	BGSL	Quartz	-	*N*	Juyal *et al.* (2003)
Tajpura II	5	Obstacle	*Y*	MAAD	BGSL	Quartz	-	*N*	Juyal *et al.* (2003)
Dabka	2	poorly organised	*Y*	MAAD	BGSL	Quartz	-	*N*	Juyal *et al.* (2003)
Khudala	23	parabolic	*Y*	MAAD	TL/BGSL/IRSL	Mixed	*N*	*N*	Kar *et al.* (2001)

Table 2.2. Luminescence ages from the Thar dunes reported elsewhere and not included in the INQUA dunes atlas chronologic database. ***[Y/N= data available/ not available]***

Sample location	Ages (#)	Dune type	Depth data	Protocol	Luminescence type	Mineral	Fading correction	Age model	Reference
Budhapushkar	8	*N*	*Y*	MAAD	TL	Quartz	-	*N*	Singhvi *et al.* (1994)
16R	13	*N*	*Y*	MAAD/SAR	TL/OSL	Quartz	-	*N*	Singhvi *et al.* (2010)
Nachna	3	*Interdune*	*Y*	MAAD	TL	Quartz	-	*N*	Chawla *et al.* (1992)
Bikampur	4	*N*	*Y*	MAAD	TL	Quartz	-	*N*	Chawla *et al.* (1992)
Awai	4	*N*	*Y*	MAAD	TL	Quartz	-	*N*	Chawla *et al.* (1992)
Amarpura	3	*N*	*Y*	MAAD	TL	Quartz	-	*N*	Singhvi *et al.* (1982)
Bagor	3	*N*	*Y*	MAAD	TL	Quartz	-	*N*	Singhvi *et al.* (1982)
Langhnaj	2	*N*	*Y*	MAAD	TL	Quartz	-	*N*	Singhvi *et al.* (1982)

2.4. Review of previously published Thar dune chronologies

Nearly all the published luminescence ages reported from the Thar dunes so far have some element of unreliability in them compared to present day standards of luminescence ages, owing to the combination of one or more factors, discussed below. This is not a criticism of the early works; rather it reflects on the developments and improvements that have occurred in luminescence dating protocols over the years. These elements are important to the interrogation of existing luminescence data and chronology, and the meaningful interpretation of records in terms of geomorphological and palaeoenvironmental changes. Further, these elements help in selecting field sites, adopting sampling strategy and setting up a robust protocol for dating.

2.8.1. Fieldwork strategies

The Identification of key sampling regions, which include spatial coverage that embraces geographic variability in the Thar, is an important objective in the thesis. As a result, the review of investigated sites and fieldwork strategies in published literature becomes important. So far, the application of intensive dunefield sampling programmes has been less prevalent in the Thar compared to many other deserts worldwide such as the Kalahari in Africa (Telfer and Thomas, 2007; Stone and Thomas, 2008), the Rub' al Khali in Arabia (Leighton *et al.*, 2013; Atkinson *et al.*, 2011), the Negev in Israel (Roskin *et al.*, 2011a) and the Strzelecki and Tirari in Australia (Fitzsimmons *et al.*, 2007). The published luminescence chronologies (and the subsequent interpretation of ages) mainly stem from scattered and sporadic records with variable spatial coverage (Figure

2.4) and various ranges of sampling depths. In some studies, there is a bias towards focussing on deep trenches (often associated with the expansion of irrigation canals into the region) to establish the antiquity of dune accumulation phases in the desert (Kar, 2013; Dhir *et al.*, 2010). As a result, the Holocene histories are sometimes not recorded, which have subsequently been interpreted as a lull in aeolian activity (Singhvi and Kar, 2004). Hesse (2016) notes this issue in the context of Australian dunes and highlights that under-representation of upper deposits might withhold useful insight into zones of reworking, erosion, and depositional structures. Some studied Thar dune sites are also marked by the absence of published information about the location and depth of dated sediments (Table 2.1). Whilst the absence of location could be attributed to the absence of sophisticated navigational devices during the time of actual fieldwork, lack of depth data cannot be explained.

In many studies in the Thar, the type and morphological description of dunes is often missing or ambiguous (Table 2.1). There are instances of contradictory descriptions as well between original citations and later reviews. For example, as per the Singhvi and Kar (2004) record in the INQUA dunes atlas database (Lancaster *et al.*, 2016), the sampled dune site Jamsar in northern Thar is a parabolic dune, while Thomas *et al.* (1999) describe it as a linear dune site. The inability to procure aerial photographs due to government restrictions, the poor resolution in old Google Earth images and an altered modern landscape, owing to agricultural activity imply that it is difficult to pin-point the exact dune form and sampling location. Since different dune types display varying levels of sensitivity to external factors like vegetation, sediment supply, wind direction, the geomorphologic understating of their development is critical to interpreting

palaeoenvironments (Lancaster, 2008; Thomas, 2013). Sampling strategy and location within a dune may also impact on the chronology produced and it is important to know the details of sampled dune to understand process based of dune systems and their diverse response to drivers of accumulation (e.g. Telfer and Thomas, 2007; Stone and Thomas, 2008; Telfer, 2011). As a result, all the required information related to a sampled dune section and retrieved sample was duly noted in this thesis and considered while interpreting dune ages. Similar to that of sampling depth and dune type data, numerous discrepancies in D_e and $\dot{D}$ values in diverse papers have also been noted leading to different luminescence ages published in different papers for same sample coded. Together, these factors offer limited scope to integrate dune records from different sites with one another, and make robust interrogation of existing data sets difficult for palaeoenvironmental purposes.

2.8.2. Use of Multiple Aliquot Additive Dose methods for D_e calculations

It is noteworthy that all the published Thar Desert dune ages used multiple aliquot additive dose (MAAD) methods to determine D_e (as summarised in Tables 2.1 and 2.2), which is required to calculate a luminescence age (equation 1). Though these were widely used in 1980s and 1990s, MAAD methods are now largely redundant due to various reasons.

First, D_e is determined using multiple sub-samples (aliquots) for different irradiation doses assuming that the natural D_e of each aliquot is the same. This is only a valid for truly homogenous sample where each grain has received same extent of bleaching during transportation and is exposed to an identical dose-rate

during burial. This usually does not happen in nature where different grains have different sedimentation histories and thus each aliquot behaves differently. Secondly, D_e is generated by the extrapolation of the dose response curve (DRC) (Figure 2.6) and which critically depends on the mathematical function used. For example, use of linear extrapolation may give an imprecise value for D_e as DRCs show sub-linearity in both old and young samples (Felix and Singhvi, 1997; Aitken, 1998). Third, the growth plot does not in itself give information about linearity or otherwise in the dose region below zero added dose (i.e. left of the vertical axis in Figure 2.6). There is the possibility that in this region, for young samples, the slope of the growth curve increases with increase in dose (i.e. supralinear growth), indicating an increase in sensitivity. This is a problem when TL dating is applied and failing to correction can lead to considerable shortfall in age (Aitken, 1998). Collectively, these issues add a relatively large uncertainty to MAAD age, and consequently majority of published Thar dune ages have 15-60 % uncertainty associated with them.

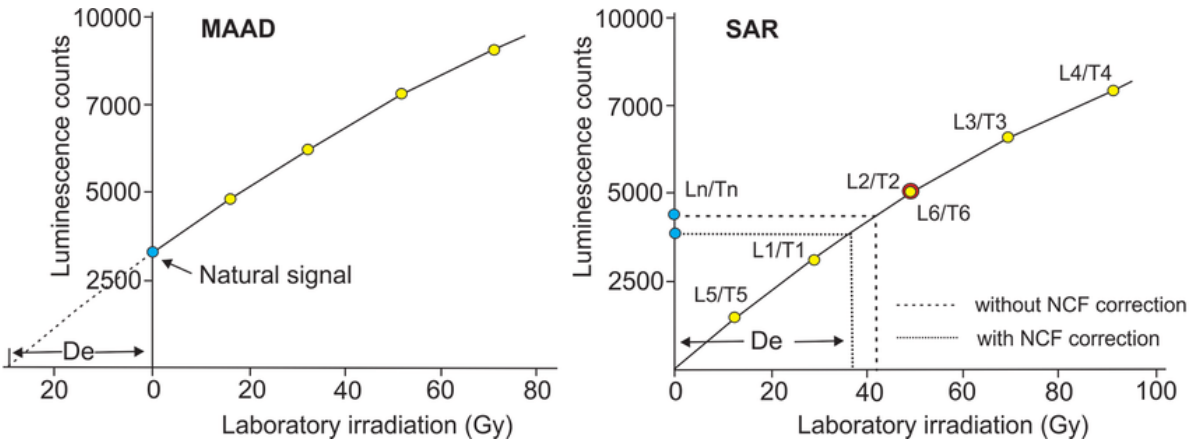


Figure 2.6. Examples of multiple aliquot additive dose (MAAD) and single aliquot regenerative (SAR) dose method used in OSL dating (Chaudhary, 2015).

The more useful Single Aliquot Regeneration (SAR) method (Murray and Wintle, 2000; Wintle and Murray, 2006), which corrects for sensitivity changes and generates D_e by interpolation and has replaced MAAD since year 2000, has not been employed yet in the context of dunes from the Thar interior yet. Singhvi *et al*. (2010), however, presented five SAR OSL ages from an archaeologically significant dune along the eastern margin of the Thar, though they used MAAD TL ages for the interpretation of dune records.

2.8.3. Lack of fading correction of IRSL ages

Several studies in the past used the infra-red stimulated luminescence (IRSL) signal from feldspar for luminescence age calculation (e.g. Kar *et al.*, 1998; Kar *et al.*, 2001; Dhir *et al.*, 2010; Table 2.1). As one of the goals of previous studies was to establish the antiquity of the Thar and samples were collected from deep trenches, IRSL signal was rightly favoured over quartz signal for its higher saturation limits (Thomas *et al*., 1999; Kar *et al*., 2004). Although IRSL is favourable for dating of older sediments, some feldspar signals are athermally unstable (termed anomalous fading) resulting in signal loss during the burial period (Wintle 1973; Wallinga *et al.*, 2001; Huntley and Lian, 2006). This phenomenon can hamper the reliable luminescence dating of feldspars by underestimating the ages, if the signal loss is not corrected for. Several correction methods have been developed based on laboratory measurements of the fading rate in the sample (e.g. Huntley and Lamothe, 2001; Kars *et al.*, 2008; Kars and Wallinga, 2009) and to obtain a stable luminescence signal in feldspars (e.g. Thomsen *et al.*, 2008; Buylaert *et al.*, 2009). For the published IRSL ages from the Thar, fading corrections were not made. When dating samples from a

parabolic dune in the central Thar, Andrews *et al.* (1998) suggested that K-feldspars did not show any age underestimation or anomalous fading by showing concordance of the few IRSL ages with OSL ages; albeit the OSL ages had large uncertainties. This observation was adopted in later studies (e.g. Kar *et al.*, 2001; Dhir *et al.*, 2010) and consequently, no IRSL ages from the Thar were fading-corrected. Recently, Dave *et al.* (2019) reviewed previously dated samples from the northern margin of the Thar and showed that the TL and IRSL ages on the same sample yielded ages of ~154 ka to ~41 ka respectively (Banerjee,1996). Dave *et al.* (2019) suggested possibilities of incomplete TL bleaching in the former and/or anomalous fading issues in the latter age, and emphasised on the need to date the samples afresh using quartz OSL if fading corrections were not done on feldspar samples.

2.5. Conclusions

This chapter has presented an overview of how dune accumulation chronologies are generated using luminescence dating and detailed basic principles of the same. Details of the previous work conducted in the Thar using luminescence dating, as included in the INQUA dunes atlas chronologic database as well as reported elsewhere, are next set out. The previously published chronologies are discussed and included in Chapter 6 in the context of *AI* methodology. The chapter then provides a review of the published Thar dune luminescence ages (a total of 186) in the context of methods these were generated, and further justifies the need for intensive dunefield sampling and application of a modern and robust luminescence dating protocols in the Thar Desert, as adopted in this thesis and discussed in the following chapter.

Chapter 3: Materials and methods

3.1 Introduction

As established in the previous chapter, the Thar Desert lacks a reliable chronological framework based on dunefield-based investigations and modern luminescence dating protocols, therefore, integrating aeolian system records with growing multiproxy framework of past environmental dynamics difficult. Consequently, a key part of this thesis to identify appropriate sites in the Thar for fieldwork. This chapter gives the introduction of the sampled dunefields and the rationale of choosing them followed by the description of the sampled dune sites, adopted sampling strategy and number of samples retrieved for dating, and additional sedimentological analyses. Since an essential focus of this thesis is to generate dune accumulation using OSL dating, this chapter also outlines the laboratory procedures for the extraction of pure quartz and the instrumentation used to measure OSL signals, followed by the details of chosen dating protocol, quality assessment tests and signal analyses undertaken to determine a sample D_e. The chapter then discusses the measurement and calculation of $\dot{D}$. The chapter concludes with the presentation of the calculated OSL ages, implications of which are discussed in the following chapters.

3.2. Study areas

The Thar is divided into four zones, based on climate and land use pattern indices, namely the Arid Western Plain (Zone 1; 133073 km^2), the Irrigated North-Western Plain (Zone 2; 20557 km^2), the Transitional Plains of Inland Drainage Basin (Zone 3; 31329 km^2) and the Transitional Plains of Luni Basin (Zone 4; 22951 km^2) (Moharana *et al*., 2013) (Figure 3.1). Of these four zones, majority of dunefields are located in Zone 1, which is the key zone of interest in this thesis.

As discussed earlier, previous geochronological studies in the Thar were based on sporadic, scattered sampling of dunes (and not dunefields) across wide geographic areas, often reflecting where exposures within dune sediments were available due to, for example, constructional or quarrying activity. In this thesis, following dunefields were selected to meet the aim and address research questions:

Jodhpur dunefield in the central Thar.

- The region is dominated by parabolic dunes, and thus provides an opportunity to investigate the principal dune type in the Thar.
- As the region is densely populated, it allows investigation of the effect of anthropogenic activities on sensitive parabolic dunes [RQ 2].
- The central Thar has been subject to several studies previously (e.g. Thomas et al., 1999; Kar et al., 2004), therefore provides an opportunity to compare records generated using older and new field and lab protocols.

Bikaner dunefield in the northern Thar.

- The region hosts linear dunes, and thus permits the first analysis of linear dune development in the Thar.
- Being far from Jodhpur region, it further allows testing of spatial variation in dune accumulation histories [RQ 1].

Suratgarh dunefield along the Ghaggar-Hakra palaeochannel forming the northern margin of the Thar.

- Source bordering dunes in this region have been investigated (e.g. Shitaoka *et al*., 2012; Singh *et al*., 2016) and further research has been

recommended for better understanding of changing environmental conditions in the region.

- The dunefield complements parallel investigations by Durcan *et al.,* 2019.

Furthermore, all three regions of Jodhpur, Bikaner and Suratgarh (Figure 3.1) are classified as arid to semi-arid, with mean annual precipitation of 200-400 mm. The dunes in these three regions are relatively stable under natural conditions, hence offering a fitting opportunity to examine the timing and amplitude of dune accumulation in the past and its correlation with variations in monsoonal precipitation. As aerial photography of the Thar is classified in India and are not available outside of the military, Google Earth™ was used to identify potential study areas. Important details specific to each region are briefly summarised in subsections below, with further information provided in Chapters 4,5 and 6.

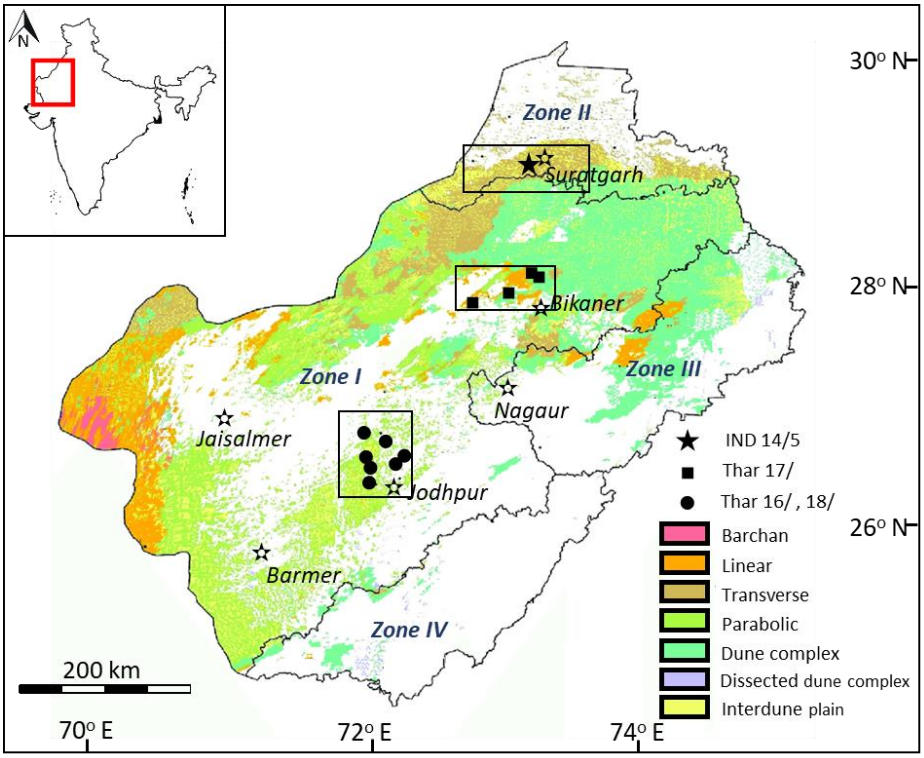


Figure 3.1. Distribution of different dune types in the Thar and the locations of investigated dunefields (boxed) (after Moharana *et al.*, 2013).

3.2.1. Jodhpur dunefield

The Jodhpur dunefield, located in the east-central Thar, is dominated by parabolic dunes (Figure 3.1). Five dunes were sampled in March 2016 and November 2017 (Table 3.1), and at each dune site, samples were collected from the dune noses, which were 10-25 m high (Figure 3.2). Dune arms were sampled at two sites, and since the aliquots from these samples yielded nearly indiscernible luminescence signals, other sites were not investigated (for more details see Section 4.2.1). In general, sampled sections comprised soft and dry structureless sand with laminations seen only near the top of section. One site, Thar 16/8 (Chamu Canal) was chosen for sampling to check consistency with results published from the site by Dhir *et al.* (2010); however, the exact section could not be located. Two samples from an exposed gully with presumably same stratigraphy were collected instead (see Figure G.1C; Appendix G).

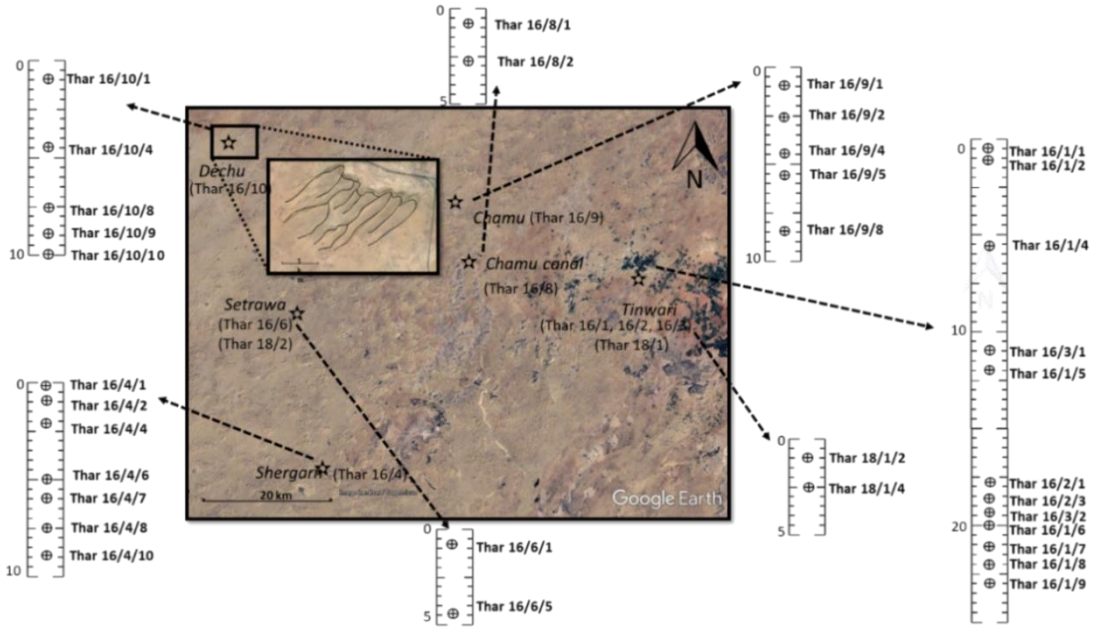


Figure 3.2. The location of sampled dunes in the Jodhpur dunefield with their schematic logs (in metres). Samples which have been dated from this dunefield are marked with the logs (see Chapter 4)

Table 3.1. Details of all the samples analysed and discussed in this thesis.

Site Name	Region	Sample Code	Altitude (m)	Latitude (degrees)	Longitude (degrees)	Section depth (m)	Sampling location	Samples analysed (#)
Suratgarh	Suratgarh	IND 14/5	150	29.3259	73.8827	26	Dune complex face	6
Tinwari	Jodhpur	Thar 16/1-3	272	26.5839	72.8162	23	Parabolic dune nose	12
Tinwari 2	Jodhpur	Thar 18/1	279	26.5794	72.8142	2	Parabolic dune arm	2
Shergarh	Jodhpur	Thar 16/4	248	26.3312	72.2882	9	Parabolic dune nose	7
Setrawa	Jodhpur	Thar 16/6	319	26.6019	72.2887	5	Parabolic dune nose	2
Setrawa 2	Jodhpur	Thar 18/2	277	26.5967	72.2855	5	Parabolic dune arm	2
Chamu Canal	Jodhpur	Thar 16/8	291	26.6579	72.6061	3	Parabolic dune arm	2
Chamu	Jodhpur	Thar 16/9	293	26.6685	72.5701	8.2	Parabolic dune nose	5
Dechu	Jodhpur	Thar 16/10	245	26.8186	72.3032	10.2	Parabolic dune nose	5
Jaisalmer Bypass 1	Jaisalmer	Thar 17/2	200	28.1373	73.3428	9	Linear dune axis	6
Nal	Jaisalmer	Thar 17/4	215	28.0331	73.2095	11	Linear dune axis	4
Bajrang Dohra	Jaisalmer	Thar 17/5	208	28.0602	73.2685	8.7	Linear dune axis	5
Jaisalmer Bypass 2	Jaisalmer	Thar 17/6	200	28.1364	73.3329	9.5	Linear dune axis	4

3.2.2. Bikaner dunefield

In the Bikaner region in the northern Thar, four linear dunes (oriented in NE-SW direction) were sampled in April 2017 (Table 3.1; Figure 3.3). The sampled dunes were partially vegetated with a rounded profile, and height ranged between 8.5-11 m (relative to adjacent interdune area) with <10 km crestline length. At all four sites, the dune axis was targeted for sampling to obtain dune core sediment presumed to be least affected by lateral dune movement as well as being the locations that preserve the maximum thickness of sediments in the dune bodies. No distinct stratigraphic change was observed at any site as sections were largely structureless (see Section 5.2.1.; Chapter 5).

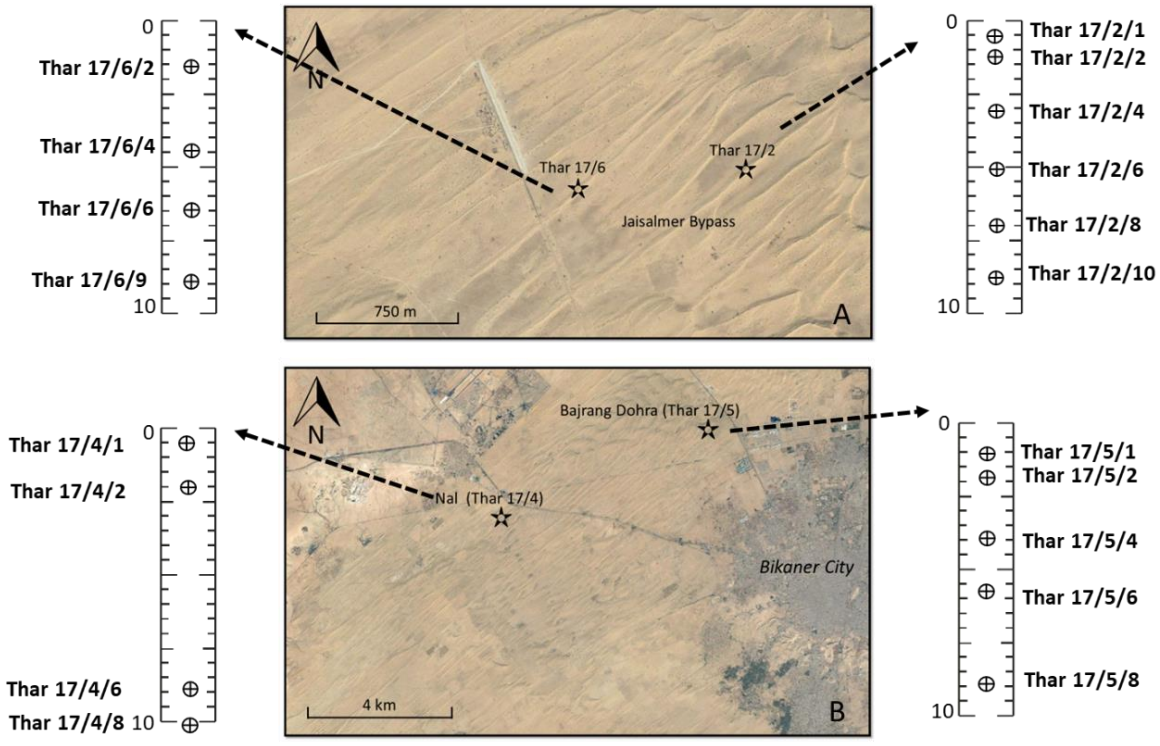


Figure 3.3. The location of sampled dunes in the Bikaner dunefield with their schematic logs (in metres). Samples which have been dated from this dunefield are marked with the logs (see Chapter 5).

3.2.3. Suratgarh region

The Suratgarh dunefield is situated on the northern desert margin next to Ghaggar-Hakra palaeochannel. Six samples from a ~26 m high dune associated with the palaeochannel (IND 14/5) (Figure 3.4) were collected by Julie Durcan and David Thomas in December 2014. These samples complement the recent study by Durcan *et al.* (2019), which reveal that Ghaggar-Hakra was a highly dynamic geomorphic system, particularly in middle to late Holocene. Being a preliminary study, the authors suggested that the need for further research to expand our understanding of changing palaeoenvironmental conditions in the region under fluctuating monsoon regimes (see Chapter 6).

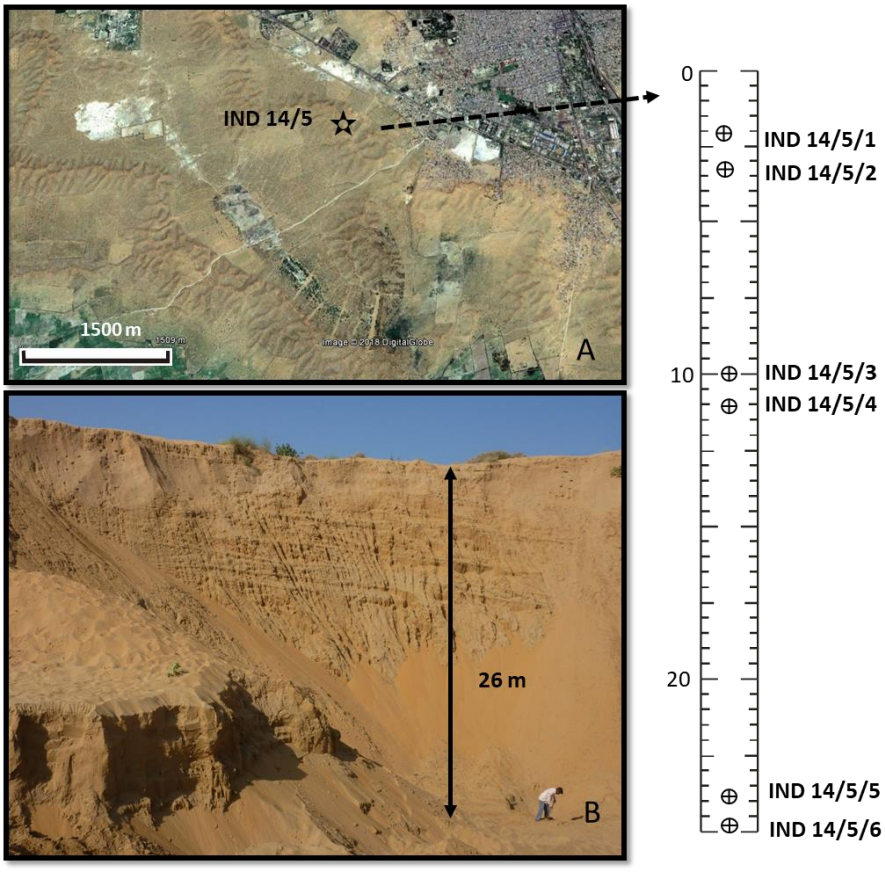


Figure 3.4. (A) The location of sampled dune in the Suratgarh dunefield in the northern Thar. (B) Exposed section of the dune where the six samples were retrieved from (as marked in the schematic log).

3.2.4. Sampling strategy

Samples were collected from vertical sections, with access achieved by cutting steps into the exposed face (see Figure 4.1). The sections were dug deeper with the help of hydraulic digger (Figure 3.5) until a hard calcrete rich layer was hit (e.g. Thar 16/1, Thar 17/4) or sediment collapse risk prevented further sampling (e.g. Thar 16/4, Thar 17/6). A major advantage of using hydraulic digger is the ability to view the entire section, therefore allowing to adopt a sampling strategy that is specific to each site. It also allows samples to be collected both at regular intervals as well as from particular horizon of interest, as done by Atkinson *et al*. (2011) in the context of sampling dunes in the Rub' al-Khali. This approach also eliminates the potential problem of retrieving a mixed sample from across a stratigraphic contact, which is a risk in 'blind' sample retrieval from drilling cores (Atkinson *et al*., 2012). During the fieldwork, wherever possible, a high sampling resolution was adopted with samples collected at regular 0.5 to 1.0 m intervals, unless field examination revealed changes in stratigraphy or sedimentology, in which case additional sampling was carried out to bracket such features like stratigraphic discontinuities (e.g. Thar 16/9) or distinct sedimentology (e.g. Thar 16/10). Stratigraphic features, where present, may be helpful in environmental interpretation in order to support assessments of chronologies, especially regarding the presence of accumulation hiatuses (Leighton *et al.*, 2013).

At sites where sections were big (> 20 m; e.g. IND 14/5, Thar 16/1) and central parts were inaccessible, samples from the upper and basal parts were collected. Samples were retrieved by inserting opaque black tubes (~20 cm length, ~5 cm diameter) into the cleaned face, and when tubes were full, those

were carefully closed with opaque lids, taped and marked before safely placing in light-proof bags. Sediment from potentially light exposed ends were removed and used for sedimentological analyses, including particle size analysis, and water, carbonate and organic contents, with the aim of substantiating further context to their depositional history. The details of different sedimentological analyses adopted are outlined in Appendix B and the results are included in Chapter 4 (Table 4.1), Chapter 5 (Table 5.1) and Appendix G (Table G.3).



Figure 3.5. Examples of dune sections being deepened with the aid of a hydraulic digger. (A). Crest of a linear dune Thar 17/6. (B) Nose of a parabolic dune Thar 16/1.

3.2.4. Dating strategy

After sampling, as discussed in previous section, a total of 90 samples were collected from twelve sampled dune sections from three dunefields. But all samples were not dated as luminescence dating of sediments is a lengthy, labour-intensive, and time-consuming procedure.

Preliminarily, from each sampled dune section, samples from top, middle and bottom units were first opened. Then, initial range finder tests (Roberts *et al*.,

2009; Durcan *et al*., 2010) were performed to identify appropriate samples in the laboratory for measurement and processing in full. A range finder test provides rapid age estimates, albeit with lower levels of precision and accuracy than would be expected from fully prepared samples, by simplifying laboratory preparation procedure (e.g. Durcan *et al*., 2010). To establish an approximate range finder D_e, sub-samples were treated with chemicals quickly (1 hour in concentrated HCl, followed by HF and HCl treatments ; Durcan *et al*., 2010) and six large aliquots were measured. If two samples, from the section, yielded comparable values, intermediate samples were not dated. For example, a total of five samples were collected from site Thar 16/6 (Figure 3.6A), but quick range finder analysis suggested that samples Thar 16/6/1 and 16/6/5 had comparable D_es, therefore, three immediate samples were not dated. Full methodical analyses on samples Thar 16/6/1 and Thar 16/6/5 later resulted in the same age from top and bottom units (i.e. 0.07 ± 0.01 ka) (Figure 3.6B). Similar approach was applied in other dune sections (e.g. between samples Thar 17/4/2 - 17/4/6, Thar 17/6/6 - 17/6/9 etc) to save labour and machine time.

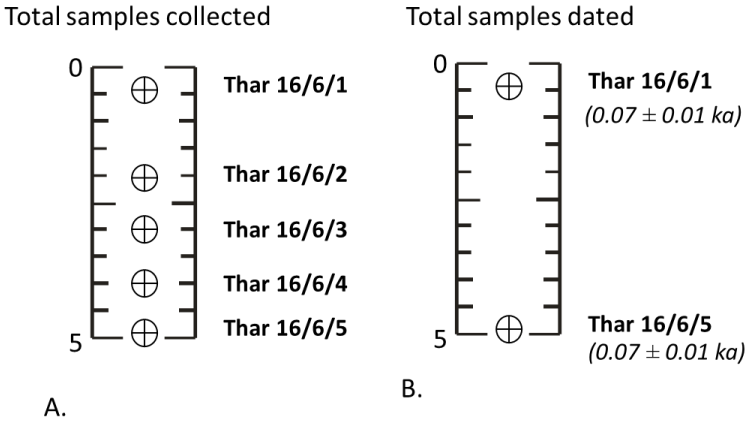
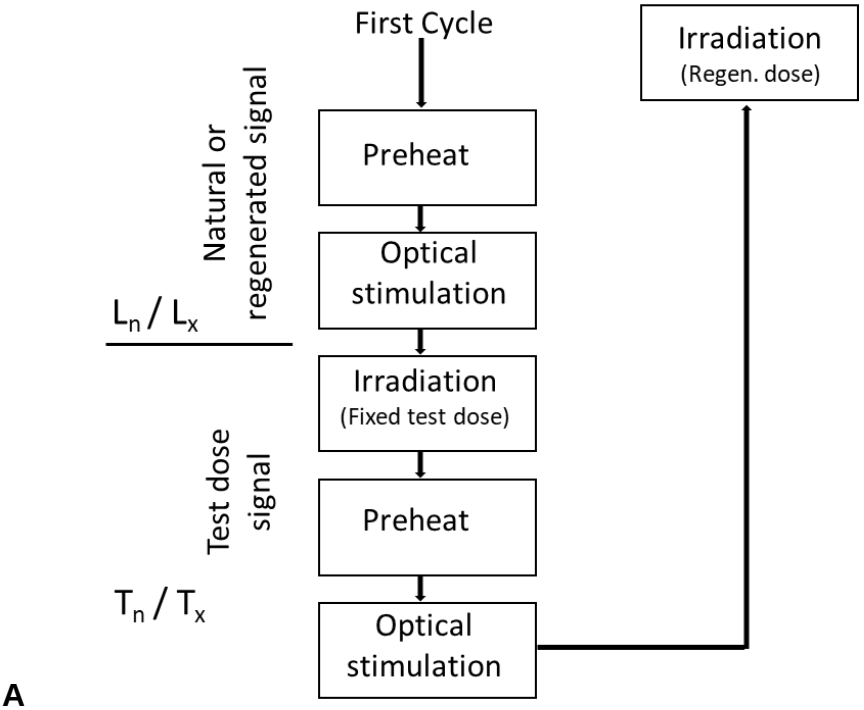


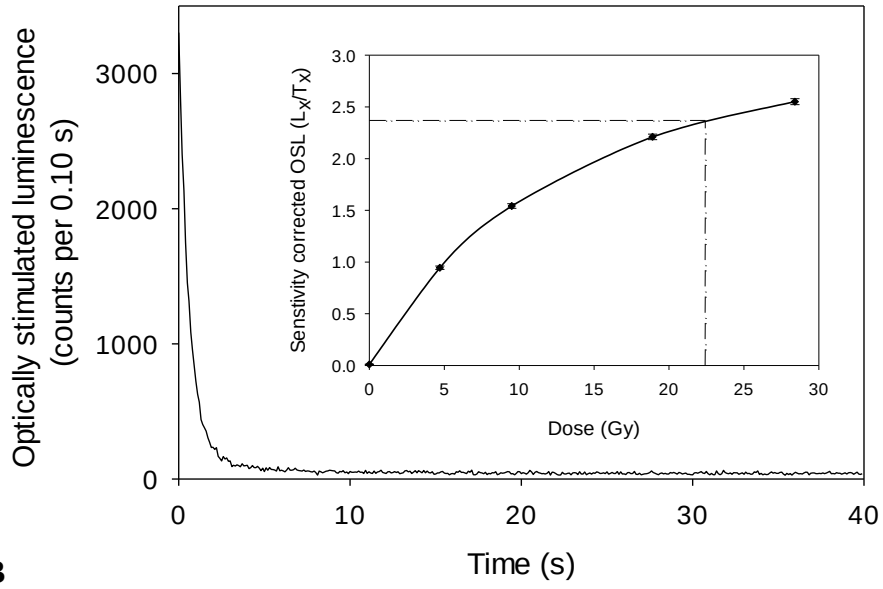
Figure 3.6. (A) Samples collected during the field from site Thar 16/6 (in m). (B) Samples dated after adopting range finder approach. Since Thar 16/6/1 and 16/6/5 resulted in the same age, intermediate samples were not dated.

3.3. Laboratory methods: equivalent dose determination

As discussed in Section 2.2, where the principles of luminescence dating are presented, the determination of the amount of radiation that a sample has absorbed during the burial period is integral to the calculation of a luminescence age. Equivalent dose or D_e is the amount of laboratory irradiation required to replicate the natural luminescence signal. The single aliquot regenerative (SAR) protocol of Murray and Wintle (2000, 2003) has become the routinely applied measurement protocol for D_e determination. The main advantage of the SAR protocol over previous approaches is the ability to detect, monitor and correct for any sensitivity change during measurement. Using the SAR protocol (summarised in Figure 3.7A), a sample is pre-heated to remove any unstable signal from shallow, less stable OSL traps, prior to measurement of the luminescence signal produced during stimulation with light (L). Following measurement of the natural luminescence signal (L_n), a fixed laboratory irradiation (test dose) is applied, followed by pre-heating and measurement of the test dose signal (T_n). A series of SAR cycles, each applying different laboratory regenerative doses is applied to establish the relationship between laboratory irradiation and the luminescence signal (the dose response curve; DRC). The sensitivity corrected luminescence signal (L_n/T_n) can then be interpolated onto the DRC to determine D_e (Figure 3.7B).



A



B

Figure 3.7. A. Generalised SAR protocol (after Murray and Wintle, 2000). B. An example of OSL signal and DRC from an aliquot of sample IND 14/5/4.

3.3.1. Sample preparation

To isolate a clean, pure quartz fraction for dating samples were opened in subdued orange-light conditions in the Oxford Luminescence Dating (OLD) Laboratory, University of Oxford. The light-exposed sample ends were removed and used for sedimentological analyses (Appendix B) and the protocol in Figure 3.8 was applied to all samples.

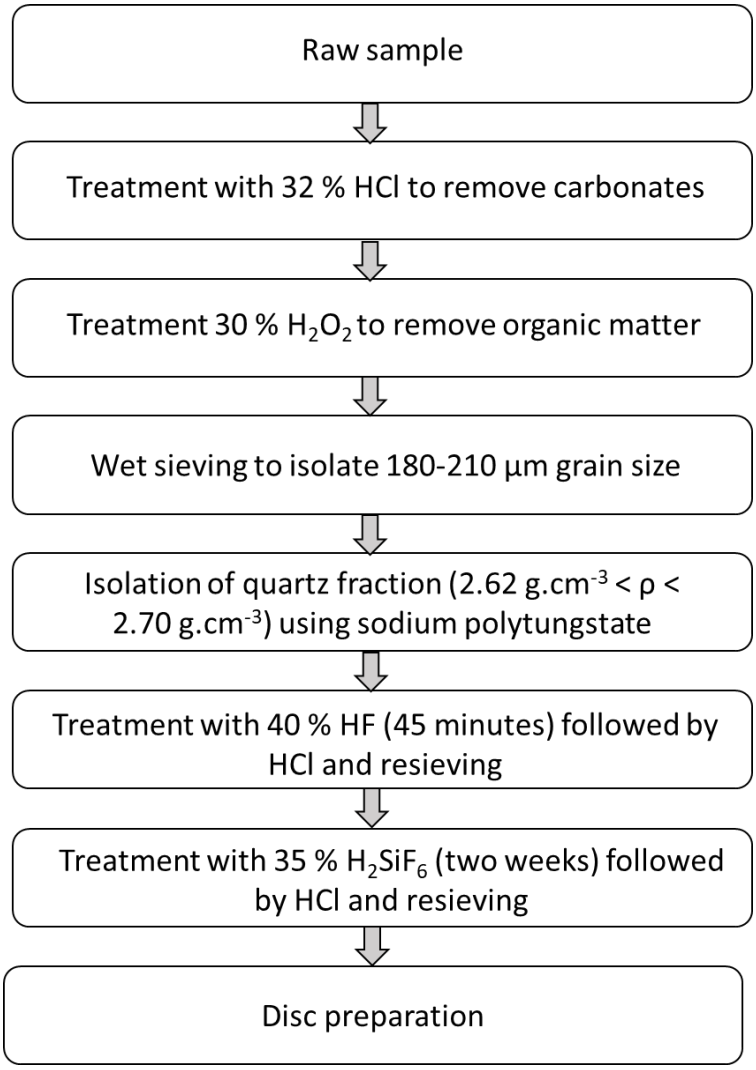


Figure 3.8. Summary of the laboratory treatment used to prepare samples for measurement of luminescence signal.

For dating, prepared samples were mounted onto aluminium discs (9.8 mm in diameter). Discs were cleaned, and aliquots of different sizes (2, 5 and 8 mm) were made by placing a mask over the disc and spraying the exposed area with Silkospray silicone oil. Grains were adhered to the disc in a monolayer. An estimate of the number of grains on different sized aliquots is shown in Table 3.2, calculated after methods described in Heer *et al.* (2012) and using the R luminescence package (Kreutzer *et al.*, 2017). For single grain measurements, aluminium discs 9.8 mm in diameter were used, each with 100 holes (300 µm in diameter and depth) arranged in a ten by ten grid.

Table 3.2. Estimated number of grains per multiple grain aliquot for different aliquot sizes. Calculations are based assuming a monolayer of spherical grains within a circular area of the specified diameter, and a packing density of 0.65 (Heer *et al.*, 2012)). Visual counting of grains using a hand-held lens verified these estimates.

Grain Size	Aliquot size	Aliquot diameter	Number of grains
180-210 µm	Small	2 mm	68
180-210 µm	Medium	5 mm	427
180-210 µm	Large	8 mm	1094

3.3.2. Luminescence signal measurement

All the measurements were conducted at the OLD laboratory using one of four Risø TL/OSL-DA-15 automated readers (named “Atlas”, “Bacchus”, “Cyclops” & “Delphi”). These readers can measure up to 48 aliquots per measurement run and can provide optical stimulation using a variety of light sources in the form of continuous wave (CW-), linearly modulated (LM-) and pulsed (P) OSL (Bøtter-Jensen *et al.*, 2003). They are fitted with a hot plate which lifts the sample into

measurement position and can heat up to 700°C prior to and during measurement. Delphi is fitted with a green (525 nm) LED array, and all other machines are fitted with blue (470 nm) LED arrays. These LEDs emit at 16 $mW.cm^{-2}$ (Altas), 28 $mW.cm^{-2}$ (Bacchus), 31 $mW.cm^{-2}$ (Cyclops) and 64 $mW.cm^{-2}$ (Delphi) (as of May 2015). All four readers are fitted with an infrared (IR) LED array (wavelength 870 nm and maximum stimulation power ~145 mW cm^{-2}). Cyclops has a single grain attachment, allowing for the measurement of single grains. The stimulation source is a 10-$mW.cm^{-2}$ green (532nm) laser diode which focusses to a <20 µm diameter, with a maximum estimated energy at the sample of 50 W cm^{-2} (Risø DTU, 2009). $^{90}Sr/^{90}Y$ beta sources were used for all irradiation and the dose rates varied between machines between 3.5 and 4 Gy. $minute^{-1}$ as of August 2018 and were last calibrated using Risø calibration quartz in February 2018. A bialkali photomultiplier tube (PMT) fitted with 7.5 Hoya U-340 detection filter (to prevent any scattered stimulation light from reaching the PMT) was used for the detection of luminescence emission. This filter transmits between 250 and 390 nm, with peak transmission in the ultraviolet at 340 nm (Bøtter-Jensen *et al.*, 2003).

3.3.3. Single grain assessment of luminescence signals

Single-grain OSL measurements from many studies have shown that the number of grains emitting a luminescence signal varies considerably from sample to sample (Duller, 2008). Duller *et al.* (2000) examined various samples including coastal sands from Mozambique and frost-wedge cast sands from Denmark, and observed a range of behaviour in their samples, with 95 % of the light sum originating from between 5 % and 50 % of the grains across a range of sedimentary quartz samples. However, grains from glacial deposits in Scotland and Chile showed different behaviour with ~30% of the grains emitting 90% of

the total light sum (Duller, 2006). In the case of aeolian sands from South Africa, only a small percentage (~10%) of grains have a measurable OSL response (Jacobs *et al.*, 2003a; Jacobs *et al.*, 2003b).

To investigate the proportion of grains emitting a luminescence signal from the Thar, single grain analyses was undertaken for ten samples (Table 3.3). 500 grains of each sample (grain size 180-210 μm) were bleached twice in the luminescence reader, given a laboratory of 50 Gy and then a post-IR SAR cycle was applied. The number of grains giving a luminescence signal discernible (e.g. Figure 3.9) from the machine background were counted. Single grain analyses of samples showed that between 2.4 and 4.0 % of measured grains gave a signal (Table 3.3). Assuming this is the case across the suite of samples dated, the small aliquots used for dating in this study should have 2-3 luminescing grains per disc, medium aliquots 10-17 grains, and large aliquots 26-45 grains (see Table 3.2). This should be sufficient for allowing heterogeneity in underlying dose distributions to be identified.

Table 3.3. Summary of the results of single grain analyses conduced on selected samples.

Sample	Grains measured	Number of grains giving measurable luminescence signal (percentage)
Thar 16/1/9	500	13 (2.6)
Thar 16/4/2	500	12 (2.4)
Thar 16/4/10	500	12 (2.4)
Thar 16/10/10	500	20 (4.0)
Thar 17/2/5	500	14 (2.8)
Thar 17/4/2	500	16 (3.2)
Thar 17/4/8	500	13 (2.6)
Thar 17/5/6	500	14 (2.8)
Thar 17/6/6	500	18 (3.6)
Thar 17/6/9	500	17 (3.4)

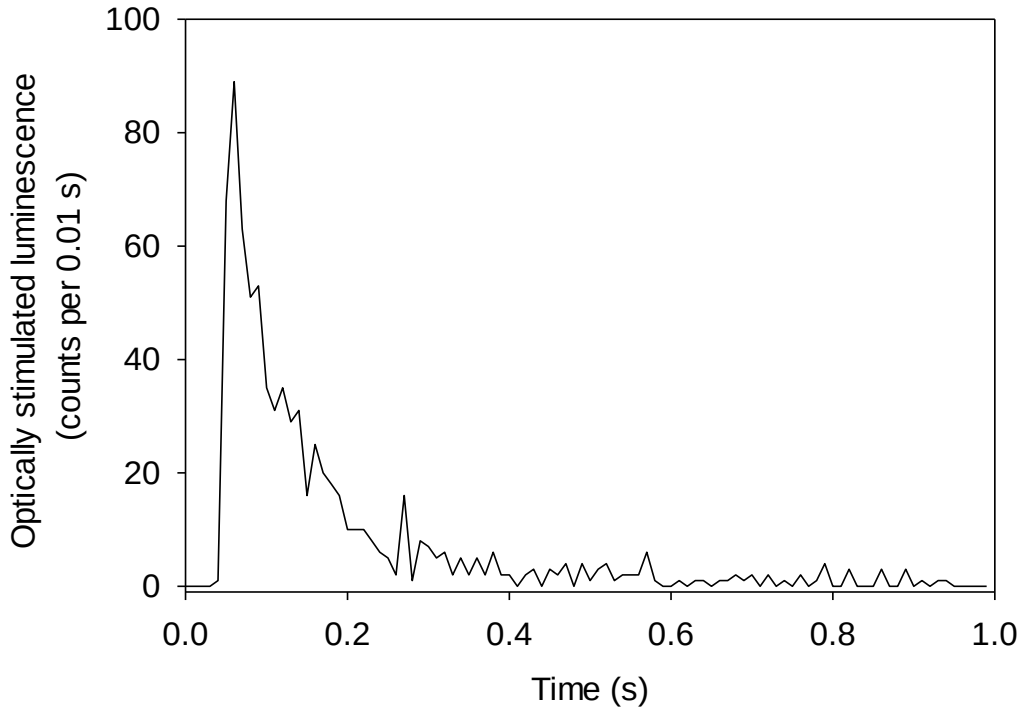


Figure 3.9. An OSL signal from a single grain of quartz from sample Thar 16/10/10 with an D_e of approximately 10 Gy.

3.3.4. Combined dose recovery and pre-heat plateau tests

There are several tests which can be used to investigate the performance of the SAR protocol, one of which is a pre-heat plateau test. As the SAR protocol involves thermal treatments in the form of pre-heats and cut-heats to remove charge from thermally unstable traps, heating a sample can invoke sensitivity change during the measurement protocol. To test the impact of varying the temperature of the pre-heat, Murray and Wintle (2000) suggest a pre-heat plateau test, which enables the assessment of the temperature dependence of D_e values and allows the most suitable pre-heat temperature for a sample to be selected. To remove the variability arising from heterogeneous D_e values, a combined dose

recovery and pre-heat plateau test was undertaken. This involved bleaching the natural D_e and giving a known laboratory dose to samples prior to undertaking the pre-heat plateau test. 10 samples from different sites were chosen for these tests. For each sample, 4-6 aliquots had their natural signals removed and were given a laboratory dose which close to their natural signal, and then the aliquots were pre-heated at a range of temperature between 200°C and 300°C (Table 3.4). The examples of pre-heat plateaux for two studied samples are shown in Figure 3.10. The ratio between the recovered and administered dose is given as a function of pre-heat temperature, for all aliquots satisfying the rejection criteria (discussed in Section 3.3.7). For all ten samples, pre-heats of 220-240°C were typically more consistent with unity (within 10 %), and thus, these pre-heats were used (220°C for Suratgarh (IND) samples and 240°C for Jodhpur and Bikaner (Thar) samples.

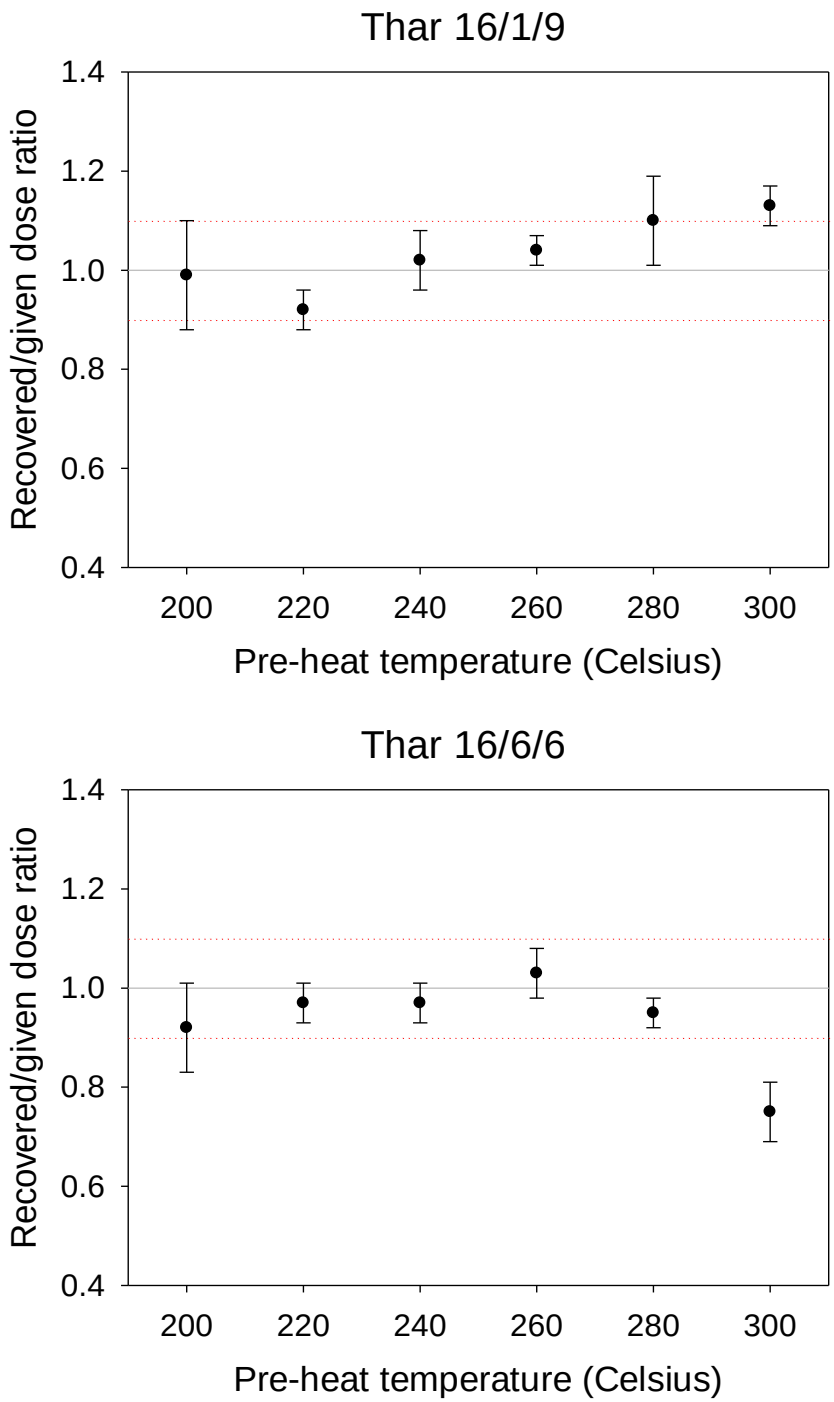


Figure 3.10. Combined dose recovery and pre-heat plateau tests for selected samples. Shown is the average D_e and standard error (one sigma) of accepted aliquots.

Table 3.4. Summary of the combined pre-heat and dose recovery tests undertaken, including the given dose, the number of aliquots at each pre-heat temperature which satisfy all rejection criteria (Section 3.3.7) and the mean ratio and standard deviation between the recovered and administered dose at the selected pre-heat temperature of 240°C for all but sample IND 14/5/3 for which 220°C temperature was selected.

Sample	Given Dose (Gy)	Aliquots accepted (aliquots measured)						Recovered/Given dose
		200°C	220°C	240°C	260°C	280°C	300°C	
Thar 16/1/1	3	3 (6)	4 (6)	4 (6)	3 (6)	2 (6)	1 (6)	0.91 ± 0.06
Thar 16/1/9	20	2 (6)	1 (6)	3 (6)	1 (6)	4 (6)	1 (6)	1.02 ± 0.06
Thar 16/4/10	20	2 (6)	1 (6)	1 (6)	2 (6)	4 (6)	2 (6)	0.94 ± 0.03
Thar 16/9/8	20	4 (6)	4 (6)	5 (6)	6 (6)	4 (6)	1 (6)	0.99 ± 0.12
Thar 16/10/1	7	2 (4)	3 (4)	5 (4)	3 (4)	3 (4)	2 (4)	0.94 ± 0.09
Thar 16/10/10	20	3 (6)	2 (6)	5 (6)	4 (6)	5 (6)	4 (6)	0.93 ± 0.09
Thar 17/4/2	17	4 (4)	3 (4)	3 (4)	4 (4)	1 (4)	1 (4)	0.96 ± 0.03
Thar 17/6/6	17	4 (4)	3 (4)	3 (4)	4 (4)	1 (4)	1 (4)	0.97 ± 0.04
Thar 17/6/2	9	4 (4)	3 (4)	3 (4)	4 (4)	1 (4)	1 (4)	0.93 ± 0.06
IND 14/5/3	20	4 (6)	6 (6)	2 (6)	3 (6)	3 (6)	0 (6)	0.96 ± 0.05

3.3.5. Dose recovery tests

Dose recovery tests (DRTs) are another important quality check to further test the suitability of the selected SAR protocol and assess the overall ability of the measurement protocol to recover a known laboratory dose given in the laboratory (Wintle and Murray, 2006). A DRT involves the removal of the natural trapped electron population from the sample and measuring the luminescence after giving a fixed dose, thus mimicking the resetting of the sample at the time of the event being sampled (Murray and Wintle, 2003). In this study, DRTs were carried out on 14 samples from different sites. The natural signal from small aliquots of sample (Table 3.5) was bleached using two blue light stimulations for 1000 s at 20°C, with a 10000 s pause between the two stimulations so that there is time for any charge transferred into the 110°C trap to thermally decay (Murray and Wintle, 2003). The aliquots were then irradiated with a known dose which was close to the expected natural dose of the sample. The selected post-IR blue SAR protocol was then run, followed by screening of signals using the rejection criteria discussed in Section 3.3.7 and calculation of the mean D_e and standard deviation. Wintle and Murray (2006) suggest this ratio should be close to unity (within 10 %) if the chosen protocol for D_e determination is working sufficiently, which was the case with all the studied samples (Table 3.5).

Table 3.5. The details of dose recovery tests conducted on the samples in this study.

Sample	Given Dose (Gy)	Aliquots measured (accepted) (#)	Recovered/Given Dose Ratio
Thar 16/1/2	2	12 (10)	0.95 ± 0.05
Thar 16/1/7	18	10 (8)	0.93 ± 0.06
Thar 16/3/2	16	10 (8)	0.94 ± 0.07
Thar 16/4/4	3	12 (9)	0.99 ± 0.06
Thar 16/6/1	1.8	12 (10)	1.02 ± 0.10
Thar 16/8/1	20	12 (10)	0.95 ± 0.07
Thar 16/9/4	1.8	12 (8)	0.97 ± 0.07
Thar 16/10/10	18	12 (9)	0.98 ± 0.10
Thar 17/2/4	20	12 (9)	0.92 ± 0.04
Thar 17/4/8	20	10 (9)	0.95 ± 0.04
Thar 17/5/1	2	10 (7)	1.01 ± 0.06
Thar 17/6/2	2	10 (8)	1.00 ± 0.07
Thar 17/6/6	20	10 (8)	0.96 ± 0.05
IND 14/5/1	20	12 (8)	0.91 ± 0.03

3.3.6. The post-IR SAR protocol used in the study

A post-IR blue SAR protocol (Banerjee *et al.*, 2001; Roberts and Wintle, 2001) has been used in this study (Table 3.6). This protocol involves an additional stimulation with IR-diodes prior to the visible light stimulation to remove the luminescence signal from any remaining IR-response minerals (e.g. feldspars) prior to stimulation with blue/green LEDs (post-IR OSL) to measure the quartz OSL signal. Roberts (2007) assessed the effectiveness of this protocol in isolating a luminescence signal dominated by quartz and suggested that chemical isolation of the quartz component to be essential, as the protocol may not successfully eradicate the contribution of feldspar to the OSL signal on stimulation with blue diodes in case of polymineralic samples.

Therefore, this protocol was chosen as a further precaution against any residual feldspar contamination remaining after laboratory preparation. This post IR-blue SAR protocol followed that of Murray and Wintle (2000) presented in Table 3.6 and consisted of measurement of the natural luminescence signal, followed by 4-5 regeneration doses to characterise the DRC. Two 0 Gy dose (one after natural dose and one after the highest dose) cycles were given to check for recuperation. A repeat measurement of the first non-zero dose, to check the recycling ratio was also made (Section 3.3.7).

Table 3.6. The post -IR blue SAR protocol used in the study (after Murray and Wintle, 2000; Banerjee *et al*., 2001; Wintle and Roberts, 2001; Wintle and Murray, 2006) on the basis of results from preheat and dose recovery tests.

Step	Treatment	Observe
1	Beta irradiation (zero for natural)	
2	Pre-heat at 220/240°C for 10 s	
3	IR stimulation at 50°C for 100 s	
4	OSL stimulation at 125°C for 40 s	L_x
5	Test dose	
6	Cut-heat at 160°C for 10 s	
7	IR stimulation at 50°C for 100 s	
8	OSL stimulation at 125°C for 40 s	T_x

3.3.7. Analyses of luminescence signals

The quartz continuous wave (CW)-OSL signal is composed of the signal originating from various components (‘fast’, ‘medium’ and ‘slow’) (Bailey *et al.*, 1997; Jain *et al.*, 2003; Singarayer and Bailey, 2003). Of these, the fast component is considered the most suitable for OSL dating because it has a long

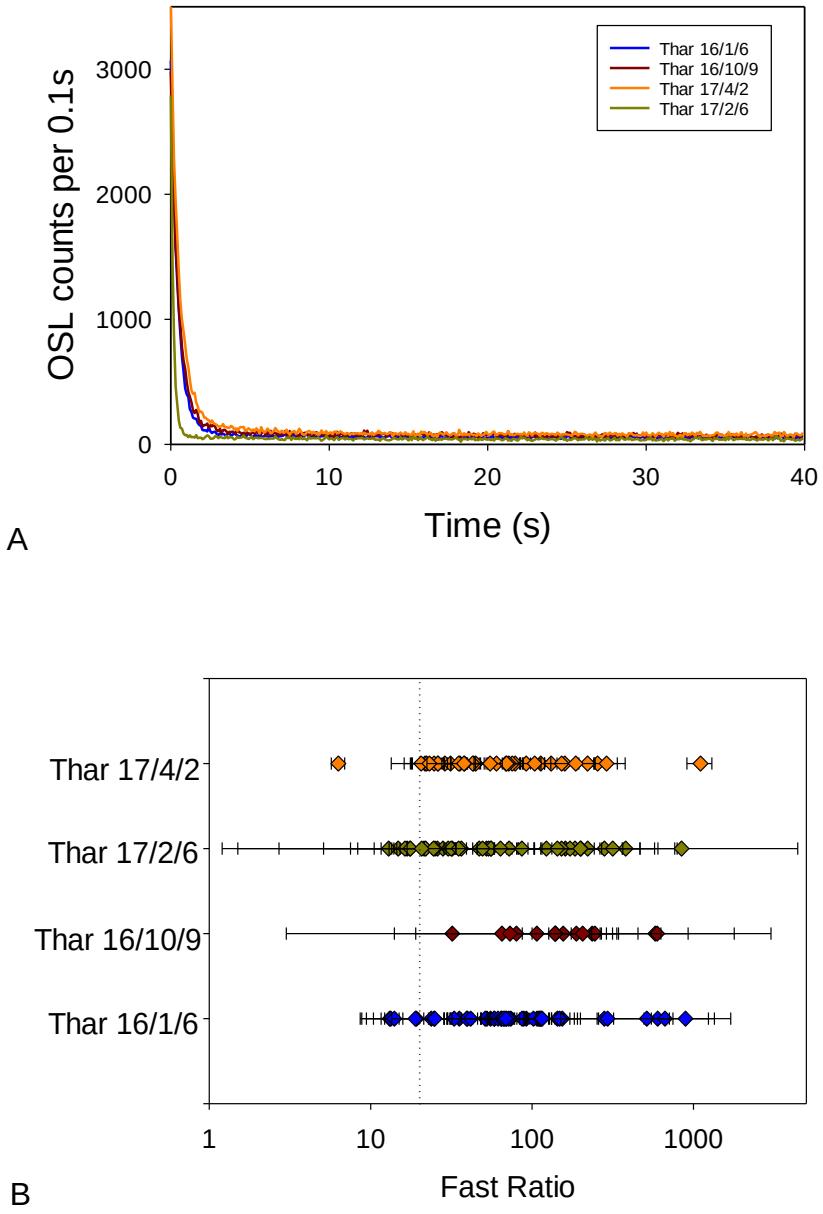


Figure 3.11. A. OSL decay curves shown by aliquots of selected samples. B. Fast ratios of all aliquots of the same selected samples.

lifetime (Wintle and Murray, 1998), stable thermal properties (Singarayer and Bailey, 2003) relatively low recuperation when compared to other components (Jain *et al.*, 2003) and is readily bleachable in nature. The SAR protocol has also been tested on samples with fast-dominated CW-OSL signals (e.g. Murray and Olley, 2002). In this study, aliquots generally generated signals with a which

decayed rapidly (near exponentially) to background levels with a few seconds of stimulation, which is expected from a quartz OSL signal (Figure 3.11). Here, D_es were calculated from the signal measured during the first 1 s of stimulation, with the mean background over the last 10 s subtracted. The use of the fast ratio (Durcan and Duller, 2011) suggested that these signals are dominated by fast component in the initial part of the OSL signal and therefore suitable for dating (Figure 3.11).

Wintle and Murray (2006) suggest some internal checks when using the SAR protocol to assess, identify and remove erroneous signals which may lead to inaccurate D_e determinations. In this thesis, the following rejection criteria have been routinely applied to individual D_e signals, and signals which do not satisfy one or more criteria were not included in final sample D_e determination.

Signal levels

To ensure that the signals are bright enough to be discernible from the background of the measurement equipment, adequate signal levels were assessed using the background rejection criterion of Jacobs *et al.* (2006). Signals where the first test dose signal (T_n) was less than three times the standard deviation of the background ($T_n > 3\sigma$ BG) were included in D_e calculation, while indiscernible signals were excluded (Figure 3.12). Also, to ensure that the reproducibility of T_x signals for sensitivity correction, signals with a test dose error >10% were also rejected.

Recycling ratio

The recycling ratio (Murray and Wintle, 2000) provides a check that the SAR protocol is successfully correcting for any sensitivity change induced during

the measurement procedure. In this check, the ratio between the sensitivity corrected luminescence signal from one of the first regenerative doses is compared to one of the final, identical regenerative doses, because sensitively change is considered progressive (Wintle and Murray, 2006). Signals were rejected when the recycling ratio was in excess of ± 10 % of unity (taking uncertainties into account) following Wintle and Murray (2006) (Figure 3.13).

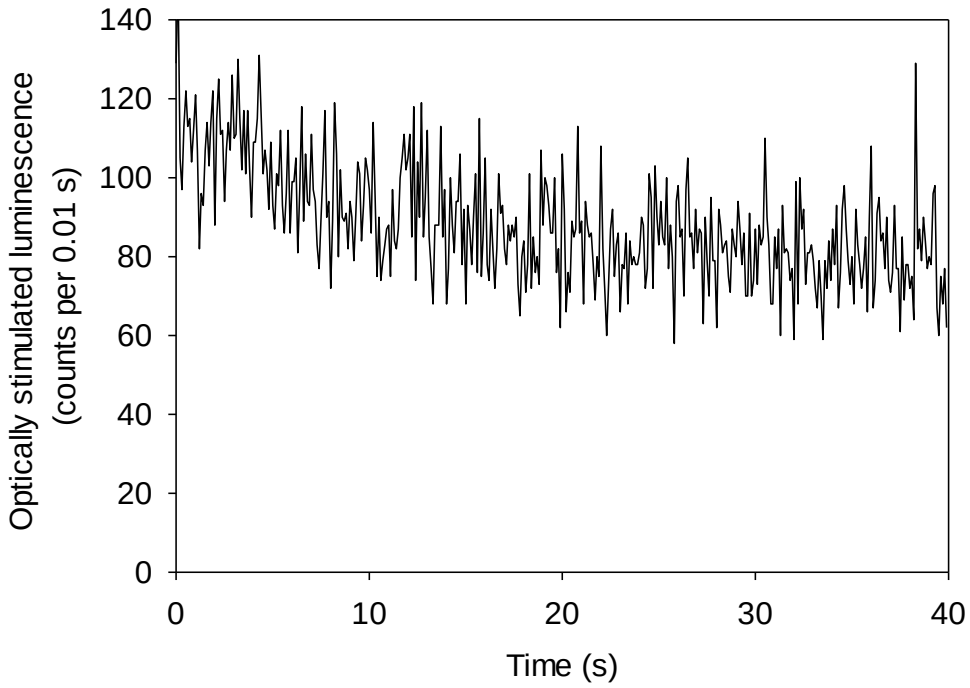


Figure 3.12. An example of signal (of sample Thar 16/6/1) failing signal level rejection criteria as the signal is not discernible from the background after a 5 Gy dose.

Recuperation

The amount of luminescence measured after a zero dose has been given is termed as recuperation (Aitken and Smith, 1988), and to monitor this, a zero dose is measured as part of the SAR cycle and the sensitivity corrected signal from this measurement is compared with the natural signal (Wintle and Murray,

2006). In this thesis, an aliquot was rejected if the percentage of recuperation ($[L_0/T_0]/[L_n/T_n]$) was more than 5 %. For young samples, calculating recuperation as a percentage of the natural may result in an exaggerated recuperation value, due to the calculation of a percentage from a small value (e.g. Reimann *et al.*, 2012; Durcan, 2012). Therefore, for samples with a D_e of less than 1.5 Gy (with age of < 500 a), recuperation was calculated as an absolute value (in Gy) and aliquots which had a regenerated dose less than 0.25 Gy after a 0 Gy dose were accepted.

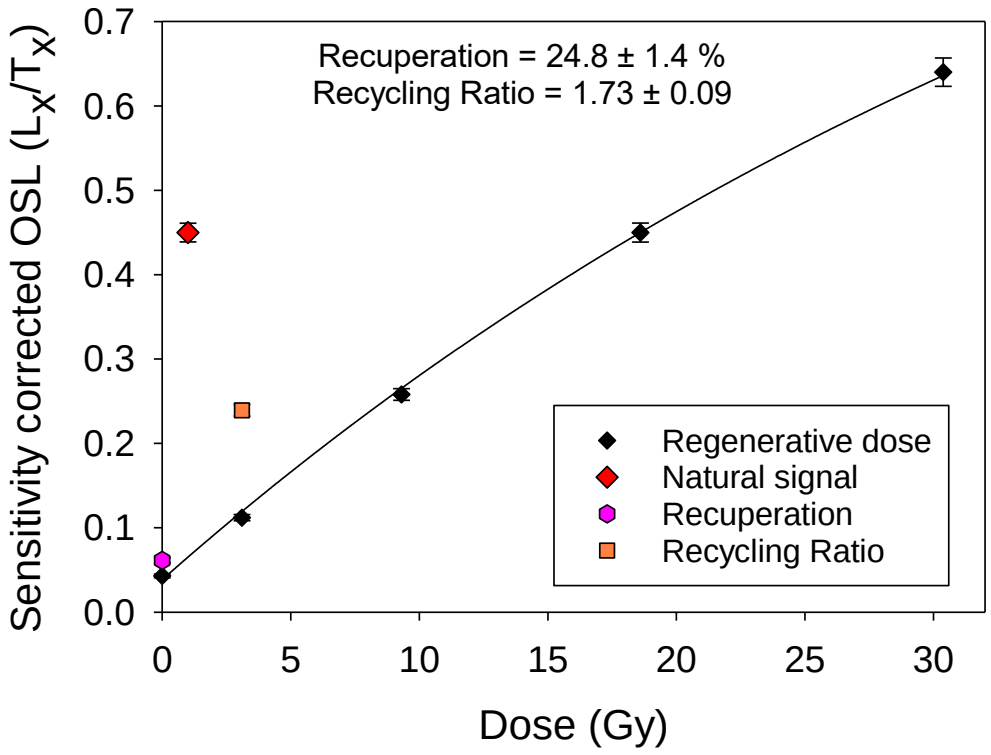


Figure 3.13. An example of a DRC (of sample Thar 17/5/4) failing on recuperation (> 5 %) and recycling ratio criteria (not consistent with unity).

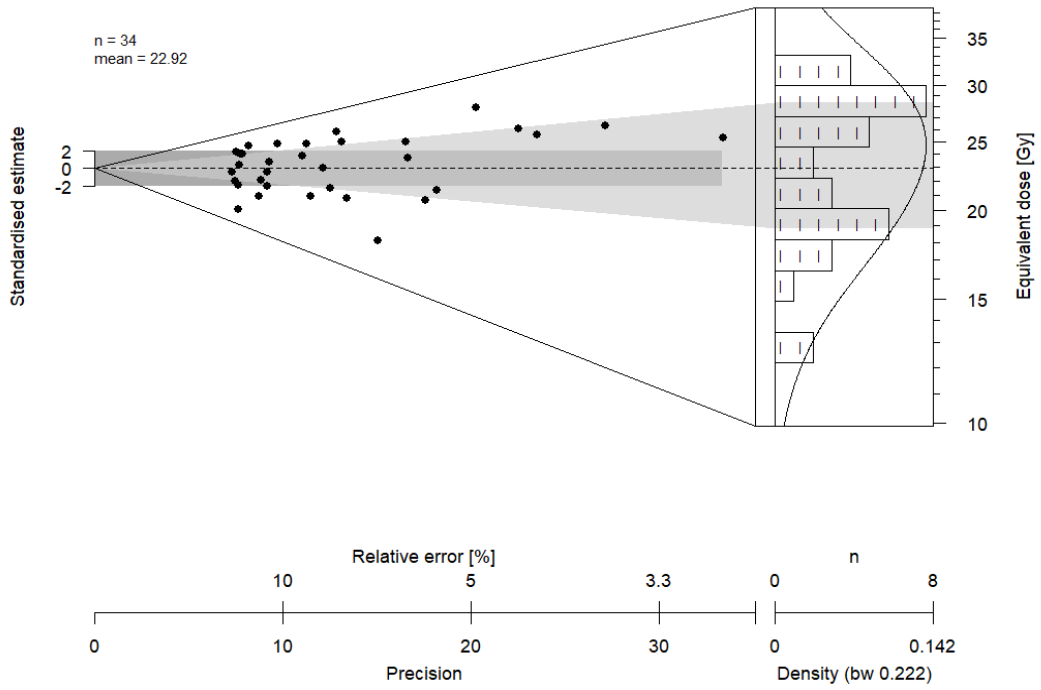
Table 3.7 shows the number of aliquots measured and the percentage of signals failing the rejection criterion. On average, 60 % of all measured aliquots were used for D_e calculation, ranging between 30 % (Thar 16/6/1) and 90 % (Thar

17/2/10) for individual samples (Table 3.7). Many aliquots measured during this study failed to satisfy at least one of the rejection criteria outlined (Table 3.7) and were excluded from dose distribution analysis. Generally, samples had less than 10 % of the total number of aliquots failing on signal levels, and for samples where a higher than average number of signals are rejected (e.g. IND 14/5 samples), that could be due to low number of grains giving a luminescence signal. On average less than 15 % aliquots were rejected on the basis of recuperation, although higher numbers are seen for samples with low D_e values (e.g. Thar 16/1/5) which may reflect the sensitivity of low doses to recuperation caused by thermal transfer (Murray and Olley, 2002). On average, one-third of aliquots were rejected on the basis of the recycling ratio (10 % of unity; though the majority of signals were with 20 % of unity) and its implication is that a known dose cannot be recovered precisely and that systematic errors of a few % are likely to occur when SAR is used to obtain D_e (Wintle and Murray, 2006).

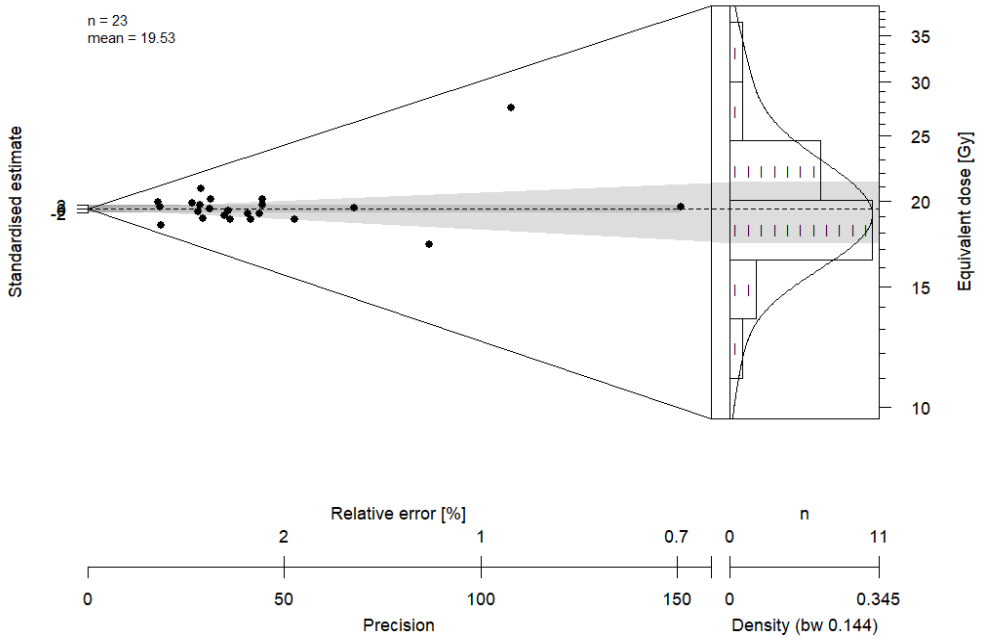
D_e distributions

In this thesis, over-dispersion (σ_d) or heterogeneity in the measured D_e distributions is relatively low, and ranges between 20 % and 35 % (including uncertainties) for the majority of samples with D_es greater than 1 Gray (Table 3.7). Heterogeneity in D_e distributions can originate due to various factors, and mild microdosimetric variability is hypothesised to explain variability in D_es in this thesis (see sections 4.3.2 and 5.3.2 for details). For the majority of samples measured in this study, dose distributions vary symmetrically around a central value (e.g. Figure 3.14), and therefore the central age model (CAM) of Galbraith *et al.* (1999), has been selected for use following the rationale of Rowan *et al.* (2012), Parton *et al.* (2015) and Durcan *et al.* (2019). CAM assumes that the true

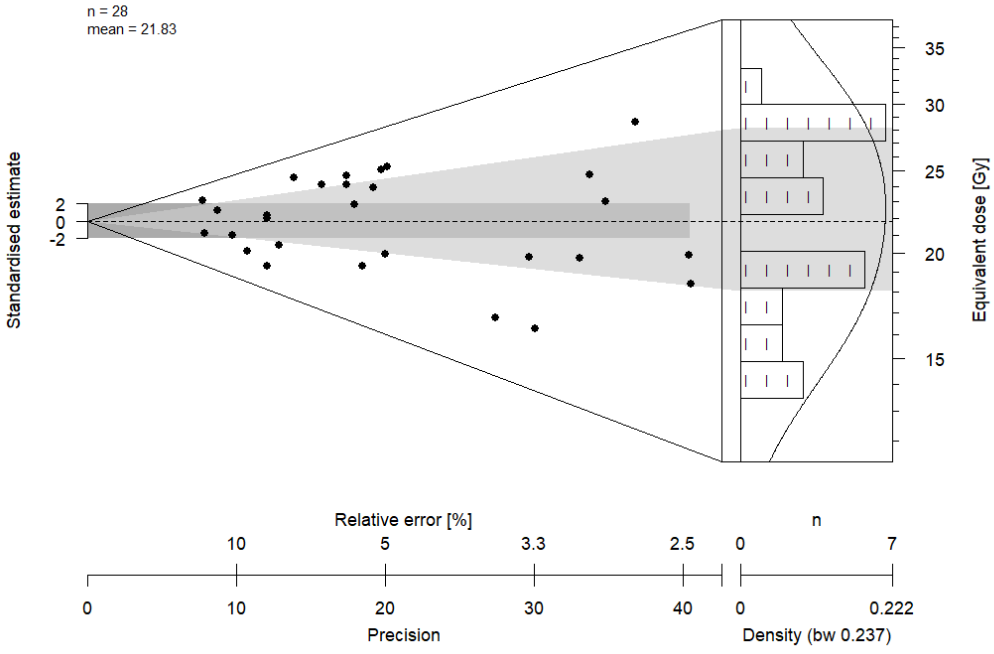
D_e is drawn from a normal distribution but external factors above measurement errors contribute to the over-dispersion (Galbraith *et al.*, 1999). CAM D_es were calculated in the R Luminescence Package v. 0.4.4 (Kreutzer *et al.*, 2017), and are provided in Table 3.7. Two samples were considered to be in saturation and for which a minimum D_e was calculated (discussed more fully in section 5.3.2). in detail in Chapter 5 (Paper 2). D_e distributions are displayed using abanico plots (Dietze *et al.*, 2016) which is a combination of two parts, a bivariate radial plot (Galbraith, 1988; Galbraith and Roberts, 2012) on the left side and a univariate plot (a kernel density estimate) on the right side. Each individual D_e value is plotted on a graph of precision/relative standard error against a standardised scale (usually shown as ±2σ, equivalent to 95 % confidence interval) and log D_e scale. Two examples are shown in Figure 3.14.



A



B



C

Figure 3.14. Abanico Plot (plotted using ShinyPlot; Dietze *et al.*, 2016) of individual D_es of sample (A) IND 14/5/3, (B) Thar 17/5/4 and (C) Thar 16/8/1. The sample D_es are shown by the dashed line and ±2σ by the grey shaded area.

Table 3.7. Summary of the total number of aliquots measured per sample, percentage of aliquots (of total measured aliquots) failing each criterion, over-dispersion (σ_d), and CAM D_es.

Samples	Aliquots Measured (#)	Aliquots accepted (%)	Failing on Signal levels (%)	Failing on Recuperation (%)	Failing on Recycling Ratio (%)	σ_d (%)	CAM D_e (Gy)
Thar 16/1/1	28	71.4	0.0	3.6	25.0	47.2 ± 8.1	0.90 ± 0.10
Thar 16/1/2	32	78.1	3.1	3.1	15.6	19.2 ± 3.7	0.88 ± 0.06
Thar 16/1/4	46	60.9	0.0	2.2	37.0	28.7 ± 4.3	1.18 ± 0.07
Thar 16/1/5	48	45.8	0.0	41.7	27.1	28.9 ± 4.5	2.38 ± 0.15
Thar 16/1/6	48	77.1	2.1	10.4	20.8	24.1 ± 2.9	14.31 ± 0.58
Thar 16/1/7	38	71.1	7.9	7.9	26.3	30.0 ± 4.1	17.21 ± 1.01
Thar 16/1/8	38	57.9	10.5	23.7	21.1	25.1 ± 3.9	20.71 ± 1.13
Thar 16/1/9	42	71.4	4.8	21.4	26.2	28.6 ± 3.8	22.70 ± 1.26
Thar 16/3/1	44	45.5	6.8	20.5	52.3	39.7 ± 8.4	1.62 ± 0.17
Thar 16/3/2	29	69.0	3.4	10.3	31.0	29.3 ± 4.8	12.07 ± 0.82
Thar 16/4/1	42	47.6	9.5	9.5	42.9	63.4 ± 16.0	0.44 ± 0.09
Thar 16/4/2	45	44.4	6.7	11.1	46.7	22.7 ± 13.7	0.36 ± 0.08
Thar 16/4/4	32	78.1	3.1	6.3	12.5	31.9 ± 4.9	1.89 ± 0.13
Thar 16/4/6	30	70.0	10.0	23.3	23.3	30.2 ± 4.7	4.67 ± 0.31
Thar 16/4/7	45	53.3	8.9	31.1	24.4	26.5 ± 4.3	4.47 ± 0.26
Thar 16/4/8	38	71.1	13.2	5.3	26.3	20.2 ± 2.9	22.84 ± 0.91
Thar 16/4/10	52	59.6	3.8	23.1	38.5	19.1 ± 2.7	23.03 ± 0.84
Thar 16/6/1	68	30.9	11.8	2.9	69.1	62.5 ± 16.0	0.16 ± 0.03
Thar 16/6/5	52	42.3	7.7	5.8	57.7	72.0 ± 14.5	0.15 ± 0.03
Thar 16/9/1	32	62.5	9.4	15.6	9.4	39.3 ± 10.3	0.16 ± 0.02

Samples	Aliquots Measured (#)	Aliquots accepted (%)	Failing on Signal levels (%)	Failing on Recuperation (%)	Failing on Recycling Ratio (%)	σ_d (%)	CAM D_e (Gy)
Thar 16/9/2	35	74.3	2.9	2.9	20.0	64.1 ± 12.1	0.18 ± 0.03
Thar 16/9/4	37	56.8	5.4	5.4	32.4	55.1 ± 9.3	0.24 ± 0.03
Thar 16/9/5	29	72.4	10.3	0.0	27.6	31.8 ± 6.1	0.31 ± 0.02
Thar 16/9/8	52	48.1	5.8	23.1	25.0	37.6 ± 5.6	7.65 ± 0.61
Thar 16/10/1	50	44.0	10.0	6.0	44.0	25.8 ± 9.6	0.15 ± 0.01
Thar 16/10/4	50	52.0	6.0	10.0	32.0	61.0 ± 12.3	0.15 ± 0.02
Thar 16/10/8	50	42.0	10.0	28.0	44.0	35.5 ± 6.7	1.58 ± 0.14
Thar 16/10/9	26	76.9	11.5	3.8	19.2	28.8 ± 4.8	12.80 ± 1.04
Thar 16/10/10	64	46.9	6.3	15.6	31.3	26.2 ± 3.7	11.45 ± 0.56
Thar 18/1/2	30	76.7	10.0	0.0	23.3	73.6 ± 13.5	0.11 ± 0.02
Thar 18/1/4	26	84.6	7.7	0.0	15.4	76.2 ± 12.1	0.35 ± 0.06
Thar 17/2/1	38	68.4	5.3	7.9	18.4	34.3 ± 4.8	1.22 ± 0.08
Thar 17/2/2	36	61.1	11.1	16.7	36.1	36.6 ± 6.1	8.36 ± 0.78
Thar 17/2/4	46	54.3	0.0	13.0	32.6	28.0 ± 4.0	19.74 ± 1.18
Thar 17/2/6	43	48.8	9.3	30.2	25.6	22.3 ± 3.7	19.82 ± 1.04
Thar 17/2/8	27	77.8	7.4	11.1	14.8	24.3 ± 3.8	19.64 ± 1.05
Thar 17/2/10	30	90.0	0.0	3.3	10.0	-	> 125
Thar 17/4/1	32	65.6	6.3	9.4	25.0	28.4 ± 4.4	8.24 ± 0.51
Thar 17/4/2	35	68.6	11.4	2.9	25.7	27.0 ± 3.9	20.39 ± 1.13
Thar 17/4/6	48	50.0	4.2	16.7	43.8	37.0 ± 5.5	24.97 ± 1.94
Thar 17/4/8	43	69.8	9.3	9.3	14.0	24.8 ± 3.3	25.23 ± 1.15
Thar 17/5/1	28	78.6	10.7	0.0	17.9	44.3 ± 8.0	0.32 ± 0.03
Thar 17/5/2	36	55.6	5.6	5.6	33.3	42.8 ± 6.8	2.51 ± 0.24
Thar 17/5/4	46	50.0	19.6	21.7	32.6	19.2 ± 2.9	19.53 ± 0.79

Samples	Aliquots Measured (#)	Aliquots accepted (%)	Failing on Signal levels (%)	Failing on Recuperation (%)	Failing on Recycling Ratio (%)	σ_d (%)	CAM D_e (Gy)
Thar 17/5/6	46	43.5	13	13	56.5	27.9 ± 4.8	18.75 ± 1.23
Thar 17/5/8	33	72.7	3.0	0.0	24.2	-	> 127
Thar 17/6/2	34	64.7	5.9	8.8	26.5	33.0 ± 5.3	0.84 ± 0.06
Thar 17/6/4	35	57.1	14.3	40.0	37.1	29.4 ± 5.0	3.72 ± 0.26
Thar 17/6/6	34	67.6	8.8	17.6	26.5	30.4 ± 4.5	20.08 ± 1.07
Thar 17/6/9	46	43.5	4.3	8.7	50.0	21.6 ± 3.9	22.10 ± 1.15
IND 14/5/1	30	66.7	13.3	13.3	23.3	21.8 ± 3.8	18.99 ± 0.97
IND 14/5/2	46	43.5	10.9	15.2	47.8	22.4 ± 5.4	22.6 ± 1.21
IND 14/5/3	48	70.8	6.3	22.9	27.1	22.6 ± 3.2	23.02 ± 0.96
IND 14/5/4	28	64.3	3.6	7.1	25.0	12.6 ± 2.8	28.75 ± 1.01
IND 14/5/5	60	48.3	13.3	25.0	48.3	28.8 ± 4.3	28.9 ± 1.65
IND 14/5/6	28	64.3	14.3	14.3	35.7	30.0 ± 5.9	25.78 ± 2.04
Thar 16/2/1	42	46.0	8.0	14.0	32.0	32.7 ± 4.3	24.55 ± 1.84
Thar 16/2/3	50	54.8	7.1	11.9	26.2	26.7 ± 4.1	25.28 ± 1.43
Thar 16/8/1	48	58.3	6.3	22.9	16.7	24.3 ± 3.5	21.82 ± 1.04
Thar 16/8/2	68	33.8	13.2	36.8	35.3	31.9 ± 4.9	24.43 ± 1.66

3.4. Environmental dose rate determination

The exposure of a mineral grain to ionising radiation causes electron trapping in the grain's crystal structure (Wintle, 2008) and the nature, amount and rate of this ionisation is significant for luminescence age calculation, because it forms the denominator of the age equation, which is known as the Ḋ. The sources of ionising radiation that contributes to the trapped charge in mineral grains can be internal to a grain or externally derived from the environment. Internal Ḋ originates from radioactive elements present within the lattice of the mineral grain and while using quartz, the effect of internal Ḋ is usually considered to be negligible (Preusser *et al.*, 2008; 2009). External Ḋs comprise all radiation coming from the surrounding environment, primarily from isotopes of uranium (^{238}U and ^{235}U) and thorium (^{232}Th) decay chains and potassium (^{40}K) (Aitken, 1985). Radioactive decay from trace concentrations of these radionuclides interact with atoms of surrounding material such as quartz or feldspar. Alpha (α)- particles (two neutrons and two protons) interact strongly with electrons due to their double positive charge and slow velocity. They therefore lose energy quickly and have a short range (~20 μm in quartz) (Aitken 1998). Beta (β)-particles (high energy electron and neutrino) have a much lower linear energy transfer and hence a greater range (~3 mm). Gamma (γ)-rays can travel ~30 cm through sediment (Aitken 1998). An additional component of the external dose is contributed by cosmic rays from outer space. The Earth is shielded from most cosmic rays by the atmosphere and by the Earth's magnetic field. Therefore, only a small proportion reaches the Earth's surface and penetrate sediments. The cosmic dose contribution decreases with depth, particularly rapidly in the uppermost metre (Prescott and Hutton, 1994).

The calculation of the total environmental Ḋ can be summarised by:

$$\dot{D} = \dot{D}_{\alpha} + \dot{D}_{\beta} + \dot{D}_{\gamma} + \dot{D}_{cosmic} \qquad \textit{Equation 2}$$

where $\dot{D}_{\alpha}$ = environmental dose from alpha radiation, which can be internal and external to the grain, $\dot{D}_{\beta}$ = beta dose rate, again internal and external, $\dot{D}_{\gamma}$ = gamma dose rate, and $\dot{D}_{cosmic}$ = cosmic dose rate.

3.4.1. Internal dose rate

Quartz is considered an inert mineral containing very low, if any, levels of U, Th and K (Preusser *et al.*, 2008; 2009). Aitken (1998) suggests that contribution of internal Ḋ from a quartz grain is negligible, which has been verified in a few studies, and has been measured using thick source alpha counting or instrumental neutron activation analysis. Feathers and Migliorini (2001) based on their experiments on Congolese quartz found values of internal Ḋ between 0.01 Gy. ka^{-1} and 0.05 Gy. ka^{-1}, while Vandenberghe *et al.* (2008) calculated an upper limit for the internal Ḋ of 0.01 ± 0.00 Gy. ka^{-1} for Dutch floodplain sediments. In both studies, these very low internal Ḋs make negligible difference to their external Ḋs. Likewise, Armitage and King (2013) used a very low internal Ḋ 0.03 ± 0.006 Gy. ka^{-1} in their studies of hearths from Libya. Whilst internal Ḋs should be measured and included when determining chronologies in low external Ḋ environments, in this study, where the mean Ḋ is 2.30 ± 0.25 Gy. ka^{-1}, the inclusion of an assumed internal Ḋ would have a negligible effect on final Ḋ calculation and has therefore not been included.

3.4.2. External dose rate

As discussed, a sample receives external radiation due to the emission of alpha and beta particles, and gamma rays during radionuclide decay, and cosmic rays. However, for quartz dating where the sample has been etched to remove the alpha irradiated outer layer of the grains, calculation of $\dot{D}_{\alpha}$ is not required. Therefore, the sum of $\dot{D}_{\beta}$, $\dot{D}_{\gamma}$ and $\dot{D}_{cosmic}$ comprises the external $\dot{D}$ for coarse grain quartz ages.

In this thesis, $\dot{D}_{\beta}$ and $\dot{D}_{\gamma}$ were calculated from radionuclide concentrations measured using Inductively Coupled Plasma Mass Spectrometry/Optical Emission Spectrometry (see Appendix C). Across the suite of analysed samples, radionuclide concentrations are relatively consistent (Table 3.8). These values are consistent with the values of Mejdahl (1979), who suggests a typical sample comprises 3 ppm U, 12 ppm Th and 1-2% K ($\dot{D}$ ~1.5-2.2 Gy.ka^{-1}). Radionuclide concentrations were converted into infinite matrix $\dot{D}$s using the conversion factors of Guerin *et al.* (2011). Infinite matrix $\dot{D}$s require adjustments, including grain size, etching and water content. The range of beta particles may be comparable to the diameter of grains under investigation, thus $\dot{D}_{\beta}$ is corrected for grain size attenuation effects, using the attenuation factors of Guerin *et al.* (2012) (see Appendix D). Secondary attenuation caused by chemical etching of quartz grains is adjusted using Bell (1979)'s attenuation factors. $\dot{D}_{\gamma}$ does not require any grain size related attenuation correction, however, moisture in the sediment matrix attenuates both $\dot{D}_{\beta}$s and $\dot{D}_{\gamma}$s which would otherwise reach the grain and contribute to the total $\dot{D}$ (Guérin *et al.*, 2012).

In this thesis, all the samples have a measured water content between 0.1 and 5.2 % (Table B1; Appendix B), and $\dot{D}$s were corrected for using a standard

water content of 5 ± 2 %. The chosen value was considered sensible because of three reasons: 1. previous studies from the Thar used this value (e.g. Thomas *et al.*, 1999; Singhvi and Kar, 2004; Singhvi *et al.*, 2010); 2. the annual rainfall in the study region is less than 400 mm.yr^{-1} with rains occurring over a few spells during monsoon months of July to September. Other than these months, the region remains dry; 3. the samples were dry at the time of collection with very limited signs of water retention shown by deeper samples; therefore, the sampled units were well drained. Nevertheless, it is impossible to accurately measure the concentration of water in the substrate over the buried geologic time, which also means uncertainties in dose rate (and therefore age) calculations are added. The correction of water content for $\dot{D}_\beta$ and $\dot{D}_\gamma$ were made using the equations in Aitken and Xie (1990) following those proposed by Zimmerman (1971) (Appendix D).

The contribution of the cosmic rays to the overall $\dot{D}$ is usually small, however, it should be included in estimates of the external $\dot{D}$ (Aitken, 1985). The contribution from cosmic rays comprises two components- the 'soft' and 'hard' component. The 'soft' component of cosmic radiation, largely electrons, is observed to penetrate shallow depths of up to 167 g.cm^{-2} (Barbouti and Rastin, 1983) about 50 cm of overburden (Aitken, 1985). The 'hard' component, composed of muons, penetrates to greater depths (Aitken, 1985). In this study, $\dot{D}_{cosmic}$ has been calculated following the calculations of Prescott and Hutton (1994). This involves the calculation of the cosmic dose rate at the depth of sampling, calculation of the geomagnetic latitude and the application of a correction of altitude and geomagnetic latitude. A worked example of $\dot{D}_{cosmic}$ calculation is outlined in Appendix D. All $\dot{D}$s calculations were made using the DRAC (v1.2) software of Durcan *et al.* (2015), an open access, web-based

program which enables Ḋ calculation for trapped charge dating applications. All calculations have been made with the assumption that environmental Ḋs have remained unchanged since deposition, and that decay chains are in radionuclide equilibrium. A worked example of Ḋ is presented in Appendix D and demonstrates that the manual and DRAC Ḋ determinations are consistent.

3.4.3. Total environmental dose rate

For the majority of samples, ~50-60 % of Ḋ is derived from $\dot{D}_{\beta}$, and ~30-45 % from $\dot{D}_{\gamma}$. The contribution of $\dot{D}_{cosmic}$ is up to 10 % of total Ḋ which decreases to ~2 % with depth. This is important to note since previous studies from the Thar assumed a constant $\dot{D}_{cosmic}$ of 0.15 ± 0.03 Gy.ka^{-1} throughout a sampled section (Singhvi and Kar, 2004; Thomas *et al.*, 1999; Kar *et al.*, 2001), which would have induced a systematic uncertainty in their Ḋ estimates. In general, the majority of calculated Ḋ values vary between 2.0 and 2.5 Gy.ka^{-1} (Figure 3.15). Sample Thar 16/9/2 has the highest Ḋ (3.24 ± 0.18 Gy.ka^{-1}) that is be attributed to higher K content (and subsequently $\dot{D}_{\beta}$) (Table 3.8). Samples from the northern Thar site IND 14/5 show relatively higher Ḋ values and are comparable to published studies from the region (Saini and Mujtaba, 2010; Durcan *et al.* 2019). The calculated Ḋ values from Jodhpur and Bikaner are consistent with values published in earlier studies from the Thar (e.g. Andrews *et al.*, 1998; Thomas *et al.*, 1999; Kar *et al.*, 2001; Singhvi and Kar, 2004; Dhir *et al.*, 2010).

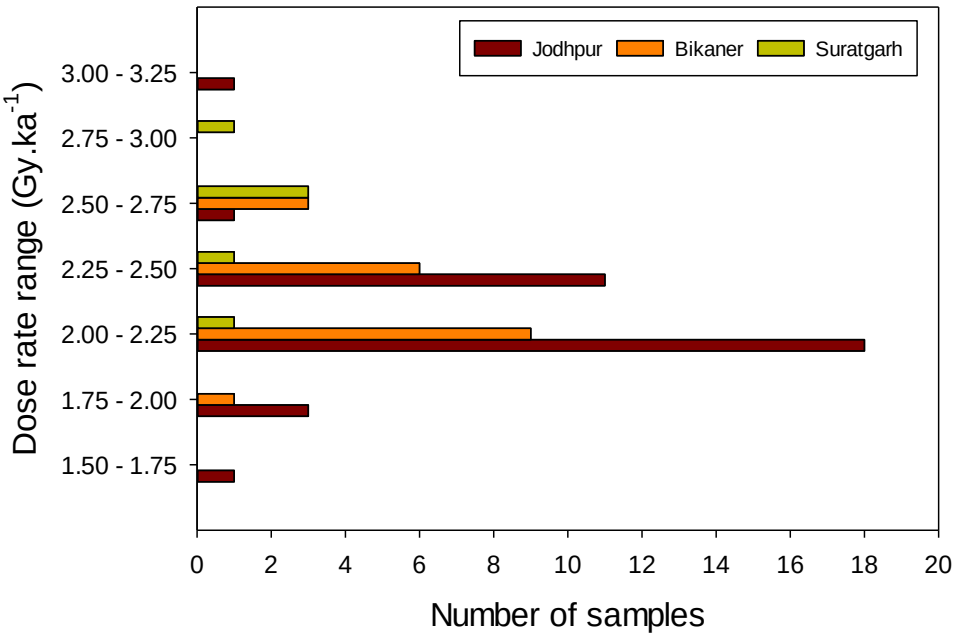


Figure 3.15. Distribution of total Ḋ of samples determined in this study.

Table 3.8. Radionuclide concentrations, beta, gamma and cosmic dose rates, and OSL ages for all samples in this study.

Sample	Depth (m)	U ± 10 % (ppm)	Th ± 10 % (ppm)	K ± 10 % (%)	$\dot{D}_\beta$ (Gy.ka^{-1})	$\dot{D}_\gamma$ (Gy.ka^{-1})	$\dot{D}_{cosmic}$ (Gy.ka^{-1})	Total $\dot{D}$ (Gy.ka^{-1})	Age (ka)
Thar 16/1/1	0.5	0.72	4.66	1.43	1.17 ± 0.11	0.62 ± 0.04	0.21 ± 0.02	2.00 ± 0.12	0.45 ± 0.06
Thar 16/1/2	0.7	1.01	7.86	1.46	1.28 ± 0.11	0.81 ± 0.05	0.19 ± 0.01	2.28 ± 0.12	0.39 ± 0.03
Thar 16/1/4	6.0	0.87	7.76	1.44	1.25 ± 0.11	0.78 ± 0.05	0.10 ± 0.01	2.14 ± 0.12	0.55 ± 0.05
Thar 16/1/5	14.0	1.0	7.83	1.55	1.34 ± 0.12	0.83 ± 0.06	0.05 ± 0.01	2.22 ± 0.13	1.07 ± 0.09
Thar 16/1/6	20.0	0.95	7.39	1.47	1.27 ± 0.11	0.78 ± 0.05	0.03 ± 0.00	2.09 ± 0.12	6.86 ± 0.49
Thar 16/1/7	21.0	0.91	7.41	1.47	1.27 ± 0.11	0.78 ± 0.05	0.03 ± 0.00	2.07 ± 0.12	8.30 ± 0.69
Thar 16/1/8	22.0	1.19	9.14	1.37	1.27 ± 0.10	0.86 ± 0.06	0.03 ± 0.00	2.16 ± 0.12	9.60 ± 0.74
Thar 16/1/9	23.0	0.79	5.47	1.17	1.01 ± 0.09	0.61 ± 0.04	0.03 ± 0.00	1.64 ± 0.10	13.85 ± 1.11
Thar 16/3/1	11.0	1.11	8.76	1.57	1.39 ± 0.12	0.88 ± 0.06	0.07 ± 0.01	2.34 ± 0.13	0.68 ± 0.08
Thar 16/3/2	19.0	1.09	8.18	1.42	1.27 ± 0.11	0.82 ± 0.06	0.03 ± 0.00	2.12 ± 0.12	5.69 ± 0.50
Thar 16/4/1	0.3	0.81	8.10	1.33	1.17 ± 0.10	0.77 ± 0.05	0.22 ± 0.02	2.16 ± 0.11	0.20 ± 0.03
Thar 16/4/2	1.0	0.73	6.51	1.61	1.33 ± 0.12	0.75 ± 0.05	0.18 ± 0.02	2.26 ± 0.13	0.16 ± 0.03
Thar 16/4/4	2.0	0.88	7.05	1.54	1.31 ± 0.11	0.78 ± 0.05	0.16 ± 0.02	2.24 ± 0.13	0.84 ± 0.08
Thar 16/4/6	5.0	0.96	7.40	1.54	1.32 ± 0.11	0.80 ± 0.05	0.11 ± 0.01	2.23 ± 0.13	2.09 ± 0.18
Thar 16/4/7	6.0	1.07	8.11	1.58	1.37 ± 0.12	0.85 ± 0.06	0.10 ± 0.01	2.33 ± 0.13	1.92 ± 0.16
Thar 16/4/8	7.0	1.02	8.66	1.48	1.31 ± 0.11	0.85 ± 0.06	0.09 ± 0.01	2.25 ± 0.13	10.14 ± 0.69
Thar 16/4/10	9.0	0.94	6.37	1.28	1.12 ± 0.10	0.69 ± 0.05	0.08 ± 0.01	1.88 ± 0.11	12.25 ± 0.82
Thar 16/6/1	0.5	1.1	8.87	1.27	1.18 ± 0.10	0.82 ± 0.06	0.21 ± 0.02	2.20 ± 0.11	0.07 ± 0.01
Thar 16/6/5	5.0	0.86	6.92	1.53	1.30 ± 0.11	0.77 ± 0.05	0.11 ± 0.01	2.18 ± 0.13	0.07 ± 0.01
Thar 16/9/1	1.5	1.43	9.97	1.29	1.25 ± 0.10	0.91 ± 0.06	0.17 ± 0.02	2.33 ± 0.12	0.07 ± 0.01
Thar 16/9/2	2.5	1.55	11.43	2.16	1.90 ± 0.16	1.19 ± 0.08	0.15 ± 0.02	3.24 ± 0.18	0.06 ± 0.01
Thar 16/9/4	4.5	0.8	7.43	1.06	0.97 ± 0.08	0.67 ± 0.05	0.12 ± 0.01	1.76 ± 0.09	0.14 ± 0.02

Sample	Depth (m)	U ± 10 % (ppm)	Th ± 10 % (ppm)	K ± 10 % (%)	$\dot{D}_{\beta}$ (Gy.ka^{-1})	$\dot{D}_{\gamma}$ (Gy.ka^{-1})	$\dot{D}_{cosmic}$ (Gy.ka^{-1})	Total $\dot{D}$ (Gy.ka^{-1})	Age (ka)
Thar 16/9/5	5.5	1.00	8.01	1.58	1.36 ± 0.12	0.84 ± 0.06	0.11 ± 0.01	2.31 ± 0.13	0.13 ± 0.01
Thar 16/9/8	8.5	1.12	9.19	1.35	1.24 ± 0.10	0.85 ± 0.06	0.08 ± 0.01	2.18 ± 0.12	3.52 ± 0.34
Thar 16/10/1	1.0	0.91	7.84	1.26	1.13 ± 0.09	0.75 ± 0.05	0.18 ± 0.02	2.06 ± 0.11	0.07 ± 0.01
Thar 16/10/4	3.7	0.84	6.46	1.51	1.27 ± 0.11	0.74 ± 0.05	0.13 ± 0.01	2.14 ± 0.12	0.07 ± 0.01
Thar 16/10/8	8.2	1.08	10.01	1.5	1.36 ± 0.11	0.92 ± 0.06	0.08 ± 0.01	2.36 ± 0.13	0.67 ± 0.07
Thar 16/10/9	9.2	1.32	10.35	1.54	1.42 ± 0.12	0.97 ± 0.07	0.07 ± 0.01	2.47 ± 0.13	5.19 ± 0.51
Thar 16/10/10	10.2	1.18	7.94	1.36	1.23 ± 0.10	0.81 ± 0.05	0.07 ± 0.01	2.11 ± 0.12	5.43 ± 0.40
Thar 18/1/2	1.0	0.85	7.31	1.57	1.33 ± 0.12	0.79 ± 0.05	0.18 ± 0.02	2.30 ± 0.13	0.05 ± 0.01
Thar 18/1/4	2.0	1.08	9.54	1.45	1.31 ± 0.11	0.89 ± 0.06	0.16 ± 0.02	2.36 ± 0.13	0.15 ± 0.03
Thar 17/2/1	0.8	0.72	5.33	1.52	1.24 ± 0.11	0.68 ± 0.05	0.19 ± 0.02	2.10 ± 0.12	0.58 ± 0.05
Thar 17/2/2	0.9	0.78	6.70	1.36	1.17 ± 0.10	0.71 ± 0.05	0.18 ± 0.02	2.06 ± 0.11	4.07 ± 0.44
Thar 17/2/4	3.0	0.89	7.36	1.44	1.25 ± 0.11	0.85 ± 0.05	0.14 ± 0.01	2.24 ± 0.12	8.81 ± 0.71
Thar 17/2/6	5.0	1.24	9.07	1.33	1.24 ± 0.10	0.86 ± 0.06	0.11 ± 0.01	2.21 ± 0.12	8.97 ± 0.67
Thar 17/2/8	7.0	1.38	10.83	1.27	1.25 ± 0.10	0.94 ± 0.06	0.09 ± 0.01	2.28 ± 0.12	8.62 ± 0.64
Thar 17/2/10	9.0	1.08	8.18	1.41	1.26 ± 0.11	0.82 ± 0.05	0.08 ± 0.01	2.15 ± 0.12	> 58
Thar 17/4/1	0.5	1.70	12.72	1.44	1.44 ± 0.11	1.10 ± 0.07	0.21 ± 0.02	2.74 ± 0.14	3.01 ± 0.24
Thar 17/4/2	2.0	1.27	9.47	1.36	1.27 ± 0.10	0.89 ± 0.06	0.16 ± 0.02	2.32 ± 0.12	8.79 ± 0.67
Thar 17/4/6	9.0	1.33	10.36	1.44	1.35 ± 0.11	0.95 ± 0.06	0.08 ± 0.01	2.37 ± 0.13	10.52 ± 0.99
Thar 17/4/8	11.0	1.27	8.66	1.37	1.26 ± 0.10	0.85 ± 0.06	0.06 ± 0.01	2.17 ± 0.12	11.61 ± 0.82
Thar 17/5/1	1.4	0.72	6.06	1.56	1.28 ± 0.11	0.72 ± 0.05	0.17 ± 0.02	2.17 ± 0.13	0.15 ± 0.02
Thar 17/5/2	1.6	1.39	12.37	1.39	1.36 ± 0.11	1.04 ± 0.07	0.17 ± 0.02	2.56 ± 0.13	0.98 ± 0.10
Thar 17/5/4	3.7	0.94	6.75	1.43	1.23 ± 0.11	0.74 ± 0.05	0.13 ± 0.01	2.11 ± 0.12	9.27 ± 0.64
Thar 17/5/6	5.7	0.85	5.53	1.45	1.21 ± 0.11	0.68 ± 0.05	0.11 ± 0.01	2.00 ± 0.12	9.38 ± 0.82
Thar 17/5/8	8.7	1.75	13.53	1.41	1.44 ± 0.11	1.13 ± 0.08	0.08 ± 0.01	2.65 ± 0.13	> 48

Sample	Depth (m)	U ± 10 % (ppm)	Th ± 10 % (ppm)	K ± 10 % (%)	$\dot{D}_\beta$ ($Gy.ka^{-1}$)	$\dot{D}_\gamma$ ($Gy.ka^{-1}$)	$\dot{D}_{cosmic}$ ($Gy.ka^{-1}$)	Total $\dot{D}$ ($Gy.ka^{-1}$)	Age (ka)
Thar 17/6/2	2.0	1.29	10.41	1.43	1.34 ± 0.11	0.95 ± 0.06	0.16 ± 0.02	2.44 ± 0.13	0.34 ± 0.03
Thar 17/6/4	4.0	1.05	8.28	1.47	1.30 ± 0.11	0.83 ± 0.06	0.13 ± 0.01	2.26 ± 0.12	1.65 ± 0.15
Thar 17/6/6	6.0	1.16	8.37	1.34	1.22 ± 0.10	0.82 ± 0.05	0.10 ± 0.01	2.14 ± 0.12	9.38 ± 0.71
Thar 17/6/9	9.5	1.41	10.59	1.39	1.33 ± 0.11	0.96 ± 0.06	0.07 ± 0.01	2.35 ± 0.12	9.39 ± 0.69
IND 14/5/1	2.0	1.80	10.60	1.48	1.43 ± 0.11	1.02 ± 0.07	0.16 ± 0.02	2.61 ± 0.13	7.28 ± 0.52
IND 14/5/2	3.0	1.80	10.10	1.47	1.42 ± 0.11	0.99 ± 0.07	0.14 ± 0.02	2.55 ± 0.13	8.86 ± 0.66
IND 14/5/3	10.0	1.30	7.30	1.47	1.31 ± 0.11	0.81 ± 0.05	0.07 ± 0.02	2.19 ± 0.13	10.51 ± 0.73
IND 14/5/4	11.0	2.30	13.70	1.39	1.48 ± 0.11	1.19 ± 0.08	0.06 ± 0.02	2.74 ± 0.13	10.51 ± 0.64
IND 14/5/5	25.0	2.80	15.50	1.34	1.54 ± 0.11	1.31 ± 0.09	0.02 ± 0.02	2.88 ± 0.13	10.05 ± 0.76
IND 14/5/6	26.0	2.20	11.30	1.36	1.41 ± 0.11	1.07 ± 0.07	0.02 ± 0.02	2.50 ± 0.13	10.33 ± 0.97
Thar 16/2/1	21.0	1.50	13.79	1.43	1.43 ± 0.11	1.12 ± 0.08	0.03 ± 0.02	2.58 ± 0.13	9.53 ± 0.87
Thar 16/2/3	22.0	1.26	9.00	1.34	1.25 ± 0.10	0.86 ± 0.06	0.03 ± 0.02	2.14 ± 0.13	11.83 ± 0.93
Thar 16/8/1	2.0	1.13	9.91	1.22	1.16 ± 0.09	0.86 ± 0.06	0.16 ± 0.02	2.18 ± 0.13	10.01 ± 0.70
Thar 16/8/2	3.0	1.65	10.32	1.36	1.33 ± 0.10	0.96 ± 0.06	0.14 ± 0.02	2.43 ± 0.13	10.04 ± 0.85

3.5. OSL ages

OSL ages in this study have been calculated by the division of the determined D_es by the calculated Ḋs. In total, 60 OSL ages from 14 sites have been calculated. The absolute values of these OSL ages range between 0.05 ± 0.01 ka (Thar 18/1/2) ka and 13.85 ± 1.11 ka (Thar 16/1/9), with most samples dating from within the Holocene. Age uncertainties vary between 6 and 20 %, and the larger uncertainties are associated with the younger ages that have more over-dispersed dose distributions, and lower precision due to dim signals (e.g. Madsen and Murray, 2009). Nevertheless, the uncertainties associated with ages reported in this thesis are considerably lower than that of previously published ages (20-60 %; Singhvi and Kar, 2004). In addition, two samples have been defined as saturated and therefore a minimum age only has been calculated (this is discussion in further detail in Section 5.3.2). The calculated ages are in stratigraphic order within a sampled section and these ages are discussed in site context in chapters 4, 5 and 6.

3.6. Conclusions

The chapter has discussed the three studied dunefield sites in Jodhpur, Bikaner and Suratgarh regions, which fall between 200-400 mm isohyets today, where dunes are stable under natural conditions, therefore, serving as ideal locations to meet the aims and objectives of this study (outlined in Chapter 1). In total, 90 samples were retrieved for OSL dating and sedimentological analyses after intensive sampling from these dunefields, of which 60 samples were dated after adopting a dating strategy to save labour and machine time.

This chapter has further outlined the laboratory treatment and measurement protocols used for D_e determination. From single grain analyses, it has been shown that between 2-4 % of quartz grains per aliquot give a discernible luminescence signal. The modified post-IR blue SAR protocol has been used for D_e determination, and regular dose recovery and pre-heat plateau test results demonstrate the suitability of the selected protocol for dating. Standard rejection criteria were used to screen all signal and remove potentially erroneous D_e determinations prior to sample D_e determination. Examination of dose distributions show that for the majority of samples, over-dispersion is relatively low and hence the CAM model was used to calculate sample D_e. $\dot{D}$ measurements and calculations have also been discussed. Final age calculations for the 60 dated samples show that ages are in good stratigraphic agreement by site, and mostly date to the Holocene. The geomorphological and palaeoenvironmental interpretations of these ages are presented in the following chapters.

Chapter 4: Holocene dune activity in the Thar Desert, India (Paper 1)

This paper has been published in Earth Surface Processes and Landforms (44; pp. 1407-1418; see Appendix E) and the following version has been adopted to reduce repetition (e.g. between figures) across the chapters that are based on papers.

Abstract

The Thar Desert dune system in north-west India and eastern Pakistan provides a rich archive of past environmental, geomorphological and climatic change. Much of the knowledge about the timing of dune accumulation in the Thar stems from scattered and sporadic records, based on older luminescence dating protocols. If the Thar dune record is to be incorporated within a growing multiproxy framework of past climate and environmental dynamics, it is necessary to generate a systematic record of the timing of dunefield accumulation. From this, relationships to climate and other drivers of dune activity may then be better established. To this end, an intensive programme of field sampling and OSL dating was carried out from a dunefield in the east-central Thar Desert. This study presents the first detailed Holocene dune accumulation history from the region, and sheds light on the development of the multi-generational parabolic dune systems. In contrast to previously published work, we identify the importance of the Holocene and the last millennium as periods with a number of preserved accumulation phases. OSL ages suggest that accumulation was persistent during the early and middle Holocene (within 11.7- 5.5 ka), late Holocene (2-1 ka), as well as two major phases in the last millennium (600 – 200 a and within the last 70 a). Potential drivers of dune mobility in the last century include a strong anthropogenic dimension. Rapid net accumulation is recorded in the last 70 years, with rates varying between 2 and 5 m/ year, in an environment where agricultural pressures have increased dramatically with the advent of irrigation schemes expanding into dunefield areas.

Keywords: Thar Desert, optically stimulated luminescence (OSL) dating, parabolic dunes, Holocene, geomorphological change.

4.1. Introduction

The Thar Desert forms an integral part of the arid lands of western India and eastern Pakistan, between the Aravalli hills in the east and the Indus plains to the west. The desert is often considered as the easternmost extension of the vast Saharo-Arabian subtropical desert belt (Singhvi and Kar 2004; Roy *et al.*, 2009), and is dominated by aeolian bedforms of various dimensions and forms. Many sand dune types have been identified in the region, including parabolic, transverse, linear, star and network dunes (Figure 2.4) (Wasson *et al.*, 1983; Kar 1993). The desert is located in a transitional but dominant south-west monsoon regime, which not only controls wind seasonality, precipitation and vegetation cover, but also implies that minor perturbations in monsoon dynamics may impact the geomorphic processes, including aeolian dynamics, in this seasonally semi-arid to arid region. The extensive dune systems in the Thar therefore provide an opportunity to understand temporal changes in aeolian dynamics during the late Quaternary.

The first application of luminescence dating to aeolian sands anywhere occurred in the Thar Desert (Singhvi *et al.*, 1982), and this seminal study inspired a move from qualitative assessments of long term dune accumulation histories to temporally specific records. The Thar was one of the leading deserts in luminescence dating applications to aeolian sediments, and in the 35 years since this first application, numerous dune sites have been dated in the region (e.g. Chawla *et al.*, 1992; Singhvi *et al.*, 1994; Kar *et al.*, 1998; Thomas *et al.*, 1999), with dated records used to address the long-standing debate surrounding the potentially recent anthropogenic origins of the Thar Desert, as suggested in early studies by Piggot (1950) and Bryson and Barreis (1967). However, the sampling

and dating strategies employed in earlier luminescence dating studies focussed largely on accessing deep trenches in basal sediments, often associated with the expansion of irrigation canals into the region, for establishing the antiquity of aeolian episodes and finding major phases of dune accumulations (Kar, 2013; Dhir *et al.*, 2010). More recent studies have tended to focus on the desert margins, within the context of aeolian-fluvial interactions (e.g. Juyal *et al.*, 2006; Saini *et al.*, 2009; Saini and Mujtaba., 2012; Giosan *et al.*, 2012; Shitaoka *et al.*, 2012; Durcan *et al.*, 2019).

To date, the application of systematic and intensive dunefield sampling programmes has been less prevalent in the Thar than in other deserts, such as the Kalahari in Africa (Stone and Thomas, 2008), the Rub' al Khali in Arabia (Leighton *et al.*, 2013; Atkinson *et al.*, 2011) and the Strzelecki and Tirari in Australia (Fitzsimmons *et al.*, 2007). In the Thar, the focus on deeper sequences has potentially resulted in a bias towards older accumulation phases, with relatively younger accumulation phases not sampled. Singhvi and Kar (2004) note that existing data sets provide little opportunity to understand the impact of climate and humans on desert evolution and geomorphological processes during the late Holocene. Interrogation of existing geochronological data is also hampered by a common absence of detailed locational and sampling depth data within published records. In addition, all 146 luminescence ages from the Thar Desert dune systems listed in INQUA dunes atlas chronologic database (Lancaster *et al.*, 2016) utilised multiple aliquot protocols, which are associated with relatively large age uncertainties (e.g. Stokes, 1994). Both instrumental and methodological advances in luminescence dating, including the single aliquot regenerative (SAR) dose protocol (e.g. Murray and Wintle, 2000; 2003; Wintle

and Murray, 2006) and single grain luminescence dating (e.g. Duller, 2003; 2008) provide the potential for more robust age calculation. In the context of geochronological improvements, and rapid anthropogenic land clearance and disturbance in the Thar Desert, conducting a systematic analysis of Thar dune accumulations chronologies becomes an important research priority. Therefore, the aim of this chapter is to present new dune accumulation records from the Thar Desert, following intensive sampling and the application of modern luminescence dating protocols, and to assess spatial variability within a dunefield. This study allows a more temporally-complete assessment of the region's dune accumulation history and provides an insight into the dune evolution in this arid to semi-arid dryland zone.

4.2. Study Site and methods

The aeolian landforms in the Thar are dominated by various types of dunes which cover ~50% of the region (Kar *et al.*, 1993; Moharana *et al.*, 2013), the majority of which occur in western Rajasthan, India (Figure 2.4) and adjoining parts in Pakistan. The present study focusses on the Shergarh-Dechu region in the Arid Western Plain of the central Thar, which is dominated by parabolic dunes. These parabolic dunes form a clustered 'rake-like' appearance (Figure 4.1A), with longer arms in the middle of the parabolic cluster and gradually shorter arms on each side. The arms can be up to 2500 m long, with inter-arm spacing ranging between 150 m and 650 m. These 'rake-like' parabolic dunes have rounded noses which contain more than 35% sand volume in the dunes (Kar *et al.*, 2004). The Shergarh-Dechu region is classified as arid to semi-arid, with mean annual precipitation typically varying between 250 – 400 mm and dunes are relatively stable under natural conditions. In the present-day conditions, winds in the region

increase in strength from March onward, peaking in June and decline after the arrival of monsoonal precipitation in July. This context provides an ideal location for examining the timing and amplitude of spatial changes in aeolian activity in the past and its correlation with variations in monsoonal precipitation.

4.2.1. Site selection and sampling

Five dunes sites (Tinwari, Shergarh, Setrawa, Chamu and Dechu) were sampled to test the spatial variability of dune accumulation histories within the dunefield (Figure 4.1A). Samples were collected from vertical sections, by carefully cutting steps through the nose and arms of the dunes using hydraulic diggers (Figure 4.1B, C). At Tinwari site, samples were collected from the 23 m deep section located in the nose of the dune (Thar 16/1, Thar 16/3). Four samples were collected from the dune arm from a 2 m deep pit, situated 500 m from the dune nose (Thar 18/1). Similarly, at Setrawa samples were collected from a 7 m deep section located in the nose of the dune (Thar 16/6) and another 7 m section from a section in the dune arm, located ~600 m from the nose (Thar 18/2). The samples from dune arms generated very young ages with indiscernible OSL signal sometimes, therefore, at Shergarh (Thar 16/4), Chamu (Thar 16/9) and Dechu (Thar 16/10), samples were collected from 9.0 m, 8.5 m and 10.2 m deep sections respectively, all located near the nose of the dune only. The sediment faces of dug sections were cleaned prior to sampling. Samples were collected by hammering black light tight tubes into the cleared sediment face, and a resolution of 1.0 m interval was adopted where possible taking into account accessibility and sediment collapse risks, with additional sampling carried out to bracket the fine bedding structures observed at the top of the dunes.

4.2.2. Sedimentological analyses

Grain size analyses were conducted using a Malvern Mastersizer Hydro 2000 laser grain analyser and analysed using Gradistat (Blott, 2000) following the method of Folk and Ward (1957). Colour analysis was conducted on oven-dried samples using a Munsell colour chart. Organic and carbonate contents were determined by heating the sediment to 550^{o} C and 950^{o} C respectively, following the process outlined in Heiri *et al.* (2001) (Appendix B).

4.2.3. Luminescence dating

Samples were opened in subdued orange-light conditions in the Oxford Luminescence Dating Laboratory, University of Oxford. The light-exposed sample ends were removed and used for sedimentological analyses and measurement of radionuclide concentrations. Sediments were treated with hydrochloric acid and hydrogen peroxide to remove carbonate and organic matter, and were sieved to isolate the 180-210 µm grain size fraction. Quartz mineral grains were isolated by heavy liquid (sodium polytungstate) density separation. Hydrofluoric acid was used to remove the alpha-irradiated outer surface of the quartz grains. Initial tests indicated feldspar contamination, and therefore samples were treated with fluorosilicic acid for two weeks to reduce persistent feldspar contamination. Sediments were treated with hydrochloric acid after each chemical etch to remove any fluoride precipitate, prior to re-sieving.

OSL measurements were made using Risø DA-15 TL/OSL readers (Bøtter-Jensen *et al.*, 2003), fitted with either blue (470 nm) or green (525 nm) LEDs and ^{90}Sr/^{90}Y beta sources with dose rates varying between 3.5 and 4 Gy/minute. Luminescence signals were detected through a bialkali photomultiplier tube, fitted with 7.5 mm Hoya U-340 filters. A post-IR blue SAR

protocol (Banerjee *et al.*, 2001; Murray and Wintle, 2000) was used to calculate D_e as a further precaution against any residual feldspar contamination. Following pre-heat plateau and dose recovery tests, a pre-heat of 240° C for 10 seconds and a cut-heat of 160° C for 0 s were selected for use. Samples were stimulated with infra-red light (870 nm) at 50° C for 100 s, prior to measurement of the blue/green stimulated luminescence at 125° C for 40 s. Sediment was adhered to aluminium discs using silicon spray and small aliquots were used for all but three samples. Small aliquots had a diameter of 2 mm (~70 grains per disc), medium had a 5 mm diameter (~425 grains) and large aliquots an 8 mm (~1100 grains) (e.g. Heer *et al.*, 2012). Single grain analyses were done on four samples, Thar 16/1/9, 16/4/2, 16/4/10 and 16/10/10, to establish the number of luminescence grains giving light in response to a laboratory beta dose. 500 grains of each of these samples were given a 50 Gy dose and the number of grains giving a luminescence signal discernible above machine background were counted.

Luminescence signals were screened using a standard set of rejection criteria (e.g. Jacobs *et al.*, 2006). Signals were included in D_e calculation when 1) recuperation was either less than 5% (where sample D_e was greater than 1.5 Gy) or 0.25 Gy (for D_es less than 1.5 Gy); 2) the recycling ratio was within 10% of unity including uncertainties (Murray and Wintle, 2003); and 3) test dose signal were at least 3σ greater than the background. Final D_e determinations were calculated using the central age model (CAM) of Galbraith *et al.* (1999), using the R Luminescence package (Kreutzer *et al.*, 2017). In addition, DRTs were carried out on samples Thar 16/1/2, Thar 16/1/7, Thar 16/3/2, Thar 16/4/4, Thar 16/6/1, Thar 16/9/4 and Thar 16/10/10, which provided dose recovery ratios of 0.95 ± 0.05, 0.93 ± 0.06, 0.94 ± 0.07, 0.99 ± 0.06, 1.0 ± 0.10, 0.97 ± 0.07, 0.98 ± 0.10

respectively, indicating that the post-IR blue SAR protocol, analyses and methods used for D_e determination can successfully recover an applied laboratory dose.

Environmental Ḋs were calculated from radionuclide concentrations measured using inductively coupled plasma mass spectrometry at the Scottish University Environmental Research Centre. Infinite-matrix dose rates were calculated using the conversion factors of Guerin *et al.* (2011) and were adjusted for attenuation by grain size (Guerin *et al.*, 2012), chemical etching (Bell,1979) and a moisture content of 5 ± 2 %. The $\dot{D}_{cosmic}$ was calculated according to Prescott and Hutton (1994), and all Ḋ calculations were made using DRAC (v1.2) software of Durcan *et al.* (2015).

Figure 4.1. (A) The location of sampled dune sites Tinwari (26.58397 N, 72.81615 E; 26.579361 N, 72.814240 E), Setrawa (26.60192 N, 72.28866 E; 26.596704 N, 72.285504 E), Shergarh (26.33122 N, 72.28821 E), Dechu (26.81859 N, 72.30316 E) and Chamu (26.66854 N, 72.57005 E); all of which are located within the arid to semi-arid Shergarh-Dechu region located on the Arid Western Plain. (B). A schematic representation of sampling sections within a parabolic dune. (C). An example of the sampled section at Shergarh (Thar 16/4). Samples were collected by cutting steps into the dune section to allow access to undisturbed sediment. An offset sample Thar 16/4/10 offset was collected after calculating the depth profile along the main trench. Inset, an OSL sample tube hammered into the cleared sediment face. The presence of laminations demonstrates a lack of post-depositional disturbance. (D) The schematic view of sampled sections with

OSL ages (ka). Sample depths are in metres. Most sites consisted of homogeneous dune sands, with the exception of some weak laminations, which are indicated by the curved lines.

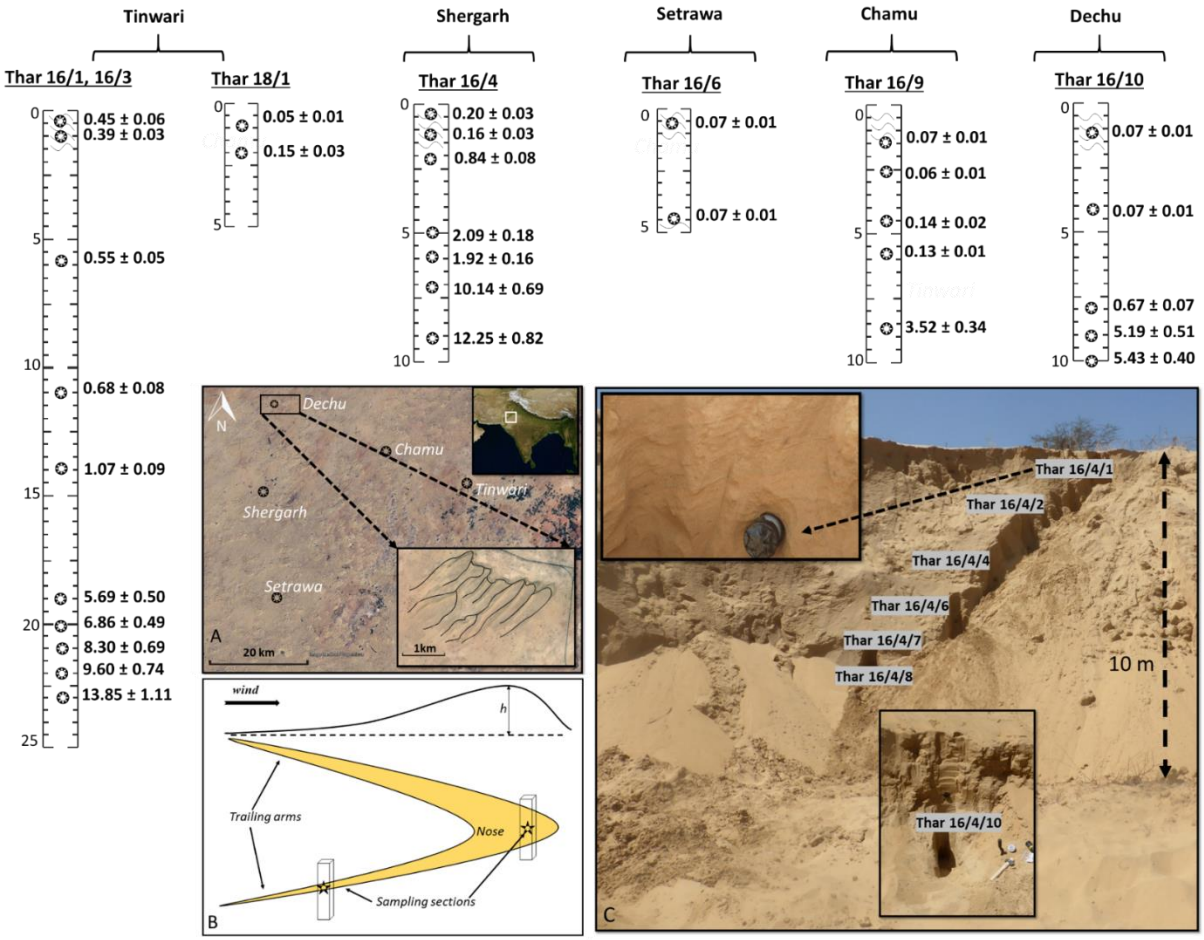


Table 4.1. Sedimentology of samples showing Munsell colour, grain size statistics (in microns), organic and carbonate content

Sample	Munsell colour	Mean (μm)	Sand (%)				Silt (%)	Clay (%)	Sorting*	Skewness**	Kurtosis***	Organic content (%)	Carbonate content (%)
			Coarse	Medium	Fine	Very Fine							
Thar 16/1/1	10 YR 6/6	185.5	0	25.4	64.5	10.1	0	0	1.478 (MWS)	-0.109 (FS)	1.123 (L)	0.88	0.64
Thar 16/1/2	10 YR 6/4	198.2	0	24.2	67.8	7.9	0	0	1.386 (WS)	-0.001 (S)	0.965 (M)	0.72	0.92
Thar 16/1/4	10 YR 5/4	172.1	0	12.3	71	16.6	0	0	1.380 (WS)	-0.002 (S)	0.962 (M)	0.56	0.84
Thar 16/1/5	10 YR 5/4	177.6	0.1	22.6	55.8	14.2	6.8	0.5	1.895 (MS)	-0.300 (FS)	1.844 (VL)	0.84	1.07
Thar 16/1/6	10 YR 5/4	171.9	0	20.7	56.5	10.5	11.5	0.8	2.084 (PS)	-0.386 (VFS)	2.255 (VL)	1.54	1.38
Thar 16/1/7	10 YR 5/4	173.8	0	21.1	56.8	10.4	10.8	0.8	2.054 (PS)	-0.376 (VFS)	2.238 (VL)	1.15	1.5
Thar 16/1/8	10 YR 6/4	162.3	0	10.5	66.5	17.2	5.7	0.1	1.739 (MS)	-0.305 (VFS)	2.077 (VL)	0.92	3.32
Thar 16/1/9	10 YR 6/4	189.4	0.1	25.6	57.8	8	8.1	0.4	1.917 (MS)	-0.345 (VFS)	2.186 (VL)	1.15	3.12
Thar 16/3/1	10 YR 7/4	186.9	0.3	26.2	54.5	13.7	5.2	0	1.763 (MS)	-0.232 (FS)	1.513 (VL)	0.79	1.1
Thar 16/3/2	10 YR 7/4	152.5	0	18.4	51.9	15	13.6	1.1	2.287 (PS)	-0.420 (VFS)	2.099 (VL)	1.75	1.82
Thar 16/4/1	10 YR 6/6	229.9	1.1	40.2	54	4.7	0	0	1.446 (MWS)	-0.004 (S)	0.949 (M)	0.69	0.87
Thar 16/4/2	10 YR 6/4	224.4	2	38	52.4	7.6	0	0	1.509 (MWS)	0.006 (S)	0.944 (M)	0.53	0.71
Thar 16/4/4	10 YR 6/4	193.6	0.1	24.5	63.7	11.7	0	0	1.437 (MWS)	0.011 (S)	0.954 (M)	0.62	2.96
Thar 16/4/6	10 YR 6/4	203.3	0.7	31.2	55.2	10.7	2.2	0	1.528 (MWS)	-0.030 (S)	0.980 (M)	0.79	0.76
Thar 16/4/7	10 YR 6/4	189.2	0.4	26.9	54.6	9	8.2	0.9	2.035 (PS)	-0.340 (VFS)	2.207 (VL)	0.95	1.02
Thar 16/4/8	10 YR 6/4	193.6	0.4	27.3	56.7	9.6	5.5	0.4	1.851 (MS)	-0.285 (FS)	1.923 (VL)	0.79	1.31
Thar 16/4/10	10 YR 6/4	184.3	0	20	65.8	14.2	0	0	1.426 (MWS)	0.001 (S)	0.946 (M)	0.66	2.71

Sample	Munsell colour	Mean (μm)	Sand (%)				Silt (%)	Clay (%)	Sorting*	Skewness**	Kurtosis***	Organic content (%)	Carbonate content (%)
			Coarse	Medium	Fine	Very Fine							
Thar 16/6/1	10 YR 5/4	190.2	0	23	64.4	12.6	0	0	1.433 (MWS)	0.004 (S)	0.946 (M)	0.78	1.41
Thar 16/6/5	10 YR 5/4	212.7	1	35	52.8	9.8	1.3	0	1.525 (MWS)	-0.039 (S)	0.959 (M)	0.78	1.38
Thar 16/9/1	10 YR 7/4	269.8	5.6	52	39.6	1.8	0.9	0	1.491 (MWS)	-0.021 (S)	0.951 (M)	0.99	1.33
Thar 16/9/2	10 YR 7/4	197.3	0.1	26	63.4	10.5	0	0	1.430 (MWS)	-0.003 (S)	0.957 (M)	0.68	1.4
Thar 16/9/4	10 YR 7/4	192	0	23.6	64.3	12	0	0	1.431 (MWS)	--0.002 (S)	0.951 (M)	0.76	1.45
Thar 16/9/5	10 YR 7/4	187.1	0.7	26.2	53.7	15.4	3.9	0.1	1.606 (MWS)	-0.065 (S)	1.045 (M)	0.71	1.44
Thar 16/9/8	10 YR 6/4	168.7	0.2	22.1	52.1	14.1	10.4	1.1	2.194 (PS)	-0.369 (VFS)	2.140 (VL)	1.53	1.48
Thar 16/10/1	10 YR 5/4	200.3	0	24.8	68.3	6.9	0	0	1.374 (WS)	0.001 (S)	0.956 (M)	0.69	1.05
Thar 16/10/4	10 YR 5/4	196.2	0	23.1	68.7	8.2	0	0	1.383 (WS)	0.002 (S)	0.963 (M)	0.71	1.09
Thar 16/10/8	10 YR 5/4	219.2	0.5	35.4	58.6	5.5	0	0	1.423 (MWS)	0.002 (S)	0.958 (M)	0.61	0.79
Thar 16/10/9	10 YR 5/4	189	0.6	27.7	52.1	12.3	6.5	0.2	1.904 (MS)	-0.277 (FS)	1.759 (VL)	0.76	1
Thar 16/10/10	10 YR 5/4	183.9	0.1	24.6	56.2	13	6.1	0	1.806 (MS)	-0.271 (FS)	1.691 (VL)	1.64	1.53
Thar 18/1/2	10 YR 5/4	178.6	0	15	71.3	13.7	0	0	0.462 (WS)	0.001 (S)	0.957 (M)	0.46	0.77
Thar 18/1/4	10 YR 5/4	166.5	0	8.2	74.9	16.9	0	0	0.424 (WS)	-0.001 (S)	0.973 (M)	0.54	0.81

* MWS= moderately well sorted, WS= well sorted, MS= moderately sorted, PS= poorly sorted.

** FS= finely skewed, VFS= very finely skewed, S= symmetrical.

*** L= leptokurtic, VL= very leptokurtic, M= mesokurtic.

Table 4.2. Summary OSL data. D_e, $\dot{D}$, and ages are shown to two decimal places, with all calculations made prior to rounding. All dates are relative to the year 2018. D_es were measured from small aliquots of sample with the exception of Thar 16/4/1 and 16/4/2 (medium aliquots) and Thar 16/4/10 (large aliquots).

Sample	Depth (m)	Discs accepted (measured)	Over-dispersion (%)	CAM D_e (Gy)	Beta $\dot{D}$ ($Gy.ka^{-1}$)	Gamma $\dot{D}$ ($Gy.ka^{-1}$)	Cosmic $\dot{D}$ ($Gy.ka^{-1}$)	Envir $\dot{D}$ ($Gy.ka^{-1}$)	Age (ka)
Thar 16/1/1	0.5	20 (28)	47.2 ± 8.1	0.90 ± 0.10	1.17 ± 0.11	0.62 ± 0.04	0.21 ± 0.02	2.00 ± 0.12	0.45 ± 0.06
Thar 16/1/2	0.7	25 (32)	19.2 ± 3.7	0.88 ± 0.06	1.28 ± 0.11	0.81 ± 0.05	0.19 ± 0.01	2.28 ± 0.12	0.39 ± 0.03
Thar 16/1/4	6	28 (46)	28.7 ± 4.3	1.18 ± 0.07	1.25 ± 0.11	0.78 ± 0.05	0.10 ± 0.01	2.14 ± 0.12	0.55 ± 0.05
Thar 16/1/5	14	22 (48)	28.9 ± 4.5	2.38 ± 0.15	1.34 ± 0.12	0.83 ± 0.06	0.05 ± 0.01	2.22 ± 0.13	1.07 ± 0.09
Thar 16/1/6	20	37 (48)	24.1 ± 2.9	14.31 ± 0.58	1.27 ± 0.11	0.78 ± 0.05	0.03 ± 0.00	2.09 ± 0.12	6.86 ± 0.49
Thar 16/1/7	21	27 (38)	30.0 ± 4.1	17.21 ± 1.01	1.27 ± 0.11	0.78 ± 0.05	0.03 ± 0.00	2.07 ± 0.12	8.30 ± 0.69
Thar 16/1/8	22	22 (38)	25.1 ± 3.9	20.71 ± 1.13	1.27 ± 0.10	0.86 ± 0.06	0.03 ± 0.00	2.16 ± 0.12	9.60 ± 0.74
Thar 16/1/9	23	30 (42)	28.6 ± 3.8	22.70 ± 1.26	1.01 ± 0.09	0.61 ± 0.04	0.03 ± 0.00	1.64 ± 0.10	13.85 ± 1.11
Thar 16/3/1	11	20 (44)	39.7 ± 8.4	1.60 ± 0.17	1.39 ± 0.12	0.88 ± 0.06	0.07 ± 0.01	2.34 ± 0.13	0.68 ± 0.08
Thar 16/3/2	19	20 (29)	29.3 ± 4.8	12.07 ± 0.82	1.27 ± 0.11	0.82 ± 0.06	0.03 ± 0.00	2.12 ± 0.12	5.69 ± 0.50
Thar 16/4/1	0.3	20 (42)	63.4 ± 16.0	0.44 ± 0.09	1.17 ± 0.10	0.77 ± 0.05	0.22 ± 0.02	2.16 ± 0.11	0.20 ± 0.03
Thar16/4/2	1	20 (45)	22.7 ± 13.7	0.36 ± 0.08	1.33 ± 0.12	0.75 ± 0.05	0.18 ± 0.02	2.26 ± 0.13	0.16 ± 0.03
Thar 16/4/4	2	25 (32)	31.9 ± 4.9	1.89 ± 0.13	1.31 ± 0.11	0.78 ± 0.05	0.16 ± 0.02	2.24 ± 0.13	0.84 ± 0.08
Thar 16/4/6	5	21 (30)	30.2 ± 4.7	4.67 ± 0.31	1.32 ± 0.11	0.80 ± 0.05	0.11 ± 0.01	2.23 ± 0.13	2.09 ± 0.18
Thar 16/4/7	6	24 (45)	26.5 ± 4.3	4.47 ± 0.26	1.37 ± 0.12	0.85 ± 0.06	0.10 ± 0.01	2.33 ± 0.13	1.92 ± 0.16

Sample	Depth (m)	Discs accepted (measured)	Over-dispersion (%)	CAM D_e (Gy)	Beta Ḋ ($Gy.ka^{-1}$)	Gamma Ḋ ($Gy.ka^{-1}$)	Cosmic Ḋ ($Gy.ka^{-1}$)	Envir Ḋ ($Gy.ka^{-1}$)	Age (ka)
Thar 16/4/8	7	27 (38)	20.2 ± 2.9	22.84 ± 0.91	1.31 ± 0.11	0.85 ± 0.06	0.09 ± 0.01	2.25 ± 0.13	10.14 ± 0.69
Thar 16/4/10	9	31 (52)	19.1 ± 2.7	23.03 ± 0.84	1.12 ± 0.10	0.69 ± 0.05	0.08 ± 0.01	1.88 ± 0.11	12.25 ± 0.82
Thar 16/6/1	0.5	21 (68)	62.5 ± 16.0	0.16 ± 0.03	1.18 ± 0.10	0.82 ± 0.06	0.21 ± 0.02	2.20 ± 0.11	0.07 ± 0.01
Thar 16/6/5	5	22 (52)	72.0 ± 14.5	0.15 ± 0.03	1.30 ± 0.11	0.77 ± 0.05	0.11 ± 0.01	2.18 ± 0.13	0.07 ± 0.01
Thar 16/9/1	1.5	20 (32)	39.3 ± 10.3	0.16 ± 0.02	1.25 ± 0.10	0.91 ± 0.06	0.17 ± 0.02	2.33 ± 0.12	0.07 ± 0.01
Thar 16/9/2	2.5	26 (35)	64.1 ± 12.1	0.18 ± 0.03	1.90 ± 0.16	1.19 ± 0.08	0.15 ± 0.02	3.24 ± 0.18	0.06 ± 0.01
Thar 16/9/4	4.5	21 (37)	55.1 ± 9.3	0.24 ± 0.03	0.97 ± 0.08	0.67 ± 0.05	0.12 ± 0.01	1.76 ± 0.09	0.14 ± 0.02
Thar 16/9/5	5.5	21 (29)	31.8 ± 6.1	0.31 ± 0.02	1.36 ± 0.12	0.84 ± 0.06	0.11 ± 0.01	2.31 ± 0.13	0.13 ± 0.01
Thar 16/9/8	8.5	25 (52)	37.6 ± 5.6	7.65 ± 0.61	1.24 ± 0.10	0.85 ± 0.06	0.08 ± 0.01	2.18 ± 0.12	3.52 ± 0.34
Thar 16/10/1	1	22 (50)	25.8 ± 9.6	0.15 ± 0.01	1.13 ± 0.09	0.75 ± 0.05	0.18 ± 0.02	2.06 ± 0.11	0.07 ± 0.01
Thar 16/10/4	3.7	26 (50)	61.0 ± 12.3	0.15 ± 0.02	1.27 ± 0.11	0.74 ± 0.05	0.13 ± 0.01	2.14 ± 0.12	0.07 ± 0.01
Thar 16/10/8	8.2	21 (50)	35.5 ± 6.7	1.58 ± 0.14	1.36 ± 0.11	0.92 ± 0.06	0.08 ± 0.01	2.36 ± 0.13	0.67 ± 0.07
Thar 16/10/9	9.2	20 (26)	28.8 ± 4.8	12.80 ± 1.04	1.42 ± 0.12	0.97 ± 0.07	0.07 ± 0.01	2.47 ± 0.13	5.19 ± 0.51
Thar 16/10/10	10.2	30 (64)	26.2 ± 3.7	11.45 ± 0.56	1.23 ± 0.10	0.81 ± 0.05	0.07 ± 0.01	2.11 ± 0.12	5.43 ± 0.40
Thar 18/1/2	1	23 (30)	73.6 ± 13.5	0.11 ± 0.02	1.33 ± 0.12	0.79 ± 0.05	0.18 ± 0.02	2.30 ± 0.13	0.05 ± 0.01
Thar18/1/4	2	22 (26)	76.2 ± 12.1	0.35 ± 0.06	1.31 ± 0.11	0.89 ± 0.06	0.16 ± 0.02	2.36 ± 0.13	0.15 ± 0.03

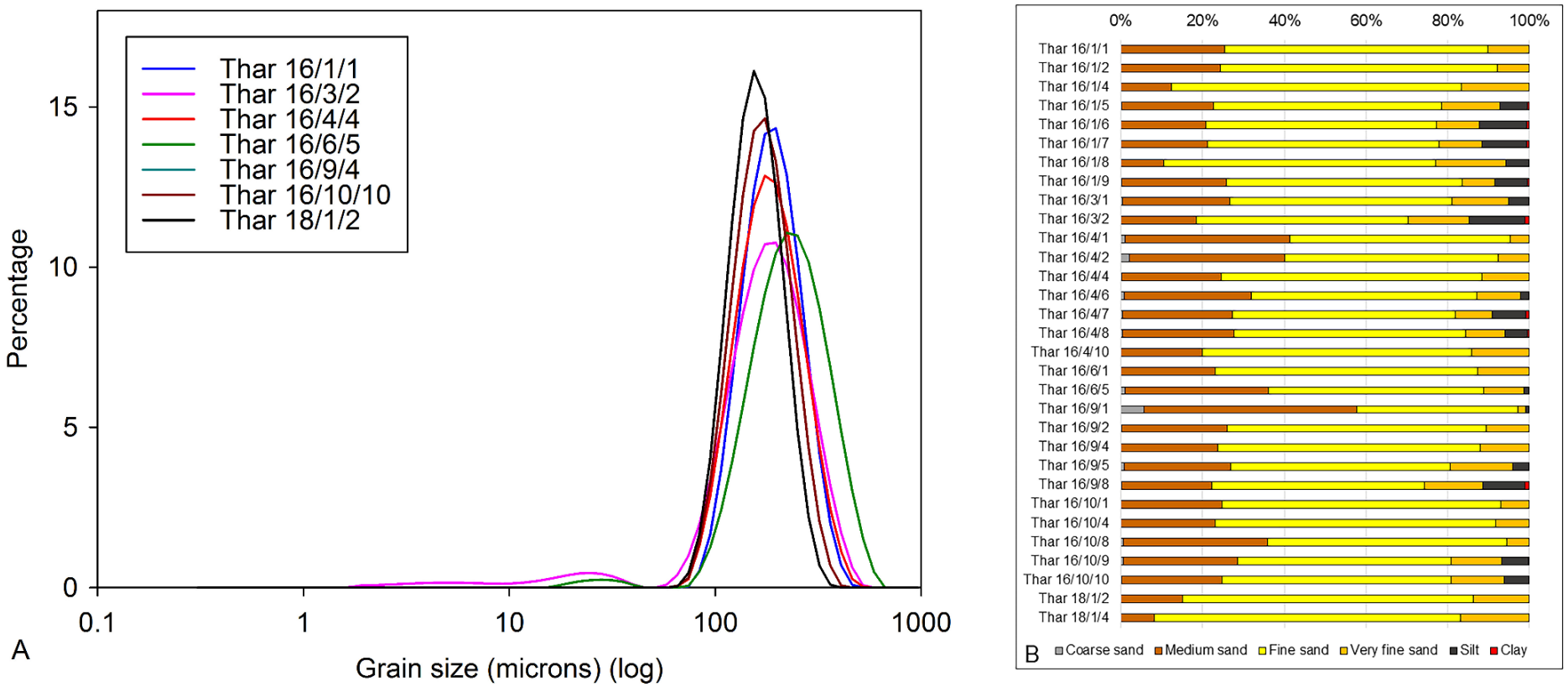


Figure 4.2. (A) Grain size distribution data for selected samples, and (B) The percentage distribution of different grain sizes for all the samples.

4.3. Results

4.3.1. Sedimentology

All sampled dune sections have a unimodal, dominantly medium to fine sand distribution with mean size varying between ~150 and ~270 μm (Table 4.1; Figure 4.2A). Silt component ranges between 0 and 15%, and there is less than 1.1% clay for all samples (Figure 4.2B). At each site, the upper part of the sampled parabolic crests consists exclusively of unimodal fine sand (for example, samples Thar 16/1/1, 16/1/2, 16/4/1, 16/4/2, 16/9/1, 16/9/2, 16/10/1) with an absence of finer silt and clay (Figure 4.2B), reflecting proximity to an active dune surface. Samples are negatively skewed, mostly very leptokurtic or mesokurtic, and sorting of the younger sediments varies between moderately well to well sorted (Table 4.1). The dune sediments are homogenous in colour within each dune, with yellowish brown as the predominant colour (Table 4.1). Generally, the samples contain 0.5 % to 2.0 % carbonates (by weight), except for some basal units at Tinwari and Shergarh, which have slightly higher contents (~3 %) and are adjacent to underlying pedogenic calcretes. The organic content in the samples is less than 2.0 % by weight (Table 4.1).

4.3.2. Luminescence dating

OSL age data are presented in Table 4.2 and in Figure 4.1. OSL signals from the sample were sufficiently bright to differentiate from machine background levels (Figure 4.3). Use of the fast ratio (Durcan and Duller, 2011) suggests the dominance of the fast component in the initial part of the OSL signal. Single grain analyses of samples showed that between 2.4 and 4.0 % of measured grains gave a discernible luminescence signal after a 50 Gy dose, suggesting that on

average, small aliquots in this study should have 2-3 luminescing grains per disc, medium 10-17 grains, and large 26-45 grains. Therefore, in the presence of very few luminescing grains per multi-grain aliquot, any heterogeneity in dose distributions will be identifiable.

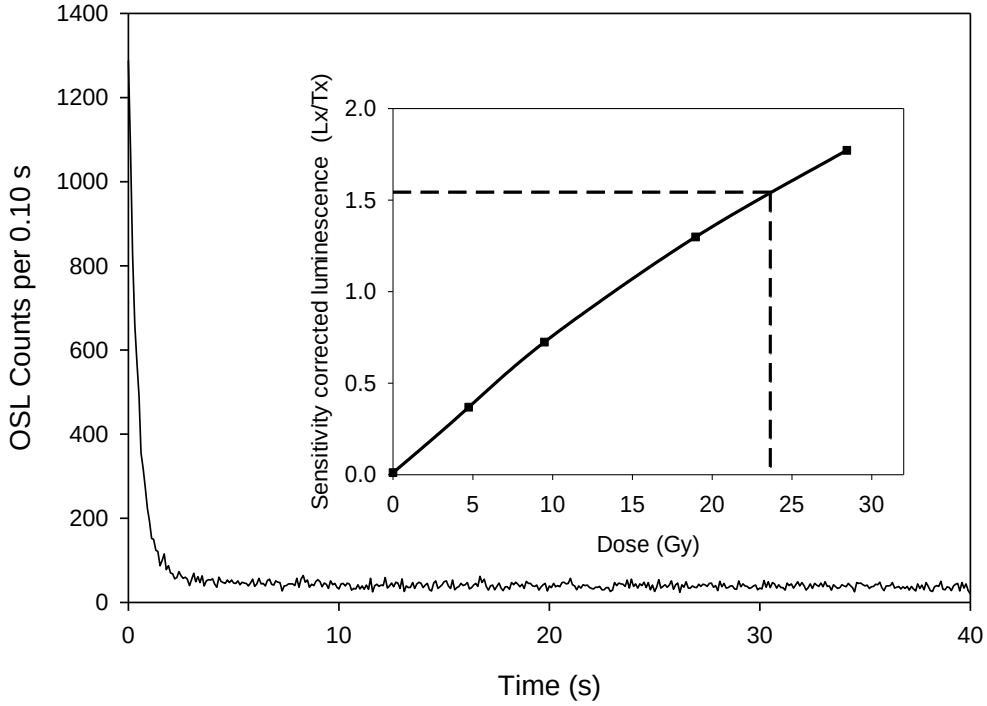


Figure 4.3. An example of OSL signal from a small aliquot of sample Thar 16/1/8. Inset, corresponding DRC fitted using an exponential function.

Over-dispersion (σ_d) or heterogeneity in D_e distributions beyond that expected from intrinsic variability, for this suite of ages is relatively low, and ranges between 20 % and 35 % (including uncertainties) for samples with D_es greater than 1 Gray (Table 4.2). Variability in D_e distributions can originate from a multitude of factors including partial bleaching of sediments prior to deposition (e.g. Olley *et al.*, 2004), environmental dose rate heterogeneity (e.g. Nathan *et al.*, 2003), and post-depositional mixing like bioturbation (e.g. Bateman *et al.*,

2007). Given the depositional environmental in this study, partial bleaching of sediments prior to deposition is unlikely, given the efficiency of bleaching during aeolian transport, and asymmetry in D_e distributions is not observed. Visual evidence for post depositional mixing was not observed during sampling, and undisturbed sediments were targeted for dating (e.g. Figure 4.1C, inset). Therefore, mild microdosimetric variability is hypothesised (but not confirmed) to explain variability in D_es. σ_d for young samples (where D_e < 1 Gy) is slightly higher (35 – 75 %; Table 4.2), although this should be expected in the mathematic context of low D_es providing small denominators, which amplifies σ_d values. Large σ_d values are commonly seen in young samples, and for example, Arnold *et al.* (2009) report σ_d values up to 208 % for samples less than 350 years of age. For the majority of samples measured in this study, dose distributions vary symmetrically around a central value (e.g. Figure 4.4), and therefore the central age model of Galbraith *et al.* (1999), has been selected for use, following the approach of Durcan *et al.* (2019) and references therein.

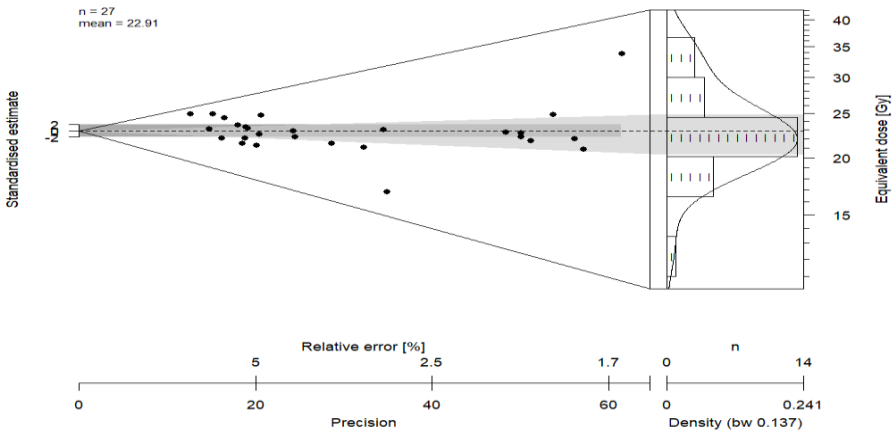


Figure 4.4. Abanico Plot (plotted using ShinyPlot; Dietze *et al.*, 2016) of individual D_es of sample Thar 16/4/8. The sample D_e of 22.84 ± 0.91 Gy is shown by the dashed line and ±2σ by the grey shaded area.

The suite of OSL ages in this study presents evidence of a dynamic aeolian environment throughout the Holocene in the east-central part of the Thar Desert. The oldest sample is Thar 16/1/9 at Tinwari, which is the easternmost sample site (Figure 4.1A), dating to 13.85 ± 1.11 ka at a 23 m depth. For the most part, ages are consistent with depth (within uncertainties), and there is a general trend for phases of large units of up to ~6 m of sediment to accumulate within relatively short periods of time, with more distinctive, older phases recorded at greater depth; for example, at Chamu the upper 5.5 m section accumulated in last 150 years and is underlain by 3.52 ± 0.34 ka old unit (Thar 16/9/8). Likewise, at Tinwari, the upper 6 m dune section accumulated at the rate of ~1 m/century whilst the lower 3 m dune section accumulated at ~0.4 m/ka (Table 4.2; Figure 4.5). Several periods of dune accumulation have been identified including at least one site in each dune recording dune activity and accumulation in the last 500 years (Figure 4.5). The sampled sand dunes at Tinwari (Thar 16/1/1, Thar 16/1/2 and Thar 16/1/4), Shergarh (Thar 16/4/1 and Thar 16/4/2) and Dechu (Thar 16/10/8) all record accumulation between 200 and 600 years, while samples from Setrawa (Thar 16/6/1 and Thar 16/6/5), Chamu (Thar 16/9/1, Thar 16/9/2) and Dechu (Thar 16/10/1 and, Thar 16/10/4) and Tinwari (18/1/2) all provide ages that show the accumulation of 3-4 m of dune sand in second half of twentieth century (0.07 ± 01 ka, 0.06 ± 01 ka and 0.05 ± 0.01 ka; Figure 4.5).

4.4. Discussion

4.4.1. Holocene dune activity in the region

The oldest OSL ages of 13.85 ± 1.11 ka and 12.25 ± 0.82 ka, observed at Tinwari and Shergarh demonstrate the relative youth of dune bodies in the region. Since these ages were determined from samples collected from the noses of parabolic dunes, these pre-Holocene records are more likely to reflect last period of reworking. The presence of sparse calcified nodules and plant roots also attest to the greater stability of these dunes (Wasson *et al.*, 1983). Previously published luminescence ages from the Thar, even though with large errors, do not include evidence of dune building during the early Holocene (Singhvi and Kar, 2004; Prasad and Enzel, 2006; Figure 4.6), yet this had been identified as a period marked by strong south-west monsoon winds based on the enhanced upwelling off the coast of Oman (Gupta *et al.*, 2003; Figure 4.7). The sites investigated in this study provide evidence of early Holocene aeolian activity and dune building, with sand accumulation ages between 10.14 ± 0.69 ka (Thar 16/4/8) and 9.60 ± 0.74 ka (Thar 16/1/8), and accumulation continuing 6.86 ± 0.49 ka (Thar 16/1/6). The dunes experienced accumulation in the middle Holocene at ~5 ka (Thar 16/3/2, Thar 16/10/9 and Thar 16/101/10) and then at ~3.5 ka (Thar 16/9/8). These ages coincide with a period of lower precipitation between 5.0-3.5 ka, as recorded in the annually laminated (varved) marine records of north-eastern Arabian Sea (von Rad *et al.*, 1999; Figure 4.7).

The east-central part of the Thar Desert was previously thought to have stabilised after ~3.5 ka, with more recent dune accumulation confined to the presently arid western Thar (Kar *et al.*, 1998; Thomas *et al.*, 1999). Kar *et al.* (2004) noted very little trace of dune accumulation from ~5 ka onward in the

eastern and southern part of the desert. Our data identify widespread late Holocene dune accumulation in the eastern Thar as well (1.92 ± 0.16 ka at Thar 16/4/7 and 1.07 ± 0.09 ka at Thar 16/1/5). Recent studies by Durcan *et al.* (2019) have also identified dune accumulation in the northern margin of the desert, along the Ghaggar-Hakra palaeochannel, at ~1.9 ka and ~2.2 ka, linking dune activity with the gradual drying of the fluvial channel. Together, the suite of ages from different regions provides an emerging picture of widespread aeolian accumulation in the late Holocene. Establishing the precise spatial extent of Thar Desert dune activity at this time will require additional new records of dune accumulation timing form further regions in the system.

Thomas *et al.* (1999) and Singhvi and Kar (2004) noted that existing data sets provide little opportunity to establish whether dune activity had been a feature of recent centuries. Of the previously published luminescence ages from dunes in the region, only one age, from Chamu (Thomas *et al.*, 1999) is from the last one thousand years, and this is a modern age of 0.06 ± 0.01 ka, with others falling predominantly in the 10-100 ka period (Figure 4.6). By intensively sampling dune profiles, our study has identified at least two recent phases of dune accumulation, between 600 and 200 years ago and very recently, in the last 70 years (Figure 4.5). It is notable that other precipitation proxy records available for this part of Asia, like the marine core proxy rainfall record of Von Rod *et al.* (1999) from the Arabian Sea or the oxygen-isotope record from a stalagmite from southern Oman (Fleitmann *et al.*, 2003) identify reduced rainfall 600-200 years ago (Figure 4.7). Closer to the study area, Singhvi and Kar (2004) noted that the Luni River, ~100 km distant, did not record any flooding during this period.

The twentieth century ages, recorded in the dunes as a result of preservation bias towards younger sediments (Bailey and Thomas, 2014), indicate the sensitivity of parabolic dunes to environmental disturbances. These ages coincide with India's independence, expansion of irrigational network and mechanised farming in the most arid districts, and the subsequent rise in human population in the desert region, which together have increased the potential for activation of dune sands. Degradation of natural vegetation has been widespread since then, as most of the permanent pasture lands in dunefield areas were very severely exploited for fuelwood and fodder. Uprooting of sand binder shrubs species, like *Calligonum polygonoides* and *Leptadenia pyrotechnica*, to make way for crops, has also aided sand transport (Kar, 2009). Unrestricted over-pumping of groundwater to support both livestock and arable agriculture is resulting in the gradual emptying of aquifers, and increasing salinity in the region (Rodell *et al.*, 2009), which bears a direct implication for the stability of parabolic dunes in the region. The expansion of agriculture including an increase in intensification has been known to reactivate parabolic dunes in Nyírség in Hungary (Kiss *et al.*, 2012) and Horqin sandfields in Inner Mongolia, China (Zhao *et al.*, 2007), and the acceleration of dune accumulation in the last 70 years (Figure 4.5) suggests that the same has occurred in this part of the Thar Desert.

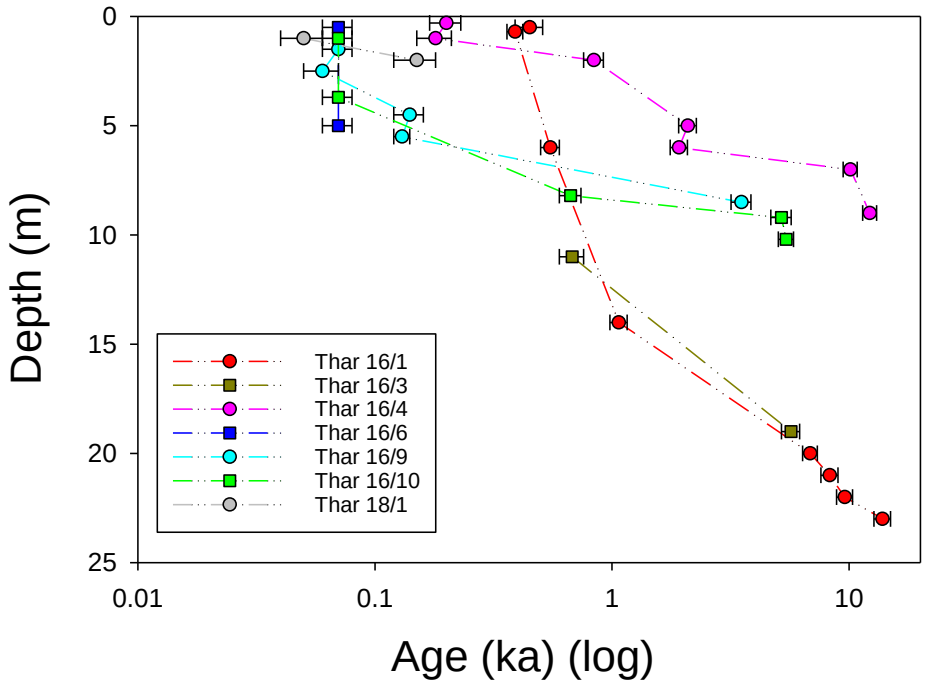


Figure 4.5. Age-depth plot for the OSL ages presented in Table 4.2. The steep lines denote the timing of periods of high dune accumulation, for example, Thar 16/1 shows a high accumulation between 500-1000 years ago at the rate of ~1.6 m/century. Likewise, the vertical line of Thar 16/6 shows the rapid accumulation of 5 m of dune 70 years ago.

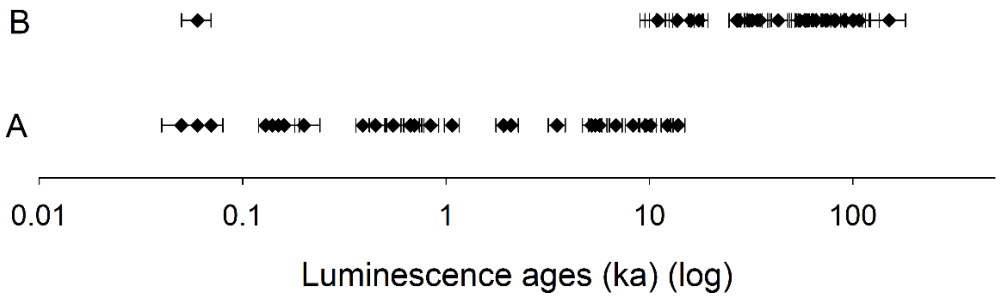


Figure 4.6. Comparison of the OSL dune age data from this study (A) with the previously published TL and OSL ages (B) from the Shergarh-Dechu basin in the Thar Desert (Thomas *et al.*, 1999 (n=2); Singhvi and Kar, 2004 (n=16); Dhir *et al.*, 2010 (n=13)).

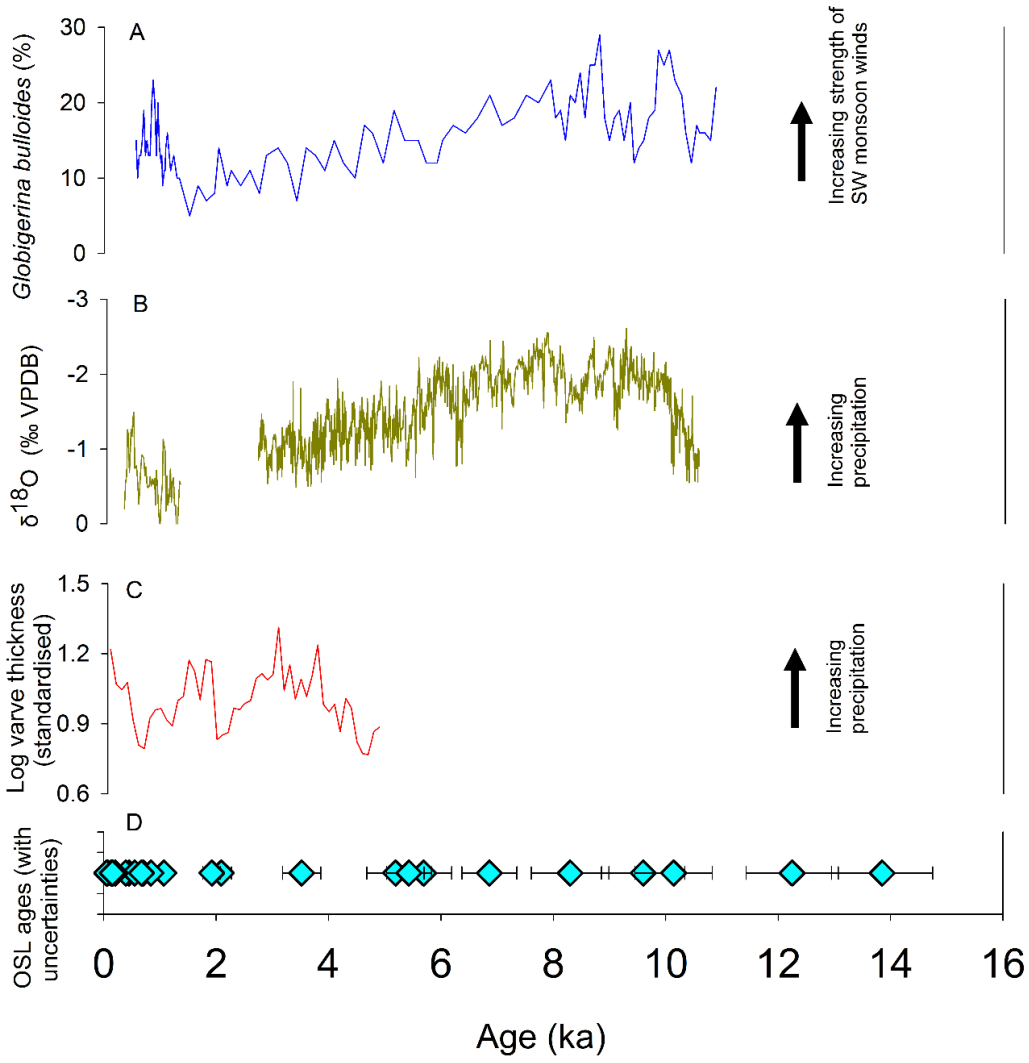


Figure 4.7. (A) *G. bulloides* percentage from core ODP 723 A core off Oman coast in the Arabian Sea, as a proxy for SW Monsoon wind strength (Gupta *et al.*, 2003). (B) Oxygen-isotope record from a stalagmite in Qunf, southern Oman reflecting as a proxy of monsoon precipitation for the periods 10.3-2.7 ka and 1.4-0.4 ka (Fleitmann *et al.*, 2003). (C) A reconstruction of annually laminated (varved) marine sediment thickness record from cores SO 90 39KG/56KA, NE Arabian Sea, as a proxy for monsoon precipitation (von Rad *et al.*, 1999). (D) The OSL ages and uncertainties calculated in this study.

4.4.2. Implications for the timing and evolution of parabolic dunes

Parabolic dunes tend to form in partially vegetated aeolian landscapes and are sensitive to both environmental and human controls. The formation, development and morphology of parabolic dunes involve complex interactions between an initial surface blowout, the strength and directional variability of the wind, the source and amount of sand involved, the density and type of vegetation, and salinity and levels of groundwater (Pye and Tsoar, 1990; Nield and Baas, 2008; Hugenholtz and Wolfe, 2006; Langford *et al.*, 2009). Under deteriorating vegetation cover conditions and anthropogenic disturbances, parabolic dunes can transform to more mobile, non-parabolic dunes (e.g. transverse dunes, barchans; Hack, 1941; Anton and Vincent, 1986). Once reactivated, the mobility of these dunes may last for decades or centuries depending upon the wind energy in the arid environments (Bullard *et al.*, 1997; Hugenholtz and Wolfe 2005).

In the study region, dune reactivation in recent times and subsequent aeolian accumulation has led to the multi-generational development of parabolic dunes. The luminescence chronology presented shows that the parabolic dunes in the region accumulated during late Pleistocene-Early Holocene. The parallelism of dune arms implies prevailing winds have been unidirectional since their accumulation (e.g. Wasson *et al.*, 1983). Modern disturbances linked to land use pressures have resulted in the reactivation of sand dunes and this has resulted in formations of new crescentic features atop parabolic dunes (Figure 4.8), which Wadhawan (1998) described as products of low energy flows. These superimposed features show migratory characteristics (Figure 4.8) in the way that they propagate further downwind, presenting an advancement of the bedform, and producing sets of weak laminations, which are observed on the top of all the

sampled dune sites (Figure 4.1C, inset). The quantification of the migratory trait is hampered by a Government restriction on access to aerial photography however, the luminescence chronology confirms that these superimposed features are episodic and young in nature. At Setrawa dune site, large aliquots from two samples collected from a dune arm (at 2.5 m and 7.5 m respectively) 650 m away from the nose, generated very low, indiscernible OSL signals and therefore demonstrate that these superimposed features have been deposited very recently. This was also the case at Tinwari, where two samples collected from a dune arm (at 1 m and 2 m depth) 500 m from the dune nose were accumulated less than 150 years ago (Thar 18/1/2 and Thar 18/1/4). The absence of older ages at such depths from these arms not only shows evidence of a large scale recent reactivation, but also suggests that these migratory superimposed features are depositing sand near the nose of the dunes. As a result, the sets of parabolic dunes are developing high transverse wall-like features (C↔D, Figure 4.9), which act as major zone of accumulation. The OSL ages show rapid net accumulation in recent times on the top half of these wall-like features, resting unconformably on the top of older, stabilised aeolian deposits. Such features are similar to the barchanoid-parabolic transitional dunes described recently by Yan and Baas (2017) using simulation results from the Extended-DECAL (Discrete Eco-geomorphic Aeolian Landscapes model of Nield and Baas (2008) and Baas and Nield (2010) and empirical data from fieldwork in Inner Mongolia, China. Although the transition of parabolic dunes to other dune types has been observed in various dune systems around the world (Pye and Tsoar, 1990), there has been very little investigation of them; the majority of which are based on aerial photographs (Yan and Baas, 2015). This study from a

parabolic dunefield in the Thar presents OSL dating as a powerful chronometric tool to understand geomorphic transformations of dunes over longer time scales.

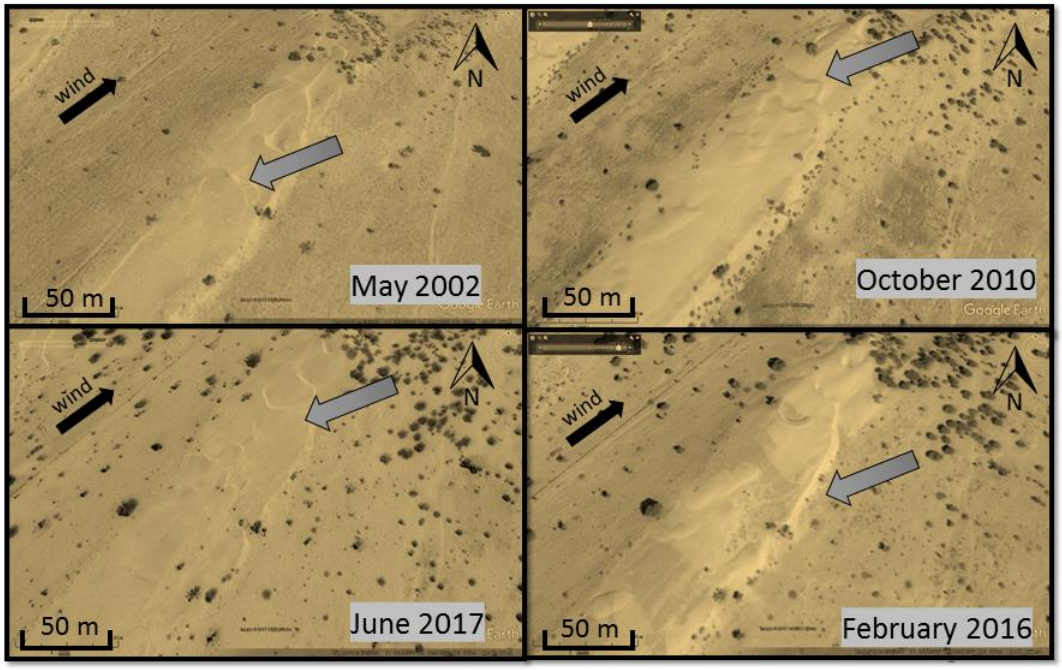


Figure 4.8. Meso-scale ephemeral transverse accretionary dune forms forming on the top of a parabolic dune arm in Dechu (Thar 16/10). The grey arrows point at their forward propagation over the past 15 years (clockwise). Satellite imagery courtesy of 2018 Google Earth Pro© 2018.

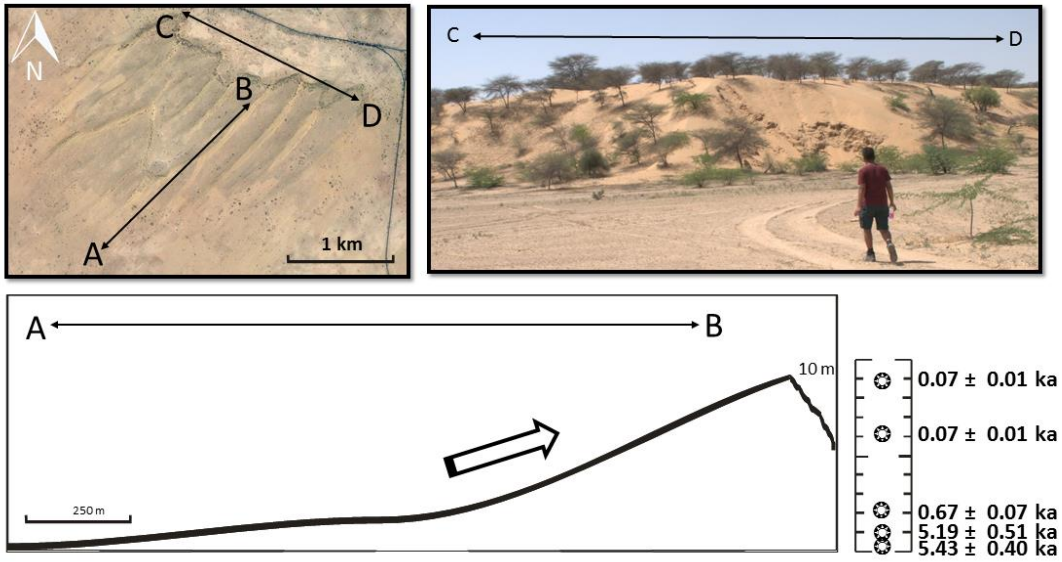


Figure 4.9. The NW-SE alignment of the transverse wall-like feature (C↔D) and their forepart appearance at Dechu (Thar 16/10). Note, the rapid ~4 m dune accumulation in last 70 years in the downwind direction, potentially caused by formation and movement of Meso-scale ephemeral transverse features as shown in Figure 4.8 .

4.5. Conclusions

This study has presented a new history of desert dune accumulation in the eastern-central Thar Desert by applying OSL dating to a series of intensively sampled sections through dune sedimentary bodies. It demonstrates that the development of dunes in this region has been both more complex and more recent than previous investigations have suggested. The main parabolic dunefield present today is largely a function of late Pleistocene-early Holocene dune accumulation, which is significantly more recent than the previous chronologies presented by Singhvi and Kar (2004) and Dhir *et al.* (2010). Furthermore, there is a strong record of dune activity and disturbance in recent

millennia and centuries, particularly during the last 70 years when a significantly expanded human presence in the landscape coincides with the widespread disturbance of dune surfaces and the development of superimposed transverse bedforms. These new bedforms seem to favour the formation of wall-like transverse features downwind. The history of the Thar Desert dune landscape demonstrates the interplay of natural and anthropogenic processes in landscape development, and the susceptibility of this marginally arid region to land use pressures today.

The chapter has presented the first dunefield based Holocene records of dune accumulation by investigating a parabolic dunefield in the central Thar. However, to test spatial variability of dune accumulation histories across the desert and address RQ1, another dunefield investigation is required. Therefore, the following Chapter 5, continuing the systematic fieldwork approach and robust dating protocols adopted in this Chapter 4, investigates a linear dunefield in the northern Thar.

Chapter 5: Analysis of late Quaternary linear dune development in the Thar Desert, India. (Paper 2)

This paper has been published in Geomorphology (344; pp. 90-98; see Appendix F) and the following version has been adopted to reduce repetition (e.g. between figures) across the chapters that are based on papers.

Abstract

Linear dunes are the most widespread dune type worldwide and act as important geoproxies of late Quaternary environmental change in deserts. They are less common in the Thar Desert, India than other dune types, especially parabolic forms, and to date their development history is poorly understood. Here we investigate a linear dunefield in the northern Thar through analysis of a series of excavated full dune profile sites and the application of optically stimulated luminescence (OSL) dating to provide chronometric control. Results show that linear dunes have been present since at least ~58 ka and were active throughout much of the Holocene. The early Holocene, a period marked by strong ISM winds (e.g., Gill *et al.*, 2017), has been shown as the last major phase of dune accumulation recorded in all sites, with ages ranging from ~11.6-8.6 ka. Two spatially restricted records of dune accumulation have also been identified during the later part of Holocene: ~4-3 ka and ~2-1 ka, attributed to localised reworking within the dunes. The suite of luminescence ages generated from the study region confirms the principle recognised in other dunefields (e.g., the southwest Kalahari; Stone and Thomas, 2008) and theoretically (Bailey and Thomas, 2014) that age records from individual dunes are unlikely to capture the developmental history of dunefields.

Keywords: *Thar Desert, optically stimulated luminescence (OSL) dating, linear dunes, the Holocene, geomorphological change.*

5.1. Introduction

A range of dune forms are present in the Thar Desert including parabolic, linear, transverse, star and network (e.g. Wasson *et al.*, 1983; Kar, 1993; Moharana *et al.*, 2013; Figure 2.4). The organisation and orientation of these dunes reflects the role of dominant south-west monsoon winds, which have governed aeolian dynamics regionally during the late Quaternary. The presence of superimposed forms, for example young meso-scale dunes on older, bigger parabolic dunes (Srivastava *et al.*, 2019b) attests to a more complex history of dune dynamics in the Thar.

Linear dunes, which are the most common desert dune type worldwide, including palaeo-dunes in semi-arid and arid landscapes (Lancaster, 1982; Tsoar, 1989) are relatively uncommon in the Thar. These dunes cover an area of approximately 11,200 km^2, representing around 7.5 % of all aeolian landforms in the Thar, where parabolic dunes are the most commonly observed dune type (Wasson *et al.*, 1983; Kar, 1993; Moharana *et al.*, 2013). Thar linear dunes occur mostly in the border zone between India and Pakistan in Jaisalmer district in the western part of the desert (Kar, 1987). Other studies have mapped smaller areas of linear dunes in the northern Thar near Bikaner (Saxena and Singh, 1976; Kumar *et al.*, 1993) and the central Thar near Jodhpur (Verstappen, 1968; Kar, 1993) (Figure 2.4). Many of these smaller dunefields, however, have since been flattened to make way for the expansion of irrigated agriculture, removing landforms and prohibiting their analysis.

Linear dunes in the Thar have often been considered as an ‘old system’ (e.g. Pandey *et al.*, 1964; Kar, 1993; Singhvi and Kar, 2004; Kar, 2014) with natural vegetation forming an integral part of the dune bodies. The length of these

dunes varies across the Thar from more than 10 km in Jaisalmer to 1-2 km in Bikaner and includes dunes forms which vary from Y-junctions to clusters of 5-8 linear dunes joining at acute angles which gradually merge with surrounding parabolic or transverse dunefields (Kar, 1987, 1993, 2014). The Y-junction pattern is similar to that of vegetated linear dunes in the north-western Negev (Tsoar and Moller, 1986; Tsoar *et al.*, 2008) and the south-western Kalahari (Thomas and Shaw, 1991; Bullard *et al.*, 1995).

Linear dunes have the potential to offer long-term records of past aeolian episodes because of their accumulatory nature (Thomas 1992; Livingstone and Thomas, 1993; Munyikwa, 2005; Telfer *et al.*, 2010), and thus are considered important geoproxy records (Telfer and Hesse, 2013; Thomas, 2013). The accumulation histories of linear dunes reconstructed using luminescence dating have been frequently and consistently used for palaeoenvironmental reconstructions in dryland environments, notably in the southern Africa (e.g. Stokes *et al.*, 1997, O'Connor and Thomas, 1999, Telfer and Thomas, 2007, Stone and Thomas, 2008), Australia (e.g. Lomax *et al.*, 2003, Fitzsimmons *et al.*, 2007), Israel (Roskin *et al.*, 2011a,b) and the Arabian Peninsula (e.g. Glennie and Singhvi, 2002; Atkinson *et al.*, 2013; Leighton *et al.*, 2013). As a result, almost a third of the luminescence ages from drylands listed in the INQUA dunes atlas chronologic database are from linear dunes (Lancaster *et al.*, 2016). In contrast, there are no ages in the database from linear dunes in the Thar Desert because the majority of chronometric studies to date have focussed on parabolic dunes (Thomas *et al.*, 1999; Kar *et al.*, 2001; Singhvi and Kar, 2004; Dhir *et al.*, 2010; Srivastava *et al.*, 2019b). The aim of this work, therefore, is to apply a spatially intensive sampling strategy and modern luminescence dating techniques to

develop a linear dunefield chronology from the Thar and integrate it into existing knowledge of the geomorphic evolution of the Thar dunes and regional palaeoenvironmental interpretations arising from such results.

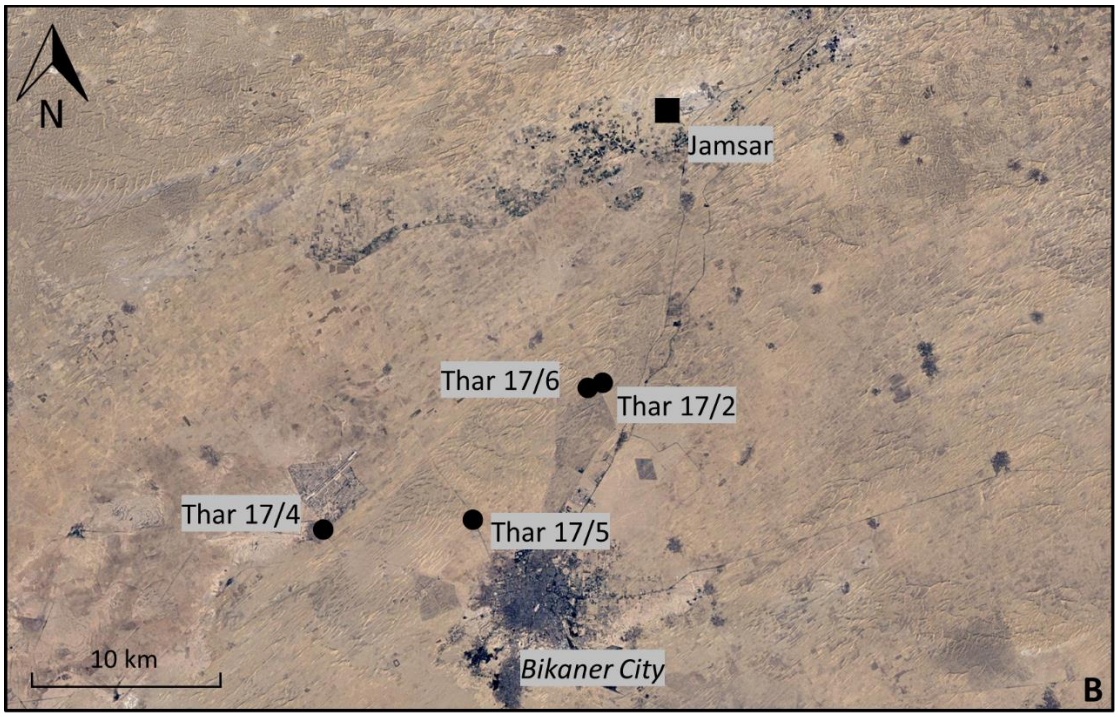


Figure 5.1. Sampled linear dune sites (closed circles): Thar 17/2 (28.13728 N, 73.34283 E), Thar 17/4 (28.03315 N, 73.20950 E), Thar 17/5 (28.06017 N, 73.26852 E) and Thar 17/6 (28.13641 N, 73.33286 E) in Bikaner dunefield in the northern Thar. See Figure 2.4 for the distribution of dunefields and the location of Bikaner linear dunefield in the northern Thar.

5.2. Study sites and methods

5.2.1. Study sites

The focus of this study is a ~500 km^2 area of the linear dunefield in the Bikaner area of the northern Thar (Figure 5.1). This area was selected because of its central location, accessibility, and representativeness, based on Google Earth assessment of the linear dunes in the Thar. The Bikaner dunefield today comprises a semiarid to arid landscape with a mean annual precipitation of 200-300 mm and an interannual rainfall coefficient of variation of 47 %. The dunes here are colonised to a varying degree by natural vegetation such as *Lasiurus sindicus, Capparis decidua, Calligonum polygonoides etc.* Dunes range in height from 5 m to 20 m above the interdune areas and are <10 km in crestline length. The orientation of these dunes is in the SW direction controlled by the dominant ISM winds (Figure 5.2A).

To identify the timing of periods of linear dune accumulation, field sampling for luminescence dating was conducted at four sites across the dunefield (Figure 5.1): Jaisalmer Bypass (Thar 17/2 and Thar 17/6), Nal (Thar 17/4) and Bajrang Dohra (Thar 17/5) sites. The two Jaisalmer Bypass sites, Thar 17/2 and Thar 17/6, are located <500 m apart near the northern edge of the dunefield. The other two sites, Thar 17/4 and Thar 17/5 fall in the central and south-central part of the dunefield. These were sampled to explore spatial and temporal variability in dune accumulation histories, with the number of sites analysed reflecting accessibility, the logistics of excavating exposures, and the number of samples generated that could effectively be dated while ensuring each sample location was represented by enough samples to capture accumulation histories. The sampled linear dunes are 9-12 m in height relative to the adjacent interdune area and aligned in the

dominant direction of monsoon winds. At all four sites, the dune axis was targeted for sampling to obtain dune core sediment presumed to have preserve the maximum thickness of sediments within the dune bodies, and to be least affected by lateral dune movement. Sampled sections were excavated on the crest of these dunes using hydraulic excavators until a hard, calcrete rich layer, suggesting the base of the dune, was reached. The base of the dune was reached at sites Thar 17/2, 17/4 and 17/5, but not at Thar 17/6, where risk of sediment collapse prevented sampling. The dunes were composed of homogeneous, usually structureless sand with some fine laminations preserved in the top part of sampled profiles. Sediment faces in the excavated pits were cleaned prior to sampling for optically stimulated luminescence (OSL) dating. All samples were taken at least 0.5 m below the modern dune surfaces and 0.5 m above a hard, calcrete layer, by hammering black light-tight tubes into the cleaned sediment face. Sampling was performed at a 1 m interval unless field examination revealed changes in stratigraphy or sedimentology, in which case additional sampling was carried out to bracket such features.

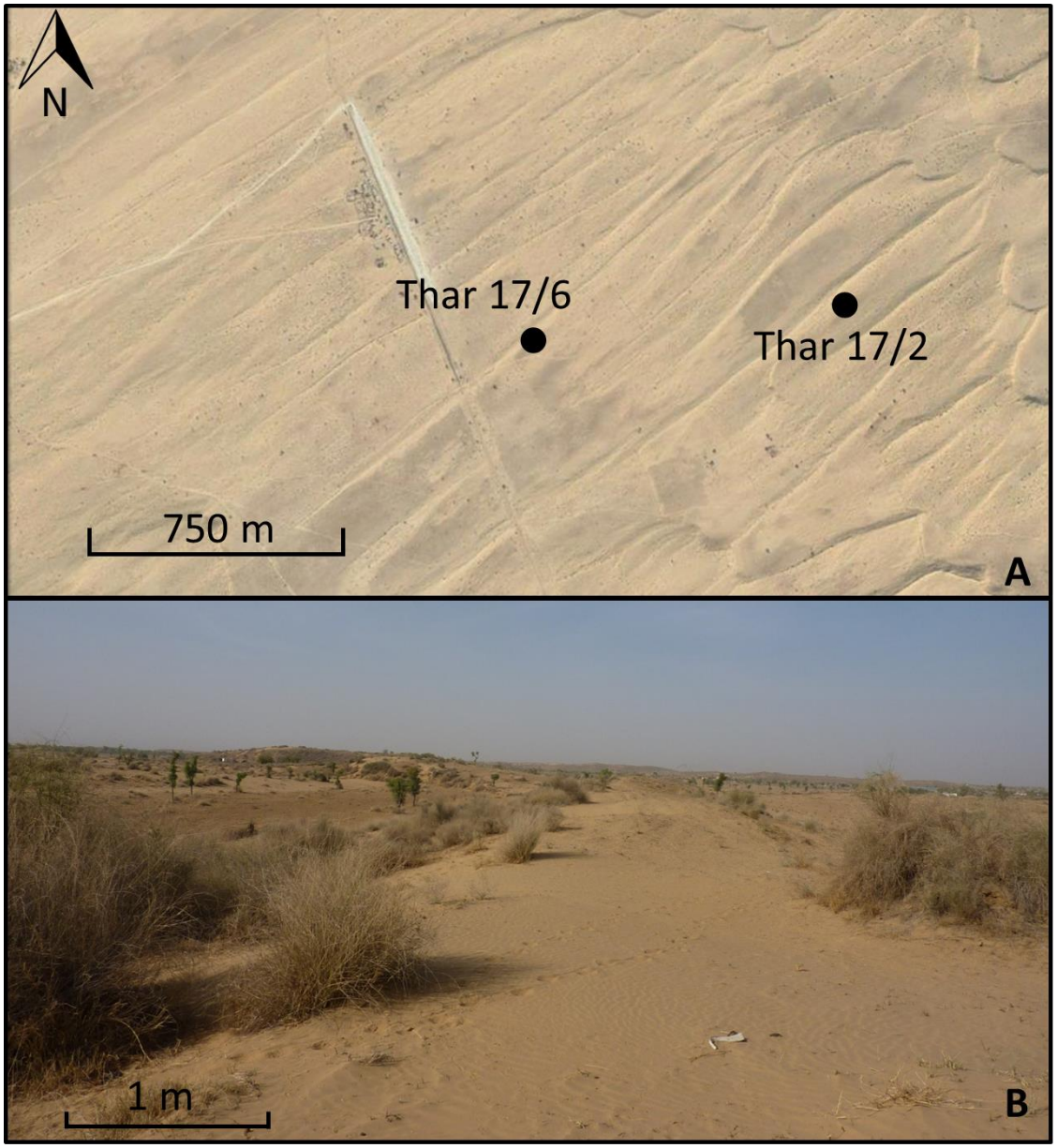


Figure 5.2. A. Linear dune pattern in the Bikaner dunefield and location of two studied sites. B. Landscape at site Thar 17/2. The photo is taken from the linear dune crest facing in NE direction.

5.2.2. Sedimentological analyses

Grain size analyses, a routine laboratory step to identify sediment characteristics, were conducted using a Malvern Mastersizer Hydro 2000 laser analyser with wet dispersion. Statistics were calculated using Gradistat (Blott and Pye, 2001) following the method of Folk and Ward (1957). Colour analysis was conducted on oven-dried samples using a Munsell colour chart. Organic and carbonate content were determined using sequential loss on ignition at 550 °C and 950 °C (Heiri *et al.*, 2001) and expressed as a percentage of the sample weight (Appendix B).

5.2.3. Sediment preparation for luminescence dating

Samples were opened and prepared in subdued orange light conditions in the Oxford Luminescence Dating Laboratory. Prior to preparation of sediment for OSL dating, light-exposed sediments from the sample tube ends were removed and reserved for Ḋ and sedimentological measurements. Sediments for luminescence dating were treated with hydrochloric acid and hydrogen peroxide to remove carbonate and organic matter, and sieved to isolate the 180-210 μm sized particles which was the modal grain size fraction and hence most appropriate to represent the bulk. Quartz mineral grains were removed from the bulk sample using sodium polytungstate density separation, which was followed by chemical etching using hydrofluoric acid to remove the alpha-irradiated outer surface of the quartz grains and fluorosilicic acid to remove persistent feldspar contamination. After chemical etching, hydrochloric acid was used to remove any fluoride precipitate, prior to re-sieving. Fully prepared dry sediment was mounted onto aluminium discs as a 2 mm (small aliquot) monolayer consisting of ~70 grains (Heer *et al.*, 2012) using Silkospray silicone oil.

5.2.4. Equivalent dose determination

D_e measurements were made using Risø DA-15 TL/OSL readers (for full reader specification see Srivastava *et al.*, 2019b) and a post-infrared blue single aliquot regenerative (SAR) dose protocol (Banerjee *et al.*, 2001). Following pre-heat plateau and DRTs, a pre-heat of 240°C for 10 s and a cut-heat of 160°C for 0 s were selected for use. The protocol comprised an infrared light (870 nm) stimulation at 50°C for 100 s prior to measurement of the blue-light stimulated ultra-violet luminescence signals at 125°C for 40 s. DRTs on samples Thar 17/2/4, 17/4/8, 17/5/1, 17/6/2, and 17/6/6, provided ratios of 0.94 ± 0.04, 0.95 ± 0.04, 1.00 ± 0.06, 1.00 ± 0.07, and 0.96 ± 0.05, respectively, indicating the suitability of the applied protocol. To ascertain the average number of luminescing signals, single grain analyses of samples on samples Thar 17/2/4, Thar 17/4/2, Thar 17/4/8, Thar 17/5/6, Thar 17/6/6 and Thar 17/6/9 was undertaken, and showed that between 2.4 and 5.0 % of the measured 500 grains gave a discernible luminescence signal after a 50 Gy dose.

Luminescence signals were included in final D_e calculation when the following rejection criteria were satisfied: 1) recuperation less than 5 % (where sample D_e was greater than 1.5 Gy) or 0.25 Gy (for D_es less than 1.5 Gy); 2) recycling ratio within 10 % of unity, including uncertainties (Murray and Wintle, 2003); and 3) test dose signals 3σ greater than the background. Final D_e determinations for each sample were based upon at least 20 accepted aliquots and were calculated in the R Luminescence package (Kreutzer *et al.*, 2017) using the central age model (CAM) (Galbraith *et al.*, 1999).

5.2.5. Dose rate determination

Radionuclide concentrations (^{232}Th, ^{238}U and ^{40}K) were measured using inductively coupled plasma mass spectrometry at the Scottish University Environmental Research Centre, East Kilbride. Infinite-matrix dose rates were calculated using the conversion factors of Guerin *et al.* (2011) and were adjusted for attenuation by grain size and chemical etching using the datasets of Guerin *et al.* (2012) and Bell (1979) respectively, as well as a moisture content of 5 ± 2 %. Following Prescott and Hutton (1994), $\dot{D}_{cosmic}$ were determined from sample longitude, latitude, altitude, and depth. All Ḋ calculations were made using the DRAC (v1.2) software of Durcan *et al.* (2015).

5.3. Results

5.3.1. Sedimentology

Sedimentological data are provided in Table 5.1. The samples are consistent in colour within each dune. The majority of samples are unimodal (Figure 5.3A), predominantly composed of medium to fine sand, with silt and clay components varying between 0 - 23.5 % and 0 - 1.2 % respectively (Figure 5.3B). Mean grain sizes are within the range of ~105–220 μm, comparable with linear dune sediments, for example in north-eastern Rub' al Khali in Arabia (Leighton *et al.*, 2013) and the north-western Negev (Roskin *et al.*, 2011a). Most samples are well to moderately well sorted with symmetrical and mesokurtic distributions (Table 5.1). The organic content by weight is less than 2 %, while carbonate content by weight increases with depth in a section, varying between ~1 and ~5 %. These organic and carbonate values are consistent with other recently reported values from Thar parabolic dune sands (Srivastava *et al.*, 2019b).

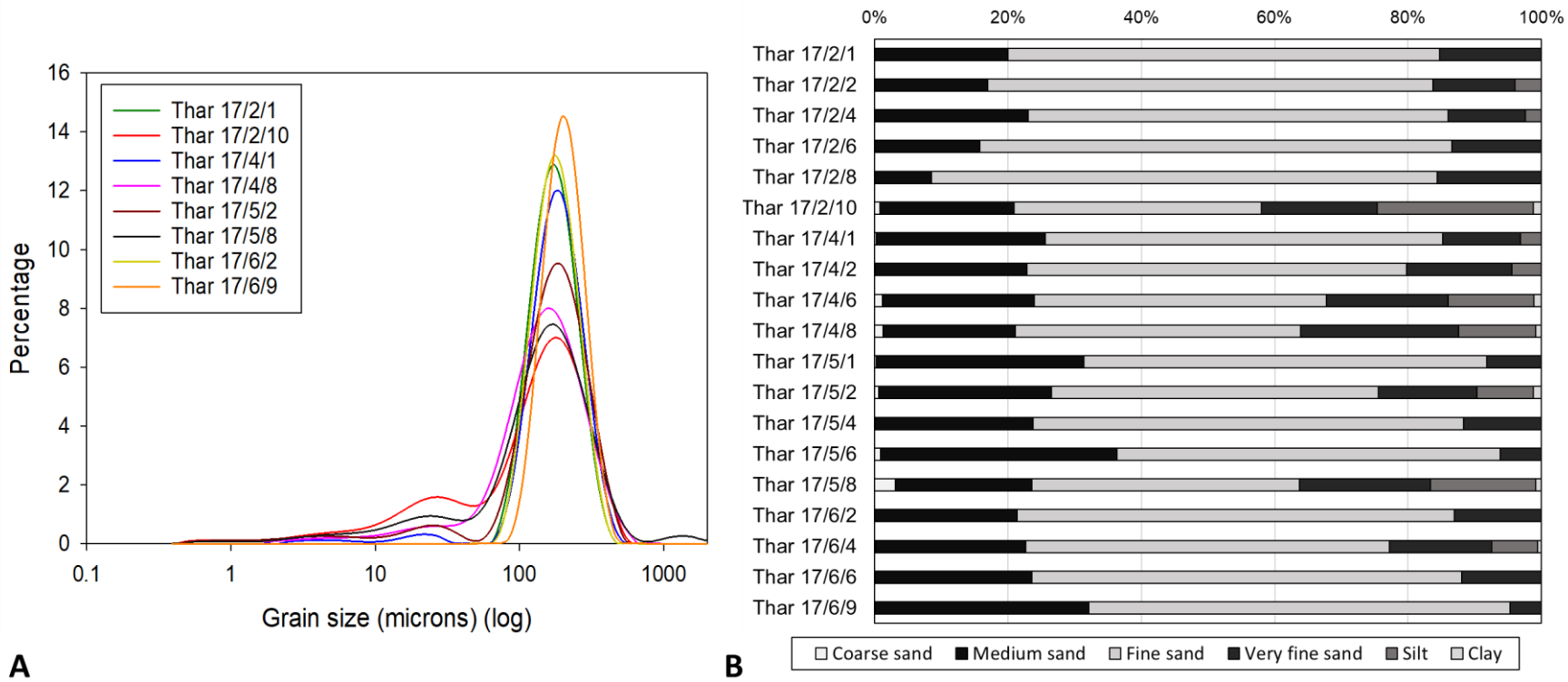


Figure 5.3. A. Grain size distribution by volume for selected samples from each sampled dune. B. The percentage distribution of different grain sizes for all the samples. Clay <2 μm; silt = 2-63 μm; very fine sand = 63-125 μm; fine sand= 125-250 μm, medium sand = 250-500 μm; and coarse sand = 500-1000 μm (Blott and Pye, 2001 and references therein).

Table 5.1. Sedimentology of samples showing Munsell colour, grain size statistics (in microns), organic and carbonate content.

Sample	Munsell colour	Mean (μm)	Sand (%)				Silt (%)	Clay (%)	Sorting*	Skewness**	Kurtosis***	Organic content (%)	Carbonate content (%)
			Coarse	Medium	Fine	Very Fine							
Thar 17/2/1	10 YR 5/4	183	0	20	64.7	15.3	0	0	1.439 (MWS)	-0.001 (S)	0.952 (M)	0.62	1.8
Thar 17/2/2	10 YR 5/4	178.5	0	17	66.7	12.3	4	0	1.447 (MWS)	-0.086 (S)	1.072 (M)	0.76	2.31
Thar 17/2/4	10 YR 5/4	188.8	0	23	63	11.6	2.4	0	1.459 (MWS)	-0.037 (S)	0.994 (M)	0.87	2.8
Thar 17/2/6	10 YR 5/4	179.9	0	15.8	70.8	13.4	0	0	1.382 (WS)	0.000 (S)	0.956 (M)	0.72	2.1
Thar 17/2/8	10 YR 5/4	168.3	0	8.5	75.9	15.6	0	0	1.336 (WS)	0.001 (S)	0.965 (M)	0.6	3.88
Thar 17/2/10	10YR 5/4	106.8	0.8	20.1	37.1	17.4	23.4	1.2	3.114 (PS)	-0.470 (VFS)	1.226 (L)	1.36	3.94
Thar 17/4/1	10 YR 6/4	191.1	0.3	25.3	59.6	11.7	3.1	0	1.500 (MWS)	-0.051 (S)	1.013 (M)	0.58	1.7
Thar 17/4/2	10 YR 6/4	180.2	0.1	22.8	56.9	15.8	4.4	0	1.569 (MWS)	-0.088 (S)	1.063 (M)	0.87	2.24
Thar 17/4/6	10 YR 6/4	154.3	1.2	22.8	43.8	18.2	12.9	1.1	2.399 (PS)	-0.356 (VFS)	1.747 (VL)	0.71	2.6
Thar 17/4/8	10 YR 6/4	149	1.3	19.8	42.8	23.7	11.6	0.8	2.192 (PS)	-0.258 (FS)	1.463 (L)	0.98	5.06
Thar 17/5/1	10 YR 6/4	208.3	0.3	31.1	60.4	8.2	0	0	1.441 (MWS)	-0.006 (S)	0.952 (M)	0.88	1.9
Thar 17/5/2	10 YR 6/4	176.6	0.6	25.9	49.1	14.8	8.5	1.2	2.134 (PS)	-0.322 (VFS)	1.877 (VL)	0.87	1.96
Thar 17/5/4	10 YR 6/4	192.4	0.1	23.7	64.5	11.7	0	0	1.429 (MWS)	0.006 (S)	0.952 (M)	0.51	2.1
Thar 17/5/6	10 YR 6/4	219	0.9	35.5	57.4	6.2	0	0	1.446 (MWS)	0.009 (S)	0.952 (M)	0.48	2.48
Thar 17/5/8	10 YR 6/4	140.4	3.1	20.5	40.1	19.9	15.8	0.8	2.584 (PS)	-0.343 (VFS)	1.567 (VL)	1.65	3.85
Thar 17/6/2	10 YR 5/4	187.5	0	21.4	65.5	13.1	0	0	1.425 (MWS)	0.002 (S)	0.946 (M)	0.6	1.09

Sample	Munsell colour	Mean (μm)	Sand (%)				Silt (%)	Clay (%)	Sorting*	Skewness**	Kurtosis***	Organic content (%)	Carbonate content (%)
			Coarse	Medium	Fine	Very Fine							
Thar 17/6/4	10 YR 5/4	175.7	0.2	22.5	54.5	15.3	6.9	0.6	1.932 (MS)	-0.295 (FS)	1.838 (VL)	0.59	2.2
Thar 17/6/6	10 YR 5/4	191.7	0.1	23.5	64.4	12	0	0	1.431 (MWS)	0.007 (S)	0.951 (M)	0.56	3.21
Thar 17/6/9	10 YR 5/4	214.6	0.1	32	63.2	4.7	0	0	1.381 (WS)	-0.003 (S)	0.956 (M)	0.52	2.78

* MWS= moderately well sorted, WS= well sorted, MS= moderately sorted, PS= poorly sorted.

** FS= finely skewed, VFS= very finely skewed, S= symmetrical.

*** L= leptokurtic, VL= very leptokurtic, M= mesokurtic

5.3.2. Luminescence dating

In general, measured luminescence signals from small aliquots are bright enough to be discernible from the background (Figure 5.4A) and are dominated by the quartz fast component in the initial part of the OSL signal (fast ratio > 20; Durcan and Duller, 2011). Single grain analyses confirm the low levels of luminescence sensitivity to dose (2-3 luminescing grains per disc), which ensures that any heterogeneity in D_e distributions should be identified. The heterogeneity or over-dispersion (σ_d), in D_e distributions for the majority of samples in this study ranges between 20 % and 45 % (Table 5.2), with slightly higher values (~45%) observed for two of the younger samples. These σ_d values are in line with values calculated from other single aliquots of dune samples in the central Thar (σ_d = 20-40 %; Srivastava *et al.*, 2019b), single grains of dune samples from the northern Thar margin (σ_d = 30-50 %; Durcan *et al.*, 2019) and are comparable to linear dunes studies elsewhere (e.g. the Negev, σ_d = 10-60 %; Roskin *et al.*, 2011a). Overdispersion can be caused by a combination of intrinsic factors, such as natural variability of quartz (Thomsen *et al.*, 2012 and references therein), as well as extrinsic sources, such as heterogeneous bleaching (e.g. Olley *et al.*, 2004), post-depositional mixing of sediments (e.g. Bateman *et al.*, 2003; 2007; Kristensen, 2015), and dosimetric variability (e.g. Nathan *et al.*, 2003; Mayya *et al.*, 2006); and instrumental sources which have a small contribution (e.g. Thomsen *et al.*, 2005; Cunningham *et al.*, 2011). As discussed, the observed σ_d values for this suite of data is relatively low, and in line with other published values from aeolian, dryland contexts. σ_d values from DRTs were <5 %, and therefore we hypothesise external factors as the source of the observed variability. σ_d due to incomplete bleaching is unlikely, given the deposition by aeolian processes

(Duller, 2004; Singhvi and Porat, 2008), and samples were carefully collected from visibly undisturbed strata, which should minimise D_e variability as a result of post-depositional mixing. We, therefore, hypothesise mild microdosimetric variability as a source of variability in D_e distributions. It has been demonstrated empirically and through modelling that microdosimetric variability may contribute significantly to variations in D_es for well-bleached samples (up to ~45- 50 %; see Mayya *et al.*, 2006; Cunningham *et al.*, 2012; Guérin *et al.*, 2015; Jankowski and Jacobs, 2018). In this context of relatively low σ_d values, which are in line with other published studies, and given that the D_e distributions tend to be symmetrical around a central value (e.g. Figure 5.4B), the CAM (Galbraith *et al.*, 1999) has been used for final D_e calculation. This follows the rationale of other dryland-based studies, such as Parton *et al.* (2015) and Durcan *et al.* (2019).

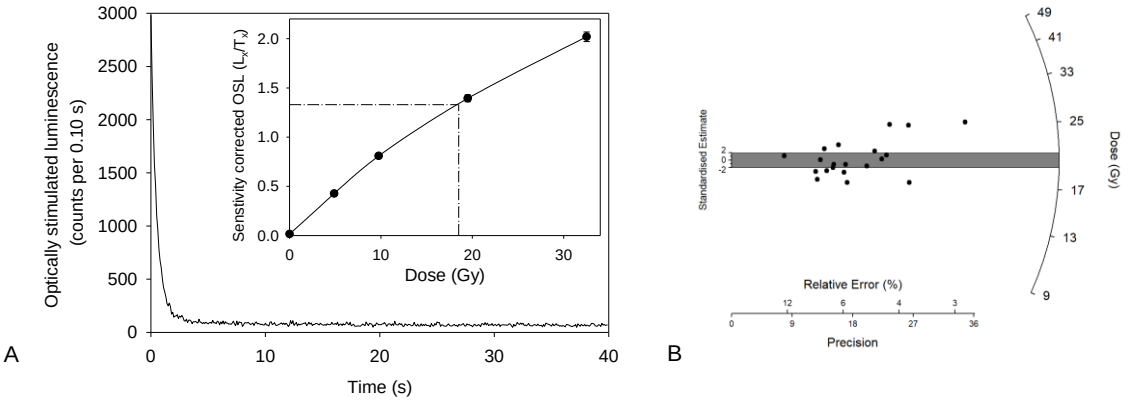


Figure 5.4. A. An example OSL signal from sample Thar 17/2/6, and the DRC from the same aliquot (inset) B. Radial plot of individual D_es for Thar 17/2/6 (σ_d = 23 %).

Calculation of minimum ages

One of the factors which limits the upper dateable range of OSL dating is signal saturation. A quartz OSL signal can be considered saturated if either the natural signal does not intercept the DRC or if the natural signal interpolates onto the flat, asymptotic part of the DRC (e.g. Figure 5.5). Interpolation of the natural signal from the asymptote of the saturated DRC results in a large and asymmetric uncertainty in D_e (Murray *et al.*, 2002; Murray and Funder, 2003) and therefore should be avoided where possible. Wintle and Murray (2006) suggest that a prudent upper dating limit for saturated signals is the $2D_0$ parameter, which represents ~85% of the upper saturation point obtained from the DRC. D_0 is derived from the fitting of the DRC with a single saturating exponential function, $I=I_0$ (1- $\exp^{-D/D0}$) where I is the OSL intensity after a dose (D), I_0 is the saturation intensity and D_0 is the dose level characteristic of the DRC (Wintle and Murray, 2006).

In this study, a signal was considered saturated if there was no interpolation on the DRC or if the calculated D_e was greater than $2D_0$. A sample was considered saturated when more than 50 % of measured accepted aliquots were saturated, and a minimum age was calculated using the mean $2D_0$ values of all accepted aliquots. These minimum ages are reported to the nearest integer and without an uncertainty, reflecting that the 'true' D_e is in excess of quoted minimum. Two samples are considered saturated (Table 5.2): Thar 17/2/10 (15/27 aliquots saturated) and Thar 17/5/8 (14/24) and yielded minimum ages of >58 ka and >48 ka respectively.

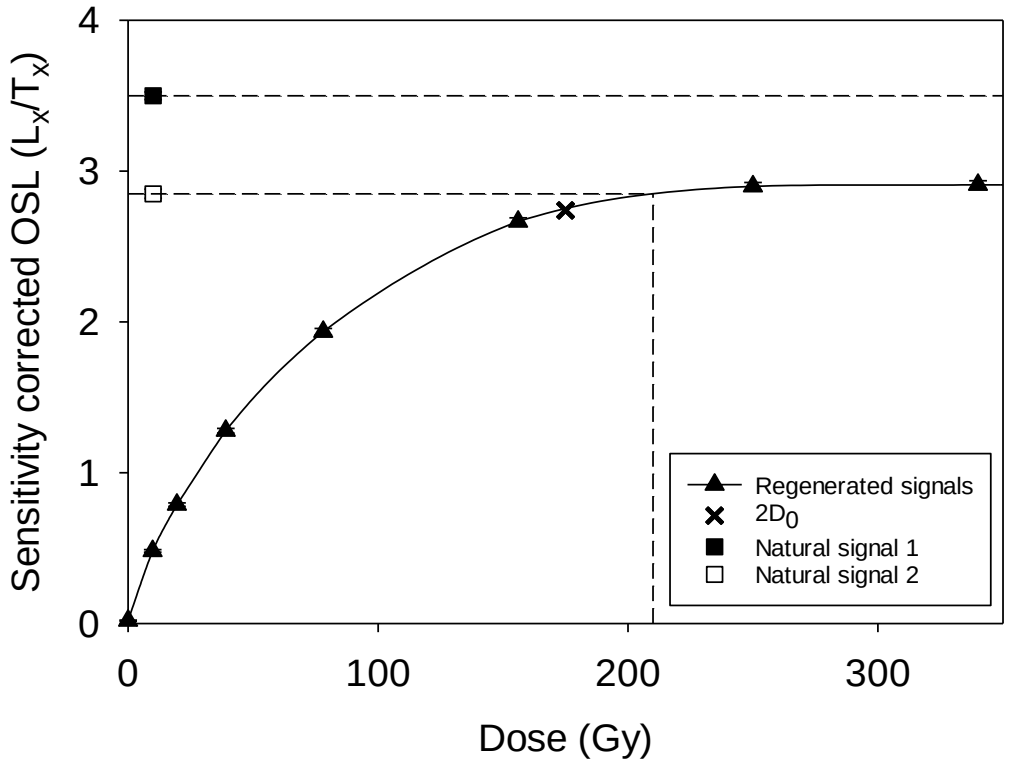


Figure 5.5. The two types of OSL signal considered saturated in this study. i) where natural signal does not intercept the DRC (natural signal 1 square symbol) and ii) when the interpolated D_e exceeds $2D_0$ (natural signal 2 open square symbol).

Luminescence ages

A summary of the luminescence dating results is provided in Table 5.2 along with stratigraphic sections (Figure 5.6A) and age-depth profiles (Figure 5.6B). At all four sites, OSL ages (including uncertainties) are in stratigraphic order and 17 of the 19 samples date to the Holocene, 10 of which date to the early part of the Holocene. Site Thar 17/2 depicts a Pleistocene feature with the oldest age at 9 m depth having a minimum age of >58 ka. At 7 and 3 m depths, sample ages are within uncertainties: 8.81 ± 0.71 ka (Thar 17/2/8) and 8.62 ±

0.64 ka (Thar 17/2/4) old respectively. Sample Thar 17/2/1 shows that the uppermost 0.8 m of dune sediments accumulated in the last ~500 years (Thar 17/2/1) and is immediately underlain by a 4.07 ± 0.44 ka old sample at 0.9 m (Thar 17/2/2). The five samples from Thar 17/5 dune show a similar dune accumulation pattern to Thar 17/2 where the basal dune unit is at least ~48 ka old (Thar 17/5/8) and is overlain by 2 m dune which accumulated between 9.38 ± 0.82 ka (Thar 17/5/6) and 9.27 ± 0.64 ka (Thar 17/5/4). The top 1.6 m of sediments at Thar 17/5 recorded dune activity in the last ~150 years (Thar 17/5/1). The site 17/4 preserves only Holocene accumulation with the oldest sample at 11 m dating to 11.61 ± 0.82 ka (Thar 17/4/8). 7 m of dune sand accumulation occurred between 10.52 ± 0.99 ka (Thar 17/4/6) and 8.79 ± 0.67 ka (Thar 17/4/2). The uppermost sample, taken 0.5 m below the dune surface, dates to 3.01 ± 0.24 ka (Thar 17/4/1). At site Thar 17/6, between 9.5 and 6 m down section, sample ages are within uncertainties- 9.39 ± 0.69 ka (Thar 17/6/9) and 9.38 ± 0.71 ka (Thar 17/6/6) old. The top 2 m dune is recent, dating from 0.34 ± 0.03 ka (Thar 17/6/2).

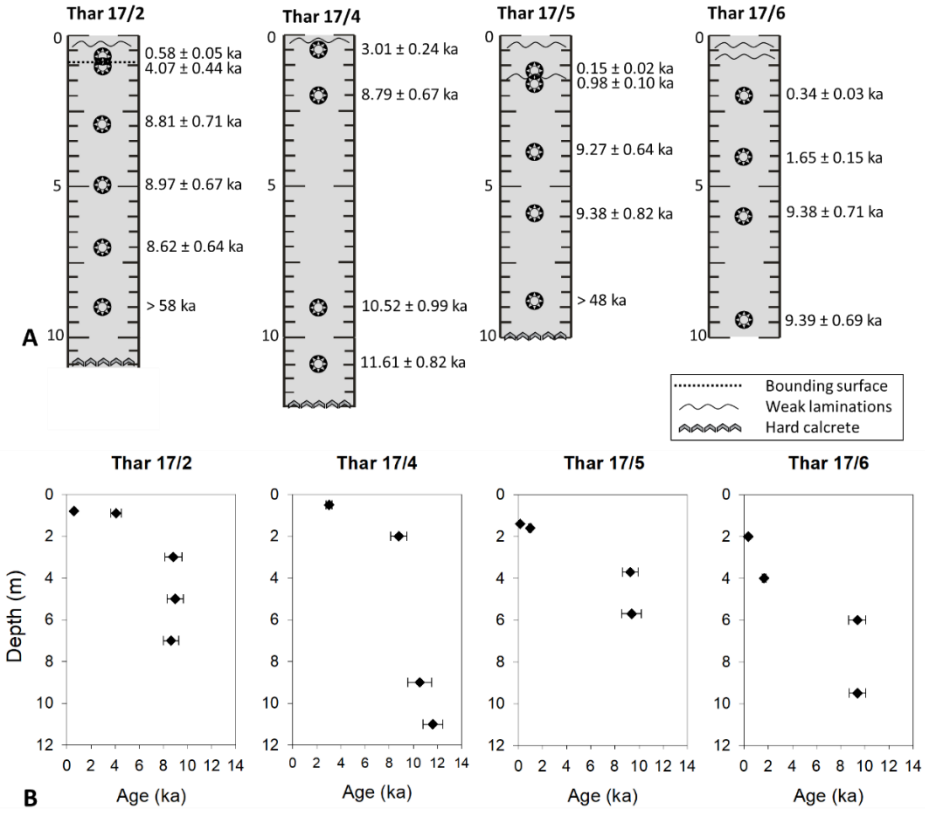


Figure 5.6. A. Stratigraphic sections and OSL ages for the sampled sites investigated in this study. Sample depth are in metres. Note the sections comprised largely homogeneous and structureless sand with very few laminations or other sedimentological features. B. Age-depth profiles for all four sites. The minimum ages for samples Thar 17/2/10 (>58 ka) and 17/5/8 (>48 ka) are not displayed.

Table 5.2. Summary OSL data. D_e, $\dot{D}$, and ages are shown to two decimal places, with all calculations made prior to rounding. Minimum D_es and ages are calculated for samples Thar 17/2/10 and Thar 17/5/8 due to signal saturation and are quoted to the nearest integer, without uncertainties. All ages are relative to the year 2018.

Sample	Depth (m)	Discs accepted (measured)	Over-dispersion (%)	D_e (Gy)	Beta $\dot{D}$ (Gy.ka^{-1})	Gamma $\dot{D}$ (Gy.ka^{-1})	Cosmic $\dot{D}$ (Gy.ka^{-1})	Envir $\dot{D}$ (Gy.ka^{-1})	Age (ka)
Thar 17/2/1	0.8	26 (38)	34.3 ± 4.8	1.22 ± 0.08	1.24 ± 0.11	0.68 ± 0.05	0.19 ± 0.02	2.10 ± 0.12	0.58 ± 0.05
Thar 17/2/2	0.9	22 (36)	36.6 ± 6.1	8.36 ± 0.78	1.17 ± 0.10	0.71 ± 0.05	0.18 ± 0.02	2.06 ± 0.11	4.07 ± 0.44
Thar 17/2/4	3	25 (46)	28.0 ± 4.0	19.74 ± 1.18	1.25 ± 0.11	0.85 ± 0.05	0.14 ± 0.01	2.24 ± 0.12	8.81 ± 0.71
Thar 17/2/6	5	21 (43)	22.3 ± 3.7	19.82 ± 1.04	1.24 ± 0.10	0.86 ± 0.06	0.11 ± 0.01	2.21 ± 0.12	8.97 ± 0.67
Thar 17/2/8	7	21 (27)	24.3 ± 3.8	19.64 ± 1.05	1.25 ± 0.10	0.94 ± 0.06	0.09 ± 0.01	2.28 ± 0.12	8.62 ± 0.64
Thar 17/2/10	9	27 (30)	-	>125	1.26 ± 0.11	0.82 ± 0.05	0.08 ± 0.01	2.15 ± 0.12	> 58
Thar 17/4/1	0.5	21 (32)	28.4 ± 4.4	8.24 ± 0.51	1.44 ± 0.11	1.10 ± 0.07	0.21 ± 0.02	2.74 ± 0.14	3.01 ± 0.24
Thar 17/4/2	2	24 (35)	27.0 ± 3.9	20.39 ± 1.13	1.27 ± 0.10	0.89 ± 0.06	0.16 ± 0.02	2.32 ± 0.12	8.79 ± 0.67
Thar 17/4/6	9	24 (48)	37.0 ± 5.5	24.97 ± 1.94	1.35 ± 0.11	0.95 ± 0.06	0.08 ± 0.01	2.37 ± 0.13	10.52 ± 0.99
Thar 17/4/8	11	30 (43)	24.8 ± 3.3	25.23 ± 1.15	1.26 ± 0.10	0.85 ± 0.06	0.06 ± 0.01	2.17 ± 0.12	11.61 ± 0.82
Thar 17/5/1	1.4	22 (28)	44.3 ± 8.0	0.32 ± 0.03	1.28 ± 0.11	0.72 ± 0.05	0.17 ± 0.02	2.17 ± 0.13	0.15 ± 0.02
Thar 17/5/2	1.6	20 (36)	42.8 ± 6.8	2.51 ± 0.24	1.36 ± 0.11	1.04 ± 0.07	0.17 ± 0.02	2.56 ± 0.13	0.98 ± 0.10
Thar 17/5/4	3.7	23 (46)	19.2 ± 2.9	19.53 ± 0.79	1.23 ± 0.11	0.74 ± 0.05	0.13 ± 0.01	2.11 ± 0.12	9.27 ± 0.64
Thar 17/5/6	5.7	20 (46)	27.9 ± 4.8	18.75 ± 1.23	1.21 ± 0.11	0.68 ± 0.05	0.11 ± 0.01	2.00 ± 0.12	9.38 ± 0.82
Thar 17/5/8	8.7	24 (33)	-	>127	1.44 ± 0.11	1.13 ± 0.08	0.08 ± 0.01	2.65 ± 0.13	> 48

Sample	Depth (m)	Discs accepted (measured)	Over-dispersion (%)	D_e (Gy)	Beta Ḋ ($Gy.ka^{-1}$)	Gamma Ḋ ($Gy.ka^{-1}$)	Cosmic Ḋ ($Gy.ka^{-1}$)	Envir Ḋ ($Gy.ka^{-1}$)	Age (ka)
Thar 17/6/2	2	22 (34)	33.0 ± 5.3	0.84 ± 0.06	1.34 ± 0.11	0.95 ± 0.06	0.16 ± 0.02	2.44 ± 0.13	0.34 ± 0.03
Thar 17/6/4	4	20 (35)	29.4 ± 5.0	3.72 ± 0.26	1.30 ± 0.11	0.83 ± 0.06	0.13 ± 0.01	2.26 ± 0.12	1.65 ± 0.15
Thar 17/6/6	6	24 (34)	30.4 ± 4.5	20.08 ± 1.07	1.22 ± 0.10	0.82 ± 0.05	0.10 ± 0.01	2.14 ± 0.12	9.38 ± 0.71
Thar 17/6/9	9.5	20 (46)	21.6 ± 3.9	22.10 ± 1.15	1.33 ± 0.11	0.96 ± 0.06	0.07 ± 0.01	2.35 ± 0.12	9.39 ± 0.69

5.4. Discussion

Previous chronometric investigations of dunes in the northern Thar Desert have been limited and have focussed chiefly on transverse and parabolic dunes (Kar *et al.*, 1998; Thomas *et al.*, 1999). These studies often relied on sampling pre-existing exposures and used older and now mostly redundant multiple aliquot luminescence dating techniques (Duller, 2004). The ages from these studies provided evidence of middle to late Holocene dune activity (Kar *et al.*, 1998; Thomas *et al.*, 1999; Singhvi and Kar, 2004). The oldest ages in our new suite of data are from full depth profiles of sites Thar 17/5 and Thar 17/2. Though these two ages of > 48 ka (Thar 17/5/8) and > 58 ka (Thar 17/2/10) are minimum age estimates, they are still considerably older than the records in previously published chronologies (Thomas *et al.*, 1999; Singhvi and Kar, 2004), and provide the first reported occurrence of pre-Holocene dune activity in the northern Thar. This is important considering previous studies from southern, central and eastern Thar have presented dune records dating to >50 ka and attested to the antiquity of the desert (Chougaonkar *et al.*, 1999; Dhir *et al.*, 2010; Singhvi *et al.*, 2010) while records from the northern Thar dunes were limited to the Holocene.

A significant component of our new dataset is evidence of early Holocene dune accumulation, and importantly this is recorded at all four sites, spanning 11.61 ± 0.82 ka to 8.62 ± 0.64 ka (Figure 5.6B). Thick sediment accumulations are recorded during this period: 2 m and 3.5 m of sediment occurred at ~9.4 ka at sites Thar 17/5 and Thar 17/6 respectively. At site Thar 17/2, a 4 m thick dune accumulation dates to slightly later (~8.8 ka), and at Thar 17/4, the lowermost 7 m dune sand accumulated between 11.61 ± 0.82 ka and 8.79 ± 0.67 ka. At this site this translates to an estimated accumulation rate of ~2.5 $m.ka^{-1}$. Regionally,

comparable early Holocene net accumulation rates have been reported from NE-SW trending linear dune studies in the monsoon dominated northeast Rub 'al-Khali Desert (Atkinson *et al.*, 2011, 2012). The early Holocene has been identified as a period marked by strong monsoonal winds compared to the late Holocene, evidenced by the enhanced upwelling off the coast of Oman (Gupta *et al.*, 2003; Figure 5.7) and a large wind stress curl across the western Arabian Sea (Gill *et al.*, 2017; Figure 5.7). Within the Thar Desert, the parabolic dunefield ~200 km south of the study area (Srivastava *et al.*, 2019b) and dunes associated with the Ghaggar-Hakra palaeochannel along the northern desert margin (Durcan *et al.*, 2019) also recorded early Holocene accumulation. The data presented here demonstrate that the last major widespread dune accumulation in the Thar was not limited to the late glacial period (~17 - ~11 ka), but that major aeolian dynamism persisted into the early Holocene until ~8.6 ka.

In our study, only two dates identify middle to late-Holocene dune accumulation (4.07 ± 0.44 ka at Thar 17/2/2 and 3.01 ± 0.24 ka at Thar 17/4/1 (Table 5.2), both of which were sampled from within 1 m of the dune crest. The middle to late- Holocene dune activity, which resulted in thinner sediment accumulations compared to the early Holocene, suggests that dune activity in the region was less pervasive in terms of dune accumulation during the later part of the Holocene, with thicker units reflecting periods of more intensive dune activity (Telfer *et al.*, 2010). Two sites (Thar 17/5 and 17/6) record seemingly more localised dune accumulation between 1.65 ± 0.15 - 0.98 ± 0.11 ka, which could be spatially restricted in nature or the result of localised reworking within the dune system. Unlike the early Holocene, the age depth profiles are more variable between the four studied sites during the middle and late Holocene (Figure 5.6B)

suggesting that individual dune profiles do not capture temporally comprehensive accumulation phases even in a spatially intensive dunefield. Telfer *et al.* (2010) and Bailey and Thomas (2014), through their modelling work, have suggested that preservation potential is unlikely to be equal spatially and temporally within a dune system, due to the interaction of exogenous and endogenous (stochastic) influences on accumulation. Stone and Thomas (2008), in their study of linear dunes in the southwest Kalahari, also showed that only some accumulation phases are consistently recorded between dunes and individual dune profiles do not offer a temporal record even for a small region. Likewise, Telfer et al. 2017 demonstrated in the Strzelecki Desert that adjacent dunes have completely different records. Here, the younger phases of dune accumulation are preserved in pockets in three studied dunes, while absent in Thar 17/4, where the uppermost sample (0.5 m from the crest) yielded an age of 3.01 ± 0.24 ka. The absence of any common accumulation phases dating to the late Holocene could be due to differential preservation between the dunes or phases being missed in sampling. However, sampling at shallow depth of 0.5 m at Thar 16/4 should have minimised sampling bias towards younger phases. Likewise, at Thar 17/2 there is a jump from 0.58 ± 0.05 ka (Thar 17/2/1) to 4.07 ± 0.44 ka (Thar 17/2/2) over just 0.1 m, where a bounding surface exists, suggests that missing an accumulation phase through sampling is not likely to be the major cause.

Although the INQUA dunes atlas chronologic database does not include any dated linear dune sites in the Thar, there are records from at least one dune site from Jamsar in the Bikaner region (Figure 5.1B). Thomas *et al.* (1999) described the sampled feature as a linear dune site while later reviews designated it as a parabolic dune (Singhvi and Kar, 2004; Lancaster *et al.*, 2016).

Jamsar, which appears to be a linear dune site from Google Earth analysis, was a 3.9 m exposed dune section on the margins of an ephemeral lake studied by Thomas *et al.* (1999) and the authors reported 6 luminescence ages suggesting dune activity between 5.3 ± 0.7 ka and 4.7 ± 0.9 ka, and within the last 2000 years (Figure 5.7). These ages were calculated using the multiple aliquot additive dose (MAAD) protocol that was widely used in the early decades of luminescence dating applications to sediments. It must be noted that earlier protocols did not explicitly check for changes in luminescence sensitivity, therefore potentially adding an element of unreliability to them (Stokes *et al.*, 2000; Duller, 2004). Duller and Augustinus (2006) demonstrated the importance of checking the validity of luminescence dating results obtained using older protocols by dating the same samples from a stabilised linear dune in Tasmania and showed that MAAD protocol methods overestimated D_e values by up to 84 % compared against SAR. Singhvi *et al.* (2010) presented SAR and MAAD ages for four dune samples from the Thar where MAAD ages overestimated the SAR ages by 15-53%. It is therefore possible that previously published ages from Jamsar dune feature (Thomas *et al.*, 1999) are likely maximum ages for sediment accumulation.

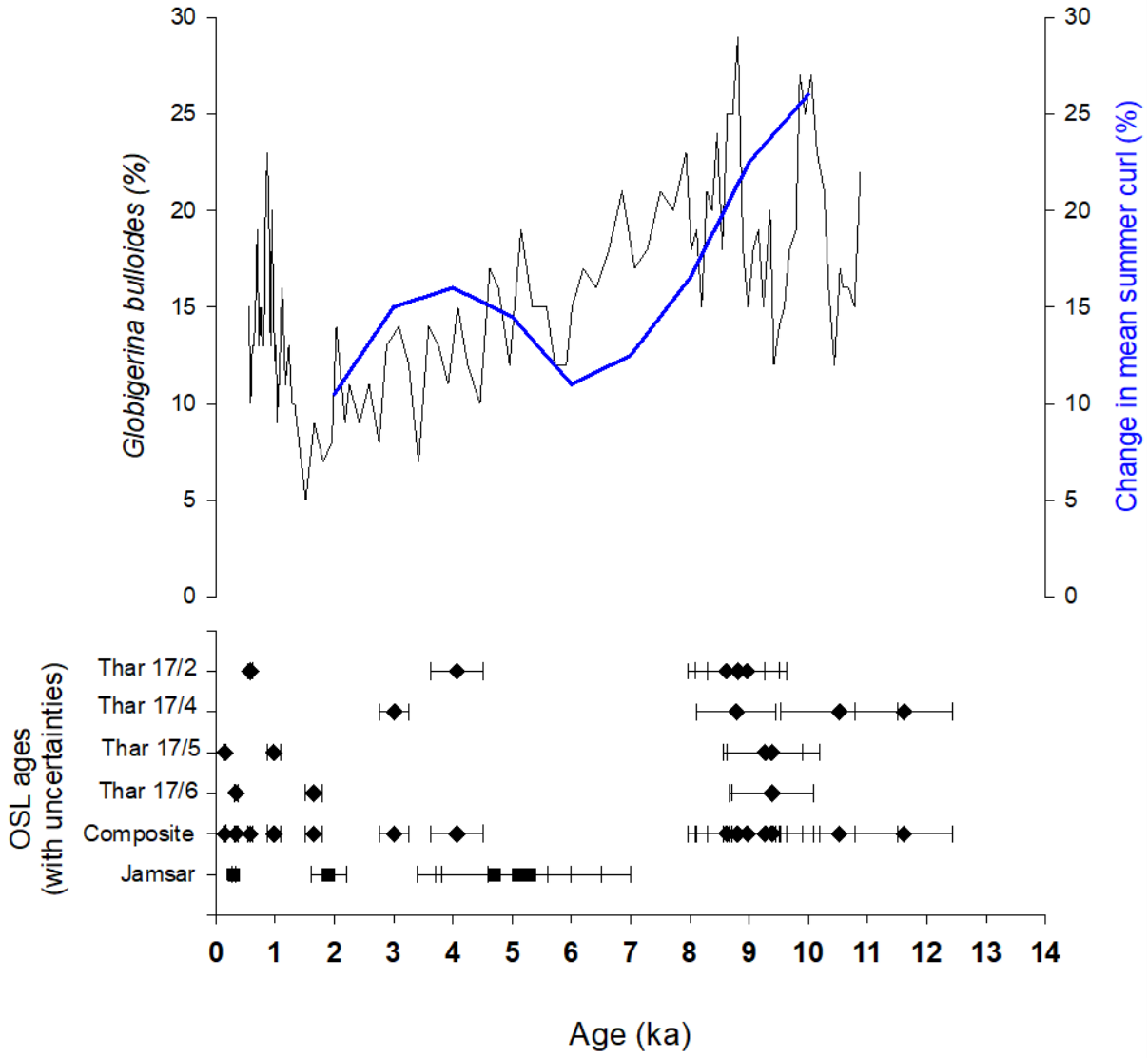


Figure 5.7. Thar linear dune OSL ages plotted against reconstructions of *G. bulloides* percentage (Gupta *et al.*, 2003) and percentage change in wind stress curl (blue) (Gill *et al.*, 2017). The diamonds represent the ages determined in this study using post IR blue SAR protocol, while the squares are the MAAD OSL ages calculated by Thomas *et al.* (1999).

The ages from the last millennium have been calculated at the crestal parts of three of the four studied dune sites (Figure 5.6A). The site Thar 17/2 recorded 0.8 m of dune accumulation in last ~500 years, Thar 17/5 recorded 1.4 m of

accumulation in last ~150 years and Thar 17/6 recorded 2 m of accumulation in the last ~350 years. These thicker units reflect the preservation bias towards younger sediments (Bailey and Thomas, 2014) and the absence of any late Holocene feature at site Thar 17/4 further confirm that individual dune profiles only provide partial information about the past changes. The parabolic dunes in the vicinity of the study area have also witnessed dune accumulation in the last millennium but those are significantly widespread with higher accumulation rates (Srivastava *et al.*, 2019b). This difference in dune accumulation rates could be attributed to parabolic dunes being more sensitive to natural and anthropogenic disturbances (e.g. Hugenholtz and Wolfe, 2005; Girardi and Davis, 2010), and the changing landscape in the Thar (Srivastava *et al.*, 2019b and references therein). Nevertheless, the modern ages not only suggest that the Thar linear dunes remained active in later parts of the Holocene but also question whether these dunes can be grouped under an 'old system' as previously implied (e.g. Pandey *et al.*, 1964; Kar, 1993; Singhvi and Kar, 2004). Similar active and partially-active linear dunes have also been reported from the Negev (Roskin *et al.*, 2011a), the Kalahari (Telfer and Thomas, 2007), the Strzelecki (Lomax *et al.*, 2003) and the Tirari Deserts (Fitzsimmons *et al.*, 2007).

5.5. Conclusions

This study presents a suite of OSL ages from intensively sampled linear dunes in the Thar Desert, India. The dataset show variability in dune activity between sites in terms of timing and nature of dune accumulation. In general, the record is characterised by consistent and rapid dune accumulation in the early Holocene, and multiple, distinct phases during the middle and late Holocene. The

early Holocene period is the most active dune accumulation period which correlates with other Thar dunes records (Srivastava *et al.*, 2019b) and wider regional geoproxy evidence. The OSL ages show that the linear dunes in the Thar have remained active, accumulating sediment during the Holocene. The accumulation of up to 2 m of dune sediment in recent times rules out the earlier notion of classifying linear dunes as belonging to an 'old' Thar Desert system. The suite of ages also presents the first reported records of pre-Holocene dune activity in the northern Thar, albeit as minimum ages, and affirms findings from other desert dunefields that linear dunes preserve a relatively longer chronology. As dune records are increasingly being incorporated to wider palaeoenvironmental studies, our study emphasises on the importance of intensive dunefield sampling, rather than focusing on single dune profiles which do not capture temporally comprehensive accumulation phases, as done in the majority of previous studies in the Thar.

Collectively, Chapters 4 and 5 have provided 50 chronologies of dune accumulation (to address RQs 1 and 2). The next step is to assess palaeoenvironmental changes in the Thar and address research question 3, which requires integration of dune accumulation records with other geochemical proxies. In the following Chapter 6, this is achieved by quantifying Thar dunes records (both old and new) through a mathematical model of Accumulation Intensity, and interpreting in association with other high-resolution records from various terrestrial and marine archives from the Indian subcontinent and beyond.

Chapter 6: Holocene palaeoenvironmental changes in the Thar Desert: an integrated assessment incorporating new insights from aeolian systems (Paper 3)

This paper has been accepted for publication in Quaternary Science Reviews.

Abstract

Due to the scarcity of geochemical and palaeoecological proxies in drylands, dunes have often been used as geoproxies for late Quaternary palaeoenvironmental reconstruction, with chronologies commonly provided by luminescence dating. Owing to their widespread occurrence and location in a monsoonal regime, dunes in the Thar Desert in South Asia act as important archives of past landscape change. Previous reviews have assimilated dune age data from the Thar and suggested a temporally and spatially complex record of sediment accumulation over the last ~70 ka. New luminescence age data presented in this study and from recent dunefield based investigations demonstrate a stronger Holocene record of dune building in parts of the Thar than previously suggested.

In this study, the Accumulation Intensity (*AI*) methodology is applied to new and old data sets, providing records of dune accumulation that can be analysed alongside other palaeoenvironmental records. *AI* analysis demonstrates the significance of Holocene dune accumulation in the Thar landscape, with accumulation peaks observed between ~12 and ~8 ka, centred around ~7, ~5 and ~3.5 ka, and in last two millennia. The strengthening of the Indian Summer Monsoon remains a significant influence on widespread dune accumulation in the early Holocene, but dunefields have also shown diverse and spatially intensive responses to sediment supply and anthropogenic disturbances during the late Holocene. Additionally, aeolian-fluvial sequences associated with the Ghaggar-Hakra palaeochannel along the northern margin of the Thar also display dynamic geomorphic behaviour during the Holocene. The integration and interpretation of the *AI* data with published, highly resolved geochemical proxies

of palaeoclimate, shows a complex relationship between geoproxy and geochemical records. We suggest that process studies of geomorphologic systems and their diverse responses to the same environmental stimuli must be given due consideration before deriving palaeoenvironmental interpretations. Despite the presence of over a hundred Holocene dune records from the Thar, there still remains marked spatial and temporal gaps. Further intensive investigations of distinct dunefields with a strong chronometric framework and geomorphological grasp are required to gain significant insights into wider Thar landscape and palaeoenvironmental dynamics.

Keywords: *Thar Desert, Holocene; Dune accumulation; Accumulation Intensity; palaeoenvironmental change*

6.1. Introduction

The landscape of the Thar Desert in South Asia is dominated by sand dunes of different types including parabolic, linear, and transverse, of up to 30 m in height (Kar, 1993; Singhvi and Kar, 2004; Moharana *et al*., 2013). These features have long been viewed as offering insights into landscape and climate change during the Quaternary period. Based on dune orientation, earlier studies proposed a dominant role of south-westerly Indian Summer Monsoon (ISM) winds in dune development in the Thar (e.g. Goudie *et al*., 1973; Allchin *et al*.,1978; Wasson *et al*., 1983; Kar, 1987). The ISM winds, based on meteorological observations, have been shown to exceed the threshold for sand movement in the pre-monsoon period (March to June) before the onset of rainfall (Wasson *et al*., 1983; Kar, 1993). Aeolian activity is strong during this period when vegetation is dry, and wind erosion of the terrain and subsequent sediment transportation and deposition are more pronounced (Wasson *et al*., 1983; Kar,

1993). It is only after this period of increased wind intensity that precipitation (~80% of the total annual amount) is delivered to the region, between the months of June and September, resulting in positive precipitation minus evaporation conditions. Therefore, whilst periods of more intensive monsoon activity can be associated with increased precipitation, they can also represent phases of more intensive aeolian activity. However, there was an absence of temporal control on Thar dune development until Singhvi *et al*. (1982) used thermoluminescence (TL) dating to provide the first chronometric perspective, with eight ages calculated from three dune sites. Since then over 150 dune samples in the Thar have been investigated and dated using both TL and optically stimulated luminescence (OSL) dating techniques (e.g. Andrews *et al*., 1998; Kar *et al*., 1998; Thomas *et al*., 1999; Kar *et al*., 2001; Juyal *et al*., 2003). Singhvi and Kar (2004) summarised these investigations and concluded these records provide a first-level understanding of aeolian episodes in the Thar, with Singhvi and Porat (2008) further assessing and briefly summarising key results from the Thar dunefield age data. Lancaster *et al*. (2016) collated all the Thar dune luminescence ages published in peer reviewed studies (>150) in the INQUA dune atlas chronologic database.

Despite a relatively large published luminescence age data set, the interrogation of the Thar dune records in the context of understanding past landscape dynamics has been challenging. The aeolian records need to be assessed alongside other proxy data if environmental dynamics and their drivers are to be determined. Two main reasons explain the challenges that have occurred. First, there has been a lack of spatial and temporal coverage in the available aeolian data set until recently, as shown in Figure 6.1. For instance, the central Thar dune record was represented by just three Holocene ages from two

sites, Chamu and Shergarh Trijunction (Andrews *et al*., 1998; Dhir *et al*., 2010). In contrast, the southern and northern Thar areas were the subject of several dune-based investigations, which identified major early and late Holocene dune accumulation phases respectively (Figure 6.1b). Consequently, single dune sites were often considered representative of the wider region, although they inevitably failed to capture dunefield development history and inhibited analyses of the drivers of dune accumulation. Recent dunefield based studies by Srivastava *et al*. (2019a; 2019b) have revealed significant Holocene aeolian accumulation, and presented 50 new OSL ages from a mixture of parabolic and linear dunes, demonstrating that dune accumulation was persistent throughout much of the Holocene, adding a significant late Holocene data set which was infrequently identified in earlier studies. Second, it has been difficult to integrate the aeolian age records, which have been discontinuous with other proxy records, an issue observed in other dryland contexts worldwide (Thomas and Burrough, 2012; Thomas and Bailey, 2017). Therefore, reconstructions of Holocene palaeoenvironments in the Thar rely on other terrestrial archives including fluvial records from the Thar margins (e.g. Jain and Tandon, 2003; Jain *et al*., 2004; Giosan *et al*., 2012; Durcan *et al*., 2019), and lacustrine sediments from various interior and marginal lakes (e.g. Wasson *et al*., 1984; Singh *et al*., 1990; Kajale and Deotare, 1997; Enzel *et al*., 1999; Deotare *et al*., 2004; Sinha *et al*., 2006; Dixit *et al*., 2014a, 2014b; Dixit *et al*., 2018) These records are often supplemented by regional palaeoclimatic proxies, including sedimentary and productivity records from marine sediments (e.g. Sarkar *et al*., 2000; Staubwasser *et al*. 2002; Gupta *et al*., 2003; Ivanochko *et al*., 2005; Ponton *et al*., 2012) and isotopic records from speleothems in central or north-eastern India

(Sinha *et al*., 2007, 2011a; Dutt *et al*., 2015; Berkelhammer *et al*., 2012; Band *et al*., 2018) and the Arabian peninsula (e.g. Neff *et al*., 2001; Fleitmann *et al*., 2003; Fleitmann *et al*., 2007) (Figure 6.2). These records present high resolution data, but due to their limited spatial context, diverse methodologies and different temporal ranges, landscape scale response interpretations arising from these geochemical proxies are often conflicting in nature (e.g. Prasad and Enzel, 2006; Macdonald, 2011, Band *et al*., 2018; Kaushal *et al*., 2018; Misra *et al*., 2019). Dunes, whilst widespread in the Thar landscape, remain under-utilised in environmental reconstructions, representing a valuable archive of change.

In the context of these considerations, this paper aims first to systematically analyse the both new and existing dune age data set from the Thar Desert using the numerical Accumulation Intensity (*AI*) analysis approach of Thomas and Bailey (2017; 2019). Then, focussing on the Holocene, the dune accumulation records are assessed alongside other published proxy data sets to re-evaluate landscape dynamics and change in the Thar. Finally, the new analysis is assessed in terms of potential drivers of climate, along with consideration of data gaps and issues within the existing portfolio of dune records.

6.2. Accumulation Intensity modelling

Several studies have highlighted difficulties in using dune age records in palaeoenvironmental and paleoclimate analyses. These difficulties include sampling issues (Hesse, 2016), taphonomic issues related to reworking of sediments (Bailey and Thomas, 2014), data presentation issues (Thomas and Burrough, 2012; Thomas and Burrough, 2016), and the definitive identification of controls on dune sediment transportation (Chase, 2009). To address these issues, Bailey and Thomas (2014) first developed the dune Accumulation Rate

Variability model, identifying and quantifying the drivers of dune accumulation. This was subsequently modified to the *AI* model which utilises information on the actual sedimentation process in dunes to produce temporal *AI* curves through time, which can be compared with other palaeoenvironmental proxy data sets (Thomas and Bailey, 2017). In principle, the model integrates and analyses central ages, their associated one sigma uncertainties, and sampling interval depth data, and then iteratively resamples these ages (within their uncertainties) to calculate accumulation rates. The dispersion in the resampled accumulation rates acts as a proxy for the estimated accumulation rate (Thomas and Bailey, 2017; 2019). Full mathematical detail of the model is explained in Thomas and Bailey (2017).

The model has several advantages. It calculates temporal changes in dune accumulation through time, independent of the number of samples included in the analysis, allowing the retrieval of continuous palaeoenvironmental information from dated dune sequences. Further, as the model incorporates age certainties into analyses, any apparent age inversions are handled appropriately. The *AI* method is applied to data from dunefields rather than individual dunes, and hence allows a more systematic testing of landscape-scale responses and relationships to external drivers at global and regional scales.

The model has been successfully used to compare and explain dunefield accumulation histories in the context of other deserts in southern Africa and Australia in conjunction with other continental and marine records (Thomas and Bailey, 2017). Recently, Thomas and Bailey (2019) applied the *AI* methodology to the Asian dune age data sets included in the INQUA dune atlas (Lancaster *et al*., 2016), focusing on the last 50 ka, including the records for the Thar. The

authors highlighted the shortage of paired stratigraphically related ages from investigated dune sections and absence of locational/depth data. The resultant *AI* curve was therefore noted for its relatively limited spatial coverage, as well as containing insufficient data to provide a nuanced assessment of Thar dune accumulation in the late Quaternary. This paper addresses this shortfall by incorporating recently published age records into a new *AI* analysis.

6.2.1 Data included in *AI* analysis

There were 146 Thar dune luminescence ages in the first version of the INQUA dune atlas database (Lancaster *et al*., 2016), which after updates, now includes a further 26 ages from Shitaoka *et al.* (2012) and Durcan *et al.* (2019). Recent studies have expanded the available luminescence age data set by providing 50 new dune ages (Srivastava *et al*., 2019a; Srivastava *et al*., 2019b) from the central and northern Thar.

In addition to these published ages, 10 new dune accumulation records from parabolic dunes in the central Thar and from a source-bordering dune associated with the Ghaggar-Hakra palaeochannel in the north have been determined and are included in this study. These new OSL ages, from the early to middle Holocene, have been determined using small aliquots of coarse quartz grains (180-210 μm) following the luminescence dating methods outlined in Srivastava *et al*. (2019a) (Table 6.1). The full details regarding sampling and luminescence dating results are provided in the Supplementary Information. Figure 6.1 displays the full set of available luminescence Holocene records from the database and new studies, categorised in four regions: northern, central and southern Thar, and Ghaggar-Hakra palaeochannel following geographical contexts described in original publications.

This combined data set for the Thar provides an opportunity to enhance the spatial and temporal detail of dune accumulation, to the point where Thar dune data can contribute more robustly to palaeoenvironmental analyses for the region. The full data set for this new *AI* analysis, using the methodology of Thomas and Bailey (2017), therefore comprises (see Supplementary Information for details of all records):

1. 73 dune ages, generating 59 accumulation intervals, from a total of 146 ages presented in the database from sites Thirana, Jamsar (Thomas *et al*., 1999), Chamu (Dhir *et al*., 2010), Amarsar (Singhvi and Kar, 2004), Dharoi (Juyal *et al*., 2003) and Khudala (Thomas *et al*., 1999; Kar *et al*., 2001). Many ages did not meet the required criteria for *AI* analysis due to an absence of locational or depth data, or the occurrence of age reversals which meant net accumulation could not be identified (Thomas and Bailey, 2017). Further, ages from mobile transverse dunes (e.g. Khara, Bharmasar; Figure 6.1; Kar *et al*., 1998) were excluded on the account of lower likelihood of sediment preservation (Bailey and Thomas, 2014).

2. 83 of 86 newly published ages, from two dunefields in the central Thar (Jodhpur; Srivastava *et al*., 2019b; this study) and the northern Thar (Bikaner; Srivastava *et al*., 2019a), and aeolian sequences in Shitaoka *et al*. (2012) and Durcan *et al*., (2019), generating 58 accumulation intervals.

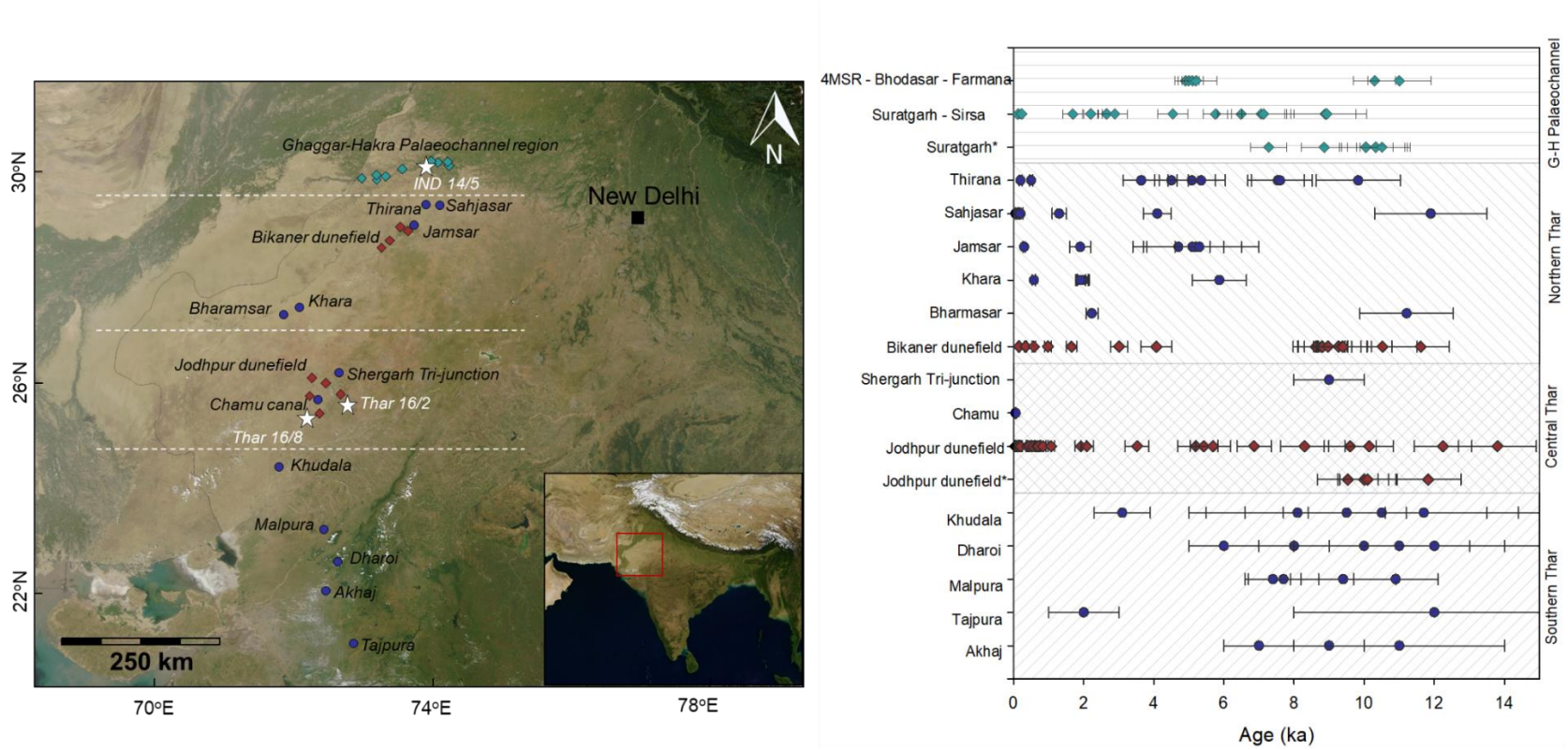


Figure 6.1. (a) The locations of studied Holocene dune sites in the Thar. Blue circles denote sites as described in Singhvi and Kar (2004) and listed in the first version of the INQUA dune database (Lancaster *et al*., 2016): Thirana, Sahjasar, Jamsar, Malpura (Thomas *et al*., 1999), Khara, Bharmasar (Kar *et al*., 1998), Chamu (Dhir *et al*., 2010), Khudala (Kar *et al*., 2001), Dharoi, Tajpura and Akhaj (Juyal *et al*., 2003); red diamonds denote sites investigated in Bikaner dunefield in the northern Thar (Srivastava *et al*., 2019a) and Jodhpur

dunefield in the central Thar (Srivastava *et al*., 2019b); blue diamonds denote sites along the Ghaggar-Hakra palaeochannel further along the northern Thar margin (Shitaoka *et al*., 2012; Durcan *et al*., 2019), white stars represent new sites included in this paper (see Supplementary Information in Appendix G). (b) Associated Holocene dune ages reported from the investigated sites. (*) represents the new ages presented in this study.

Table 6.1. Summary OSL data of new ages included in this study. D_e, $\dot{D}$ and ages are shown to two decimal places, with all calculations made prior to rounding. All ages were calculated using Central Age Model (CAM) and are relative to the year 2018.

Sample	Depth (m)	Discs accepted (measured)	Overdispersion (%)	CAM D_e (Gy)	Beta $\dot{D}$ ($Gy.ka^{-1}$)	Gamma $\dot{D}$ ($Gy.ka^{-1}$)	Cosmic $\dot{D}$ ($Gy.ka^{-1}$)	Envir $\dot{D}$ ($Gy.ka^{-1}$)	Age (ka)
Thar 16/2/1	21	23 (50)	32.7 ± 4.3	24.55 ± 1.84	1.43 ± 0.11	1.12 ± 0.08	0.03 ± 0.02	2.58 ± 0.14	9.53 ± 0.87
Thar 16/2/3	22	23 (42)	26.7 ± 4.1	25.28 ± 1.43	1.25 ± 0.10	0.86 ± 0.06	0.03 ± 0.02	2.14 ± 0.12	11.83 ± 0.93
Thar 16/8/1	2	28 (48)	24.3 ± 3.5	21.82 ± 1.04	1.16 ± 0.09	0.86 ± 0.06	0.16 ± 0.02	2.18 ± 0.11	10.01 ± 0.70
Thar 16/8/2	3	23 (68)	31.9 ± 4.9	24.43 ± 1.66	1.33 ± 0.10	0.96 ± 0.06	0.14 ± 0.02	2.43 ± 0.13	10.04 ± 0.85
IND 14/5/1	2	20 (30)	21.8 ± 3.8	18.99 ± 0.97	1.43 ± 0.11	1.02 ± 0.07	0.16 ± 0.02	2.61 ± 0.13	7.28 ± 0.52
IND 14/5/2	3	20 (46)	22.4 ± 5.4	22.60 ± 1.21	1.42 ± 0.11	0.99 ± 0.07	0.14 ± 0.02	2.55 ± 0.13	8.86 ± 0.66
IND 14/5/3	10	34 (48)	22.6 ± 3.2	23.02 ± 0.96	1.31 ± 0.11	0.81 ± 0.05	0.07 ± 0.02	2.19 ± 0.13	10.51 ± 0.73
IND 14/5/4	11	18 (28)	12.6 ± 2.8	28.75 ± 1.01	1.48 ± 0.11	1.19 ± 0.08	0.06 ± 0.02	2.74 ± 0.14	10.51 ± 0.64
IND 14/5/5	25	29 (60)	28.8 ± 4.3	28.90 ± 1.65	1.54 ± 0.11	1.31 ± 0.09	0.02 ± 0.02	2.88 ± 0.14	10.05 ± 0.76
IND 14/5/6	26	18 (28)	30.0 ± 5.9	25.78 ± 2.04	1.41 ± 0.11	1.07 ± 0.07	0.02 ± 0.02	2.50 ± 0.13	10.33 ± 0.97

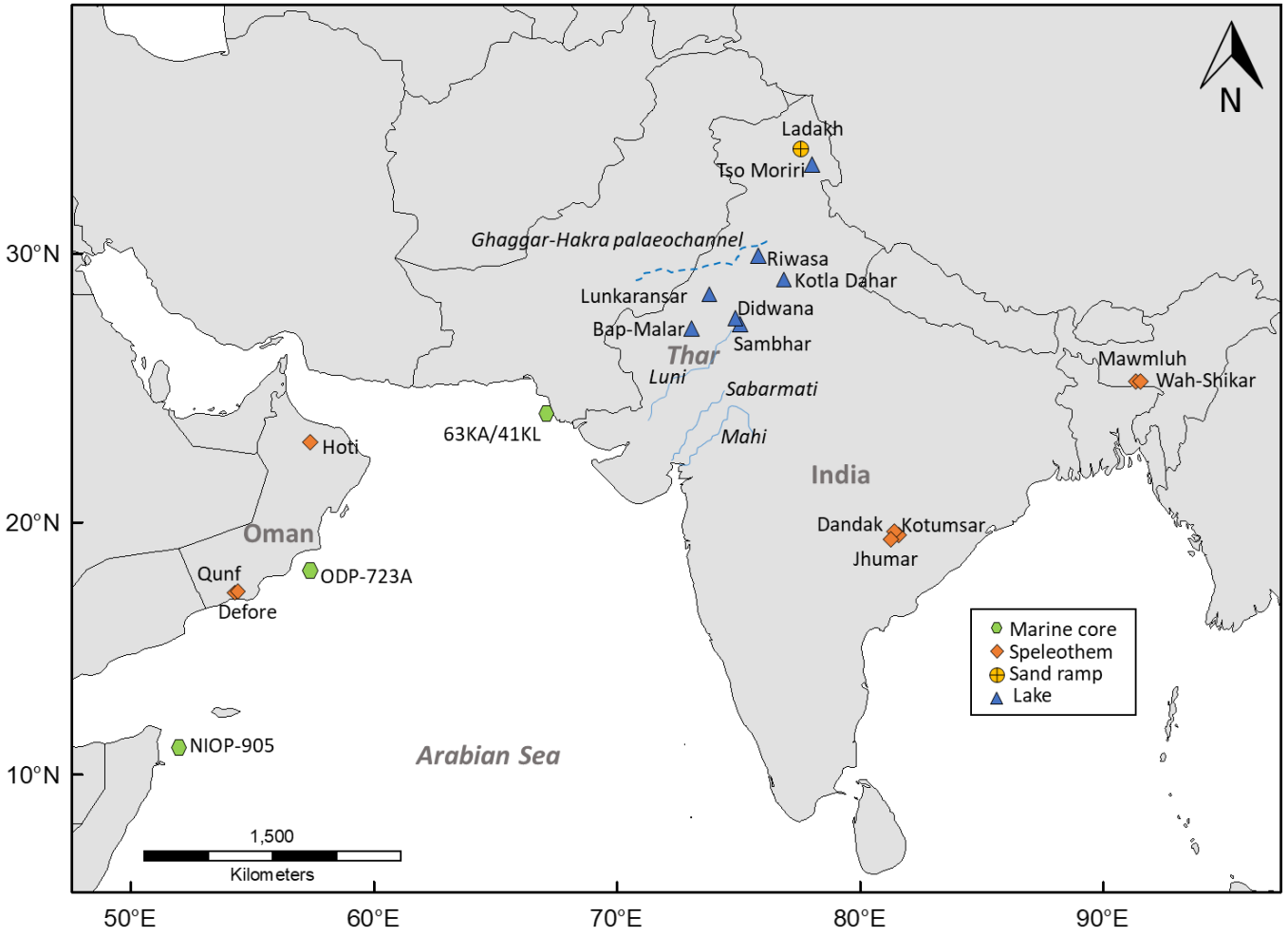


Figure 6.2. The locations of different types of proxies from north-western India and beyond as discussed in this chapter.

6.2.2 A new *AI* record for the Thar Desert

The new Holocene *AI* record for the Thar Desert is presented in Figure 6.3. For contrast, Figure 6.3a shows the initial Thar *AI* plot from Thomas and Bailey (2019), based only on the ages included in the original dune atlas database (Lancaster *et al*., 2016). Figure 6.3b shows the *AI* plot from the recently published OSL ages from parabolic and linear dunefields in the central and northern Thar (Srivastava *et al*., 2019a; Srivastava *et al*., 2019b), aeolian sequences along the Ghaggar-Hakra palaeochannel (e.g. Shitaoka *et al*., 2012; Durcan *et al*., 2019) and ten new OSL ages presented in this study (Table 6.1). Figure 6.3c shows the integrated results of *AI* analysis generated after combining all the Thar dune records included in Figure 6.3a and 3b.

The broadest accumulation peak falls within the late Pleistocene and early to middle Holocene period, extending from ~14 to ~6 ka based on >40 individual ages. The breadth of the peak in Figure 3a and 3c occurs as a result of the larger age uncertainties associated with the previously published ages, which are in the range ~ ±10-40 % (Table G.2). The new and recently published OSL ages (this study; Srivastava *et al*., 2019a; Srivastava *et al*., 2019b) have lower uncertainties (less than ±10%), which when incorporated into the *AI* model results in a narrower accumulation peak (Figure 6.3b). Thomas and Bailey (2017) discuss this in their paper, commenting that as uncertainties increase, peak broadness increases and peaks become less refined (see Figure 4A, 4B of Thomas and Bailey, 2017). Regardless of the resolution, the early Holocene is a period of high aeolian accumulation in the Thar Desert.

In the middle to late Holocene, as shown in Figure 6.3b, peaks are centred at ~7, ~5 and ~3.5 ka. Interestingly, there are no peaks or secondary ‘shoulders’

observed between ~5 and ~3.5 ka despite the presence of six luminescence ages (Figure 6.1). It can be explained in the context of underlying principles of *AI* analysis as these six ages have been calculated from different sampling locations in the Thar and hence associated accumulation thickness cannot be calculated. Another important consideration is that due to nature of y axis resolution, sometimes minor rises may not be displayed unless magnified (e.g. southern Kalahari dunefield; Thomas and Bailey, 2017).

The late Holocene peaks are notably absent from the original analysis from dune database records (Figure 6.3a). Prior to the recent application of intensive sampling through full dune sediment profiles, studies tended to exclude the upper few metres of dune sediments from investigation, sampling deeper sections, and therefore potentially under-representing the late Holocene records. With the inclusion of new data in this *AI* analysis, strong peaks appear in the late Holocene centred around ~2 ka and ~1 ka, with the most nuanced one based on 14 ages representing the last two centuries. Unlike the early Holocene peaks, the late Holocene *AI* peaks increase in size due to younger ages having narrower one sigma error ranges (causing accumulation concentrated towards the central age) and probabilistic likelihood of better preservation of younger accumulation phases (Bailey and Thomas, 2014).

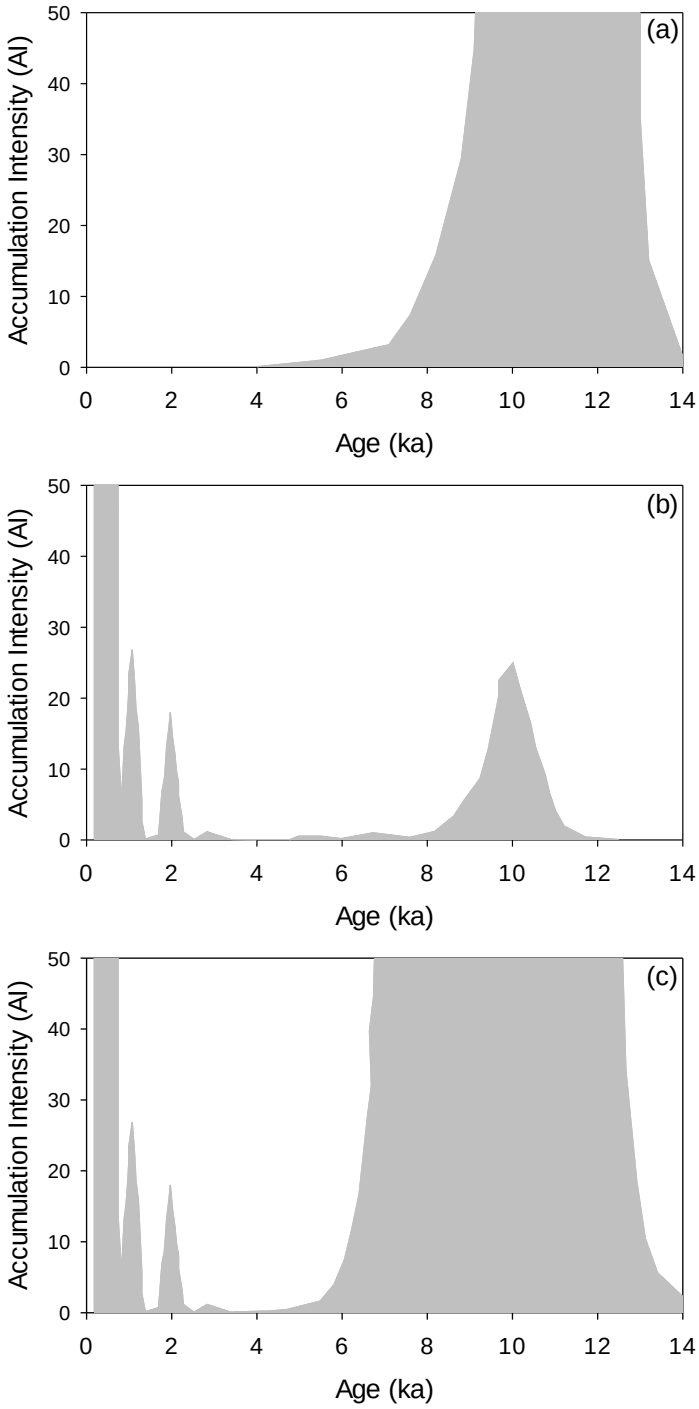


Figure 6.3. (a). Holocene *AI* plots for the Thar based on dune luminescence ages first listed in the INQUA dune atlas chronologic database (Lancaster *et al.*, 2016). (b). based on recent studies (Shitaoka *et al.*, 2012; Durcan *et al.*, 2019; Srivastava *et al.*, 2019a; Srivastava *et al.*, 2019b; this study). (c). all combined.

6.3. Drivers of Thar landscape change during the Holocene

6.3.1 Early Holocene (~11.7 - ~8.2 ka)

As the Thar lies in a monsoonal regime, the ISM winds remain one of the major drivers of dune accumulation in the desert (Wasson *et al*., 1983; Kar, 1993; Singhvi and Kar, 2004; Srivastava *et al*., 2019a). As shown by the strongest peak in the *AI* plot (Figure 6.3) and >30 individual luminescence ages from dunefields (Figure 6.1), the Thar landscape experienced widespread dune accumulation during the early Holocene. At least 3 parabolic dune sites in the central Thar and 4 linear dune sites in the northern Thar have been shown to have recorded accumulation between 12.2 ± 0.8 ka and 8.7 ± 0.6 ka, with net dune accumulation up to 3.5 m per year (Srivastava *et al*., 2019a; Srivastava *et al*., 2019b). The new ages presented in this paper are also consistent with these published early Holocene records (Table 6.1). The basal ages from a parabolic dune near Jodhpur (Thar 16/2; Figure 6.1) date to 9.53 ± 0.87 ka (Thar 16/2/1) and 11.83 ± 0.93 ka (Thar 16/2/3). The samples investigated from another parabolic dune Thar 16/8 also display consistency and further give evidence of an early Holocene dune accumulation between 10.01 ± 0.70 ka (Thar 16/8/1) and 10.04 ± 0.85 ka (Thar 16/8/2). Dunes at the northern margin of the Thar, associated with the Ghaggar-Hakra palaeochannel system, also record early Holocene aeolian accumulation. Six samples from one such source-bordering dune in the northern Thar margin show a rapid ~16 m thick dune accumulation between 10.05 ± 0.76 ka and 10.51 ± 0.73 ka (site IND 14/5; Table 6.1). The shallower samples at this site record dune activity at 7.28 ± 0.52 ka and 8.86 ± 0.66 ka at depths of 2 and 3 m (Table 6.1). Shitaoka *et al*. (2012) and Maemoku *et al*. (2012) dated sediments from nearby dunes to report accumulation between ~15-10 ka,

however, the extent of accumulation cannot be compared because their studies are based on ⩽2 samples from each dune. From the same area, Durcan *et al*. (2019), also used OSL dating to report aeolian accumulation dating to 8.93 ± 1.14 ka at 0.5 m and 8.89 ± 0.88 ka from uppermost 3.3 m of a dune in the same dunefield. Further to the north in the cold desert of Ladakh, Kumar *et al*. (2017) investigated five sand ramps using sedimentology and OSL dating and identified a phase of persistent high sedimentation rate between ~12 and ~8 ka. In the southern Thar, fluvial records from the Luni River suggest incision during this phase, which was followed by sheet flow aggradation between ~9 and ~5 ka (Jain and Tandon, 2003). Further south, records from the perennial Mahi and Sabarmati Rivers also indicate that these rivers incised during the early Holocene primarily governed by accelerated fluvial activity and large runoff as a response to enhanced ISM (Srivastava *et al*., 2001; Jain and Tandon, 2003; Jain *et al*., 2004).

The strong *AI* peaks, consistent with thick dune accumulation records from the Thar and beyond attest to a wider dynamic landscape response in the early Holocene. This period was marked by precessionally forced changes in insolation resulting in the intensification of the monsoon systems (Berger and Loutre, 1999; Wang *et al*., 2005), as evidenced in an array of terrestrial and marine proxies. In terrestrial records from north-western India, a $\delta^{18}O$ study conducted on ostracods from palaeolake Riwasa sediments (Figure 6.4) by Dixit *et al*. (2014b) showed that lake levels were high between ~9.4 and ~8.3 ka, in concurrence with the early Holocene monsoon strengthening. The other lakes in the Thar (notably Sambhar, Didwana, Bap-Malar and Lunkaransar),however, show differences in the onset timings of fluctuations in levels and salinity throughout the Holocene

(Figure 6.4). Lake level peaks do not directly correlate with the early Holocene ISM strength, as the high lake levels were reported to have occurred in the middle Holocene (Prasad and Enzel, 2006; Macdonald, 2011; Misra *et al*., 2019). Furthermore, Lake Sambhar in the eastern Thar does not record any evidence of complete desiccation (Sinha *et al*., 2006). These differences, which highlight the difficulties in considering individual lake records as representative of the regional picture, may be due to a multitude of reasons including differences in their geographic locations and groundwater discharges, resulting in different hydrological responses to rainfall changes as well as basin size, depth and morphology (e.g. Bowler, 1986); differences in the proxy records analysed in individual studies resulting in diverse interpretations (e.g. Burrough and Thomas, 2009); differences in employed dating methods and interpretive resolutions (e.g. Cohen, 2003) and finally the additional possibility of winter rainfall also contributing to the hydrology of some of the basins (Enzel *et al*., 1999; Prasad and Enzel, 2006).

The published Holocene speleothem records are scarce within the peripheral domain of the ISM in the Indian subcontinent and do not often cover the entire Holocene period (e.g. Yadava and Ramesh, 1999; Dixit and Tandon, 2016; Kaushal *et al*., 2018; Band *et al*., 2018 and references therein). Nevertheless, more negative $\delta^{18}O$ values reported from speleothem records in the Mawmluh Cave, north-eastern India suggest an enhanced ISM precipitation in the early Holocene (Berkelhammer *et al*., 2015; Dutt *et al*., 2015). The other high-resolution $\delta^{18}O$ records from speleothems in Oman also indicate a rapid increase in ISM strength between ~10.6 and ~9.7 ka in southern Oman (Qunf and Defore Caves) and between ~10.1 and ~9.2 ka in northern Oman (Hoti Cave)

(Figure 6.4; Fleitmann *et al*., 2003; Fleitmann *et al*., 2007) which is consistent with widespread early Holocene dune accumulation in the Thar.

Holocene ISM variability has been inferred from the Arabian Sea sedimentary records as the region experiences upwelling driven by this monsoon system. Gupta *et al*. (2003) presented a high-resolution foraminifer (*Globigerina bulloides*) productivity record of wind strength from a core off the coast of Oman (ODP- 723). This suggested an early Holocene strengthening of the ISM marked by discrete weak intervals (Figure 6.4). Another productivity record based on *Neogloboquadrina dutertrei* from south-western Arabia Sea core NIOP-905 also shows broad consistency with Gupta *et al*. (2003)'s observations (Ivanochko *et al*., 2005). Staubwasser *et al*. (2002) presented a record of the Indus River discharge using *Globigerinoides ruber* $\delta^{18}O$ from core 63KA/41KL off Pakistan, and suggested strengthening of the ISM between ~12 and 11 ka BP with maximum Indus water discharge at ~9.4 ka. Gill *et al*. (2017) hypothesised teleconnections from the Pacific and based on sea surface temperature proxies from 27 locations scattered across the equatorial Pacific revealed the greatest ISM wind stress curl during this period. The correlation between upwelling and wind strength proxies from the Arabian Sea and enhanced phases of dune accumulation thus most likely suggest an in-phase relationship between general intensification of the ISM and dune accumulation in the early Holocene.

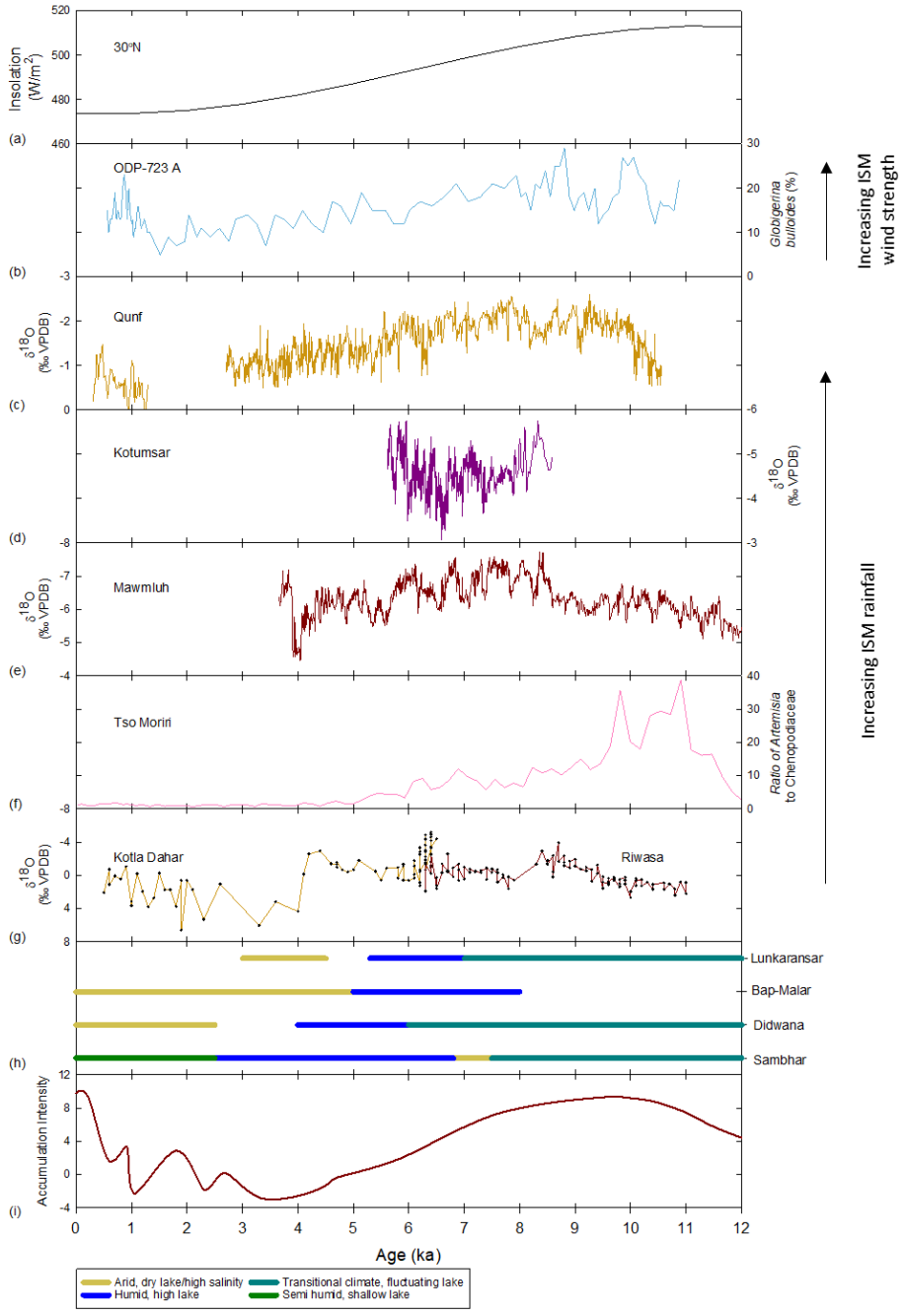


Figure 6.4. (a). Summer insolation (W/m^2) at 30^{0}N (from Berger and Loutre, 1999). (b). *G. bulloides* percentage from a marine core ODP-723A off Oman (Gupta *et al*., 2003). (c). δ^{18}O record (‰ Vienna Peedee belemnite; VPDB) from a stalagmite in the Qunf Cave, southern Oman (Fleitmann *et al*., 2003). (d). δ^{18}O record (‰ VPDB) from the Kotumsar Cave, central India (Band *et al*., 2018). (e). δ^{18}O record (‰ VPDB) from the Mawmluh Cave, north-eastern

India (Berkelhammer *et al*., 2012). (f) pollen percentage ratio of *Artemisia* to Chenopodiaceae (A/C) from Tso Moriri (Leipe *et al*., 2014) (g). Gastropod $\delta^{18}O$ record (‰ VPDB) from palaeolakes Kotla Dahar (Dixit *et al*., 2014a) and Riwasa (Dixit *et al*., 2014b). (h) Schematic representation of Holocene palaeolimnological history of four inland lakes in the Thar (Wasson *et al*., 1984; Kajale and Deotare, 1997; Deotare *et al*., 1998; Enzel *et al*., 1999; Sinha *et al*., 2006); (i) Summary *AI* curve for the Thar dune records as analysed in this study.

6.3.2 Middle Holocene (~8 - ~4.2 ka)

The middle Holocene, in contrast to the early Holocene, has fewer records of dune accumulation which come from scattered sites. In the *AI* plots, this period has therefore fewer and more minor peaks (Figure 6.3c). As shown in Figure 6.1b there is a relative lull in recorded dune accumulation between ~8.5 ka and ~7 ka in the northern and central Thar, although there are luminescence ages from dune sites in the southern Thar that show evidence of dune accumulation (Singhvi and Kar, 2004). Juyal *et al*. (2003) associated southern Thar dune activity with the availability of sediment from a large alluvial plain of regional rivers, notably the Mahi and the Sabarmati, in combination with lower sea-levels, increasing sediment availability to the wind, resulting in source-proximal dune accumulation despite the weaker ISM.

Several high-resolution records have suggested variability in ISM strength during the middle Holocene (Gupta *et al*., 2003; Wang *et al*., 2005; Dixit *et al*., 2014a). Based on stalagmite $\delta^{18}O$ records from the Kotumsar Cave in central

India, Band *et al*. (2018) showed that the intensity of ISM gradually declined between ~8.5 ka and ~6.5 ka, which was followed by a steady increase between ~6.3 and ~5.6 ka (Figure 6.4). The brief period of re-intensification can also be observed in $\delta^{18}O$ records from other Qunf and Mawmluh Caves (Fleitmann *et al*., 2003; Berkelhammer *et al*., 2012; Figure 6.4). There are two dune sites in the northern (Jamsar) and central (Jodhpur) Thar where dune accumulation was recorded in this phase, as reflected in the form of minor *AI* peak in Figure 6.3b. Other geochemical records indicate further weakening of the ISM after ~5 ka as evidenced from high $\delta^{18}O$ values in Kotla Dahar palaeolake along the northern Thar margin (Dixit *et al*., 2014a; Figure 6.4), low *Artemisia* to Chenopodiaceae pollen ratios from Tso Moriri Lake in northern India (Leipe *et al*., 2014; Figure 6.4) and higher $\delta^{18}O$ values in speleothem record from Mawmluh in north-eastern India (Berkelhammer *et al*., 2012; Figure 6.4). Despite a relatively weaker ISM, dune accumulation is recorded along the Thar's north-eastern fringe during the middle Holocene, coincident with enhanced fluvial activity. Saini and Mujtaba (2010) and Durcan *et al*. (2019) dated silty sand fluvial sediments from the Ghaggar-Hakra palaeochannel and reported fluvial deposition during this phase which continued to ~4 ka. Multiple source bordering dunes in the vicinity, also recorded dune activity (Shitaoka *et al*., 2012; Maemuku *et al*., 2012). Durcan *et al*. (2019) suggested this concurrence of dune and fluvial activity to be related to changing hydrological conditions of the palaeochannel, with the drying of the fluvial system resulting an increase of sediment supply available for entrainment. They hypothesised that dune accumulations on the floodplain of the Ghaggar-Hakra channel are sourced from reworking of the fluvial sediments. Similar co-occurrence has been shown in the context of landscape dynamics near Cooper

Creek in the Lake Eyre basin in central Australia where dune activity on the floodplain has direct sediment influx from the fluvial system (Cohen *et al*., 2010; Maroulis *et al*., 2007). Based on these data, it is evident that dune accumulation occurred over a large area of the Thar Desert and its margins during the middle Holocene, attributable to enhanced sediment supply from ephemeral fluvial channels set against the backdrop of a weakening ISM. Further the coeval fluvial activity records suggest that during the middle to late Holocene, the landscape along the Ghaggar-Hakra palaeochannel possibly acquired a state of balance, which Li and Coulthard (2015) describe as a geomorphic setting where both fluvial and aeolian processes operate together.

The middle Holocene palaeolimnological histories of the Thar lakes have often been compared with the timing of dune accumulation to test a potential relationship. For instance, Thomas *et al*. (1999) studied a palaeolake in the northern Thar (near Jamsar) and hypothesised antiphase behaviour between dune accumulation and lake aridity at ~5 ka that during a period of relatively increased aridity, lake dried up which facilitated sand mobilisation. Prasad and Enzel (2006) also compared the middle Holocene 'dune formation' episodes in the southern Thar with aridity records from nearby lakes and suggested further analyses of the available regional climate record. However, establishing any such relationship requires careful assessment of each geomorphic system individually and their response to external factors. For example, lakes that are groundwater or distant-catchment fed could be wet in locations where dunes are also active (accumulating), as the forcing factors (local wind /aridity, distant moisture source) do not conflict as evidenced in the case of dunes and lakes in Badain Jaran Desert, Inner Mongolia, China (Yang *et al*., 2003; Yang *et al*., 2010). Further,

dunes can be active, and lakes wet over annual/decadal cycles in regions with strongly seasonal climates, which is a characteristic of monsoon environments such as the Thar. For instance, when Lake Bap-Malar recorded high levels between ~8 ka and ~5 ka (Kajale and Deotare, 1997) (Figure 6.4), parabolic dunes in the nearby dunefield (Srivastava *et al*., 2019b) were also accumulating during the period. Therefore, a complex, nonlinear relationship should be expected between lake hydrological changes and dune records.

6.3.3 Late Holocene (~4.2 ka - ~present)

In the late Holocene, two minor peaks are observed between ~3.5 ka and ~1.5 ka (Figure 6.3c), calculated from dune records from the central and northern dunefields. Late Holocene dune records, however, remain scarce from the southern Thar (Figure 6.1), with only 2 of the 18 luminescence ages from this area recording late Holocene accumulation (Figure 6.1b). As the *AI* method focusses on the time period in which sediments accumulated rather than treating individual ages as discrete dune activity phases (Thomas and Bailey, 2017), peaks between ~3.5 and ~1.5 ka suggest the beginning of a phase of accumulation instead of an activity phase. Interestingly, the late Holocene, due to weakening of the ISM and reduced monsoonal precipitation, represented a phase of pronounced aridity in the Thar. Jain and Tandon (2003) and Jain *et al*. (2004), based on sedimentological analyses and luminescence dating, suggested that the streams of rivers in the southern Thar became defunct. Several lakes in the Thar like the Bap-Malar, Didwana, Lunkaransar also showed high salinity levels or dried up during this phase (Wasson *et al*., 1984; Singh *et al*., 1990; Kajale and Deotare, 1997; Deotare, 1998; Enzel *et al*., 1999). Whilst

the records of dune accumulation in the backdrop of weakening ISM are sparse, the drying lakes and river sources acted as potential local sources of sediment supply, and hence the *AI* peaks appear, even during a period of weakened ISM intensity.

In Figure 6.3c, two *AI* peaks are observed: one centred around ~1 ka and the other representing the recent century. In the last millennium, based on $\delta^{18}O$ values from a speleothem from the Wah Shikar Cave in north-eastern India, it has been suggested that ISM strength was variable, and coincided with intervals of droughts in the subcontinent (Gupta *et al*., 2019). Other speleothem studies from the Dandak and Jhumar Caves in central India (Sinha *et al*. 2007; Sinha *et al*., 2011a; Sinha *et al*., 2011b; Berkelhammer *et al*., 2010) also reported weaker ISM conditions attributable to drought conditions across large part of the country. In the Thar, there is recurring evidence from different dune sites of continuous dune activity coinciding with some of the historically reported long droughts. These droughts during 1255-1258, 1309-1313, 1868-1870, 1899-1905 and 1935-39 have been attributed to weak and erratic summer monsoons (Sharma 1966; Narain and Kar, 2005). The relationship between drought events with dune activity has been investigated in some detail in the context of dunefields in the Kalahari (Thomas and Leason, 2005; Thomas and Burrough, 2012) and the Nebraska Sandhills (Miao *et al*., 2007; Hanson *et al*., 2009; Buckland *et al*., 2019) to demonstrate geomorphological consequences in the landscape. It could be hypothesised that during drought events, vegetation on dunes and groundwater levels fell affecting the stability of dunes and exposing their surfaces to reactivation.

While a strengthening of the ISM in recent centuries has been suggested based on marine productivity records (e.g. Anderson *et al*., 2002; Anderson *et al*., 2010) and speleothem geochemistry from the Indian subcontinent (e.g. Gupta *et al*., 2019; Sinha *et al*., 2011a), Gill *et al*. (2017) suggest that precipitation over northwest India today is approximately 40% lower when compared to Early Holocene levels.. Instrumental meteorological data collection began during the mid-19th century in the Thar Desert, and shows that fluctuations in rainfall inter-annually, but no long term increase or decrease (Sontakke *et al*., 1993; Parthasarathy *et al*., 1994). From field observations made throughout the year, Singhvi and Kar (2004) observed increased levels of sand mobility in areas of significant human pressure, which they suggested to be greater now than during the Late Quaternary period. This is seen in the late Holocene strong *AI* peaks in Figure 6.3c, which are comparable to the pronounced early Holocene *AI* peaks, and are more likely to be the result of significant anthropogenic disturbances in the Thar landscape. Since the subcontinent's independence seventy years ago, the human population has seen a four-fold rise in the Thar as land reforms and the construction of irrigation canals has increased access and agricultural potential (Kar *et al*., 2014; Dhir, 2018). Today, the population density of the Thar is over 100 people/km^2 which surpasses not just other arid but many temperate regions too. Increased livestock grazing, mechanised ploughing on dune slopes and excessive groundwater pumping have all led to a significant deterioration in vegetation cover and dune reactivation. Srivastava *et al*. (2019b) have shown that sensitive parabolic dunes in the central Thar have recorded accumulation rates up to 5 m per year in the recent century. Similar cases of anthropogenic drivers of dune activity have also been observed in semi-arid regions of China

(e.g. Yang *et al*., 2011; Xu *et al*., 2019; Zhang and Huisingh, 2018) and the Negev (Tsoar, 2008; Roskin *et al*., 2013).

6.4. Conclusions

There are now more than 100 Holocene luminescence ages calculated from dunes in the Thar Desert. This new *AI* analysis identifies multiple peaks of dune accumulation, notably between ~12-~8 ka, and centred around ~7, ~5 and ~3.5 ka. The strongest peaks are observed in recent centuries. The widespread early Holocene dune accumulation is most likely to have occurred as a response to the period of strengthened ISM that is recorded in the other proxies from the subcontinent and beyond (e.g. Gupta *et al*., 2003; Fleitmann *et al*., 2003; Gill *et al*., 2017). During the middle to late Holocene, when the ISM started to weaken gradually, sediment supply facilitated by drying river channels in the northern Thar, and anthropogenic disturbances in the central Thar have been significant drivers of dune activity (e.g. Durcan *et al*., 2019; Srivastava *et al*., 2019b). The dune ages cannot be translated simply to derive palaeoclimatic interpretation as they display a nonlinear and complex relationship with rainfall and aridity, much like the dune records from the Kalahari (Chase, 2009), the Arabia (Atkinson *et al*., 2011; Leighton *et al*., 2014) and the Negev (Roskin *et al*., 2011). Thar fluvial and lacustrine records also present a picture of dynamic yet divergent responses to drivers during the Holocene. Along the northern margin of the Thar, the Ghaggar-Hakra system shows a concurrence of fluvial and dune activities during the middle to late Holocene. The lake records from the Thar also show complex relationships with ISM variations, and it is therefore unsurprising that dune accumulation periods do not necessarily relate to lake low phases. These

complex geomorphic responses over time in the Thar, and the lack of clear correlations between both lake/dune dynamics and ISM changes inferred form marine records, indicates that landscape dynamics are likely driven by the complex interplay of regional and more local drivers.

This study with the application of *AI* analysis, has allowed an enhanced recognition of the complexity of landscape development in the Holocene. However, there still remain challenges in constructing a holistic picture of landscape dynamics as the Thar is under-sampled spatially and temporally with few intensive dunefield based studies. Being an extensive desert with many distinct dune types, further dunefield based studies are needed to represent the complexity of geomorphic evolution of the Thar landscape through time.

Chapter 7: Implications and conclusions

7.1. Introduction

The research in this thesis has sought to investigate the timing of dune accumulation in the Thar Desert, India during the late Quaternary, in relation to potential drivers of dune activity. In doing so, the thesis addresses three key research questions:

RQ1. When did dune accumulation occur during the late Quaternary in response to drivers of landscape change?

RQ2.Given the large and dense population that the Thar hosts, what is the effect of anthropogenic pressure on dune activity?

RQ3. What do the dune records reveal about the late Quaternary geomorphological and regional palaeoenvironmental changes in the Thar?

This chapter draws together the findings of the three papers (Chapters 4-6) to directly answer these three questions. It discusses the implications of key findings for wider research including fieldwork in drylands, development of parabolic and linear dunes, and suitability of dunes as proxies of desert climate change. The chapter then briefly discusses some recommendations for future luminescence dating based studies of aeolian features in the Thar, and ends with offering overall conclusions.

7.2. Addressing thesis research questions

7.2.1. RQ1. When did dune accumulation occur during the late Quaternary in response to drivers of landscape change?

The body of work presents the first application of a robust luminescence dating (SAR) protocol to a series of samples retrieved from intensively investigated dune sections in the Thar. The dune ages, as determined and presented in Chapter 3, have revealed a new and significant history of late Quaternary dune accumulation in the Thar, with a strong late Holocene record (Figure 7.1). Two linear dune samples from the northern Thar provide the first reported occurrence of pre-Holocene dune activity in the region and demonstrate that the dunes have been present in the region since at least ~58 ka (Chapter 5). This is important since the antiquity of the Thar dunefields had been a contested topic, and older records were reported from the central and southern Thar (Singhvi and Kar, 2004; Chapter 2). The absolute OSL ages in this thesis are predominantly Holocene in age, ranging between 0.05 ± 0.01 ka and 13.85 ± 1.11 ka. The pattern of calculated dune luminescence ages displays two primary characteristics: 1) phases of dune accumulation throughout the Holocene, and 2) two intense periods of accumulation around the early Holocene and in the last millennium. As shown in Figure 7.1, the records of early Holocene dune accumulation have been reported from various dune sites. Interestingly, these records were unfrequently reported in previous studies, despite of this period being marked by strengthened ISM winds. Prasad and Enzel (2006) attributed this absence to seemingly large uncertainties associated with previously published ages, while Kar *et al.* (2004) discussed the presence of this phase of accumulation from dune records from the southern margin of the Thar. As discussed in Chapters 4, 5 and 6, early Holocene accumulation periods match with other dune records from monsoon dominated

dunefields in the north-eastern Rub'al Khali (Atkinson *et al.*, 2011, Atkinson *et al.*, 2012) as well as an array of other geochemical and palaeoecological records from other terrestrial and marine archives (Chapters 4 and 5). Multiple spatially heterogeneous middle and late Holocene records of dune activity have been reported at ~4-3, 2-1, 0.6-0.2 and 0.07 ka, from linear, parabolic and source-bordering dunes, which are attributed to more regional factors including sediment supply facilitated by drying river channels and alluvial plains of regional rivers, and anthropogenic disturbances (Chapter 6).

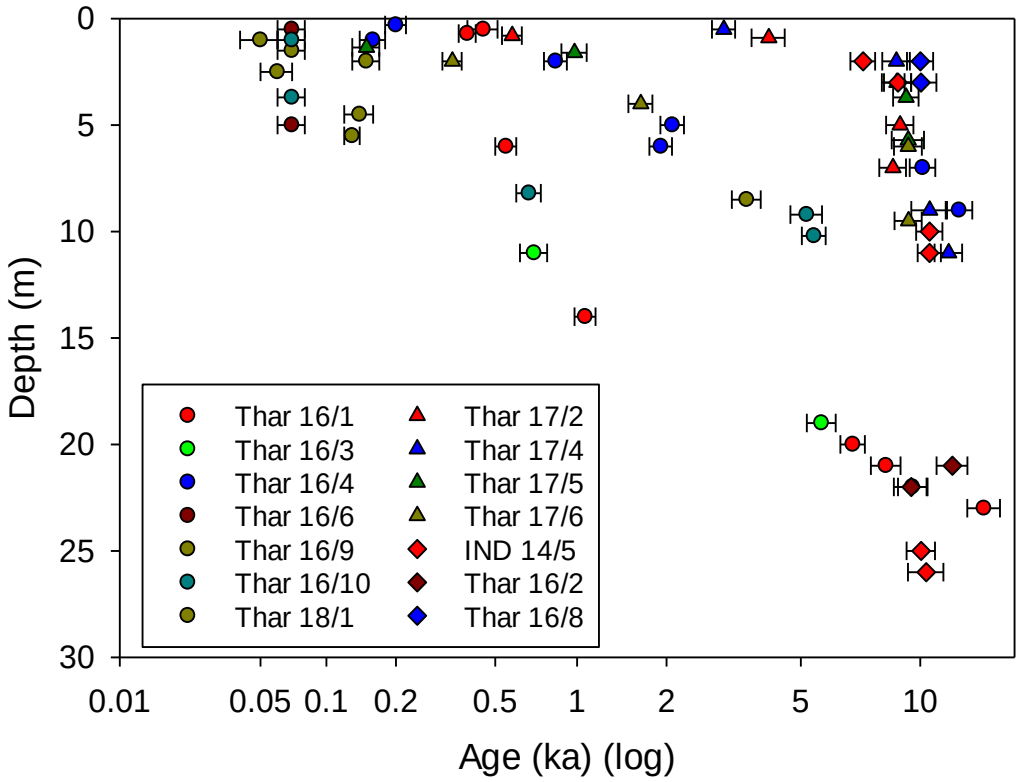


Figure 7.1. Age-depth plot for the absolute OSL ages presented in this thesis. The two minimum ages for samples Thar 17/2/10 and Thar 17/5/8 are not shown here. Samples beginning with code Thar 16/ are from parabolic dunes, Thar 17/ from linear dunes and IND 14/5 is a source bordering dune.

In summary, new and different phases of Holocene dune accumulation, both temporally and spatially, have been identified in this thesis. This formed the first step towards understanding the controls operating on dune development and the palaeoenvironmental conditions which lead to accumulation, which were discussed in Chapters 4-6 and summarised in the following section as response to RQ2 and RQ3.

7.2.2. RQ2. Given the large and dense population that the Thar hosts, what is the effect of anthropogenic pressure on dune activity?

As outlined in Chapter 2, in previously published ages, pulling apart of distinct phases of dune accumulation and their interrogation in terms of potential drivers was limited due to large uncertainties. Singhvi and Kar (2004) in their review of Thar dune records discuss the issue of resolution in late Holocene records and associated difficulties in determining the impact of humans on the landscape. Consequently, whilst the effect of anthropogenic influences on the Thar landscape had been visible, the apparent impact on dune activity and its quantification was not possible.

In this thesis, five parabolic dunes, which are sensitive to an array of factors in the environment they exist in were investigated to address this issue (Chapter 4). For the first time, a large data set of phases in the last millennium and within the last seven decades has been identified which includes a strong anthropogenic dimension. Modern records of dune activity have been reported from investigated parabolic dunes, with dune ages ranging between 0.15 ± 0.01 ka to 0.05 ± 0.01 ka. Many dunes dune ages date to 0.07 ± 0.01 ka and younger, generating accumulation rates up to 5 m per year (Chapter 4). When these modern records are run through *AI* modelling, a strong peak is observed (Chapter 6). In Figure 6.3, it is shown that the levels of dune activity

in the last century (caused by anthropogenic disturbances) is greater than those in middle Holocene and comparable to the pronounced early Holocene *AI* peaks (Chapter 6). These modern luminescence ages coincide with India's independence, expansion of irrigational network and mechanised farming in the most arid districts, and the subsequent four-fold rise in human population in the desert region (Chapter 1), which together have increased the potential for activation of dune sands.

As shown in Figure 1.7, the Thar landscape is changing rapidly and dunefields are increasingly being replaced by agricultural lands. There's widespread degradation of natural vegetation and most of the permanent pasture lands in dunefield areas are severely exploited for fuelwood and fodder (Kar, 2014; Dhir *et al*., 2018). Uprooting of sand binder shrubs species, like *Calligonum polygonoides* and *Leptadenia pyrotechnica*, to make way for crops, has also aided sand transport (Kar, 2009). In Chapter 4, over-pumping of groundwater which results in the gradual emptying of aquifers, and increasing salinity in the region (Rodell *et al.*, 2009), has been associated with the stability of parabolic dunes in the central Thar. Other than in the Thar, the substantial effects of anthropogenic disturbances, in the last century, have also been noted in the dunefields in Hungary (Kiss *et al.*, 2012), Israel (Tsoar, 2008; Roskin *et al.*, 2013) and the vast expanses of semi-arid regions in China (e.g. Zhao *et al.*, 2007; Yang *et al*., 2011; Xu *et al*., 2019; Zhang and Huisingh, 2018).

A direct implication of the rapidly changing Thar landscape is to prioritise and conduct fieldwork in the regions which are undergoing landscape alterations due to agricultural or urban expansions. In Chapter 4, it was discussed that how the trailing arms of parabolic dunes are being flattened to make way for agricultural land, as there is immense demand for land clearance in the region. Because of rapidly changing landscape, it has become impossible to revisit sites investigated in earlier studies and

do comparative investigations- an issue highlighted in Chapter 2. Nevertheless, this scenario instead offers an opportunity to understand and quantify anthropogenically-induced dune accumulation and migration rates which will then be useful for planning future land use practises.

7.2.3. RQ3. What do the dune records reveal about the late Quaternary geomorphological and regional palaeoenvironmental changes in the Thar?

Geomorphological changes

Parabolic and linear dunes are the two principal dune types investigated in this study. The OSL age data set shows that these dominant Thar dune types continued to accumulate through modern times, and therefore, their classification as 'old system' dunes as previously implied, does not hold true (Chapter 5). As more dunes are investigated, further evidence of modern reactivations is rather observed in the Thar.

Parabolic dunes, being widespread in arid and semi-arid regions worldwide, are also the second most widely studied dune type worldwide in terms of chronological investigations (~15 %; Lancaster *et al.*, 2016). As discussed in Chapter 4 (Section 4.4.2), these dunes are very sensitive to environmental deteriorations. In the last century, due to the anthropogenic disturbances, these dunes in the central Thar have reactivated and shown modern accumulation of up to ~5 m per year. In the context of dunefields in Canadian Prairies, Hugenholtz and Wolfe (2005) discuss how after reactivation, mobility of such dunes may last for decades or centuries. Whilst the nose of these dunes in the Thar are anchored by dense vegetation, migratory transverse features are forming atop dune arms which are propagating downwind and depositing sand (Figure 4.9). This has resulted in the transition of parabolic dunes to the

barchanoid-parabolic transitional dunes. Mathematical modelling has been previously used to demonstrate such geomorphic transformation (e.g. Yan and Baas, 2017), but in this thesis luminescence dating has been presented as a method not to just reveal such transformations but also allow their quantification, therefore, offering a new avenue for parabolic dunes studies in other susceptible semi-arid to arid areas.

Linear dunes are the most studied dune type worldwide, and in the context of the Thar, their investigation is presented for the first time in this thesis (Chapter 5). Thar linear dunes have been shown to have preserved evidence of older and multiple phases of past periods of dune activity, just like linear dunes elsewhere (Thomas, 2013). The mechanism of the formation of linear dunes in the Thar is a contested topic. While the luminescence ages presented in this thesis do not allow formative assessment of linear dune formation in the Thar, the ages can still be used to substantiate a theory proposed in earlier studies. Verstappen (1968) studied a parabolic-linear dunefield in the Jodhpur region and suggested that gradual blowing away of previously formed parabolic dune's noses and subsequent elongation of the arms formed linear dunes; the theory was later supported by Singh (1982) and Wasson *et al*. (1983). The length and spacing of trailing arms of parabolic dunes, and length between two linear dunes vary considerably throughout the Thar (e.g. Figures 4.9 and 5.2), therefore, in the absence of obvious spatial differences nature of dune accumulation becomes a vital factor to discuss the aforementioned theory.

However, as discussed in Chapter 4, it is the nose of parabolic dunes (in the Jodhpur region) which are the major zones of accumulation (late Pleistocene-early Holocene in age) where the maximum sand volume lies (Figure 4.9), while the arms are lower in height (~ 4 m) with noted evidence of thick modern accumulation. In contrast, nature of dune accumulation in linear dunes in significantly different as

shallow samples (< 1 m) from linear dunes from the Bikaner dunefield provide evidence of considerably older phases of accumulation (Figure 5.6). The ages presented in this thesis, therefore, suggest that it is very unlikely that Thar linear dunes are remnant of parabolic dunes particularly in the Jodhpur-Bikaner region. Similar divergence between parabolic and linear dune types have been noted in an aeolian setting in the Bolivian Chaco, where the author recommends chronological data for a more detailed reconstruction of nature and timing of dune activity to substantiate their formation theories (May, 2013).

Palaeoenvironmental changes

In this study, the *AI* methodology has been applied to new set of chronologies generated as well as old dates, and generated *AI* peaks have been analysed alongside other palaeoenvironmental records (variability in the ISM and associated aridity) to allow an enhanced recognition of the complexity of the Thar landscape development and reconstruct regional palaeoenvironmental changes (Chapter 6).

The widespread early Holocene dune accumulation records generate a broad distinctive *AI* peak and show an in-phase relationship with increased productivity records and strengthened ISM winds deduced from the Arabian Sea sediments, high precipitation records inferred from oxygen isotope ratios from speleothems in the Arabia and central India, and high lake levels along the northern Thar margin based on sedimentological and geochemical observations. Whilst there is a palaeoclimatic evidence of an enhanced ISM during the early Holocene, the correlations are equivocal in the middle and late Holocene. During the middle to late Holocene, against the backdrop of a weakening ISM, the phases of dune accumulation have been

associated with enhanced sediment supply from drying river channels in the northern Thar, and both drying river channels and a lowered (Arabian) sea level in the southern Thar. This local role of changing sediment supply has been shown as an important control on dune development in the eastern Rub'al Khali (Preusser, 2009) and the central Australia (Maroulis *et al.*, 2007). Another important control on dune development in the Thar, particularly in the last century, is anthropogenic pressure on landscape (e.g. Figure 7.1). Whilst parabolic dunes have recorded rapid accumulation in the last 70 years, with rates up to 5 m/year, such rapid and modern signatures of dune accumulation are absent from the records from the investigated linear dunefield. It is interesting because both dunefields, only ~200 km apart, experience comparable rainfall and support equally dense human and livestock populations. This further highlights the importance to consider the different sensitivities of different dune types to same external controls.

In summary, this study with the application of *AI* analysis, has allowed an enhanced recognition of the complexity of landscape development and palaeoenvironmental changes in the Thar during the late Quaternary. The lack of clear correlations between both lake levels/dune accumulation and the ISM variability, indicates that landscape dynamics are likely driven by the complex interplay of regional and more local drivers. However, whilst this thesis has presented first dunefield-based studies from the Thar, being an extensive desert, further investigations are required to represent the complexity of geomorphic evolution of the Thar landscape and paleoenvironmental reconstructions.

7.3. Future work and considerations

The development and application of new field-based and laboratory techniques allow for the future expansion of the research conducted in this thesis. This section discusses and proposes some points which could be pursued as a continuation of the thesis and hold significance in the context of other investigations globally.

7.3.1 More dunefield based studies using modern dating protocols

The results in this thesis confirm that intensive fieldwork strategies and modern dating protocols have the potential to elucidate complex dune chronologies which significantly enhance analyses of dune development. However, the accumulation history of Thar dunes and their implications for geomorphological and palaeoenvironmental significance remain under-studied when compared with other deserts (e.g. the Negev, the Rub' al Khali, the Mallee; Roskin *et al.*, 2011a; Leighton *et al.*, 2013; Lomax *et al.*, 2011) which are well dated, both spatially and in terms of full-dune profile records.

As dunefield based studies from the Thar were not prevalent until this body of work, more intensive and systematic dunefield-based chronometric studies are recommended to help further identify spatial and temporal variability across the Thar dunefields: dunefields in the arid Barmer and Jaisalmer regions (Figure 3.1) are recommended as potential field sites. Furthermore, since the records presented in this thesis are largely confined to the Holocene, future studies will be valuable to fill the research gaps concerning Thar landscape beyond the Holocene.

7.3.2. Thar dune quartz

In this thesis, quartz signals have been used to establish a chronological framework. A two-week treatment of quartz grains with fluorosilicic acid and a post IR-blue SAR protocol were adopted as further precautions against any residual feldspar contamination which was noted in earlier studies (Chapter 3). Single grain analyses show that approximately 2-4 % of quartz grains provide a measurable OSL signal after a set laboratory dose (Table 3.3). Signals from small aliquots have been shown to exhibit rapid decay dominated by the fast component (Figure 3.11). However, as discussed in Chapter 3, a large number of measured aliquots failed on one or more quality checks. One third of measured aliquots do not display good recycling behaviour within protocol which could be due to either imperfect sensitivity correction, or the presence of signal components that do not behave as required for the application of the SAR protocol (Murray and Wintle, 2000). While there are no other published detailed investigations of the Thar quartz and its luminescence properties yet for comparison, the observations made in this thesis suggest that the Thar quartz is not as bright compared to other desert dunes' quartz (e.g. south-eastern Australia, south-western Kalahari; Fitzsimmons *et al.*, 2010; Telfer, 2011) and the use of this quartz to generate a robust luminescence age could be time intensive. Another consideration is signal saturation which is an associated limitation. As discussed in Chapter 5, two linear dune samples from a northern Thar dunefield display saturation of signals after ~100 Gy. This potentially explains why over two-third of pre-Holocene Thar ages listed in the dune atlas database used IRSL signal for D_e determination (Lancaster *et al.,* 2016).

7.3.2. Thar dune feldspars

The thesis exclusively uses luminescence signal from quartz grains for dating purposes. As demonstrated in Chapter 5, the Thar quartz signals show saturation characteristics after ~100 Gy, which means the upper dateable range of OSL dating is potentially limited to ~35-45 ka (assuming Ḋ between 2.2 and 2.8 $Gy.ka^{-1}$). Investigations on potassium feldspars have shown that IRSL signals saturate at higher doses (e.g. Thomsen *et al.*, 2008; Buylaert *et al.*, 2012), therefore, extending the age range offered by quartz OSL. Recently, the post-infrared signals have been demonstrated to offer improved signal stability over IRSL signals (e.g. Zhang and Li, 2020 and references therein) and have been used to date sediments in the region to the north (Singh *et al*., 2017) and south of the Thar (Blinkhorn *et al*., 2019). Therefore, future studies could consider using feldspars. Further, as discussed in Chapter 2, 45% of the Thar dune luminescence ages in the INQUA dune atlas database were based on feldspars and not corrected for anomalous fading (Lancaster *et al*., 2016), an intrinsic phenomenon that hampers the reliability of determined ages (Spooner, 1994; Huntley and Lamothe, 2001), future investigations of the IRSL signals used for dating will provide the added benefit of checking the robustness of already published records.

7.3.3 Study of other aeolian features

In the Thar, there remains a marked unevenness in spatial extent and type of dune investigated. Prior to this thesis, over 50 % of dune records came from parabolic dunes, ~20 % from undifferentiated dunes, ~4 from transverse dunes and none from linear dunes (Lancaster *et al*., 2016). Less dominant dune types, especially linear and transverse dunes, require further investigation. Whilst linear dunes (Chapter 5) saw

first dunefield based investigations, there still remains more potential to investigate the vast linear dunefields in the Pakistani Thar, from where no luminescence dating based study of dunes has been reported to date. Future investigations are expected to offer significant insights into wider Thar landscape and palaeoenvironmental dynamics. More mobile forms such as transverse dunes should also be investigated to constrain dune migration rates due to environmental changes and anthropogenic pressure. To date, there is just one study by Kar *et al.* (1998) who investigated a 7 m high transverse dune in the Western Thar and based on five luminescence ages provided evidence of high variability in dune accumulation in the last two millennia. Sand ramps in the southern Thar are another untapped aeolian feature in the Thar which should be further explored (Figure 7.2). Investigations of sand ramps from the southern Africa have established the potential of their records in proxy-poor environments (e.g. Telfer *et al.*, 2012; Telfer *et al.*, 2014; Rowell *et al.*, 2018a).

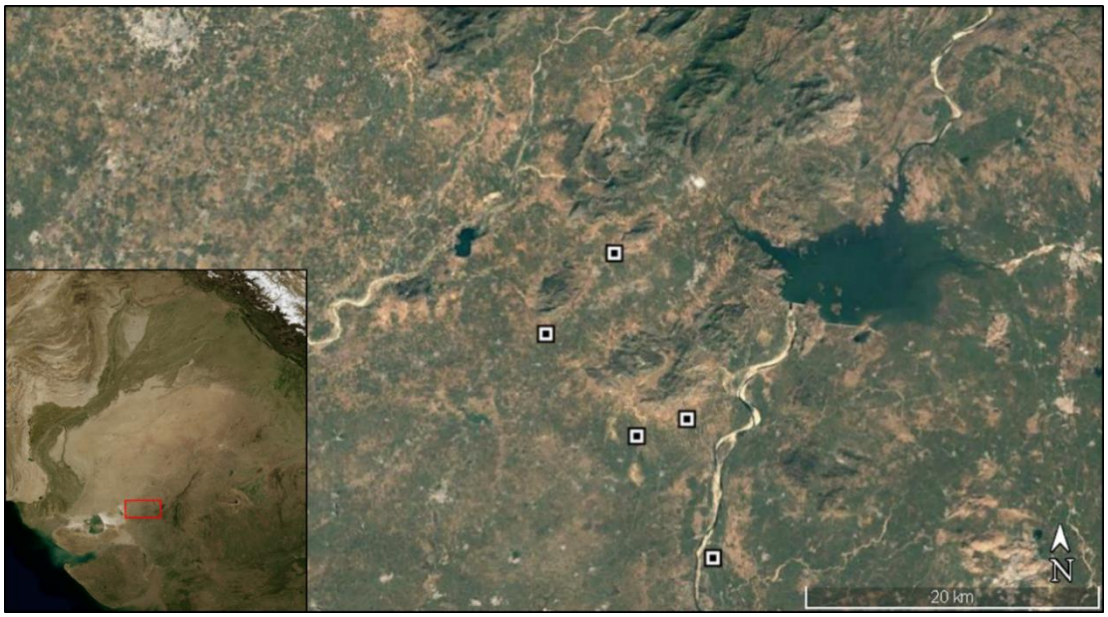


Figure 7.2. Location of a few sand ramps connected to hill slopes of the Aravalli Hills. Juyal *et al.* (2003), in their analysis of aeolian features in the southern Thar, discuss sand ramps in this region briefly.

However, as recently demonstrated by Rowell *et al.* (2018b), being complex aeolian features, the controls operating on sand ramps and the local geomorphic processes need to be identified and understood before sand ramps can be fully and reliably utilised as palaeoenvironmental archives.

7.3.4 Luminescence data quality and consistency

Whilst the contribution made by early studies on the Thar desert dunes has been duly acknowledged and included in this thesis, it is also critical to note the modern developments in scientific approaches and the necessity to then review older studies (Chapter 2). Despite once being at the forefront of application of luminescence dating to sand dunes, it has often been noted that publications presenting luminescence ages from the Thar dunes do not mention and discuss vital information like stratigraphic location, sample preparation, number of aliquots studied, over-dispersion in calculated values as well as the age models used. Collectively, this opacity of luminescence data undermines the robustness and reproducibility of ages, and affects subsequent interpretation. As noted in Chapter 6, due to under reporting of sample information more than 50 % of Thar ages from the INQUA dune atlas database were not eligible for *AI* analysis. Future studies and papers are recommended to be more thorough in data inclusion and presentation while publishing.

Prior to the work in this thesis, all the published dune ages from the Thar were based on now rarely used dating protocols that generated ages with large uncertainties (~20-60 %; Lancaster *et al.*, 2016). This thesis is the first study from the Thar in which the SAR luminescence dating protocol has been used to date aeolian dune sediments. As demonstrated in Chapters 3 and 4, with the help of a robust dating protocol, a more complex chronology with distinct phases in the late Holocene can be

identified which significantly enhances our understanding of dune development. Currently, ~20 % of all luminescence ages (from all the deserts) as listed in the INQUA dunes atlas chronologic database were determined using older protocols (Lancaster *et al.*, 2016), therefore, the reappraisal and re-analysis of these ages, in the context of methodological improvements, should be considered. This observation has been reiterated by Li and Yang (2016) who note that ~33 % of published luminescence ages from northern China and Mongolia were determined using older protocols, which led to difficulties in the assessment and interpretation of dune records.

7.4. Overall conclusions

The contribution made my early studies on the Thar Desert dunes established the potential of these dunes as the archive of past geomorphological and environmental changes (Chapter 1). However, due to lack of dunefield-based investigations and application of refined dating protocols, pulling apart of distinct phases of dune accumulation and their interrogation with other proxies in terms of potential drivers was limited (Chapter 2) (Singhvi and Kar, 2004; Singhvi and Porat, 2008; Lancaster *et al*., 2016). Therefore, with an aim to *investigate the timing of dune activity in the desert*, in relation to potential drivers of dune activity, three research questions were pursued in this thesis: (i) what are the key phases of dune activity (ii) what is the effect of anthropogenic influences on the landscape; and (iii) how can dune chronologies be interpreted most effectively to reconstruct late Quaternary environmental changes?

To address this, systematic sampling of dunes was conducted in a parabolic dunefield in the central Thar, a linear dunefield in the northern Thar and source-bordering dunefield associated with the Ghaggar-Hakra palaeochannel along the

northern Thar margin. OSL dating was used to provide a chronological framework (Chapter 3), to infer dune sensitivity to palaeoenvironmental change and the time scales over which dunes register and preserve the palaeoenvironmental record. Results, based on a suite of 60 quartz OSL ages, show that Thar dunes accumulated at least ~58 ka ago and the Holocene has been an important period with a number of preserved accumulation phases observed between ~13.85 ka and ~0.05 ka.

The suite of calculated ages shows that the development of parabolic dunes in the central Thar has been multi-generational in the geologic past, and due to modern-day significantly expanded anthropogenic disturbances, parabolic dunes have reactivated accumulating dune up to 5 m/year. These dunes are now marked by formation of superimposed young transverse features, and show geomorphic transformation to barchanoid-parabolic transitional dunes (Chapter 4). Linear dunes in the northern Thar, which are >58 ka old, remained active, accumulating sediment during the Holocene. Their investigations show that individual dunes do not capture temporally comprehensive accumulation and highlights the importance of dunefield-based studies (Chapter 5). The aeolian-fluvial sequence associated with the Ghaggar-Hakra palaeochannel along the northern Thar margin has also been shown to be a highly dynamic geomorphic system during the early Holocene (Chapter 6).

The application of *AI* methodology on the Thar dune records (both old and new data presented in this thesis) and interpretation of results in association with other high-resolution records from various terrestrial and marine archives provides important insights into the palaeoenvironmental changes in the desert (Chapter 6). The widely evidenced and thick early Holocene dune accumulation records generate prominent *AI* peaks in response to the period of strengthened ISM as noted in several other marine sediments records from the Arabian Sea and speleothem records from the

Arabia and the Indian subcontinent. During the middle and late Holocene, the Thar dunes have shown diverse and spatially heterogeneous responses to drying of river channels and lowered sea levels. In recent times, especially in the last seven decades, anthropogenic disturbances are the key driver of dune activity in the Thar.

Nevertheless, the overall synthesis of Thar accumulation records shows that whilst the dune records display a complex relationship with rainfall and aridity, they provide valuable insights into the landscape development and geomorphological change in the region, set within a robust chronological framework. As dunes are being increasingly used as geoproxies of past changes in different drylands worldwide, the findings in this thesis further attest that a more systematic and detailed approach (in terms of fieldwork and dating) is now needed to represent the complexity of a dunefield evolution through time. It becomes even more critical for investigations in other deserts which, like the Thar, are dotted by many distinct dune systems like the Nebraska Sand Hills in North America (Muhs and Budahn, 2019), the Andean Piedmont and western Pampas in South America (Tripaldi and Forman, 2007; Tripaldi and Zarate, 2016) amongst many others.

References

Aitken, M.J., 1985. *Thermoluminescence dating.* Academic Press, London.

Aitken, M.J., 1990. *Science-based dating in archaeology*. Longman, Essex.

Aitken, M.J., 1998. *Introduction to optical dating: the dating of Quaternary sediments by the use of photon-stimulated luminescence.* Oxford University Press, Oxford.

Aitken, M.J. and Smith, B.W., 1988. Optical dating: recuperation after bleaching. *Quaternary Science Reviews*, *7*(3-4), pp.387-393.

Aitken, M.J. and Xie, J., 1990. Moisture correction for annual gamma dose. *Ancient TL*, *8*(2), pp.6-9.

Allchin, B., Goudie, A. and Hegde, K., 1978. Prehistory and palaeogeography of the Great Indian Desert.

Anderson, D.M., Baulcomb, C.K., Duvivier, A.K. and Gupta, A.K., 2010. Indian summer monsoon during the last two millennia. *Journal of Quaternary Science*, 25(6), pp.911-917.

Anderson, D.M., Overpeck, J.T. and Gupta, A.K., 2002. Increase in the Asian southwest monsoon during the past four centuries. *Science*, 297(5581), pp.596-599.

Andrews, J.E., Singhvi, A.K., Kailath, A.J., Kuhn, R., Dennis, P.F., Tandon, S.K. and Dhir, R.P., 1998. Do stable isotope data from calcrete record late Pleistocene monsoonal climate variation in the Thar Desert of India? *Quaternary Research*, 50(3), pp.240-251.

Anton, D. and Vincent, P., 1986. Parabolic dunes of the Jafurah desert, eastern province, Saudi Arabia. *Journal of Arid Environments*, *11*(3), pp.187-198.

Ardon, K., Tsoar, H. and Blumberg, D.G., 2009. Dynamics of nebkhas superimposed on a parabolic dune and their effect on the dune dynamics. *Journal of Arid Environments*, *73*(11), pp.1014-1022.

Armitage, S.J. and King, G.E., 2013. Optically stimulated luminescence dating of hearths from the Fazzan Basin, Libya: a tool for determining the timing and pattern of Holocene occupation of the Sahara. *Quaternary Geochronology*, *15*, pp.88-97.

Arnold, L.J. and Roberts, R.G., 2009. Stochastic modelling of multi-grain equivalent dose (De) distributions: Implications for OSL dating of sediment mixtures. *Quaternary Geochronology*, *4*(3), pp.204-230.

Atkinson, O.A., Thomas, D.S.G., Goudie, A.S. and Bailey, R.M., 2011. Late Quaternary chronology of major dune ridge development in the northeast Rub'al-Khali, United Arab Emirates. *Quaternary Research*, *76*(1), pp.93-105.

Atkinson, O.A., Thomas, D.S.G., Goudie, A.S. and Parker, A.G., 2012. Holocene development of multiple dune generations in the northeast Rub'al-Khali, United Arab Emirates. *The Holocene*, *22*(2), pp.179-189.

Atkinson, O.A., Thomas, D.S.G., Parker, A.G. and Goudie, A.S., 2013. Late Quaternary humidity and aridity dynamics in the northeast Rub'al-Khali, United Arab Emirates: implications for early human dispersal and occupation of eastern Arabia. *Quaternary International*, *300*, pp.292-301.

Baas, A.C. and Nield, J.M., 2010. Ecogeomorphic state variables and phase-space construction for quantifying the evolution of vegetated aeolian landscapes. *Earth Surface Processes and Landforms: The Journal of the British Geomorphological Research Group*, *35*(6), pp.717-731.

Bailey, R.M. and Thomas, D.S.G., 2014. A quantitative approach to understanding dated dune stratigraphies. *Earth Surface Processes and Landforms*, 39(5), pp.614-631.

Bailey, R.M., Smith, B.W. and Rhodes, E.J., 1997. Partial bleaching and the decay form characteristics of quartz OSL. *Radiation Measurements*, *27*(2), pp.123-136.

Band, S., Yadava, M.G., Lone, M.A., Shen, C.C., Sree, K. and Ramesh, R., 2018. High-resolution mid-Holocene Indian Summer Monsoon recorded in a stalagmite from the Kotumsar Cave, Central India. *Quaternary International*, 479, pp.19-24.

Banerjee D., 1996. Thermoluminescence and Infrared Luminescence dating of alluvial sediments. Unpublished PhD Thesis.

Banerjee, D., Murray, A.S., Bøtter-Jensen, L. and Lang, A., 2001. Equivalent dose estimation using a single aliquot of polymineral fine grains. *Radiation Measurements*, *33*(1), pp.73-94.

Barbouti, A.I. and Rastin, B.C., 1983. A study of the absolute intensity of muons at sea level and under various thicknesses of absorber. *Journal of Physics G: Nuclear Physics*, *9*(12), p.1577.

Barchyn, T.E. and Hugenholtz, C.H., 2012. A process-based hypothesis for the barchan–parabolic transformation and implications for dune activity modelling. *Earth Surface Processes and Landforms*, *37*(13), pp.1456-1462.

Bateman, M.D., Boulter, C.H., Carr, A.S., Frederick, C.D., Peter, D. and Wilder, M., 2007. Detecting post-depositional sediment disturbance in sandy deposits using optical luminescence. *Quaternary Geochronology*, *2*(1-4), pp.57-64.

Bateman, M.D., Frederick, C.D., Jaiswal, M.K. and Singhvi, A.K., 2003. Investigations into the potential effects of pedoturbation on luminescence dating. *Quaternary Science Reviews*, *22*(10-13), pp.1169-1176.

Bell, W.T., 1979. Attenuation factors for the absorbed radiation dose in quartz inclusions for thermoluminescence dating. *Ancient TL*, *8*(2), p.12.

Berger, A. and Loutre, M.F., 1999. Parameters of the Earth's orbit for the last 5 Million years in 1 kyr resolution. PANGAEA.

Berkelhammer, M., Sinha, A., Mudelsee, M., Cheng, H., Edwards, R.L. and Cannariato, K., 2010. Persistent multidecadal power of the Indian Summer Monsoon. *Earth and Planetary Science Letters*, 290(1-2), pp.166-172.

Berkelhammer, M., Sinha, A., Stott, L., Cheng, H., Pausata, F.S. and Yoshimura, K., 2012. An abrupt shift in the Indian monsoon 4000 years ago. *Geophysical Monograph. Series*, 198, pp.75-87.

Blinkhorn, J., 2012. The Palaeolithic Occupation of the Thar Desert. Unpublished PhD Thesis.

Blinkhorn, J., 2013. A new synthesis of evidence for the Upper Pleistocene occupation of 16R Dune and its southern Asian context. *Quaternary International*, *300*, pp.282-291.

Blinkhorn, J., 2014. Late Middle Palaeolithic surface sites occurring on dated sediment formations in the Thar Desert. *Quaternary International*, *350*, pp.94-104.

Blinkhorn, J., Achyuthan, H. and Ajithprasad, P., 2015. Middle Palaeolithic point technologies in the Thar Desert, India. *Quaternary International*, *382*, pp.237-249.

Blinkhorn, J., Achyuthan, H., Ditchfield, P. and Petraglia, M., 2017. Palaeoenvironmental dynamics and palaeolithic occupation at Katoati, Thar Desert, India. *Quaternary Research*, *87*(2), pp.298-313.

Blinkhorn, J., Achyuthan, H., Petraglia, M. and Ditchfield, P., 2013. Middle Palaeolithic occupation in the Thar Desert during the Upper Pleistocene: the signature of a modern human exit out of Africa?. *Quaternary Science Reviews*, *77*, pp.233-238.

Blinkhorn, J., Ajithprasad, P., Mukherjee, A., Kumar, P., Durcan, J.A. and Roberts, P., 2019. The first directly dated evidence for Palaeolithic occupation on the Indian coast at Sandhav, Kachchh. *Quaternary Science Reviews*, 224, p.105975.

Blott, S.J., 2000. Grain size distribution and statistics package for the analysis of unconsolidated sediments by sieving or by laser granulometer. *Grandistat*, pp.1-6.

Blott, S.J. and Pye, K., 2001. GRADISTAT: a grain size distribution and statistics package for the analysis of unconsolidated sediments. *Earth surface processes and Landforms*, *26*(11), pp.1237-1248.

Bøtter-Jensen, L., Andersen, C.E., Duller, G.A.T. and Murray, A.S., 2003. Developments in radiation, stimulation and observation facilities in luminescence measurements. *Radiation Measurements*, *37*(4-5), pp.535-541.

Bowler, J.M., 1986. Spatial variability and hydrologic evolution of Australian lake basins: analogue for Pleistocene hydrologic change and evaporite formation. *Palaeogeography, Palaeoclimatology, Palaeoecology*, 54(1-4), pp.21-41.

Bray, H.E. and Stokes, S., 2004. Temporal patterns of arid-humid transitions in the south-eastern Arabian Peninsula based on optical dating. *Geomorphology*, *59*(1-4), pp.271-280.

Bristow, C.S., Lancaster, N. and Duller, G.A.T., 2005. Combining ground penetrating radar surveys and optical dating to determine dune migration in Namibia. *Journal of the Geological Society*, *162*(2), pp.315-321.

Bryson, R.A. and Baerreis, D.A., 1967. Possibilities of major climatic modification and their implications: Northwest India, a case for study. *Bulletin of the American Meteorological Society*, *48*(3), pp.136-142.

Buckland, C.E., Thomas, D.S. and Bailey, R.M., 2019. Complex disturbance‐driven reactivation of near‐surface sediments in the largest dunefield in North America during the last 200 years. *Earth Surface Processes and Landforms*, 44(14), pp.2794-2809.

Bullard, J.E., Thomas, D.S.G., Livingstone, I. and Wiggs, G.F.S., 1995. Analysis of linear sand dune morphological variability, southwestern Kalahari Desert. *Geomorphology*, *11*(3), pp.189-203.

Bullard, J.E., Thomas, D.S.G., Livingstone, I. and Wiggs, G.S.F., 1997. Dunefield activity and interactions with climatic variability in the southwest Kalahari Desert. *Earth Surface Processes and Landforms: The Journal of the British Geomorphological Group*, *22*(2), pp.165-174.

Burrough, S.L. and Thomas, D.S.G., 2009. Geomorphological contributions to palaeolimnology on the African continent. *Geomorphology*, 103(3), pp.285-298.

Buylaert, J.P., Murray, A.S., Thomsen, K.J. and Jain, M., 2009. Testing the potential of an elevated temperature IRSL signal from K-feldspar. *Radiation Measurements*, *44*(5-6), pp.560-565.

Cai, Y., Fung, I.Y., Edwards, R.L., An, Z., Cheng, H., Lee, J.E., Tan, L., Shen, C.C., Wang, X., Day, J.A. and Zhou, W., 2015. Variability of stalagmite-inferred Indian monsoon precipitation over the past 252,000 y. *Proceedings of the National Academy of Sciences*, 112(10), pp.2954-2959.

Census of India 2011. Provisional Population Totals. New Delhi: Government of India. http://censusindia.gov.in/2011-prov-results/

Chase, B.M., 2009. Evaluating the use of dune sediments as a proxy for palaeo-aridity: a southern African case study. *Earth-Science Reviews*, 93(1-2), pp.31-45.

Chase, B.M. and Thomas, D.S.G., 2006. Late Quaternary dune accumulation along the western margin of South Africa: distinguishing forcing mechanisms through the analysis of migratory dune forms. *Earth and Planetary Science Letters*, *251*(3-4), pp.318-333.

Chase, B.M. and Thomas, D.S.G., 2007. Multiphase late Quaternary aeolian sediment accumulation in western South Africa: timing and relationship to palaeoclimatic changes inferred from the marine record. *Quaternary International*, *166*(1), pp.29-41.

Chaudhary, S., 2015. Optically Stimulated Luminescence (OSL) Dating of Sediments from Himalaya. Journal of the Indian Institute of Science, 95(2), pp.135-146.

Chawla, S., Dhir, R.P. and Singhvi, A.K., 1992. Thermoluminescence chronology of sand profiles in the Thar Desert and their implications. *Quaternary Science Reviews*, *11*(1-2), pp.25-32.

Chougaonkar, M.P., Ragahv, M.S., Rajaguru, S.N., Kar, A., Singhvi, A.K. and Nambi, K.S.V., 1999. Luminescence dating results of dune profiles from margins of Thar desert and their implications. *Man and Environment*, *24*, pp.21-26.

Cohen, A.S., 2003. *Paleolimnology: the history and evolution of lake systems*. Oxford University Press.

Cohen, T.J., Nanson, G.C., Larsen, J.R., Jones, B.G., Price, D.M., Coleman, M. and Pietsch, T.J., 2010. Late Quaternary aeolian and fluvial interactions on the Cooper Creek Fan and the association between linear and

source-bordering dunes, Strzelecki Desert, Australia. *Quaternary Science Reviews*, *29*(3-4), pp.455-471.

Coningham, R. and Young, R., 2015. The archaeology of South Asia: from the Indus to Asoka, c. 6500 BCE–200 CE. Cambridge University Press.

Cunningham, A.C., DeVries, D.J. and Schaart, D.R., 2012. Experimental and computational simulation of beta-dose heterogeneity in sediment. *Radiation Measurements*, *47*(11-12), pp.1060-1067.

Cunningham, A.C., Wallinga, J. and Minderhoud, P.S., 2011. Expectations of scatter in equivalent-dose distributions when using multi-grain aliquots for OSL dating. *Geochronometria*, *38*(4), p.424.

Dave, A.K., Courty, M.A., Fitzsimmons, K.E. and Singhvi, A.K., 2019. Revisiting the contemporaneity of a mighty river and the Harappans: Archaeological, stratigraphic and chronometric constraints. *Quaternary Geochronology*, 49, pp.230-235.

Deotare, B.C., Kajale, M.D., Kshirsagar, A.A. and Rajaguru, S.N., 1998. Geoarchaeological and palaeoenvironmental studies around Bap–Malar playa, district Jodhpur, Rajasthan. *Current Science*, pp.316-320.

Deotare, B.C., Kajale, M.D., Rajaguru, S.N., Kusumgar, S., Jull, A.T. and Donahue, J.D., 2004. Palaeoenvironmental history of Bap-Malar and Kanod playas of western Rajasthan, Thar desert. *Journal of Earth System Science*, *113*(3), pp.403-425.

Dhir, R.P., 2018. Thar Desert: Its Land Management, Livelihoods and Prospects in a Global Warming Scenario. In *Climate Variability Impacts on Land Use and Livelihoods in Drylands* (pp. 131-147). Springer, Cham.

Dhir, R.P., Joshi, D.C. and Kathju, S., 2018. Thar Desert in retrospect and prospect. Scientific Publishers.

Dhir, R.P., Singhvi, A.K., Andrews, J.E., Kar, A., Sareen, B.K., Tandon, S.K., Kailath, A. and Thomas, J.V., 2010. Multiple episodes of aggradation and calcrete formation in Late Quaternary aeolian sands, Central Thar Desert, Rajasthan, India. *Journal of Asian Earth Sciences*, *37*(1), pp.10-16.

Dietze, M., Kreutzer, S., Burow, C., Fuchs, M.C., Fischer, M. and Schmidt, C., 2016. The abanico plot: visualising chronometric data with individual standard errors. *Quaternary Geochronology*, *31*, pp.12-18.

Dixit, Y. and Tandon, S.K., 2016. Hydroclimatic variability on the Indian subcontinent in the past millennium: review and assessment. *Earth-science reviews*, *161*, pp.1-15.

Dixit, Y., Hodell, D.A. and Petrie, C.A., 2014a. Abrupt weakening of the summer monsoon in northwest India~ 4100 yr ago. *Geology*, *42*(4), pp.339-342.

Dixit, Y., Hodell, D.A., Giesche, A., Tandon, S.K., Gázquez, F., Saini, H.S., Skinner, L.C., Mujtaba, S.A., Pawar, V., Singh, R.N. and Petrie, C.A., 2018. Intensified summer monsoon and the urbanization of Indus Civilization in northwest India. *Scientific reports*, *8*(1), p.4225.

Dixit, Y., Hodell, D.A., Sinha, R. and Petrie, C.A., 2014b. Abrupt weakening of the Indian summer monsoon at 8.2 kyr BP. *Earth and Planetary Science Letters*, *391*, pp.16-23.

Duller, G.A.T., 2003. Distinguishing quartz and feldspar in single grain luminescence measurements. *Radiation measurements*, *37*(2), pp.161-165.

Duller, G.A.T., 2004. Luminescence dating of Quaternary sediments: recent advances. *Journal of Quaternary Science*, *19*(2), pp.183-192.

Duller, G.A.T., 2006. Single grain optical dating of glacigenic deposits. *Quaternary Geochronology*, *1*(4), pp.296-304.

Duller, G.A.T., 2008. Single-grain optical dating of Quaternary sediments: why aliquot size matters in luminescence dating. *Boreas*, *37*(4), pp.589-612.

Duller, G.A.T. and Augustinus, P.C., 2006. Reassessment of the record of linear dune activity in Tasmania using optical dating. *Quaternary Science Reviews*, *25*(19-20), pp.2608-2618.

Duller, G.A.T., Bøtter-Jensen, L. and Murray, A.S., 2000. Optical dating of single sand-sized grains of quartz: sources of variability. *Radiation Measurements*, *32*(5-6), pp.453-457.

Durán, O., Schatz, V., Herrmann, H.J. and Tsoar, H., 2005. Transformation of barchans into parabolic dunes under the influence of vegetation. *arXiv preprint cond-mat/0504621*.

Durcan, J.A., 2012. Luminescence dating of sediments in Punjab, Pakistan: implications for the collapse of the Harappan Civilisation. Unpublished PhD thesis. Aberystwyth University.

Durcan, J.A. and Duller, G.A.T., 2011. The fast ratio: a rapid measure for testing the dominance of the fast component in the initial OSL signal from quartz. *Radiation Measurements*, *46*(10), pp.1065-1072.

Durcan, J.A., King, G.E. and Duller, G.A.T., 2015. DRAC: Dose Rate and Age Calculator for trapped charge dating. *Quaternary Geochronology*, *28*, pp.54-61.

Durcan, J.A., Roberts, H.M., Duller, G.A.T. and Alizai, A.H., 2010. Testing the use of range-finder OSL dating to inform field sampling and laboratory processing strategies. *Quaternary Geochronology*, *5*(2-3), pp.86-90.

Durcan, J.A., Thomas, D.S.G., Gupta, S., Pawar, V., Singh, R.N. and Petrie, C.A., 2019. Holocene landscape dynamics in the Ghaggar-Hakra palaeochannel region at the northern edge of the Thar Desert, northwest India. *Quaternary International, 501,* 317-327.

Dutt, S., Gupta, A.K., Clemens, S.C., Cheng, H., Singh, R.K., Kathayat, G. and Edwards, R.L., 2015. Abrupt changes in Indian summer monsoon strength during 33,800 to 5500 years BP. *Geophysical Research Letters*, 42(13), pp.5526-5532.

Enzel, Y., Ely, L.L., Mishra, S., Ramesh, R., Amit, R., Lazar, B., Rajaguru, S.N., Baker, V.R. and Sandler, A., 1999. High-resolution Holocene environmental changes in the Thar Desert, northwestern India. *Science*, *284*(5411), pp.125-128.

Feathers, J.K. and Migliorini, E., 2001. Luminescence dating at Katanda—a reassessment. *Quaternary Science Reviews*, *20*(5-9), pp.961-966.

Felix, C. and Singhvi, A.K., 1997. Study of non-linear luminescence-dose growth curves for the estimation of paleodose in luminescence dating: results of Monte Carlo simulations. *Radiation Measurements*, *27*(4), pp.599-609.

Fitzsimmons, K.E. and Telfer, M.W., 2008. Complexities in the preservation and interpretation of Late Quaternary dune records: examples from the Tirari Desert, Australia and the southwestern Kalahari, South Africa. *Chungará*, *30*, pp.295-308.

Fitzsimmons, K.E., Rhodes, E.J., Magee, J.W. and Barrows, T.T., 2007. The timing of linear dune activity in the Strzelecki and Tirari Deserts, Australia. *Quaternary Science Reviews*, *26*(19-21), pp.2598-2616.

Fleitmann, D., Burns, S.J., Mangini, A., Mudelsee, M., Kramers, J., Villa, I., Neff, U., Al-Subbary, A.A., Buettner, A., Hippler, D. and Matter, A., 2007. Holocene ITCZ and Indian monsoon dynamics recorded in stalagmites from Oman and Yemen (Socotra). *Quaternary Science Reviews*, *26*(1-2), pp.170-188.

Fleitmann, D., Burns, S.J., Mudelsee, M., Neff, U., Kramers, J., Mangini, A. and Matter, A., 2003. Holocene forcing of the Indian monsoon recorded in a stalagmite from southern Oman. *Science*, *300*(5626), pp.1737-1739.

Folk, R.L. and Ward, W.C., 1957. Brazos River bar [Texas]; a study in the significance of grain size parameters. *Journal of Sedimentary Research*, *27*(1), pp.3-26.

Galbraith, R.F., 1988. Graphical display of estimates having differing standard errors. *Technometrics*, *30*(3), pp.271-281.

Galbraith, R.F. and Roberts, R.G., 2012. Statistical aspects of equivalent dose and error calculation and display in OSL dating: an overview and some recommendations. *Quaternary Geochronology*, *11*, pp.1-27.

Galbraith, R.F., Roberts, R.G., Laslett, G.M., Yoshida, H. and Olley, J.M., 1999. Optical dating of single and multiple grains of quartz from Jinmium rock shelter, northern Australia: Part I, experimental design and statistical models. *Archaeometry*, *41*(2), pp.339-364.

Gangal, K., Vahia, M.N. and Adhikari, R., 2010. Spatio-temporal analysis of the Indus urbanization. *Current Science*, pp.846-852.

Gilbert, N., 2011. United Nations considers creating advisory panel on land degradation akin to IPCC. *Nature*, *477*, pp.262-264.

Gill, E.C., Rajagopalan, B., Molnar, P.H., Kushnir, Y. and Marchitto, T.M., 2017. Reconstruction of Indian summer monsoon winds and precipitation over the past 10,000 years using equatorial pacific SST proxy records. *Paleoceanography*, *32*(2), pp.195-216.

Giosan, L., Clift, P.D., Macklin, M.G., Fuller, D.Q., Constantinescu, S., Durcan, J.A., Stevens, T., Duller, G.A., Tabrez, A.R., Gangal, K. and Adhikari, R., 2012. Fluvial landscapes of the Harappan civilization. *Proceedings of the National Academy of Sciences*, 109(26), pp.E1688-E1694.

Girardi, J.D. and Davis, D.M., 2010. Parabolic dune reactivation and migration at Napeague, NY, USA: Insights from aerial and GPR imagery. *Geomorphology*, *114*(4), pp.530-541.

Glennie, K.W. and Singhvi, A.K., 2002. Event stratigraphy, paleoenvironment and chronology of SE Arabian deserts. *Quaternary Science Reviews*, *21*(7), pp.853-869.

Godfrey-Smith, D.I., Huntley, D.J. and Chen, W.H., 1988. Optical dating studies of quartz and feldspar sediment extracts. *Quaternary Science Reviews*, *7*(3-4), pp.373-380.

Goudie, A.S., 2011. Parabolic dunes: distribution, form, morphology and change. *Annals of Arid Zone*, *50*(3&4), pp.1-7.

Goudie, A.S., Allchin, B. and Hegde, K.T.M., 1973. The former extensions of the great Indian sand desert. *Geographical Journal*, pp.243-257.

Goudie, A.S., Colls, A., Stokes, S., Parker, A., White, K. and Al-Farraj, A., 2000. Latest Pleistocene and Holocene dune construction at the north-eastern edge of the Rub Al Khali, United Arab Emirates. *Sedimentology*, *47*(5), pp.1011-1021.

Guerin, G., Jain, M., Thomsen, K.J., Murray, A.S. and Mercier, N., 2015. Modelling dose rate to single grains of quartz in well-sorted sand samples: The dispersion arising from the presence of potassium feldspars and implications for single grain OSL dating. *Quaternary Geochronology*, *27*, pp.52-65.

Guérin, G., Mercier, N. and Adamiec, G., 2011. Dose-rate conversion factors: update. *Ancient TL*, *29*(1), pp.5-8.

Guérin, G., Mercier, N., Nathan, R., Adamiec, G. and Lefrais, Y., 2012. On the use of the infinite matrix assumption and associated concepts: a critical review. *Radiation Measurements*, *47*(9), pp.778-785.

Gupta, A.K., Anderson, D.M. and Overpeck, J.T., 2003. Abrupt changes in the Asian southwest monsoon during the Holocene and their links to the North Atlantic Ocean. *Nature*, *421*(6921), p.354.

Gupta, A.K., Dutt, S., Cheng, H. and Singh, R.K., 2019. Abrupt changes in Indian summer monsoon strength during the last~ 900 years and their linkages to socio-economic conditions in the Indian subcontinent. *Palaeogeography, Palaeoclimatology, Palaeoecology*, p.109347.

Gupta, A.K., Mohan, K., Das, M. and Singh, R.K., 2013. Solar forcing of the Indian summer monsoon variability during the Ållerød period. *Scientific reports*, *3*, p.2753.

Hack, J.T., 1941. Dunes of the western Navajo country. *Geographical Review*, *31*(2), pp.240-263.

Halfen, A.F., Fredlund, G.G. and Mahan, S.A., 2010. Holocene stratigraphy and chronology of the Casper dune field, Casper, Wyoming, USA. The Holocene, 20(5), pp.773-783.

Hanson, P.R., Joeckel, R.M., Young, A.R. and Horn, J., 2009. Late Holocene dune activity in the Eastern Platte River Valley, Nebraska. *Geomorphology*, *103*(4), pp.555-561.

Heer, A.J., Adamiec, G. and Moska, P., 2012. How many grains are there on a single aliquot. *Ancient TL*, *30*(1), pp.9-16.

Heiri, O., Lotter, A.F. and Lemcke, G., 2001. Loss on ignition as a method for estimating organic and carbonate content in sediments: reproducibility and comparability of results. *Journal of paleolimnology*, *25*(1), pp.101-110.

Hesse, P.P., 2010. The Australian desert dunefields: formation and evolution in an old, flat, dry continent. Geological Society, London, Special Publications, 346(1), pp.141-164.

Hesse, P.P., 2011. Sticky dunes in a wet desert: formation, stabilisation and modification of the Australian desert dunefields. *Geomorphology*, 134(3-4), pp.309-325.

Hesse, P.P., 2016. How do longitudinal dunes respond to climate forcing? Insights from 25 years of luminescence dating of the Australian desert dunefields. *Quaternary International*, *410*, pp.11-29.

Hugenholtz, C.H. and Wolfe, S.A., 2005. Recent stabilization of active sand dunes on the Canadian prairies and relation to recent climate variations. *Geomorphology*, *68*(1-2), pp.131-147.

Hugenholtz, C.H. and Wolfe, S.A., 2006. Morphodynamics and climate controls of two aeolian blowouts on the northern Great Plains, Canada. *Earth Surface Processes and Landforms: The Journal of the British Geomorphological Research Group*, *31*(12), pp.1540-1557.

Hunter, R.E., Richmond, B.M. and RHO ALPHA, T.A.U., 1983. Storm-controlled oblique dunes of the Oregon coast. *Geological Society of America Bulletin*, *94*(12), pp.1450-1465.

Huntley, D.J. and Lamothe, M., 2001. Ubiquity of anomalous fading in K-feldspars and the measurement and correction for it in optical dating. *Canadian Journal of Earth Sciences*, *38*(7), pp.1093-1106.

Huntley, D.J. and Lian, O.B., 2006. Some observations on tunnelling of trapped electrons in feldspars and their implications for optical dating. *Quaternary Science Reviews*, *25*(19-20), pp.2503-2512.

Ivanochko, T.S., Ganeshram, R.S., Brummer, G.J.A., Ganssen, G., Jung, S.J., Moreton, S.G. and Kroon, D., 2005. Variations in tropical convection as an amplifier of global climate change at the millennial scale. *Earth and Planetary Science Letters*, *235*(1-2), pp.302-314.

Jacobs, Z., Duller, G.A.T. and Wintle, A.G., 2003a. Optical dating of dune sand from Blombos Cave, South Africa: II—single grain data. *Journal of Human Evolution*, *44*(5), pp.613-625.

Jacobs, Z., Wintle, A.G. and Duller, G.A.T., 2003b. Optical dating of dune sand from Blombos Cave, South Africa: I—multiple grain data. *Journal of Human Evolution*, *44*(5), pp.599-612.

Jacobs, Z., Duller, G.A.T., Wintle, A.G. and Henshilwood, C.S., 2006. Extending the chronology of deposits at Blombos Cave, South Africa, back to 140 ka using optical dating of single and multiple grains of quartz. *Journal of Human Evolution*, *51*(3), pp.255-273.

Jain, M. and Tandon, S.K., 2003. Fluvial response to Late Quaternary climate changes, western India. *Quaternary Science Reviews*, *22*(20), pp.2223-2235.

Jain, M., Murray, A.S. and Bøtter-Jensen, L., 2003. Characterisation of blue-light stimulated luminescence components in different quartz samples: implications for dose measurement. *Radiation Measurements*, *37*(4-5), pp.441-449.

Jain, M., Tandon, S.K. and Bhatt, S.C., 2004. Late Quaternary stratigraphic development in the lower Luni, Mahi and Sabarmati river basins, western India. *Journal of Earth System Science*, *113*(3), pp.453-471.

Jankowski, N.R. and Jacobs, Z., 2018. Beta dose variability and its spatial contextualisation in samples used for optical dating: An empirical approach to examining beta microdosimetry. *Quaternary Geochronology*, *44*, pp.23-37.

Jerolmack, D.J., Ewing, R.C., Falcini, F., Martin, R.L., Masteller, C., Phillips, C., Reitz, M.D. and Buynevich, I., 2012. Internal boundary layer model for the evolution of desert dune fields. *Nature Geoscience*, *5*(3), p.206.

Juyal, N., Chamyal, L.S., Bhandari, S., Bhushan, R. and Singhvi, A.K., 2006. Continental record of the southwest monsoon during the last 130 ka: evidence from the southern margin of the Thar Desert, India. *Quaternary Science Reviews*, *25*(19-20), pp.2632-2650.

Juyal, N., Kar, A., Rajaguru, S.N. and Singhvi, A.K., 2003. Luminescence chronology of aeolian deposition during the Late Quaternary on the southern margin of Thar Desert, India. *Quaternary International*, *104*(1), pp.87-98.

Kajale, M.D. and Deotare, B.C., 1997. Late Quaternary environmental studies on salt lakes in western Rajasthan, India: a summarised view. *Journal of Quaternary Scienc*, *12*(5), pp.405-412.

Kar, A., 1987. Origin and transformation of longitudinal sand dunes in the Indian desert. *Zeitschrift fur Geomorphologie*, *31*, pp.311-337.

Kar, A., 1993. Aeolian processes and bedforms in the Thar Desert. *Journal of Arid Environments*, *25*(1), pp.83-96.

Kar, A., 2013. Quaternary geomorphic processes and landform development in the Thar Desert of Rajasthan. Landforms Process. Environ. Manag, pp.225-256.

Kar, A., 2014. The Thar or the Great Indian Sand Desert. In *Landscapes and Landforms of India* (pp. 79-90). Springer, Dordrecht.

Kar, A., Felix, C., Rajaguru, S.N. and Singhvi, A.K., 1998. Late Holocene growth and mobility of a transverse dune in the Thar Desert. *Journal of Arid Environments*, *38*(2), pp.175-185.

Kar, A., Singhvi, A.K., Juyal, N. and Rajaguru, S.N., 2004. Late Quaternary aeolian sedimentation history of the Thar Desert. *Geomorphology and Environment, ACB Publications, Kolkata*, pp.105-122.

Kar, A., Singhvi, A.K., Rajaguru, S.N., Juyal, N., Thomas, J.V., Banerjee, D. and Dhir, R.P., 2001. Reconstruction of the late Quaternary environment of the lower Luni plains, Thar Desert, India. *Journal of Quaternary Science*, *16*(1), pp.61-68.

Kars, R.H., Wallinga, J. and Cohen, K.M., 2008. A new approach towards anomalous fading correction for feldspar IRSL dating—tests on samples in field saturation. *Radiation Measurements*, *43*(2-6), pp.786-790.

Kaushal, N., Breitenbach, S.F., Lechleitner, F.A., Sinha, A., Tewari, V.C., Ahmad, S.M., Berkelhammer, M., Band, S., Yadava, M., Ramesh, R. and Henderson, G.M., 2018. The Indian Summer Monsoon from a Speleothem δ18O Perspective—A Review. *Quaternary*, *1*(3), p.29.

Kenoyer, J.M., 1998. Ancient cities of the Indus valley civilization. American Institute of Pakistan Studies.

Kenoyer, J.M., 2008. Indus urbanism: New perspectives on its origin and character. The ancient city: New perspectives on urbanism in the Old and New World, pp.183-208.

Kiss, T., Sipos, G. and Kovács, F., 2009. Human impact on fixed sand dunes revealed by morphometric analysis. *Earth Surface Processes and Landforms*, *34*(5), pp.700-711.

Kreutzer, S., Dietze, M., Burow, C., Fuchs, M.C., Schmidt, C., Fischer, M. and Friedrich, J., 2017. Luminescence: Comprehensive luminescence dating data analysis. R package version 0.7. 3.

Kristensen, J.A., Thomsen, K.J., Murray, A.S., Buylaert, J.P., Jain, M. and Breuning-Madsen, H., 2015. Quantification of termite bioturbation in a savannah ecosystem: application of OSL dating. *Quaternary Geochronology*, *30*, pp.334-341.

Kumar, A., Srivastava, P. and Meena, N.K., 2017. Late Pleistocene aeolian activity in the cold desert of Ladakh: a record from sand ramps. *Quaternary International*, *443*, pp.13-28.

Kumar, M., Goossens, E. and Goossens, R., 1993. Assessment of sand dune change detection in Rajasthan (Thar) Desert, India. *International Journal of Remote Sensing*, *14*(9), pp.1689-1703.

Kutzbach, J.E., 1981. Monsoon climate of the early Holocene: climate experiment with the earth's orbital parameters for 9000 years ago. *Science*, *214*(4516), pp.59-61.

Lancaster, N., 1982. Linear dunes. *Progress in Physical Geography*, *6*(4), pp.475-504.

Lancaster, N., 2008. Desert dune dynamics and development: insights from luminescence dating. *Boreas*, *37*(4), pp.559-573.

Lancaster, N., Wolfe, S., Thomas, D.S.G., Bristow, C., Bubenzer, O., Burrough, S.L., Duller, G.A.T., Halfen, A., Hesse, P.P., Roskin, J., Singhvi, A.K., Tsoar, H., Tripaldi, A., Yang, X., and Zarate, M. 2016. The INQUA dunes atlas chronologic database. *Quaternary international*, *410*, pp.3-10.

Langford, R.P., Rose, J.M. and White, D.E., 2009. Groundwater salinity as a control on development of eolian landscape: An example from the White Sands of New Mexico. *Geomorphology*, *105*(1-2), pp.39-49.

Leighton, C.L., Bailey, R.M. and Thomas, D.S.G., 2013. The utility of desert sand dunes as Quaternary chronostratigraphic archives: evidence from the northeast Rub'al Khali. *Quaternary Science Reviews*, *78*, pp.303-318.

Leighton, C.L., Bailey, R.M. and Thomas, D.S.G., 2014. Interpreting and modelling late Quaternary dune accumulation in the southern Arabian Peninsula. *Quaternary Science Reviews*, *102*, pp.1-13.

Leipe, C., Demske, D., Tarasov, P.E. and Members, H.P., 2014. A Holocene pollen record from the northwestern Himalayan lake Tso Moriri:

implications for palaeoclimatic and archaeological research. *Quaternary International*, 348, pp.93-112.

Li, B. and Coulthard, T.J., 2015. Mapping the interactions between rivers and sand dunes: implications for fluvial and aeolian geomorphology. *Geomorphology*, *231*, pp.246-257.

Li, C. and Yanai, M., 1996. The onset and interannual variability of the Asian summer monsoon in relation to land–sea thermal contrast. *Journal of Climate*, *9*(2), pp.358-375.

Li, H. and Yang, X., 2016. Spatial and temporal patterns of aeolian activities in the desert belt of northern China revealed by dune chronologies. *Quaternary International*, 410, pp.58-68.

Liu, Z., Harrison, S.P., Kutzbach, J. and Otto-Bliesner, B., 2004. Global monsoons in the mid-Holocene and oceanic feedback. *Climate Dynamics*, *22*(2-3), pp.157-182.

Liu, Z., Kutzbach, J. and Wu, L., 2000. Modeling climate shift of El Nino variability in the Holocene. *Geophysical Research Letters*, *27*(15), pp.2265-2268.

Livingstone, I. and Thomas, D.S.G., 1993. Modes of linear dune activity and their palaeoenvironmental significance: an evaluation with reference to southern African examples. *Geological Society, London, Special Publications*, *72*(1), pp.91-101.

Lomax, J., Hilgers, A. and Radtke, U., 2011. Palaeoenvironmental change recorded in the palaeodunefields of the western Murray Basin, South Australia–

New data from single grain OSL-dating. *Quaternary Science Reviews*, *30*(5-6), pp.723-736.

Lomax, J., Hilgers, A., Wopfner, H., Grün, R., Twidale, C.R. and Radtke, U., 2003. The onset of dune formation in the Strzelecki Desert, South Australia. *Quaternary Science Reviews*, *22*(10-13), pp.1067-1076.

Lowe, D.J., 2011. Tephrochronology and its application: a review. *Quaternary Geochronology*, *6*(2), pp.107-153.

MacDonald, G., 2011. Potential influence of the Pacific Ocean on the Indian summer monsoon and Harappan decline. *Quaternary International*, *229*(1-2), pp.140-148.

Maemoku, H., Shitaoka, Y., Nagatomo, T. and Yagi, H., 2012. Geomorphological constraints on the Ghaggar River regime during the Mature Harappan period. *Clim. Landscapes Civilizations*, *198*, pp.97-106.

Maroulis, J.C., Nanson, G.C., Price, D.M. and Pietsch, T., 2007. Aeolian–fluvial interaction and climate change: source-bordering dune development over the past~ 100 ka on Cooper Creek, central Australia. *Quaternary Science Reviews*, *26*(3-4), pp.386-404.

May, J.H., 2013. Dunes and dunefields in the Bolivian Chaco as potential records of environmental change. *Aeolian Research*, 10, pp.89-102.

Mayya, Y.S., Morthekai, P., Murari, M.K. and Singhvi, A.K., 2006. Towards quantifying beta microdosimetric effects in single-grain quartz dose distribution. *Radiation Measurements*, *41*(7-8), pp.1032-1039.

Mejdahl, V., 1979. Thermoluminescence dating: beta-dose attenuation in quartz grains. *Archaeometry*, *21*(1), pp.61-72.

Miao, X., Mason, J.A., Swinehart, J.B., Loope, D.B., Hanson, P.R., Goble, R.J. and Liu, X., 2007. A 10,000 year record of dune activity, dust storms, and severe drought in the central Great Plains. *Geology*, *35*(2), pp.119-122.

Middleton, N., Stringer, L., Goudie, A.S. and Thomas, D.S.G., 2011. The forgotten billion: MDG achievement in the drylands. In *United Nations Convention to Combat Desertification, Bonn*.

Misra, P., Tandon, S.K. and Sinha, R., 2019. Holocene climate records from lake sediments in India: Assessment of coherence across climate zones. *Earth-science reviews*, 190, pp.370-397.

Misra, V.N., 1963. Palaeolithic culture of western Rajputana. *Bulletin of the Deccan College Research Institute*, *21*, pp.85-156.

Misra, V.N. and Rajaguru, S.N., 1985. Palaeoenvironment and Prehistory of the Thar Desert, Rajastan, India. *South Asian Archaeology*, *1985*, pp.296-320.

Misra, V.N. and Rajaguru, S.N., 1986. Environnement et culture de l'Homme préhistorique dans le désert du Thar, Rajasthan, Inde. *L'anthropologie (Paris)*, *90*(3), pp.407-437.

Misra, V.N., Rajaguru, S.N., Raju, D.R., Raghavan, H. and Gaillard, C., 1982. Acheulian occupation and evolving landscape around Didwana in the Thar Desert, India. *Man and Environment*, *6*(72.86), pp.1975-1976.

Moharana, P.C., Gaur, M.C., Choudhary, C., Chauhan, J.S. and Rajpurohit, R.S., 2013. A system of geomorphological mapping for western

Rajasthan with relevance for agricultural land use. *Annals of Arid Zone*, *52*(3&4), pp.163-180.

Muhs, D.R. and Budahn, J.R., 2019. New geochemical evidence for the origin of North America's largest dune field, the Nebraska Sand Hills, central Great Plains, USA. *Geomorphology*, 332, pp.188-212.

Munyikwa, K., 2005. The role of dune morphogenetic history in the interpretation of linear dune luminescence chronologies: a review of linear dune dynamics. *Progress in Physical Geography*, *29*(3), pp.317-336.

Murray, A.S. and Funder, S., 2003. Optically stimulated luminescence dating of a Danish Eemian coastal marine deposit: a test of accuracy. *Quaternary Science Reviews*, *22*(10-13), pp.1177-1183.

Murray, A.S. and Olley, J.M., 2002. Precision and accuracy in the optically stimulated luminescence dating of sedimentary quartz: a status review. *Geochronometria*, *21*(1), pp.1-16.

Murray, A.S. and Wintle, A.G., 2000. Luminescence dating of quartz using an improved single-aliquot regenerative-dose protocol. *Radiation measurements*, *32*(1), pp.57-73.

Murray, A.S. and Wintle, A.G., 2003. The single aliquot regenerative dose protocol: potential for improvements in reliability. *Radiation measurements*, *37*(4-5), pp.377-381.

Murray, A.S, Wintle, A.G. and Wallinga, J., 2002. Dose estimation using quartz OSL in the non-linear region of the growth curve. *Radiation Protection Dosimetry*, *101*(1-4), pp.371-374.

Nanson, G.C., Chen, X.Y. and Price, D.M., 1992. Lateral migration, thermoluminescence chronology and colour variation of longitudinal dunes near Birdsville in the Simpson Desert, central Australia. *Earth Surface Processes and Landforms*, *17*(8), pp.807-819.

Narain, P. and Kar, A., 2005. *Drought in Western Rajasthan*. ICAR-Central Arid Zone Research Institute, Jodhpur.

Nathan, R.P., Thomas, P.J., Jain, M., Murray, A.S. and Rhodes, E.J., 2003. Environmental dose rate heterogeneity of beta radiation and its implications for luminescence dating: Monte Carlo modelling and experimental validation. *Radiation Measurements*, *37*(4-5), pp.305-313.

Neff, U., Burns, S.J., Mangini, A., Mudelsee, M., Fleitmann, D. and Matter, A., 2001. Strong coherence between solar variability and the monsoon in Oman between 9 and 6 kyr ago. *Nature*, *411*(6835), p.290.

Nelson, B.W., 1994. Natural forest disturbance and change in the Brazilian Amazon. *Remote Sensing Reviews*, 10(1-3), pp.105-125.

Nield, J.M. and Baas, A.C., 2008. The influence of different environmental and climatic conditions on vegetated aeolian dune landscape development and response. *Global and Planetary Change*, *64*(1-2), pp.76-92.

Nishimori, H. and Tanaka, H., 2001. A simple model for the formation of vegetated dunes. *Earth Surface Processes and Landforms: The Journal of the British Geomorphological Research Group*, *26*(10), pp.1143-1150.

O'Connor, P.W. and Thomas, D.S.G., 1999. The timing and environmental significance of late Quaternary linear dune development in western Zambia. *Quaternary Research*, *52*(1), pp.44-55.

Olley, J.M., Pietsch, T. and Roberts, R.G., 2004. Optical dating of Holocene sediments from a variety of geomorphic settings using single grains of quartz. *Geomorphology*, *60*(3-4), pp.337-358.

Owen, L.A., Bright, J., Finkel, R.C., Jaiswal, M.K., Kaufman, D.S., Mahan, S., Radtke, U., Schneider, J.S., Sharp, W., Singhvi, A.K. and Warren, C.N., 2007. Numerical dating of a Late Quaternary spit-shoreline complex at the northern end of Silver Lake playa, Mojave Desert, California: A comparison of the applicability of radiocarbon, luminescence, terrestrial cosmogenic nuclide, electron spin resonance, U-series and amino acid racemization methods. *Quaternary International*, *166*(1), pp.87-110.

Pandey, S., Singh, S. and Ghose, B., 1964. Orientation, distribution and origin of sand dunes in the central Luni basin. In *Proceedings, Symposium on Problems of Indian Arid Zone* (pp. 84-91).

Parikh, D. and Petrie, C.A., 2019. 'We are inheritors of a rural civilisation': rural complexity and the ceramic economy in the Indus Civilisation in northwest India. *World Archaeology*, pp.1-21.

Parthasarathy, B., Munot, A.A. and Kothawale, D.R., 1994. All-India monthly and seasonal rainfall series: 1871–1993. *Theoretical and Applied Climatology*, 49(4), pp.217-224.

Parton, A., Farrant, A.R., Leng, M.J., Telfer, M.W., Groucutt, H.S., Petraglia, M.D. and Parker, A.G., 2015. Alluvial fan records from southeast Arabia reveal multiple windows for human dispersal. *Geology*, *43*(4), pp.295-298.

Petrie, C.A., Khan, F., Knox, J.R., Thomas, K. and Morris, J.C., 2010. The investigation of early villages in the hills and on the plains of western South Asia. Sheri Khan Tarakai and early village life in the borderlands of north-west Pakistan, pp.7-28.

Petrie, C.A., Singh, R.N., Bates, J., Dixit, Y., French, C.A., Hodell, D.A., Jones, P.J., Lancelotti, C., Lynam, F., Neogi, S. and Pandey, A.K., 2017. Adaptation to variable environments, resilience to climate change: Investigating land, water and settlement in Indus Northwest India. *Current Anthropology*, 58(1), pp.000-000.

Piggott S. 1950. *Prehistoric India to 1000 B.C. (Penguin Books)*: Harmondsworth.

Ponton, C., Giosan, L., Eglinton, T.I., Fuller, D.Q., Johnson, J.E., Kumar, P. and Collett, T.S., 2012. Holocene aridification of India. *Geophysical Research Letters*, *39*(3).

Possehl, G.L., 2002. The Indus civilization: a contemporary perspective. Rowman Altamira.

Prasad, S. and Enzel, Y., 2006. Holocene paleoclimates of India. *Quaternary Research*, *66*(3), pp.442-453.

Prasad, S., Kusumgar, S. and Gupta, S.K., 1997. A mid to late Holocene record of palaeoclimatic changes from Nal Sarovar: a palaeodesert margin lake in western India. *Journal of Quaternary Science*, 12(2), pp.153-159.

Prescott, J.R. and Hutton, J.T., 1994. Cosmic ray contributions to dose rates for luminescence and ESR dating: large depths and long-term time variations. *Radiation measurements*, *23*(2-3), pp.497-500.

Preusser, F., 2009. Chronology of the impact of Quaternary climate change on continental environments in the Arabian Peninsula. *Competus Rendus Geoscience, 341 (*8-9), pp. 621-632.

Preusser, F., Chithambo, M.L., Götte, T., Martini, M., Ramseyer, K., Sendezera, E.J., Susino, G.J. and Wintle, A.G., 2009. Quartz as a natural luminescence dosimeter. *Earth-Science Reviews*, *97*(1-4), pp.184-214.

Preusser, F., Degering, D., Fuchs, M., Hilgers, A., Kadereit, A., Klasen, N., Krbetschek, M., Richter, D. and Spencer, J.Q., 2008. Luminescence dating: basics, methods and applications. *Eiszeitalter & Ggenwart= Quaternary Science Journal*, *57*(1/2), pp.95-149.

Pye, K. and Tsoar, H., 2008. *Aeolian sand and sand dunes*. Springer Science & Business Media.

Raghavan, H. and Courty, M.A., 1987. Holocene and Pleistocene pedo-sedimentary environments in the Thar desert (Didwana, Inde). In Micromorphologie des sols. *Réunion internationale de micromorphologie des sols*. 7 (pp. 639-646).

Raghavan, H., Rajaguru, S.N. and Misra, V.N., 1989. Radiometric dating of a Quaternary dune section, Didwana, Rajasthan. *Man and environment*, *13*, pp.19-22.

Rajagopalan, B. and Molnar, P., 2013. Signatures of Tibetan Plateau heating on Indian summer monsoon rainfall variability. *Journal of Geophysical Research: Atmospheres*, *118*(3), pp.1170-1178.

Rao, A.S. and Roy, M.M., 2012. Weather variability and crop production in arid Rajasthan. Central Arid Zone Research Institute, Indian Council of Agricultural Research.

Reimann, T., Thomsen, K.J., Jain, M., Murray, A.S. and Frechen, M., 2012. Single-grain dating of young sediments using the pIRIR signal from feldspar. *Quaternary Geochronology*, *11*, pp.28-41.

Reitz, M.D., Jerolmack, D.J., Ewing, R.C. and Martin, R.L., 2010. Barchan-parabolic dune pattern transition from vegetation stability threshold. *Geophysical Research Letters*, *37*(19).

Roberts, H.M., 2007. Assessing the effectiveness of the double-SAR protocol in isolating a luminescence signal dominated by quartz. *Radiation measurements*, 42(10), pp.1627-1636.

Roberts, H.M. and Wintle, A.G., 2001. Equivalent dose determinations for polymineralic fine-grains using the SAR protocol: application to a Holocene sequence of the Chinese Loess Plateau. *Quaternary Science Reviews*, *20*(5-9), pp.859-863.

Roberts, H.M., Durcan, J.A. and Duller, G.A.T., 2009. Exploring procedures for the rapid assessment of optically stimulated luminescence range-finder ages. *Radiation Measurements*, *44*(5-6), pp.582-587.

Rodell, M., Velicogna, I. and Famiglietti, J.S., 2009. Satellite-based estimates of groundwater depletion in India. *Nature*, *460*(7258), p.999.

Roskin, J., Katra, I. and Blumberg, D.G., 2013. Late Holocene dune mobilizations in the northwestern Negev dunefield, Israel: A response to combined anthropogenic activity and short-term intensified windiness. *Quaternary International*, 303, pp.10-23.

Roskin, J., Porat, N., Tsoar, H., Blumberg, D.G. and Zander, A.M., 2011a. Age, origin and climatic controls on vegetated linear dunes in the northwestern Negev Desert (Israel). *Quaternary Science Reviews*, *30*(13-14), pp.1649-1674.

Roskin, J., Tsoar, H., Porat, N. and Blumberg, D.G., 2011b. Palaeoclimate interpretations of Late Pleistocene vegetated linear dune mobilization episodes: evidence from the northwestern Negev dunefield, Israel. *Quaternary Science Reviews*, *30*(23-24), pp.3364-3380.

Rowan, A.V., Roberts, H.M., Jones, M.A., Duller, G.A., Covey-Crump, S.J. and Brocklehurst, S.H., 2012. Optically stimulated luminescence dating of glaciofluvial sediments on the Canterbury Plains, South Island, New Zealand. *Quaternary Geochronology*, *8*, pp.10-22.

Rowell, A., Thomas, D.S.G., Bailey, R.M., Stone, A.E.C., Garzanti, E. and Padoan, M., 2018. Controls on sand ramp formation in southern Namibia. *Earth Surface Processes and Landforms*, 43(1), pp.150-171.

Rowell, A.L., Thomas, D.S.G., Bailey, R.M. and Holmes, P.J., 2018. Sand ramps as palaeoenvironmental archives: Integrating general principles and regional contexts through reanalysis of the Klipkraal Sands, South Africa. *Geomorphology*, 311, pp.103-113.

Roy, P.D., Nagar, Y.C., Juyal, N., Smykatz-Kloss, W. and Singhvi, A.K., 2009. Geochemical signatures of Late Holocene paleo-hydrological changes from Phulera and Pokharan saline playas near the eastern and western margins of the Thar Desert, India. *Journal of Asian Earth Sciences*, *34*(3), pp.275-286.

Saini, H. and Mujtaba, S., 2010. Luminescence dating of the sediments from a buried channel loop in Fatehabad area, Haryana: insight into Vedic Saraswati River and its environment. *Geochronometria*, *37*(1), pp.29-35.

Saini, H.S., Tandon, S.K., Mujtaba, S.A.I., Pant, N.C. and Khorana, R.K., 2009. Reconstruction of buried channel-floodplain systems of the northwestern Haryana Plains and their relation to the 'Vedic'Saraswati. *Current Science*, *97*(11), pp.1634-1643.

Sarkar, A., Ramesh, R., Somayajulu, B.L.K., Agnihotri, R., Jull, A.T. and Burr, G.S., 2000. High resolution Holocene monsoon record from the eastern Arabian Sea. *Earth and Planetary Science Letters*, *177*(3-4), pp.209-218.

Sarkar, A., Ramesh, R., Somayajulu, B.L.K., Agnihotri, R., Jull, A.T. and Burr, G.S., 2000. High resolution Holocene monsoon record from the eastern Arabian Sea. *Earth and Planetary Science Letters*, *177*(3-4), pp.209-218.

Saxena, S.K. and Singh, S., 1976. Some observations on the sand dunes and vegetation of Bikaner district in Western Rajasthan [India]. *Annals of Arid Zone*.

Sharma, D. ed., 1966. *Rajasthan Through the Ages: From the earliest times to 1316 AD* (Vol. 1). Rajasthan State Archives.

Shitaoka, Y., Maemoku, H. and Nagatomo, T., 2012. Quartz OSL dating of sand dunes in Ghaggar Basin, northwestern India. *Geochronometria*, *39*(3), pp.221-226.

Singarayer, J.S. and Bailey, R.M., 2003. Further investigations of the quartz optically stimulated luminescence components using linear modulation. *Radiation Measurements*, *37*(4-5), pp.451-458.

Singh, A., Paul, D., Sinha, R., Thomsen, K.J. and Gupta, S., 2016. Geochemistry of buried river sediments from Ghaggar Plains, NW India: Multi-proxy records of variations in provenance, paleoclimate, and paleovegetation patterns in the Late Quaternary. *Palaeogeography, Palaeoclimatology, Palaeoecology*, 449, pp.85-100.

Singh, A., Thomsen, K.J., Sinha, R., Buylaert, J.P., Carter, A., Mark, D.F., Mason, P.J., Densmore, A.L., Murray, A.S., Jain, M. and Paul, D., 2017. Counter-intuitive influence of Himalayan river morphodynamics on Indus Civilisation urban settlements. *Nature Communications*, 8(1), pp.1-14.

Singh, G., Joshi, R.D., Chopra, S.K. and Singh, A.B., 1974. Late Quaternary history of vegetation and climate of the Rajasthan Desert, India. Philosophical Transactions of the Royal Society of London. B, Biological Sciences, 267(889), pp.467-501.

Singh, G., Wasson, R.J. and Agrawal, D.P., 1990. Vegetational and seasonal climatic changes since the last full glacial in the Thar Desert,

northwestern India. *Review of Palaeobotany and Palynology*, *64*(1-4), pp.351-358.

Singh, S., 1982. Types and formation of sand dunes in the Rajasthan Desert. Perspectives in Geomorphology, 4, pp.165-183.

Singhvi, A.K. and Kar, A., 2004. The aeolian sedimentation record of the Thar Desert. *Journal of Earth System Science*, *113*(3), pp.371-401.

Singhvi, A.K. and Porat, N., 2008. Impact of luminescence dating on geomorphological and palaeoclimate research in drylands. *Boreas*, *37*(4), pp.536-558.

Singhvi, A.K., Banerjee, D., Rajaguru, S.N. and Kumar, V.K., 1994. Luminescence chronology of a fossil dune at Budha Pushkar, Thar Desert: Palaeoenvironmental and archaeological implications. *Current Science*, pp.770-773.

Singhvi, A.K., Banerjee, D., Ramesh, R., Rajaguru, S.N. and Gogte, V., 1996. A luminescence method for dating 'dirty'pedogenic carbonates for paleoenvironmental reconstruction. *Earth and Planetary Science Letters*, *139*(1-2), pp.321-332.

Singhvi, A.K., Sharma, Y.P. and Agrawal, D.P., 1982. Thermoluminescence dating of sand dunes in Rajasthan, India. *Nature*, *295*(5847), p.313.

Singhvi, A.K., Williams, M.A.J., Rajaguru, S.N., Misra, V.N., Chawla, S., Stokes, S., Chauhan, N., Francis, T., Ganjoo, R.K. and Humphreys, G.S., 2010.

A~ 200 ka record of climatic change and dune activity in the Thar Desert, India. *Quaternary Science Reviews*, *29*(23-24), pp.3095-3105.

Sinha, A., Berkelhammer, M., Stott, L., Mudelsee, M., Cheng, H. and Biswas, J., 2011a. The leading mode of Indian Summer Monsoon precipitation variability during the last millennium. *Geophysical Research Letters*, 38(15).

Sinha, A., Cannariato, K.G., Stott, L.D., Cheng, H., Edwards, R.L., Yadava, M.G., Ramesh, R. and Singh, I.B., 2007. A 900‐year (600 to 1500 AD) record of the Indian summer monsoon precipitation from the core monsoon zone of India. *Geophysical Research Letters*, 34(16).

Sinha, A., Cannariato, K.G., Stott, L.D., Li, H.C., You, C.F., Cheng, H., Edwards, R.L. and Singh, I.B., 2005. Variability of Southwest Indian summer monsoon precipitation during the Bølling-Allerød. *Geology*, 33(10), pp.813-816.

Sinha, A., Stott, L., Berkelhammer, M., Cheng, H., Edwards, R.L., Buckley, B., Aldenderfer, M. and Mudelsee, M., 2011b. A global context for megadroughts in monsoon Asia during the past millennium. *Quaternary Science Reviews*, 30(1-2), pp.47-62.

Sinha, R., Smykatz-Kloss, W., Stüben, D., Harrison, S.P., Berner, Z. and Kramar, U., 2006. Late Quaternary palaeoclimatic reconstruction from the lacustrine sediments of the Sambhar playa core, Thar Desert margin, India. *Palaeogeography, Palaeoclimatology, Palaeoecology*, *233*(3-4), pp.252-270.

Sirocko, F., Sarnthein, M., Erlenkeuser, H., Lange, H., Arnold, M. and Duplessy, J.C., 1993. Century-scale events in monsoonal climate over the past 24,000 years. *Nature*, *364*(6435), pp.322-324.

Sontakke, N.A., Pant, G.B. and Singh, N., 1993. Construction of all-India summer monsoon rainfall series for the period 1844–1991. *Journal of Climate*, 6(9), pp.1807-1811.

Spooner, N.A., 1994. The anomalous fading of infrared-stimulated luminescence from feldspars. *Radiation Measurements*, *23*(2-3), pp.625-632.

Srivastava, A., Durcan, J.A. and Thomas, D.S.G., 2019a. Analysis of late Quaternary linear dune development in the Thar Desert, India. *Geomorphology*, *344*, pp.90-98.

Srivastava, A., Thomas, D.S.G. and Durcan, J.A., 2019b. Holocene dune activity in the Thar Desert, India. *Earth Surface Processes and Landforms*, *44*(7), pp.1407-1418.

Srivastava, A., Thomas, D.S.G., Durcan, J.A. and Bailey, R.M., 2020. Holocene palaeoenvironmental changes in the Thar Desert: An integrated assessment incorporating new insights from aeolian systems. *Quaternary Science Reviews*, 233, p.106214.

Srivastava, P., Juyal, N., Singhvi, A.K., Wasson, R.J. and Bateman, M.D., 2001. Luminescence chronology of river adjustment and incision of Quaternary sediments in the alluvial plain of the Sabarmati River, north Gujarat, India. *Geomorphology*, 36(3-4), pp.217-229.

Staubwasser, M., Sirocko, F., Grootes, P.M. and Erlenkeuser, H., 2002. South Asian monsoon climate change and radiocarbon in the Arabian Sea during early and middle Holocene. *Paleoceanography*, 17(4), pp.15-1.

Staubwasser, M., Sirocko, F., Grootes, P.M. and Segl, M., 2003. Climate change at the 4.2 ka BP termination of the Indus valley civilization and Holocene south Asian monsoon variability. *Geophysical Research Letters*, *30*(8).

Stokes S. 1994. *Optical dating of selected Late Quaternary aeolian sediments from Western United States, D*. Phil Thesis, University of Oxford.

Stokes, S., Thomas, D.S.G. and Shaw, P.A., 1997. New chronological evidence for the nature and timing of linear dune development in the southwest Kalahari Desert. *Geomorphology*, *20*(1-2), pp.81-93.

Stone, A.E.C. and Thomas, D.S.G., 2008. Linear dune accumulation chronologies from the southwest Kalahari, Namibia: challenges of reconstructing late Quaternary palaeoenvironments from aeolian landforms. *Quaternary Science Reviews*, *27*(17-18), pp.1667-1681.

Swezey, C., 2001. Eolian sediment responses to late Quaternary climate changes: temporal and spatial patterns in the Sahara. *Palaeogeography, Palaeoclimatology, Palaeoecology*, *167*(1-2), pp.119-155.

Telfer, M.W., 2011. Growth by extension, and reworking, of a south-western Kalahari linear dune. *Earth Surface Processes and Landforms*, *36*(8), pp.1125-1135.

Telfer, M.W. and Hesse, P.P., 2013. Palaeoenvironmental reconstructions from linear dunefields: recent progress, current challenges and future directions. *Quaternary Science Reviews*, *78*, pp.1-21.

Telfer, M.W. and Thomas, D.S.G., 2007. Late Quaternary linear dune accumulation and chronostratigraphy of the southwestern Kalahari: implications for aeolian palaeoclimatic reconstructions and predictions of future dynamics. *Quaternary Science Reviews*, *26*(19-21), pp.2617-2630.

Telfer, M.W., Bailey, R.M., Burrough, S.L., Stone, A.E.S., Thomas, D.S.G. and Wiggs, G.S.F., 2010. Understanding linear dune chronologies: insights from a simple accumulation model. *Geomorphology*, *120*(3-4), pp.195-208.

Telfer, M.W., Hesse, P.P., Perez-Fernandez, M., Bailey, R.M., Bajkan, S. and Lancaster, N., 2017. Morphodynamics, boundary conditions and pattern evolution within a vegetated linear dunefield. *Geomorphology*, *290*, pp.85-100.

Telfer, M.W., Mills, S.C. and Mather, A.E., 2014. Extensive quaternary aeolian deposits in the Drakensberg foothills, Rooiberge, South Africa. *Geomorphology*, 219, pp.161-175.

Telfer, M.W., Thomas, Z.A. and Breman, E., 2012. Sand ramps in the Golden Gate Highlands National Park, South Africa: evidence of periglacial aeolian activity during the last glacial. *Palaeogeography, Palaeoclimatology, Palaeoecology*, 313, pp.59-69.

Thamban, M., Kawahata, H. and Rao, V.P., 2007. Indian summer monsoon variability during the Holocene as recorded in sediments of the Arabian Sea: timing and implications. *Journal of oceanography*, 63(6), pp.1009-1020.

Thomas, D.S.G., 1992. Desert dune activity: concepts and significance. *Journal of Arid Environments*, *22*(1), pp.31-38.

Thomas, D.S.G., 2013. Reconstructing paleoenvironments and palaeoclimates in drylands: what can landform analysis contribute?. *Earth Surface Processes and Landforms*, *38*(1), pp.3-16.

Thomas, D.S.G. and Bailey, R.M., 2017. Is there evidence for global-scale forcing of Southern Hemisphere Quaternary desert dune accumulation? A quantitative method for testing hypotheses of dune system development. *Earth Surface Processes and Landforms*, *42*(14), pp.2280-2294.

Thomas, D.S.G. and Bailey, R.M., 2019. Analysis of late Quaternary dunefield development in Asia using the accumulation intensity model. *Aeolian Research*, *39*, pp.33-46.

Thomas, D.S.G. and Burrough, S.L., 2012. Interpreting geoproxies of late Quaternary climate change in African drylands: implications for understanding environmental change and early human behaviour. *Quaternary International*, *253*, pp.5-17.

Thomas, D.S.G. and Burrough, S.L., 2016. Luminescence-based dune chronologies in southern Africa: analysis and interpretation of dune database records across the subcontinent. *Quaternary International*, *410*, pp.30-45.

Thomas, D.S.G. and Leason, H.C., 2005. Dunefield activity response to climate variability in the southwest Kalahari. *Geomorphology*, *64*(1-2), pp.117-132.

Thomas, D.S.G. and Shaw, P.A., 1991. *The Kalahari Environment*. Cambridge University Press.

Thomas, J.V., Kar, A., Kailath, A.J., Juyal, N., Rajaguru, S.N. and Singhvi, A.K., 1999. Late Pleistocene-Holocene-history of aeolian accumulation in the Thar Desert, India. *Zeitschrift fur Geomorphologie Supplementband*, pp.181-194.

Thomsen, K.J., Murray, A.S. and Bøtter-Jensen, L., 2005. Sources of variability in OSL dose measurements using single grains of quartz. *Radiation Measurements*, *39*(1), pp.47-61.

Thomsen, K.J., Murray, A.S., Jain, M. and Bøtter-Jensen, L., 2008. Laboratory fading rates of various luminescence signals from feldspar-rich sediment extracts. *Radiation measurements*, *43*(9-10), pp.1474-1486.

Thomsen, K.J., Murray, A.S. and Jain, M., 2012. The dose dependency of the over-dispersion of quartz OSL single grain dose distributions. *Radiation Measurements*, *47*(9), pp.732-739.

Tod, J., 1832. Annals and Antiquities of Rajast'han or the Central and Western Rajpoot States of India, Volume 2. London: Smith, Elder.

Tripaldi, A. and Forman, S.L., 2007. Geomorphology and chronology of Late Quaternary dune fields of western Argentina. *Palaeogeography, Palaeoclimatology, Palaeoecology*, 251(2), pp.300-320.

Tripaldi, A. and Zárate, M.A., 2016. A review of Late Quaternary inland dune systems of South America east of the Andes. *Quaternary international*, 410, pp.96-110.

Tsoar, H., 1989. Linear dunes-forms and formation. *Progress in Physical Geography*, *13*(4), pp.507-528.

Tsoar, H., 2008. Land use and its effect on the mobilization and stabilization of the north-western Negev sand dunes. In Arid Dune Ecosystems (pp. 79-89). Springer, Berlin, Heidelberg.

Tsoar, H. and Blumberg, D.G., 2002. Formation of parabolic dunes from barchan and transverse dunes along Israel's Mediterranean coast. *Earth Surface Processes and Landforms*, *27*(11), pp.1147-1161.

Tsoar, H. and Møller, J.T., 1986. The role of vegetation in the formation of linear sand dunes. *Aeolian geomorphology*, pp.75-95.

Tsoar, H., Blumberg, D.G. and Wenkart, R., 2008. Formation and geomorphology of the North-Western Negev sand dunes. In *Arid dune ecosystems* (pp. 25-48). Springer, Berlin, Heidelberg.

United Nations, 2010. United Nations Decade: For Deserts and the Fight Against Desertification. www.un.org/en/events/desertification_decade/background.shtml

Vandenberghe, D., De Corte, F., Buylaert, J.P. and Kučera, J., 2008. On the internal radioactivity in quartz. *Radiation Measurements*, *43*(2-6), pp.771-775.

Verstappen, H.T., 1968. On the origin of longitudinal (seif) dunes. *Zeitschrift für Geomorphologie NF*, *12*, pp.200-220.

Visocekas, R., 1985. Tunnelling radiative recombination in labradorite: its association with anomalous fading of thermoluminescence. *Nuclear Tracks and Radiation Measurements (1982)*, *10*(4-6), pp.521-529.

Von Rad, U., Schaaf, M., Michels, K.H., Schulz, H., Berger, W.H. and Sirocko, F., 1999. A 5000-yr record of climate change in varved sediments from the oxygen minimum zone off Pakistan, Northeastern Arabian Sea. *Quaternary Research*, *51*(1), pp.39-53.

Wadhawan, S.K., 1998. Late Quaternary Evolution of Clustered Parabolic Megadunes in Thar Desert, India. *Quaternary Deserts and Climatic Change*, pp.185-195.

Walker, M., Head, M.J., Lowe, J., Berkelhammer, M., BjÖrck, S., Cheng, H., Cwynar, L.C., Fisher, D., Gkinis, V., Long, A. and Newnham, R., 2019. Subdividing the Holocene Series/Epoch: formalization of stages/ages and subseries/subepochs, and designation of GSSPs and auxiliary stratotypes. *Journal of Quaternary Science*, 34(3), pp.173-186.

Wallinga, J., Murray, A.S., Duller, G.A. and Törnqvist, T.E., 2001. Testing optically stimulated luminescence dating of sand-sized quartz and feldspar from fluvial deposits. *Earth and Planetary Science Letters*, *193*(3-4), pp.617-630.

Wang, L., d'Odorico, P., Evans, J.P., Eldridge, D.J., McCabe, M.F., Caylor, K.K. and King, E.G., 2012. Dryland ecohydrology and climate change: critical issues and technical advances. *Hydrology and Earth System Sciences*, *16*(8), pp.2585-2603.

Wang, Y., Cheng, H., Edwards, R.L., He, Y., Kong, X., An, Z., Wu, J., Kelly, M.J., Dykoski, C.A. and Li, X., 2005. The Holocene Asian monsoon: links to solar changes and North Atlantic climate. *Science*, 308(5723), pp.854-857.

Wasson, R.J., Rajaguru, S.N., Misra, V.N., Agrawal, D.P. and Dhir, R.P., 1983. Geomorphology, late Quaternary stratigraphy and paleoclimatology of the Thar dunefield. *Zeitschrift für Geomorphologie. Supplementband*, 45, pp.117-151.

Wasson, R.J., Rajaguru, S.N., Misra, V.N., Agrawal, D.P., Dhir, R.P., Singhvi, A.K. and Rao, K.K., 1983. Geomorphology, late Quaternary stratigraphy and palaeoclimatology of the Thar dunefield.

Wasson, R.J., Smith, G.I. and Agrawal, D.P., 1984. Late Quaternary sediments, minerals, and inferred geochemical history of Didwana Lake, Thar Desert, India. *Palaeogeography, Palaeoclimatology, Palaeoecology*, *46*(4), pp.345-372.

Wiggs, G.F.S., Baird, A.J. and Atherton, R.J., 2004. The dynamic effects of moisture on the entrainment and transport of sand by wind. *Geomorphology*, *59*(1-4), pp.13-30.

Wintle, A.G., 1973. Anomalous fading of thermo-luminescence in mineral samples. *Nature*, *245*(5421), p.143.

Wintle, A.G., 2008. Luminescence dating: where it has been and where it is going. *Boreas*, *37*(4), pp.471-482.

Wintle, A.G. and Murray, A.S., 1998. Towards the development of a preheat procedure for OSL dating of quartz. *Radiation Measurements*, *29*(1), pp.81-94.

Wintle, A.G. and Murray, A.S., 2006. A review of quartz optically stimulated luminescence characteristics and their relevance in single-aliquot regeneration dating protocols. *Radiation measurements*, *41*(4), pp.369-391.

Wintle, A.G., Shackleton, N.J. and Lautridou, J.P., 1984. Thermoluminescence dating of periods of loess deposition and soil formation in Normandy. *Nature*, *310*(5977), p.491.

Wolfe, S.A. and Hugenholtz, C.H., 2009. Barchan dunes stabilized under recent climate warming on the northern Great Plains. *Geology*, *37*(11), pp.1039-1042.

Wright, R.P., 2010. The ancient Indus: Urbanism, economy, and society (p. 1). Cambridge: Cambridge University Press.

Wu, G., Liu, Y., Zhang, Q., Duan, A., Wang, T., Wan, R., Liu, X., Li, W., Wang, Z. and Liang, X., 2007. The influence of mechanical and thermal forcing by the Tibetan Plateau on Asian climate. *Journal of Hydrometeorology*, *8*(4), pp.770-789.

Xu, D., You, X. and Xia, C., 2019. Assessing the spatial-temporal pattern and evolution of areas sensitive to land desertification in North China. *Ecological indicators*, *97*, pp.150-158.

Yadava, M.G. and Ramesh, R., 1999. *Speleothems—useful proxies for past monsoon rainfall*.

Yan, N. and Baas, A.C., 2015. Parabolic dunes and their transformations under environmental and climatic changes: Towards a conceptual framework for understanding and prediction. *Global and Planetary Change*, *124*, pp.123-148.

Yan, N. and Baas, A.C., 2017. Environmental controls, morphodynamic processes, and ecogeomorphic interactions of barchan to parabolic dune transformations. *Geomorphology*, *278*, pp.209-237.

Yang, X., Li, H. and Conacher, A., 2012. Large-scale controls on the development of sand seas in northern China. *Quaternary International*, *250*, pp.74-83.

Yang, X., Liu, T. and Xiao, H., 2003. Evolution of megadunes and lakes in the Badain Jaran Desert, Inner Mongolia, China during the last 31,000 years. *Quaternary International*, *104*(1), pp.99-112.

Yang, X., Ma, N., Dong, J., Zhu, B., Xu, B., Ma, Z. and Liu, J., 2010. Recharge to the inter-dune lakes and Holocene climatic changes in the Badain Jaran Desert, western China. *Quaternary Research*, *73*(1), pp.10-19.

Yang, X., Scuderi, L., Paillou, P., Liu, Z., Li, H. and Ren, X., 2011. Quaternary environmental changes in the drylands of China–a critical review. *Quaternary Science Reviews*, *30*(23-24), pp.3219-3233.

Zárate, M.A. and Tripaldi, A., 2012. The aeolian system of central Argentina. *Aeolian Research*, 3(4), pp.401-417.

Zhang, J. and Li, S.H., 2020. Review of the Post-IR IRSL Dating Protocols of K-Feldspar. *Methods and Protocols*, 3(1), p.7.

Zhang, Z. and Huisingh, D., 2018. Combating desertification in China: Monitoring, control, management and revegetation. *Journal of cleaner production*, *182*, pp.765-775.

Zhao, H., Lu, Y. and Yin, J., 2007. Optical dating of Holocene sand dune activities in the Horqin sand-fields in Inner Mongolia, China, using the SAR protocol. *Quaternary Geochronology*, *2*(1-4), pp.29-33.

Zhisheng, A., Clemens, S.C., Shen, J., Qiang, X., Jin, Z., Sun, Y., Prell, W.L., Luo, J., Wang, S., Xu, H. and Cai, Y., 2011. Glacial-interglacial Indian summer monsoon dynamics. science, 333(6043), pp.719-723.

Zimmerman, D.W., 1971. Thermoluminescent dating using fine grains from pottery. *Archaeometry*, *13*(1), pp.29-52.

Appendices

Appendix A: Contribution of authors

The majority of work in this thesis is author's own work, however, a small proportion has been contributed by the co-authors in the three published papers. Field sampling was conducted by the author Aayush Srivastava (AS), Dave Thomas (DT) and Julie Durcan (JD). AS conducted all of the laboratory work associated with dating sediments using luminescence techniques and preparing samples for ICP-MS measurement, and sedimentological analyses. Richard Bailey ran the *AI* model. AS also prepared all the figures and tables. After discussion with DT and JD, all papers and chapters were written by AS. DT and JD also provided comments which significantly improved the drafts of each submitted paper.

Appendix B: Sedimentological analyses

Sedimentological analyses were undertaken on all the collected samples to provide additional context to their depositional history.

Colour

The Munsell colour of samples was derived from overnight oven-dried sediments. All samples ranged between light yellowish brown (10YR 5/4) to very pale brown (10YR 7/4). Barring two samples, Thar 16/1/1 and Thar 16/4/1 (both 10YR 6/6), samples remain homogenous in colour in a sampled section.

Water content

Water content was calculated by the change in mass of a subsample between opening the sample and drying for 24h in the oven at 50°C. The change in mass was calculated as a percentage, and reduction was attributed to water loss.

Table B1. Water content for studied samples in this thesis.

Samples	*Empty Beaker (EB)* (g)	*EB+ moist sand* (g)	*EB+ dry sand* (g)	*Water content* (g)	*Water content* (%)
Thar 16/1/1	34.63	56.67	56.61	0.06	**0.27**
Thar 16/1/2	19.29	36.93	36.87	0.06	**0.32**
Thar 16/1/4	19.32	32.64	32.63	0.01	**0.08**
Thar 16/1/5	19.05	24.12	24.11	0.01	**0.24**
Thar 16/1/6	19.05	32.56	32.53	0.03	**0.22**
Thar 16/1/7	19.29	30.86	30.84	0.02	**0.15**
Thar 16/1/8	19.07	37.13	37.10	0.03	**0.18**
Thar 16/1/9	34.6	72.14	70.94	1.2	**3.30**
Thar 16/2/1	19.06	35.73	35.68	0.06	**0.36**
Thar 16/2/3	19.30	30.78	30.75	0.04	**0.33**
Thar 16/3/1	19.38	33.49	33.44	0.05	**0.35**
Thar 16/3/2	19.05	35.12	35.04	0.08	**0.48**
Thar 16/4/1	37.17	63.75	63.68	0.07	**0.26**
Thar 16/4/2	19.29	34.81	34.80	0.01	**0.06**
Thar 16/4/4	19.06	30.81	30.80	0.01	**0.10**
Thar 16/4/6	19.06	32.32	32.31	0.01	**0.10**

Thar 16/4/7	19.26	27.17	27.17	0.01	**0.10**
Thar 16/4/8	19.00	37.91	37.88	0.03	**0.15**
Thar 16/4/10	36.73	75.15	74.56	0.59	**1.56**
Thar 16/6/1	33.25	60.16	60.08	0.08	**0.30**
Thar 16/6/5	19.34	34.26	34.22	0.04	**0.27**
Thar 16/8/1	19.06	32.92	32.88	0.04	**0.30**
Thar 16/8/2	19.09	38.86	38.78	0.09	**0.44**
Thar 16/9/1	35.17	73.43	72.9	0.53	**1.40**
Thar 16/9/2	19.09	37.41	37.36	0.04	**0.24**
Thar 16/9/4	19.30	30.40	30.38	0.02	**0.20**
Thar 16/9/5	19.29	36.21	36.14	0.06	**0.39**
Thar 16/9/8	33.27	61.86	61.47	0.39	**1.38**
Thar 16/10/1	34.63	65.32	65.23	0.09	**0.29**
Thar 16/10/4	19.33	32.91	32.90	0.01	**0.07**
Thar 16/10/8	19.00	33.03	33.01	0.01	**0.09**
Thar 16/10/9	19.28	28.42	28.40	0.02	**0.19**
Thar 16/10/10	35.21	61.3	60.81	0.49	**1.91**
Thar 18/1/2	19.06	26.88	26.85	0.033	**0.42**
Thar 18/1/4	19.32	27.91	27.86	0.046	**0.54**
Thar 18/2/1	19.05	26.97	26.97	0.003	**0.04**
Thar 18/2/5	19.08	28.75	28.72	0.027	**0.28**
Thar 17/2/1	19.30	34.86	34.82	0.04	**0.26**
Thar 17/2/2	19.34	33.23	33.18	0.04	**0.32**
Thar 17/2/4	19.08	30.90	30.85	0.05	**0.38**
Thar 17/2/6	19.06	30.98	30.94	0.04	**0.34**
Thar 17/2/8	19.06	36.82	36.76	0.06	**0.36**
Thar 17/2/10	18.20	27.67	27.49	0.18	**1.96**
Thar 17/4/1	19.09	33.56	33.51	0.05	**0.31**
Thar 17/4/2	19.30	36.38	36.33	0.05	**0.31**
Thar 17/4/6	19.33	33.34	33.27	0.07	**0.50**
Thar 17/4/8	19.02	37.68	37.40	0.27	**1.49**
Thar 17/5/1	19.38	35.18	35.14	0.05	**0.30**
Thar 17/5/2	19.31	35.85	35.81	0.04	**0.26**
Thar 17/5/4	19.07	30.66	30.62	0.04	**0.31**
Thar 17/5/6	19.08	33.12	32.58	0.54	**4.03**
Thar 17/5/8	19.11	35.95	35.81	0.14	**0.84**
Thar 17/6/2	19.39	36.38	36.33	0.05	**0.30**
Thar 17/6/4	19.29	33.05	33.01	0.05	**0.35**
Thar 17/6/6	19.08	36.46	36.40	0.06	**0.32**
Thar 17/6/9	19.06	39.18	39.13	0.05	**0.25**
IND 14/5/1	33.56	97.47	97.25	0.22	**0.35**
IND 14/5/2	33.32	100.40	100.00	0.40	**0.60**
IND 14/5/3	34.90	115.80	114.80	1.00	**1.25**
IND 14/5/4	35.26	108.40	107.90	0.50	**0.69**
IND 14/5/5	34.53	96.10	95.90	0.20	**0.33**
IND 14/5/6	34.63	112.70	112.40	0.30	**0.39**

Organic and Carbonate content

The percentage weights of organic and carbonate content were calculated using sequential loss on ignition (LOI), following the procedure outlined in Heiri *et al.* (2001) and using the equations below.

$$LOI_{550} = \frac{DW_{105} - DW_{550}}{DW_{105}} \times 100$$

$$LOI_{950} = \frac{DW_{505} - DW_{950}}{DW_{105}} \times 100$$

DW_{105} is the weight of the sample dried overnight at 105°C, DW_{550} is the weight of the sample after 4 hours of combustion in the furnace at 550°C and DW_{950} is the weight of the sample after 4 hours of combustion in the furnace at 950 ^{0}C.

The combustion of sediment at 550°C gives a crude measure of a sample's organic content. The remaining ash is then heated to 905°C, a process which converted carbonates to oxides, therefore enabling the determination of the carbonate content of the sediment. Once the samples are cool and re-weighed, the difference between the ash weight and the weight lost at 950°C is multiplied by 1.36 (the difference between the molecular weights of CO_2 and CO_3) to derive the carbonate content which is then expressed as a percentage of the dry weight.

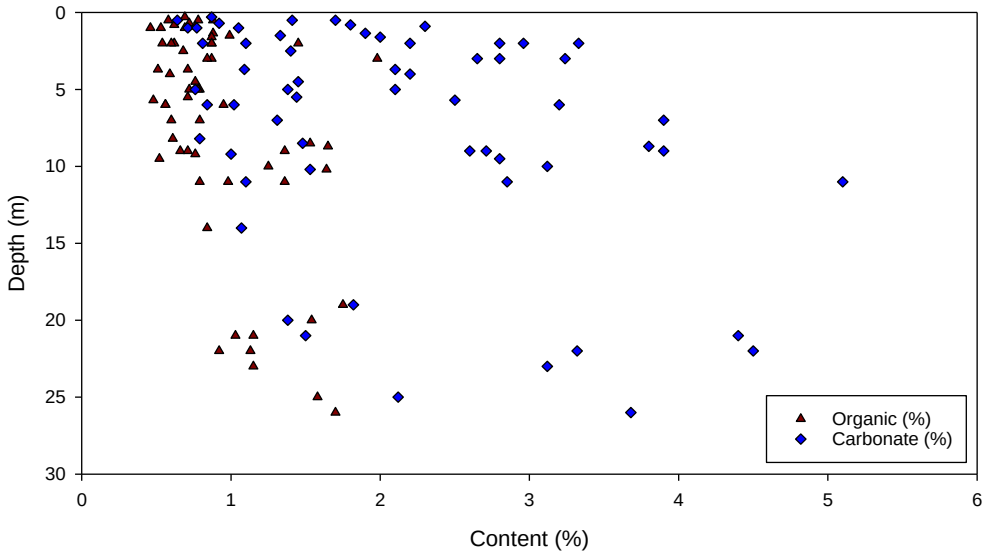


Figure B.1. Scatter plot showing the percentages of organic and carbonate contents against depth for all the studied samples.

As shown in Figure B.1, the organic content for all samples is less than 2 %, which is expected as due to low rainfall, dunes are typically devoid of decaying organic matter. Even if some traces are present, high temperatures in the region ensure rapid breakdown of organic matter. Additionally, during sampling in the field it was made sure that bioturbated units (with evidence of roots or other biogenic activities) were avoided. The carbonate content for the majority of samples is less than ~3 % (Figure B.1). For basal samples (e.g. Thar 16/1/9, Thar 17/2/3, Thar 17/5/8, Thar 17/4/8, Thar 17/2/10 etc.), it is slightly higher ranging between 4 and 5 % because of their proximity to underlying pedogenic calcretes. Since the presence of carbonates can affect the environmental dosimetry (e.g. Guérin *et al.*, 2015), samples were carefully collected away from such calcrete units. Studies have shown that Thar dunes are devoid of well-formed calcretes because of a very weak and limited vertical

redistribution of carbonate and incipient transformation of weatherable minerals (Dhir *et al.*, 2010).

Grain size analyses

Grain size analyses were conducted on a Malvern Mastersizer 2000 laser granulometer (wet dispersion technique with no pre-treatment, and addition of 20 s ultrasonic dissolution). Statistics (mean size, sorting, skewness and kurtosis) were calculated using GRADISTAT (Blott, 2000) following the scheme proposed by Folk and Ward (1957). In general, all the samples have a unimodal, dominantly fine sand distribution with most of them having mean grain size varying between 150 and 250 µm (Figures 4.3 and 5.3). The silt component ranges between 0 and 15 % for all samples, except for Thar 17/2/10 where the silt component is 23 %. The percentage of the clay component does not exceed 1.2 % for any sample.

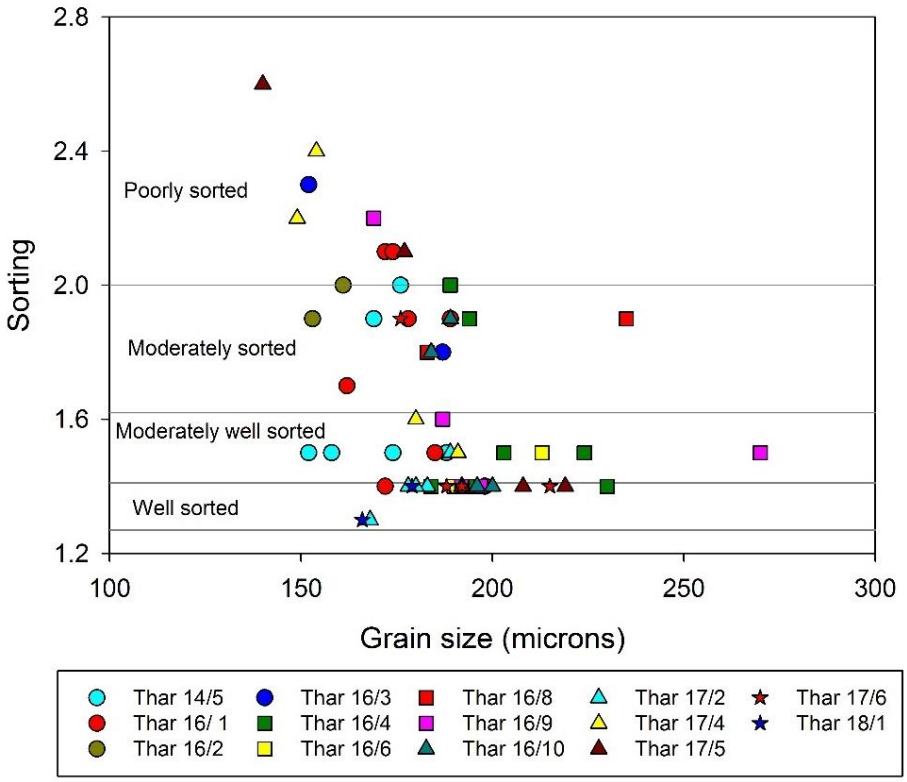


Figure B.2. Bivariate plot between grain size and sorting for studied samples. Sorting range has been chosen following the scheme of Folk and Ward (1975).

Statistical formulae used in the calculation of grain size parameters and suggested descriptive terminology following Folk and Ward (1957) (P_x is grain diameter in metric).

Mean (M_G)

$$M_G = exp\ \frac{ln\ P_{16} + ln\ P_{50} + ln\ P_{84}}{3}$$

Standard Deviation (σ_g)

$$\sigma_g = exp\left(\frac{ln\ P_{16} - ln\ P_{84}}{4} + \frac{ln\ P_5 - ln\ P_{95}}{6.6}\right)$$

Sorting	
Very well sorted	< 1.27
Well sorted	1.27 - 1.41
Moderately well sorted	1.41 - 1.62
Poorly sorted	1.62 - 2.00
Very poorly sorted	2.00 - 4.00
Extremely poorly sorted	> 16.00

Skewness (Sk_G)

$$Sk_G = \frac{ln\ P_{16}\ +\ ln\ P_{84}\ -\ 2(ln\ P_{50})}{2\ (ln\ P_{84}\ -\ ln\ P_{16})} + \frac{ln\ P_5\ +\ ln\ P_{95}\ -\ 2(ln\ P_{50})}{2\ (ln\ P_{25}\ -\ ln\ P_5)}$$

Skewness	
Very fine skewed	-0.3 to - 1.0
Fine skewed	-0.1 to - 0.3
Symmetrical	-0.1 to + 0.1
Coarse skewed	+0.1 to + 0.3
Very coarse skewed	+0.3 to + 1.0

Kurtosis (K_G)

$$K_G = \frac{ln\ P_5\ -\ ln\ P_{95}}{2.44\ (ln\ P_{25}\ -\ ln\ P_{75})}$$

Kurtosis	
Very platykurtic	< 0.67
Platykurtic	0.67 - 0.90
Mesokurtic	0.90 - 1.11
Leptokurtic	1.11 - 1.50
Very leptokurtic	1.50 - 3.00
Extremely leptokurtic	> 3.00

Heavy mineral separation

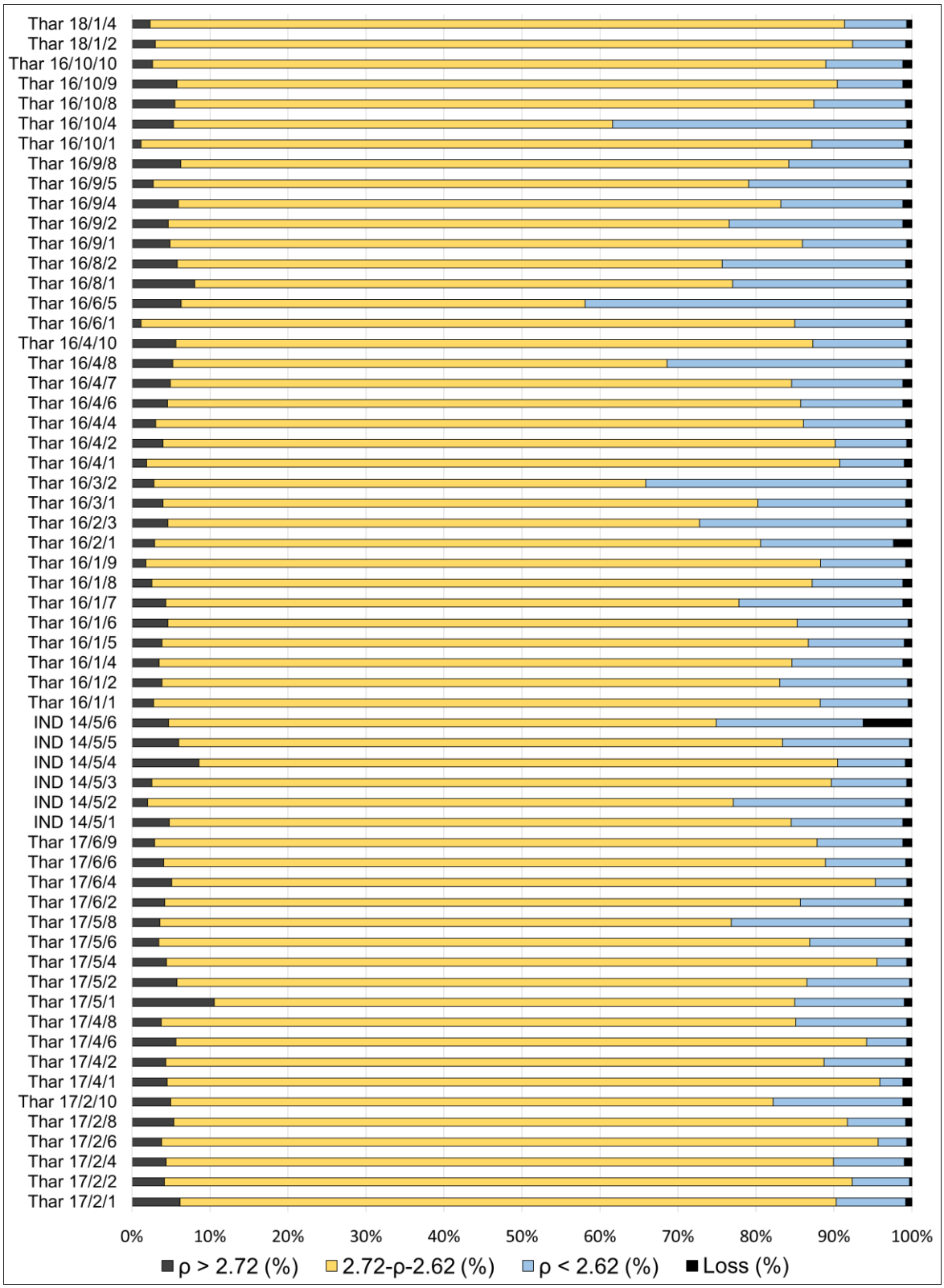


Figure B.3. The percentage of mass separated during heavy liquid density separation for all studied samples in this thesis.

Appendix C: Measurement of radionuclide concentrations

For this thesis, radionuclide concentrations were measured using inductively coupled plasma mass spectrometry performed at the Scottish Universities Environmental Research Centre, East Kilbride. Before analysis ~5-6 g of sediment was homogenised and from this, ~0.2 g was used for analysis. Dissolution was performed using conventional tri-acid (HF-HNO_3-HCl) digestion, incorporating a perchloric acid ($HClO_4$) step to ensure complete dissolution and complete evaporation of HF before going to complete dryness (V. Olive, pers. comms.). Following the digestion procedure, samples were picked up in 2.5 ml of HNO_3 (5%) and then transferred to volumetric flasks, diluted to 50 ml with HNO_3 (5%). A USGS geo-standard BCR-2 (Basalt, Columbia River) was used an internal quality check. Analyses were done on an Agilent 7500ce using an Aspire Nebulizer tuned at 0.1 ml a minute. Concentrations were calculated using a regression on 3 multi-elements standards diluted from a single solution (V. Olive. pers. Comms.).

Appendix D: Calculation of the environmental dose rate

The Ḋs in this thesis have been calculated using the DRAC (v1.2) software of Durcan *et al.* (2015). A worked calculation for sample Thar 16/1/1 is presented here to check the DRAC calculations. The radionuclide concentrations and attenuation factors are provided in Table D.1, and all uncertainties are propagated in quadrature.

Table D.1. Radionuclide concentrations, conversion factors, and the attenuation factors used in dose rate calculation for sample Thar16/1/1. Beta and gamma dose rates were also corrected for a moisture content of 5 ± 2 %.

	Radionuclide concentrations	Conversion factors (from Guerin *et al.*, 2011)		Grain size attenuation factors (Guerin *et al.*, 2012)	Etch depth attenuation factors (Bell, 1979)
		Beta	Gamma		
U	0.720 ± 0.072 ppm	0.1457 ± 0.0004	0.1116 ± 0.0002	0.0859 ± 0.007	0.939 ± 0.004
Th	0.466 ± 0.466 ppm	0.0277 ± 0.0009	0.0479 ± 0.0002	0.0803 ± 0.009	0.922 ± 0.007
K	1.430 ± 0.143 %	0.7982 ± 0.0073	0.2491 ± 0.0048	0.0927 ± 0.006	1

Calculation of the beta dose rate

The infinite matrix $\dot{D}_\beta$ is calculated by multiplying the radionuclide concentrations (Table D.1) by their conversion factor (C) values of Guerin *et al.* (2011):

$$\dot{D}_\beta = (U \times C_U^\beta \times A_U^\beta) + (Th \times C_{Th}^\beta \times A_{Th}^\beta) + (K \times C_K^\beta \times A_K^\beta)$$

$\dot{D}_\beta$ = [(0.720 ± 0.007) x (0.1457 ± 0.0277)] + [(4.660 ± 0.466) x (0.0277 ± 0.0009)] + [(1.431 ± 0.143) x (0.7982 ± 0.0073)]

$\dot{D}_{\beta}$ = (0.105 ± 0.0105) + (0.129 ± 0.0044) + (1.141 ± 0.1145)

The infinite matrix dose rates are then adjusted for attenuation by grain size and etch depth (Table D.1), as well as moisture content:

Grain size:

$\dot{D}_{\beta}$ = [(0.105 ± 0.0105) x (0.859 ± 0.007)] + [(0.129 ± 0.0044) x (0.803 ± 0.009)] + [(1.141 ± 0.1145) x (0.927 ± 0.006)]

$\dot{D}_{\beta}$ = (0.090 ± 0.0090) + (0.104 ± 0.0016) + (1.058 ± 0.1064)

Etch depth:

$\dot{D}_{\beta}$ = [(0.090 ± 0.0090) x (0.939 ± 0.004)] + [(0.104 ± 0.0016) x (0.922 ± 0.007)] + [(1.058 ± 0.1064) x (1.000 ± 0.000)]

$\dot{D}_{\beta}$ = 1.238 ± 0.102 Gy.ka^{-1}

Moisture content

$\dot{D}_{\beta,moist} = \dot{D}_{\beta,dry} / 1+1.25W$

where W is the water content (5 %) and 1.25 is the attenuation factor of Aitken (1998).

$\dot{D}_{\beta,moist}$ = (1.238 ± 0.102) / (1.063 ± 0.063)

$\dot{D}_{\beta,moist}$ = <u>1.165 ± 0.118 Gy.ka^{-1}</u>

<u>*Calculation of the gamma dose rate*</u>

By applying the conversation factors (C) of Guerin *et al.* (2011) (Table D.1) and radionuclide concentrations, $\dot{D}_{\gamma}$ is calculated as:

$\dot{D}_\gamma = (U \times C_U^\gamma) + (Th \times C_{Th}^\gamma) + (K \times C_K^\gamma)$

$\dot{D}_\gamma$ = [(0.720 ± 0.007) x (0.1116 ± 0.0002)] + [(4.660 ± 0.466) x (0.0479 ± 0.0002)] + [(1.431 ± 0.143) x (0.2491 ± 0.0048)]

$\dot{D}_\gamma$ = 0.659 ± 0.037 Gy.ka^{-1}

Gamma rays are attenuated by moisture in the sediment matrix. Using the attenuation factor of 1.14 (Aitken, 1998), the $\dot{D}_{\gamma,dry}$ is corrected for moisture by:

$\dot{D}_{\gamma,moist} = \dot{D}_{\gamma,dry}$ / 1+1.14W

where W is the water content (5% here).

$\dot{D}_{\gamma,\ moist}$ = (0.659 ± 0.037) / (1.057 ± 0.057)

$\dot{D}_{\gamma,\ moist}$ = <u>0.624 ± 0.043 Gy.ka^{-1}</u>

<u>Calculation of the cosmic dose</u>

The $\dot{D}_{cosmic}$ has been calculated using the equations in Prescott and Hutton (1994), first by calculating the $\dot{D}_{cosmic}$ from the hard and soft components of cosmic rays (Prescott and Hutton,1994) and then adjusting the $\dot{D}$ for the effect of geomagnetic latitude and altitude.

The hard component $\dot{D}_{cosmic}$ (for sample depth 0.5 m with overburden of 1.80 g.cm^{-3}) is calculated by:

$$\dot{D}_0 = \frac{6072}{((x+11.6)^{1.68} + 75)(x+212)} exp\,(-5.50 \times 10^{-4} x)$$

and the soft component is calculated by a fourth order polynomial fitted to the data in Prescott and Hutton (1998):

$$\dot{D}_0 = 3.21 \times 10^{-2}x^4 - 1.35 \times 10^{-1}x^3 + 2.21 \times 10^{-1}x^2 - 2.07 \times 10^{-1}\,x + 0.295$$

where D_0 is the uncorrected $\dot{D}_{cosmic}$ in Gy.ka^{-1}, and x is the depth in units of 100 g.cm^{-2}. The calculated value of $\dot{D}_0$ 0.209 Gy.ka^{-1}. The calculated cosmic ray dose rate is corrected for geomagnetic latitude (λ) using the equation:

$$\sin\lambda = 0.203\ \cos\theta\ \cos(\varphi - 291) + 0.979\ \sin\theta$$

where λ is the geomagnetic latitude, θ is the geographic latitude (26.58397 N here) and φ the geographic longitude (72.81615 E here) (north latitudes and east longitudes are positive).

sin λ = 0.203 cos 26.58 cos (72.82 – 291) + 0.979 sin 26.58

sin λ = 0.2953

λ = 17.182

The cosmic ray dose rate is then corrected for a geomagnetic latitude of 17.182 using the equation:

$$\dot{D}_c = \dot{D}_0 \left[F + J\ exp\ \left(\frac{h}{H}\right)\right]$$

where $\dot{D}_0$ is the cosmic dose rate prior to geomagnetic latitude correction, F, J and H are derived from Figure D.1 and h is the altitude (km).

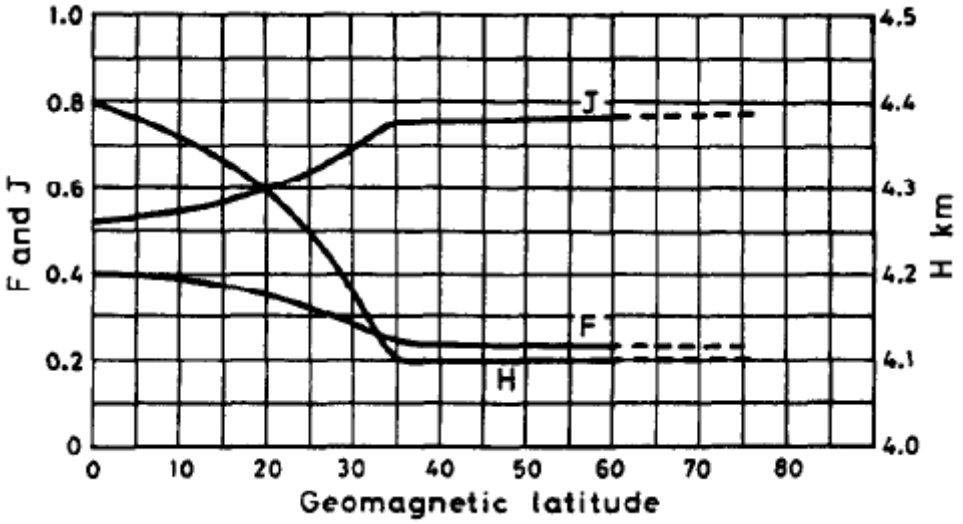


Figure D.1. The parameters required to calculate the cosmic dose rate correcting for altitude and geomagnetic latitude, after Prescott and Stephan (1982) in Prescott and Hutton (1994).

$$\dot{D}_c = 0.209 \left[0.37 + 0.575\, exp\, \left(\frac{0.272}{4.32}\right)\right]$$

The calculated value of $\dot{D}_{cosmic}$ is 0.207 ± 0.021 Gy.ka^{-1}. Note that the uncertainty is not calculated but a ± 10 % of calculated $\dot{D}_{cosmic}$ is added.

Total environmental dose

The total $\dot{D}$ is calculated as

$\dot{D} = \dot{D}_{\beta,moist} + \dot{D}_{\gamma,\ moist} + \dot{D}_{cosmic}$

$\dot{D}$ = 1.165 ± 0.118 + 0.624 ± 0.043 + 0.207 ± 0.021

$\dot{D}$ = **1.996 ± 0.121 Gy.ka^{-1}**

The $\dot{D}$ value calculated using DRAC is **1.995 ± 0.115 Gy.ka^{-1}**, which is consistent with the manual calculation presented above.

Appendix E: Paper 1 (Chapter 4) as included in journal *Earth Surface Processes and Landforms*.

EARTH SURFACE PROCESSES AND LANDFORMS
Earth Surf. Process. Landforms (2019)
© 2019 John Wiley & Sons, Ltd.
Published online in Wiley Online Library
(wileyonlinelibrary.com) DOI: 10.1002/esp.4583

Holocene Dune Activity in the Thar Desert, India

Aayush Srivastava,[1]* David S.G. Thomas[1,2] and Julie A. Durcan[1]
[1] School of Geography and the Environment, University of Oxford, Oxford OX1 3QY, United Kingdom
[2] School of Geography, Archaeology and Environmental Studies, University of the Witwatersrand, Johannesburg 2050, South Africa

Received 8 May 2018; Revised 24 December 2018; Accepted 9 January 2019

*Correspondence to: Aayush Srivastava, School of Geography and the Environment, University of Oxford, Oxford, OX1 3QY, United Kingdom. E-mail: aayush.srivastava@ouce.ox.ac.uk

ESPL
Earth Surface Processes and Landforms

ABSTRACT: The Thar Desert dune system in north-west India and eastern Pakistan provides a rich archive of past environmental, geomorphological and climatic change. Much of the knowledge about the timing of dune accumulation in the Thar stems from scattered and sporadic records, based on older luminescence dating protocols. If the Thar dune record is to be incorporated within a growing multiproxy framework of past climate and environmental dynamics, it is necessary to generate a systematic record of the timing of dunefield accumulation. From this, relationships to climate and other drivers of dune activity may then be better established. To this end, an intensive programme of field sampling and optically stimulated luminescence (OSL) dating was carried out from a dunefield in the east-central Thar Desert. This study presents the first detailed Holocene dune accumulation history from the region, and sheds light on the development of the multi-generational parabolic dune systems. In contrast to previously published work, we identify the importance of the Holocene and the last millennium as periods with a number of preserved accumulation phases. OSL ages suggest that accumulation was persistent during the early and mid-Holocene (within 11.7-5.5 ka), late Holocene (2-1 ka), as well as two major phases in the last millennium (600 – 200 a and within the last 70 a). Potential drivers of dune mobility in the last century include a strong anthropogenic dimension. Rapid net accumulation is recorded in the last 70 years, with rates varying between 2 and 5 m/year, in an environment where agricultural pressures have increased dramatically with the advent of irrigation schemes expanding into dunefield areas. © 2019 John Wiley & Sons, Ltd.

KEYWORDS: Thar Desert; optically stimulated luminescence (OSL) dating; parabolic dunes; Holocene; geomorphological change

Introduction

The Thar Desert forms an integral part of the arid lands of western India and eastern Pakistan, between the Aravalli hills in the east and the Indus plains to the west. The desert is often considered as the easternmost extension of the vast Saharo-Arabian subtropical desert belt (Singhvi and Kar, 2004; Roy *et al.*, 2009), and is dominated by aeolian bedforms of various dimensions and forms. Many sand dune types have been identified in the region, including parabolic, transverse, linear, star and network dunes (Figure 1) (Wasson *et al.*, 1983; Kar, 1993). The desert is located in a transitional but dominant south-west monsoon regime, which not only controls wind seasonality, precipitation and vegetation cover, but also implies that minor perturbations in monsoon dynamics may impact the geomorphic processes, including aeolian dynamics, in this seasonally semi-arid to arid region. The extensive dune systems in the Thar therefore provide an opportunity to understand temporal changes in aeolian dynamics during the late Quaternary.

The first application of luminescence dating to aeolian sands anywhere occurred in the Thar Desert (Singhvi *et al.*, 1982), and this seminal study inspired a move from qualitative assessments of long term dune accumulation histories to temporally specific records. The Thar was one of the leading deserts in luminescence dating applications to aeolian sediments, and in the 35 years since this first application, numerous dune sites have been dated in the region (e.g. Chawla *et al.*, 1992; Singhvi *et al.*, 1994; Kar *et al.*, 1998; Thomas *et al.*, 1999), with dated records used to address the long-standing debate surrounding the potentially recent anthropogenic origins of the Thar Desert, as suggested in early studies by Piggott (1950) and Bryson and Barreis (1967). However, the sampling and dating strategies employed in earlier luminescence dating studies focussed largely on accessing deep trenches in basal sediments, often associated with the expansion of irrigation canals into the region, for establishing the antiquity of aeolian episodes and finding major phases of dune accumulations (Dhir *et al.*, 2010; Kar, 2013). More recent studies have tended to focus on the desert margins, within the context of aeolian-fluvial interactions (e.g. Juyal *et al.*, 2006; Saini *et al.*, 2009; Giosan *et al.*, 2012; Saini and Mujtaba, 2012; Shitaoka *et al.*, 2012; Durcan *et al.*, in press).

To date, the application of systematic and intensive dunefield sampling programmes has been less prevalent in the Thar than in other deserts, such as the Kalahari in Africa (Stone and Thomas, 2008), the Rub' al Khali in Arabia (Atkinson *et al.*, 2011; Leighton *et al.*, 2013) and the Strzelecki and Tirari in Australia (Fitzsimmons *et al.*, 2007). In the Thar, the focus on deeper sequences has potentially resulted in a bias towards older accumulation phases, with relatively younger accumulation phases not sampled. Singhvi and Kar (2004) note that existing data sets provide little opportunity to understand the impact of climate and humans on desert evolution and geomorphological processes during the late Holocene. Interrogation of existing geochronological data is also hampered by a common

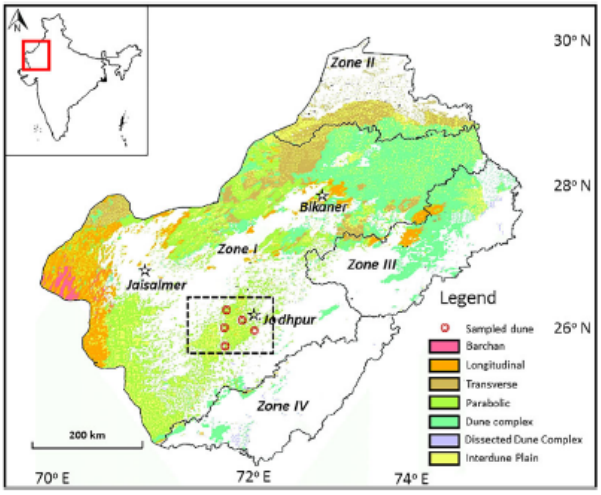


Figure 1. Based on climate and land use pattern indices, the Thar is divided into four zones, namely Arid Western Plain (Zone 1; 133073 sq. km), Irrigated North-Western Plain (Zone 2; 20557 sq. km), Transitional Plains of Inland Drainage Basin (Zone 3; 31329 sq. km) and Transitional Plains of Luni Basin (Zone 4; 22951 sq. km). The dotted box shows the Shergarh-Dechu region in Zone 1 with the location of five sampled dune sites (red wheels) and major cities (stars) (Figure modified from Moharana *et al.*, 2013). [Colour figure can be viewed at wileyonlinelibrary.com]

absence of detailed locational and sampling depth data within published records. In addition, all 146 luminescence ages from the Thar Desert dune systems listed in INQUA Dune Atlas chronologic database (Lancaster *et al.*, 2016) utilised multiple aliquot protocols, which are associated with relatively large age uncertainties (e.g. Stokes, 1994). Both instrumental and methodological advances in luminescence dating, including the single aliquot regenerative (SAR) dose protocol (e.g. Murray and Wintle, 2000, 2003; Wintle and Murray, 2006) and single grain luminescence dating (e.g. Duller, 2003; Duller, 2008) provide the potential for more robust age calculation. In the context of geochronological improvements, and rapid anthropogenic land clearance and disturbance in the Thar Desert, conducting a systematic analysis of Thar dune accumulations chronologies becomes an important research priority. Therefore, the aim of this paper is to present new dune accumulation records from the Thar Desert, following intensive sampling and the application of modern luminescence dating protocols, and to assess spatial variability within a dunefield. This study allows a more temporally-complete assessment of the region's dune accumulation history and provides an insight into the dune evolution in this arid to semi-arid dryland zone.

Study Site and Methodology

The aeolian landforms in the Thar are dominated by various types of dunes which cover ~50% of the region (Kar, 1993; Moharana *et al.*, 2013), the majority of which occur in western Rajasthan, India (Figure 1) and adjoining parts in Pakistan. The present study focusses on the Shergarh-Dechu region in the Arid Western Plain of the central Thar, which is dominated by parabolic dunes. These parabolic dunes form a clustered 'rake-like' appearance (Figure 2A), with longer arms in the middle of the parabolic cluster and gradually shorter arms on each side. The arms can be up to 2500 m long, with inter-arm spacing ranging between 150 m and 650 m. These 'rake-like' parabolic dunes have rounded nose which contains more than 35% sand volume in the dunes (Kar *et al.*, 2004). The Shergarh-Dechu region is classified as arid to semi-arid, with mean annual precipitation typically varying between 250 and 400 mm where dunes are relatively stable under natural conditions. In the present-day conditions, winds in the region increase in strength from March onward, peaking in June and decline after the arrival of monsoonal precipitation in July. This context provides an ideal location for examining the timing and amplitude of spatial changes in aeolian activity in the past and its correlation with variations in monsoonal precipitation.

Site Selection and Sampling

Five dunes sites (Tinwari, Shergarh, Setrawa, Chamu and Dechu) were sampled to test the spatial variability of dune accumulation histories within the dunefield (Figure 2A). Samples were collected from vertical sections, by carefully cutting steps through the nose and arms of the dunes using hydraulic diggers (Figure 2B, C). At Tinwari site, samples were collected from the 23 m deep section located in the nose of the dune (Thar 16/1, Thar 16/3). Four samples were collected from the dune arm from a 2 m deep pit, situated 500 m from the dune nose (Thar 18/1). Similarly, at Setrawa samples were collected from a 7 m deep section located in the nose of the dune (Thar 16/6) and another 7 m section from a section in the dune arm, located ~600 m from the nose (Thar 18/2). The samples from dune arms generated very young ages with indiscernible OSL signal sometimes, therefore, at Shergarh (Thar 16/4), Chamu (Thar 16/9) and Dechu (Thar 16/10), samples were collected from 9.0 m, 8.5 m and 10.2 m deep sections respectively, all located near the nose of the dune only. The sediment faces of dug sections were cleaned prior to sampling. Samples were collected by hammering black light tight tubes into the cleared sediment face, and a resolution of 1.0 m interval was adopted where possible taking into account accessibility and sediment collapse

© 2019 John Wiley & Sons, Ltd.

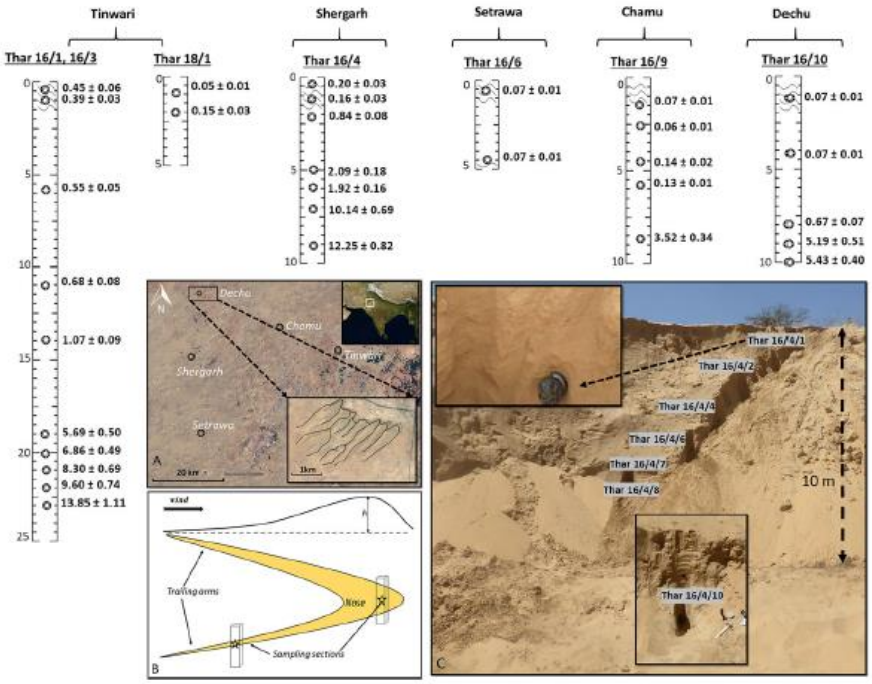


Figure 2. (A) The location of sampled dune sites Tinwari (26.58397 N, 72.81615 E; 26.579361 N, 72.814240 E), Setrawa (26.60192 N, 72.28866 E; 26.596704 N, 72.285504 E), Shergarh (26.33122 N, 72.28821 E), Dechu (26.81859 N, 72.30316 E) and Chamu (26.66854 N, 72.57005 E); all of which are located within the arid to semi-arid Shergarh-Dechu region located on the Arid Western Plain. (B). A schematic representation of sampling sections within a parabolic dune. (C). An example of the sampled section at Shergarh (Thar 16/4). Samples were collected by cutting steps into the dune section to allow access to undisturbed sediment. An offset sample Thar 16/4/10 offset was collected after calculating the depth profile along the main trench. Inset, an OSL sample tube hammered into the cleared sediment face. The presence of laminations demonstrates a lack of post-depositional disturbance. (D) The schematic view of sampled sections with OSL ages (ka). Sample depths are in metres. Most sites consisted of homogeneous dune sands, with the exception of some weak laminations, which are indicated by the curved lines. [Colour figure can be viewed at wileyonlinelibrary.com]

risks, with additional sampling carried out to bracket the fine bedding structures observed at the top of the dunes.

Sedimentological Analyses

Grain size analyses were conducted using a Malvern Mastersizer Hydro 2000 laser grain analyser and analysed using Gradistat (Blott, 2000) following the method of Folk and Ward (1957). Colour analysis was conducted on oven-dried samples using a Munsell colour chart. Organic and carbonate contents were determined by heating the sediment to 550° C and 950° C respectively, following the process outlined in Heiri *et al.* (2001).

Luminescence Dating

Samples were opened in subdued orange-light conditions in the Oxford Luminescence Dating Laboratory, University of Oxford. The light-exposed sample ends were removed and used for sedimentological analyses and measurement of radionuclide concentrations. Sediments were treated with hydrochloric acid and hydrogen peroxide to remove carbonate and organic matter, and were sieved to isolate the 180-210 µm grain size fraction. Quartz mineral grains were isolated by heavy liquid (sodium polytungstate) density separation. Hydrofluoric acid was used to remove the alpha-irradiated outer surface of the quartz grains. Initial tests indicated feldspar contamination, and therefore samples were treated with fluorosilicic acid for two weeks to reduce persistent feldspar contamination. Sediments were treated with hydrochloric acid after each chemical etch to remove any fluoride precipitate, prior to re-sieving.

OSL measurements were made using Risø DA-15 TL/OSL readers (Bøtter-Jensen *et al.*, 2003), fitted with either blue (470 nm) or green (525 nm) LEDs and $^{90}Sr/^{90}Y$ beta sources with dose rates varying between 3.5 and 4 Gy/minute. Luminescence signals were detected through a bialkali photomultiplier tube, fitted with 7.5 mm Hoya U-340 filters. A post-IR blue SAR protocol (Murray and Wintle, 2000; Banerjee *et al.*, 2001) was used to calculate equivalent doses (D_e) as a further precaution against any residual feldspar contamination. Following pre-heat plateau and dose recovery tests, a pre-heat of 240° C for 10 seconds and a cut-heat of 160° C for 0 s were selected for use. Samples were stimulated with infra-red light (870 nm) at 50° C for 100 s, prior to measurement of the blue/green stimulated luminescence at 125° C for 40 s. Sediment was adhered to aluminium discs using silicon spray and small aliquots were used for all but three samples. Small aliquots had a diameter of 2 mm (~70 grains per disc), medium

© 2019 John Wiley & Sons, Ltd.

Table I. Sedimentology of samples showing Munsell colour, grain size statistics (in microns), organic and carbonate content

Sample	Munsell colour	Mean (μm)	Coarse sand (%)	Medium sand (%)	Fine sand (%)	Very fine sand (%)	Silt (%)	Clay (%)	Sorting*	Skewness**	Kurtosis***	Organic content (%)	Carbonate content (%)
Thar 16/1/1	10 YR 6/6	185.5	0.0	25.4	64.5	10.1	0.0	0.0	1.478 (MWS)	-0.109 (FS)	1.123 (L)	0.88	0.64
Thar 16/1/2	10 YR 6/4	198.2	0.0	24.2	67.8	7.9	0.0	0.0	1.386 (WS)	-0.001 (S)	0.965 (M)	0.72	0.92
Thar 16/1/4	10 YR 5/4	172.1	0.0	12.3	71.0	16.6	0.0	0.0	1.380 (WS)	-0.002 (S)	0.962 (M)	0.56	0.84
Thar 16/1/5	10 YR 5/4	177.6	0.1	22.6	55.8	14.2	6.8	0.5	1.895 (MS)	-0.300 (FS)	1.844 (VL)	0.84	1.07
Thar 16/1/6	10 YR 5/4	171.9	0.0	20.7	56.5	10.5	11.5	0.8	2.084 (PS)	-0.386 (VFS)	2.255 (VL)	1.54	1.38
Thar 16/1/7	10 YR 5/4	173.8	0.0	21.1	56.8	10.4	10.8	0.8	2.054 (PS)	-0.376 (VFS)	2.238 (VL)	1.15	1.50
Thar 16/1/8	10 YR 6/4	162.3	0.0	10.5	66.5	17.2	5.7	0.1	1.739 (MS)	-0.305 (VFS)	2.077 (VL)	0.92	3.32
Thar 16/1/9	10 YR 6/4	189.4	0.1	25.6	57.8	8.0	8.1	0.4	1.917 (MS)	-0.345 (VFS)	2.186 (VL)	1.15	3.12
Thar 16/3/1	10 YR 7/4	186.9	0.3	26.2	54.5	13.7	5.2	0.0	1.763 (MS)	-0.232 (FS)	1.513 (VL)	0.79	1.10
Thar 16/3/2	10 YR 7/4	152.5	0.0	18.4	51.9	15.0	13.6	1.1	2.287 (PS)	-0.420 (VFS)	2.099 (VL)	1.75	1.82
Thar 16/4/1	10 YR 6/6	229.9	1.1	40.2	54.0	4.7	0.0	0.0	1.446 (MWS)	-0.004 (S)	0.949 (M)	0.69	0.87
Thar 16/4/2	10 YR 6/4	224.4	2.0	38.0	52.4	7.6	0.0	0.0	1.509 (MWS)	0.006 (S)	0.944 (M)	0.53	0.71
Thar 16/4/4	10 YR 6/4	193.6	0.1	24.5	63.7	11.7	0.0	0.0	1.437 (MWS)	0.011 (S)	0.954 (M)	0.62	2.96
Thar 16/4/6	10 YR 6/4	203.3	0.7	31.2	55.2	10.7	2.2	0.0	1.528 (MWS)	-0.030 (S)	0.980 (M)	0.79	0.76
Thar 16/4/7	10 YR 6/4	189.2	0.4	26.9	54.6	9.0	8.2	0.9	2.035 (PS)	-0.340 (VFS)	2.207 (VL)	0.95	1.02
Thar 16/4/8	10 YR 6/4	193.6	0.4	27.3	56.7	9.6	5.5	0.4	1.851 (MS)	-0.285 (FS)	1.923 (VL)	0.79	1.31
Thar 16/4/10	10 YR 6/4	184.3	0.0	20.0	65.8	14.2	0.0	0.0	1.426 (MWS)	0.001 (S)	0.946 (M)	0.66	2.71
Thar 16/6/1	10 YR 5/4	190.2	0.0	23.0	64.4	12.6	0.0	0.0	1.433 (MWS)	0.004 (S)	0.946 (M)	0.78	1.41
Thar 16/6/5	10 YR 5/4	212.7	1.0	35.0	52.8	9.8	1.3	0.0	1.525 (MWS)	-0.039 (S)	0.959 (M)	0.78	1.38
Thar 16/9/1	10 YR 7/4	269.8	5.6	52.0	39.6	1.8	0.9	0.0	1.491 (MWS)	-0.021 (S)	0.951 (M)	0.99	1.33
Thar 16/9/2	10 YR 7/4	197.3	0.1	26.0	63.4	10.5	0.0	0.0	1.430 (MWS)	-0.003 (S)	0.957 (M)	0.68	1.40
Thar 16/9/4	10 YR 7/4	192.0	0.0	23.6	64.3	12.0	0.0	0.0	1.431 (MWS)	-0.002 (S)	0.951 (M)	0.76	1.45
Thar 16/9/5	10 YR 7/4	187.1	0.7	26.2	53.7	15.4	3.9	0.1	1.606 (MWS)	-0.065 (S)	1.045 (M)	0.71	1.44
Thar 16/9/8	10 YR 6/4	168.7	0.2	22.1	52.1	14.1	10.4	1.1	2.194 (PS)	-0.369 (VFS)	2.140 (VL)	1.53	1.48
Thar 16/10/1	10 YR 5/4	200.3	0.0	24.8	68.3	6.9	0.0	0.0	1.374 (WS)	0.001 (S)	0.956 (M)	0.69	1.05
Thar 16/10/4	10 YR 5/4	196.2	0.0	23.1	68.7	8.2	0.0	0.0	1.383 (WS)	0.002 (S)	0.963 (M)	0.71	1.09
Thar 16/10/8	10 YR 5/4	219.2	0.5	35.4	58.6	5.5	0.0	0.0	1.423 (MWS)	0.002 (S)	0.958 (M)	0.61	0.79
Thar 16/10/9	10 YR 5/4	189.0	0.6	27.7	52.1	12.3	6.5	0.2	1.904 (MS)	-0.277 (FS)	1.759 (VL)	0.76	1.00
Thar 16/10/10	10 YR 5/4	183.9	0.1	24.6	56.2	13.0	6.1	0.0	1.806 (MS)	-0.271 (FS)	1.691 (VL)	1.64	1.53
Thar 18/1/2	10 YR 5/4	178.6	0.0	15.0	71.3	13.7	0.0	0.0	0.462 (WS)	0.001 (S)	0.957 (M)	0.46	0.77
Thar 18/1/4	10 YR 5/4	166.5	0.0	8.2	74.9	16.9	0.0	0.0	0.424 (WS)	-0.001 (S)	0.973 (M)	0.54	0.81

*MWS= moderately well sorted, WS= well sorted, MS= moderately sorted, PS= poorly sorted.
**FS= finely skewed, VFS= very finely skewed, S= symmetrical.
***L= leptokurtic, VL= very leptokurtic, M= mesokurtic.

© 2019 John Wiley & Sons, Ltd.

had a 5 mm diameter (~425 grains) and large aliquots an 8 mm (~1100 grains) (e.g. Heer *et al.*, 2012). Single grain analyses were done on four samples, Thar 16/1/9, 16/4/2, 16/4/10 and 16/10/10, to establish the number of luminescence grains giving light in response to a laboratory beta dose. 500 grains of each of these samples were given a 50 Gy dose and the number of grains giving a luminescence signal discernible above machine background were counted.

Luminescence signals were screened using a standard set of rejection criteria (e.g. Jacobs *et al.*, 2006). Signals were included in D_e calculation when 1) recuperation was either less than 5% (where sample D_e was greater than 1.5 Gy) or 0.25 Gy (for D_es less than 1.5 Gy); 2) the recycling ratio was within 10% of unity including uncertainties (Murray and Wintle, 2003); and 3) test dose signal were at least 3σ greater than the background. Final D_e determinations were calculated using the central age model (CAM) of Galbraith *et al.* (1999), using the R Luminescence package (Kreutzer *et al.*, 2017). In addition, dose recovery tests were carried out on samples Thar 16/1/2, Thar 16/1/7, Thar 16/3/2, Thar 16/4/4, Thar 16/6/1, Thar 16/9/4 and Thar 16/10/10, which provided dose recovery ratios of 0.95 ± 0.05, 0.93 ± 0.06, 0.94 ± 0.07, 0.99 ± 0.06, 1.0 ± 0.10, 0.97 ± 0.07, 0.98 ± 0.10 respectively, indicating that the post-IR blue SAR protocol, analyses and methods used for D_e determination can successfully recover an applied laboratory dose.

Environmental dose rates were calculated from radionuclide concentrations measured using inductively coupled plasma mass spectrometry at the Scottish University Environmental Research Centre. Infinite-matrix dose rates were calculated using the conversion factors of Guérin *et al.* (2011) and were adjusted for attenuation by grain size (Guérin *et al.*, 2012), chemical etching (Bell, 1979) and a moisture content of 5 ± 2 %. The cosmic dose rate was calculated according to Prescott and Hutton (1994), and all dose rates calculations were made using DRAC (v1.2) software of Durcan *et al.* (2015).

Results

Sedimentology

All sampled dune sections have a unimodal, dominantly medium to fine sand distribution with mean size varying between ~150 and ~270 µm (Table I; Figure 3A). Silt component ranges between 0 and 15%, and there is less than 1.1% clay for all samples (Figure 3B). At each site, the upper part of the sampled parabolic crests consists exclusively of unimodal fine sand (for example, samples Thar 16/1/1, 16/1/2, 16/4/1, 16/4/2, 16/9/1, 16/9/2, 16/10/1) with an absence of finer silt and clay (Figure 3B), reflecting proximity to an active dune surface. Samples are negatively skewed, mostly very leptokurtic or mesokurtic, and sorting of the younger sediments varies between moderately well to well sorted (Table I). The dune sediments are homogenous in colour within each dune, with yellowish brown as the predominant colour (Table I). Generally, the samples contained 0.5 % to 2.0 % carbonates (by weight), except for some basal units at Tinwari and Shergarh, which had slightly higher contents (~3 %) and are adjacent to underlying pedogenic calcretes. The organic content in the samples is less than 2.0 % by weight (Table I).

Luminescence Dating

OSL age data are presented in Table II and in Figure 2D. OSL signals from the sample were sufficiently bright to differentiate from machine background levels (Figure 4). Use of the fast ratio (Durcan and Duller, 2011) suggests the dominance of the fast component in the initial part of the OSL signal. Single grain analyses of samples showed that between 2.4 and 4.0 % of measured grains gave a discernible luminescence signal after a 50 Gy dose, suggesting that on average, small aliquots in this study should have 2-3 luminescing grains per disc, medium 10-17 grains, and large 26-45 grains. Therefore, in the presence of very few luminescing grains per multi-grain aliquot, any heterogeneity in dose distributions will be identifiable.

Over-dispersion (σ_d) or heterogeneity in D_e distributions beyond that expected from intrinsic variability, for this suite of ages is relatively low, and ranges between 20 % and 35 % (including uncertainties) for samples with D_es greater than 1 Gray (Table II). Variability in D_e distributions can originate from a multitude of factors including partial bleaching of sediments prior to deposition (e.g. Olley *et al.*, 2004), environmental dose rate heterogeneity (e.g. Nathan *et al.*, 2003), and post-depositional mixing like bioturbation (e.g. Bateman *et al.*, 2007). Given the depositional environmental in this study, partial bleaching of sediments prior to deposition is

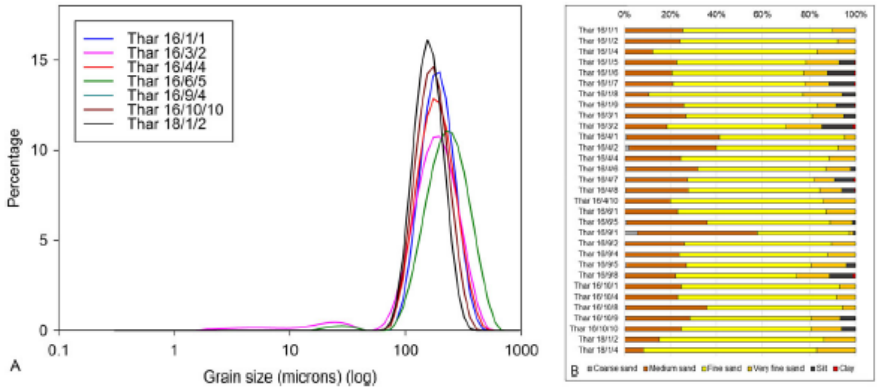


Figure 3. (A) Grain size distribution data for selected samples, and (B) The percentage distribution of different grain sizes for all the samples. [Colour figure can be viewed at wileyonlinelibrary.com]

© 2019 John Wiley & Sons, Ltd.

Table II. Summary OSL data. Equivalent doses (D_e), dose rates ($\dot{D}$), and ages are shown to two decimal places, with all calculations made prior to rounding. All dates are relative to the year 2018. D_es were measured from small aliquots of sample with the exception of Thar 16/4/1 and 16/4/2 (medium aliquots) and Thar 16/4/10 (large aliquots)

Sample	Depth (m)	Discs accepted (measured)	Over-dispersion (%)	CAM D_e (Gy)	Beta $\dot{D}$ (Gy.ka^{-1})	Gamma $\dot{D}$ (Gy.ka^{-1})	Cosmic $\dot{D}$ (Gy.ka^{-1})	Envir $\dot{D}$ (Gy.ka^{-1})	Age (ka)
Thar 16/1/1	0.5	20 (28)	47.2 ± 8.1	0.90 ± 0.10	1.17 ± 0.11	0.62 ± 0.04	0.21 ± 0.02	2.00 ± 0.12	0.45 ± 0.06
Thar 16/1/2	0.7	25 (32)	19.2 ± 3.7	0.88 ± 0.06	1.28 ± 0.11	0.81 ± 0.05	0.19 ± 0.01	2.28 ± 0.12	0.39 ± 0.03
Thar 16/1/4	6.0	28 (46)	28.7 ± 4.3	1.18 ± 0.07	1.25 ± 0.11	0.78 ± 0.05	0.10 ± 0.01	2.14 ± 0.12	0.55 ± 0.05
Thar 16/1/5	14.0	22 (48)	28.9 ± 4.5	2.38 ± 0.15	1.34 ± 0.12	0.83 ± 0.06	0.05 ± 0.01	2.22 ± 0.13	1.07 ± 0.09
Thar 16/1/6	20.0	37 (48)	24.1 ± 2.9	14.31 ± 0.58	1.27 ± 0.11	0.78 ± 0.05	0.03 ± 0.00	2.09 ± 0.12	6.86 ± 0.49
Thar 16/1/7	21.0	27 (38)	30.0 ± 4.1	17.21 ± 1.01	1.27 ± 0.11	0.78 ± 0.05	0.03 ± 0.00	2.07 ± 0.12	8.30 ± 0.69
Thar 16/1/8	22.0	22 (38)	25.1 ± 3.9	20.71 ± 1.13	1.27 ± 0.10	0.86 ± 0.06	0.03 ± 0.00	2.16 ± 0.12	9.60 ± 0.74
Thar 16/1/9	23.0	30 (42)	28.6 ± 3.8	22.70 ± 1.26	1.01 ± 0.09	0.61 ± 0.04	0.03 ± 0.00	1.64 ± 0.10	13.85 ± 1.11
Thar 16/3/1	11.0	20 (44)	39.7 ± 8.4	1.60 ± 0.17	1.39 ± 0.12	0.88 ± 0.06	0.07 ± 0.01	2.34 ± 0.13	0.68 ± 0.08
Thar 16/3/2	19.0	20 (29)	29.3 ± 4.8	12.07 ± 0.82	1.27 ± 0.11	0.82 ± 0.06	0.03 ± 0.00	2.12 ± 0.12	5.69 ± 0.50
Thar 16/4/1	0.3	20 (42)	63.4 ± 16.0	0.44 ± 0.09	1.17 ± 0.10	0.77 ± 0.05	0.22 ± 0.02	2.16 ± 0.11	0.20 ± 0.03
Thar16/4/2	1.0	20 (45)	22.7 ± 13.7	0.36 ± 0.08	1.33 ± 0.12	0.75 ± 0.05	0.18 ± 0.02	2.26 ± 0.13	0.16 ± 0.03
Thar 16/4/4	2.0	25 (32)	31.9 ± 4.9	1.89 ± 0.13	1.31 ± 0.11	0.78 ± 0.05	0.16 ± 0.02	2.24 ± 0.13	0.84 ± 0.08
Thar 16/4/6	5.0	21 (30)	30.2 ± 4.7	4.67 ± 0.31	1.32 ± 0.11	0.80 ± 0.05	0.11 ± 0.01	2.23 ± 0.13	2.09 ± 0.18
Thar 16/4/7	6.0	24 (45)	26.5 ± 4.3	4.47 ± 0.26	1.37 ± 0.12	0.85 ± 0.06	0.10 ± 0.01	2.33 ± 0.13	1.92 ± 0.16
Thar 16/4/8	7.0	27 (38)	20.2 ± 2.9	22.84 ± 0.91	1.31 ± 0.11	0.85 ± 0.06	0.09 ± 0.01	2.25 ± 0.13	10.14 ± 0.69
Thar 16/4/10	9.0	31 (52)	19.1 ± 2.7	23.03 ± 0.84	1.12 ± 0.10	0.69 ± 0.05	0.08 ± 0.01	1.88 ± 0.11	12.25 ± 0.82
Thar 16/6/1	0.5	21 (68)	62.5 ± 16.0	0.16 ± 0.03	1.18 ± 0.10	0.82 ± 0.06	0.21 ± 0.02	2.20 ± 0.11	0.07 ± 0.01
Thar 16/6/5	5.0	22 (52)	72.0 ± 14.5	0.15 ± 0.03	1.30 ± 0.11	0.77 ± 0.05	0.11 ± 0.01	2.18 ± 0.13	0.07 ± 0.01
Thar 16/9/1	1.5	20 (32)	39.3 ± 10.3	0.16 ± 0.02	1.25 ± 0.10	0.91 ± 0.06	0.17 ± 0.02	2.33 ± 0.12	0.07 ± 0.01
Thar 16/9/2	2.5	26 (35)	64.1 ± 12.1	0.18 ± 0.03	1.90 ± 0.16	1.19 ± 0.08	0.15 ± 0.02	3.24 ± 0.18	0.06 ± 0.01
Thar 16/9/4	4.5	21 (37)	55.1 ± 9.3	0.24 ± 0.03	0.97 ± 0.08	0.67 ± 0.05	0.12 ± 0.01	1.76 ± 0.09	0.14 ± 0.02
Thar 16/9/5	5.5	21 (29)	31.8 ± 6.1	0.31 ± 0.02	1.36 ± 0.12	0.84 ± 0.06	0.11 ± 0.01	2.31 ± 0.13	0.13 ± 0.01
Thar 16/9/8	8.5	25 (52)	37.6 ± 5.6	7.65 ± 0.61	1.24 ± 0.10	0.85 ± 0.06	0.08 ± 0.01	2.18 ± 0.12	3.52 ± 0.34
Thar 16/10/1	1.0	22 (50)	25.8 ± 9.6	0.15 ± 0.01	1.13 ± 0.09	0.75 ± 0.05	0.18 ± 0.02	2.06 ± 0.11	0.07 ± 0.01
Thar 16/10/4	3.7	26 (50)	61.0 ± 12.3	0.15 ± 0.02	1.27 ± 0.11	0.74 ± 0.05	0.13 ± 0.01	2.14 ± 0.12	0.07 ± 0.01
Thar 16/10/8	8.2	21 (50)	35.5 ± 6.7	1.58 ± 0.14	1.36 ± 0.11	0.92 ± 0.06	0.08 ± 0.01	2.36 ± 0.13	0.67 ± 0.07
Thar 16/10/9	9.2	20 (26)	28.8 ± 4.8	12.80 ± 1.04	1.42 ± 0.12	0.97 ± 0.07	0.07 ± 0.01	2.47 ± 0.13	5.19 ± 0.51
Thar 16/10/10	10.2	30 (64)	26.2 ± 3.7	11.45 ± 0.56	1.23 ± 0.10	0.81 ± 0.05	0.07 ± 0.01	2.11 ± 0.12	5.43 ± 0.40
Thar 18/1/2	1.0	23 (30)	73.6 ± 13.5	0.11 ± 0.02	1.33 ± 0.12	0.79 ± 0.05	0.18 ± 0.02	2.30 ± 0.13	0.05 ± 0.01
Thar18/1/4	2.0	22 (26)	76.2 ± 12.1	0.35 ± 0.06	1.31 ± 0.11	0.89 ± 0.06	0.16 ± 0.02	2.36 ± 0.13	0.15 ± 0.03

© 2019 John Wiley & Sons, Ltd.

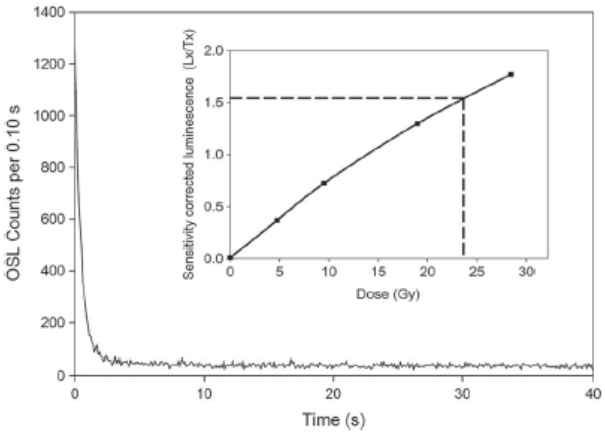


Figure 4. An example of OSL signal from a small aliquot of sample Thar 16/1/8. Inset, corresponding dose response curve fitted using an exponential function.

unlikely, given the efficiency of bleaching during aeolian transport, and asymmetry in D_e distributions is not observed. Visual evidence for post depositional mixing was not observed during sampling, and undisturbed sediments were targeted for dating (e.g. Figure 2C, inset). Therefore, mild microdosimetric variability is hypothesised (but not confirmed) to explain variability in D_es. σ_d for young samples (where $D_e < 1$ Gy) is slightly higher (35 – 75 %; Table II), although this should be expected in the mathematic context of low D_es providing small denominators, which amplifies σ_d values. Large σ_d values are commonly seen in young samples, and for example, Arnold and Roberts (2009) report σ_d values up to 208 % for samples less than 350 years of age. For the majority of samples measured in this study, dose distributions vary symmetrically around a central value (e.g. Figure 5), and therefore the central age model of Galbraith *et al.* (1999), has been selected for use, following the approach of Durcan *et al.* (in press) and references therein.

The suite of OSL ages in this study presents evidence of a dynamic aeolian environment throughout the Holocene in the east-central part of the Thar Desert. The oldest sample is Thar 16/1/9 at Tinwari, which is the easternmost sample site (Figure 2A), dating to 13.85 ± 1.11 ka at a 23 m depth. For the most part, ages are consistent with depth (within uncertainties), and there is a general trend for phases of large units of up to ~6 m of sediment to accumulate within relatively short periods of time, with more distinctive, older phases recorded at greater depth; for example, at Chamu the upper 5.5 m section accumulated in last 150 years and is underlain by 3.52 ± 0.34 ka old unit (Thar 16/9/8). Likewise, at Tinwari, the upper 6 m dune section accumulated at the rate of ~1 m/century whilst the lower 3 m dune section accumulated at ~0.4 m/ka (Table II; Figure 6). Several periods of dune accumulation have been identified including at least one site in each dune recording dune activity and accumulation in the last 500 years (Figure 6). The sampled sand dunes at Tinwari (Thar 16/1/1, Thar 16/1/2

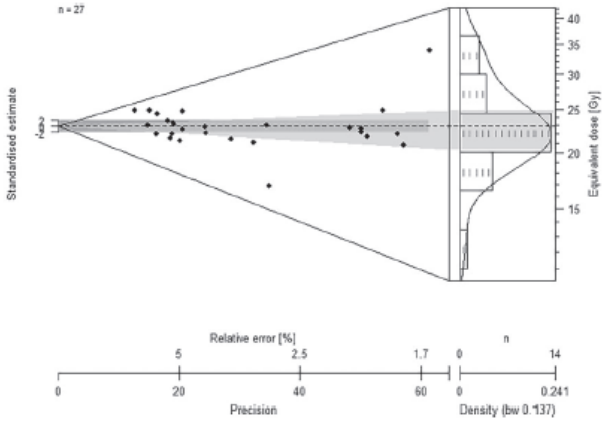


Figure 5. Abanico Plot (plotted using ShinyPlot; Dietze *et al.*, 2016) of individual D_es of sample Thar 16/4/8. The sample D_e of 22.84 ± 0.91 Gy is shown by the dashed line and ±2σ by the grey shaded area.

© 2019 John Wiley & Sons, Ltd.

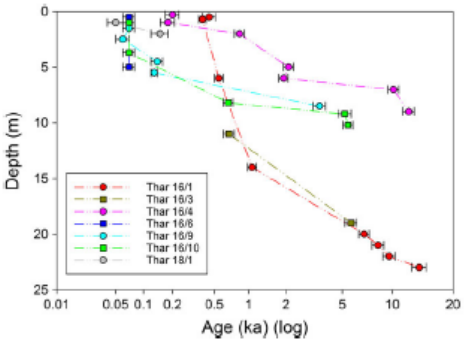


Figure 6. Age-depth plot for the OSL ages presented in Table II. The steep lines denote the timing of periods of high dune accumulation, for example, Thar 16/1 shows a high accumulation between 500 and 1000 years ago at the rate of ~1.6 m/century. Likewise, the vertical line of Thar 16/6 shows the rapid accumulation of 5 m of dune 70 years ago. [Colour figure can be viewed at wileyonlinelibrary.com]

and Thar 16/1/4), Shergarh (Thar 16/4/1 and Thar 16/4/2) and Dechu (Thar 16/10/8) all record accumulation between 200 and 600 years, while samples from Setrawa (Thar 16/6/1 and Thar 16/6/5), Chamu (Thar 16/9/1, Thar 16/9/2) and Dechu (Thar 16/10/1 and, Thar 16/10/4) and Tinwari (18/1/2) all provide ages that show the accumulation of 3-4 m of dune sand in second half of twentieth century (0.07 ± 01 ka, 0.06 ± 01 ka and 0.05 ± 0.01 ka; Figure 6).

Discussion

Holocene dune activity in the region

The oldest OSL ages of 13.85 ± 1.11 ka and 12.25 ± 0.82 ka, observed at Tinwari and Shergarh demonstrate the relative youth of dune bodies in the region. The presence of sparse calcified nodules and plant roots also attest to the greater stability of these dunes (Wasson *et al.*, 1983). Previously published luminescence ages from the Thar, even though with large errors, do not include evidence of dune building during the early Holocene (Singhvi and Kar, 2004; Prasad and Enzel, 2006; Figure 7), yet this had been identified as a period marked by strong south-west monsoon winds based on the enhanced upwelling off the coast of Oman (Gupta *et al.*, 2003; Figure 8). The sites investigated in this study provide evidence of early Holocene aeolian activity and dune building, with sand accumulation ages between 10.14 ± 0.69 ka (Thar 16/4/8) and 9.60 ± 0.74 ka (Thar 16/1/8), and accumulation continuing 6.86 ± 0.49 ka (Thar 16/1/6). The dunes experienced accumulation in the mid-Holocene at ~5 ka (Thar 16/3/2, Thar 16/10/9 and Thar 16/101/10) and then at ~3.5 ka (Thar 16/9/8). These ages coincide with a period of lower precipitation between 5.0-3.5 ka, as recorded in the annually laminated (varved) marine records of north-eastern Arabian Sea (von Rad *et al.*, 1999; Figure 8).

The east-central part of the Thar Desert was previously thought to have stabilised after ~3.5 ka, with more recent dune accumulation confined to the presently arid western Thar (Kar *et al.*, 1998; Thomas *et al.*, 1999). Kar *et al.* (2004) noted very little trace of dune accumulation from ~5 ka onward in the eastern and southern part of the desert. Our data identify widespread late Holocene dune accumulation in the eastern Thar as well (1.92 ± 0.16 ka at Thar 16/4/7 and 1.07 ± 0.09 ka at Thar 16/1/5). Recent studies by Durcan *et al.* (in press) have also identified dune accumulation in the northern margin of the desert, along the Ghaggar-Hakra palaeochannel, at ~1.9 ka and ~2.2 ka, linking dune activity with the gradual drying of the fluvial channel. Together, the suite of ages from different regions provides an emerging picture of widespread aeolian accumulation in the late Holocene. Establishing the precise spatial extent of Thar Desert dune activity at this time will require additional new records of dune accumulation timing form further regions in the system.

Thomas *et al.* (1999) and Singhvi and Kar (2004) noted that existing data sets provide little opportunity to establish whether dune activity had been a feature of recent centuries. Of the previously published luminescence ages from dunes in the region, only one age, from Chamu (Thomas *et al.*, 1999) is from the last one thousand years, and this is a modern age of 0.06 ± 0.01 ka, with others falling predominantly in the 10-100 ka period (Figure 7). By intensively sampling dune profiles, our study has identified at least two recent phases of dune accumulation, between 600 and 200 years ago and very recently, in the last 70 years (Figure 6). It is notable that other precipitation proxy records available for this part of Asia, like the marine core proxy rainfall record of Von Rad *et al.* (1999) from the Arabian Sea or the oxygen-isotope record from a stalagmite from southern Oman (Fleitmann *et al.*, 2003) identify reduced rainfall 600-200 years ago (Figure 8). Closer to the study area, Singhvi and Kar (2004) noted that the Luni River, ~100 km distant, did not record any flooding during this period.

The twentieth century ages, recorded in the dunes as a result of preservation bias towards younger sediments (Bailey and Thomas, 2014), indicate the sensitivity of parabolic dunes to environmental disturbances. These ages coincide with India's independence, expansion of irrigational network and mechanised farming in the most arid districts, and the subsequent rise in human population in the desert region, which together have increased the potential for activation of dune sands. Degradation of natural vegetation has been widespread since then, as most of the permanent pasture lands in dunefield areas were very severely exploited for fuelwood and fodder. Uprooting of sand binder shrubs species, like *Calligonum*

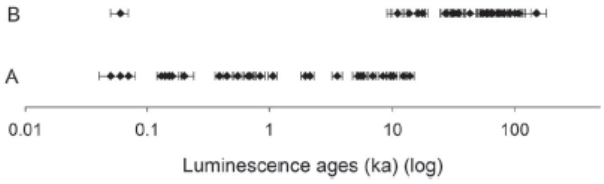


Figure 7. Comparison of the OSL dune age data from this study (A) with the previously published TL and OSL ages (B) from the Shergarh-Dechu basin in the Thar Desert (Thomas *et al.*, 1999 (*n*=2); Singhvi and Kar, 2004 (*n*=16); Dhir *et al.*, 2010 (*n*=13)).

© 2019 John Wiley & Sons, Ltd.

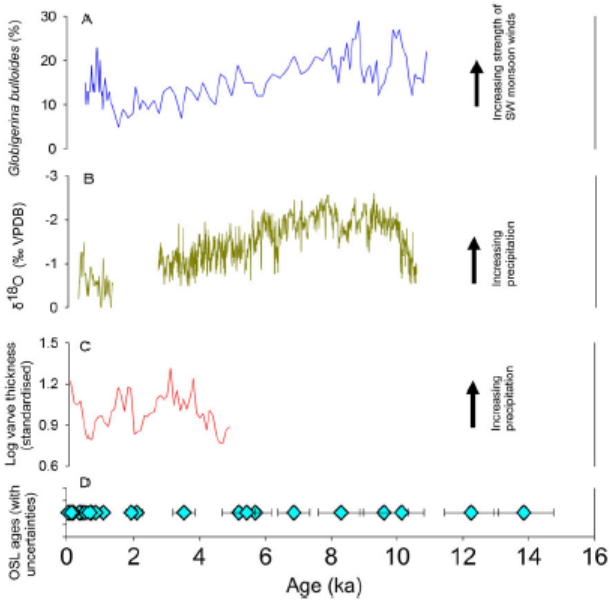


Figure 8. (A) *G. bulloides* percentage from core ODP 723 A core off Oman coast in the Arabian Sea, as a proxy for SW Monsoon wind strength (Gupta *et al.*, 2003). (B) Oxygen-isotope record from a stalagmite in Qunf, southern Oman reflecting as a proxy of monsoon precipitation for the periods 10.3-2.7 ka and 1.4-0.4 ka (Fleitmann *et al.*, 2003). (C) A reconstruction of annually laminated (varved) marine sediment thickness record from cores SO 90 39KG/56KA, NE Arabian Sea, as a proxy for monsoon precipitation (von Rad *et al.*, 1999). (D) The OSL ages and uncertainties calculated in this study. [Colour figure can be viewed at wileyonlinelibrary.com]

polygonoides and *Leptadenia pyrotechnica*, to make way for crops, has also aided sand transport (Kar *et al.*, 2009). Unrestricted over-pumping of groundwater to support both livestock and arable agriculture is resulting in the gradual emptying of aquifers, and increasing salinity in the region (Rodell *et al.*, 2009), which bears a direct implication for the stability of parabolic dunes in the region. The expansion of agriculture including an increase in intensification has been known to reactivate parabolic dunes in Nyírség in Hungary (Kiss *et al.*, 2009) and Horqin sandfields in Inner Mongolia, China (Zhao *et al.*, 2007), and the acceleration of dune accumulation in the last 70 years (Figure 6) suggests that the same has occurred in this part of the Thar Desert.

Implications for the timing and evolution of parabolic dunes

Parabolic dunes tend to form in partially vegetated aeolian landscapes and are sensitive to both environmental and human controls. The formation, development and morphology of parabolic dunes involve complex interactions between an initial surface blowout, the strength and directional variability of the wind, the source and amount of sand involved, the density and type of vegetation, and salinity and levels of groundwater (Pye and Tsoar, 1990; Hugenholtz and Wolfe, 2006; Nield and Baas, 2008; Langford *et al.*, 2009). Under deteriorating vegetation cover conditions and anthropogenic disturbances, parabolic dunes can transform to more mobile, non-parabolic dunes (e.g. Hack, 1941; Anton and Vincent, 1986). Once reactivated, the mobility of these dunes may last for decades or centuries depending upon the wind energy in the arid environments (Bullard *et al.*, 1997; Hugenholtz and Wolfe, 2005).

In the study region, dune reactivation in recent times and subsequent aeolian accumulation has led to the multi-generational development of parabolic dunes. The luminescence chronology presented shows that the parabolic dunes in the region accumulated during late Pleistocene-Early Holocene. The parallelism of dune arms implies prevailing winds have been unidirectional since their accumulation (e.g. Wasson *et al.*, 1983). Modern disturbances linked to land use pressures have resulted in the reactivation of sand dunes and this has resulted in formations of new crescentic features atop parabolic dunes (Figure 9),which Wadhawan (1998) described as products of low energy flows. These superimposed features show migratory characteristics (Figure 9) in the way that they propagate further downwind, presenting an advancement of the bedform, and producing sets of weak laminations, which are observed on the top of all the sampled dune sites (Figure 2C, inset). The quantification of the migratory trait is hampered by a Government restriction on access to aerial photography however, the luminescence chronology confirms that these superimposed features are episodic and young in nature. At Setrawa dune site, large aliquots from two samples collected from a dune arm (at 2.5 m and 7.5 m respectively) 650 m away from the nose, generated very low, indiscernible OSL signals and therefore demonstrate that these superimposed features have been deposited very recently. This was also the case at Tinwari, where two samples collected from a dune arm (at 1 m and 2 m depth) 500 m from the dune nose were accumulated less than 150 years ago (Thar 18/1/2 and Thar 18/1/4). The absence of older ages at such depths from these arms not only shows evidence of a large scale recent reactivation, but

© 2019 John Wiley & Sons, Ltd.

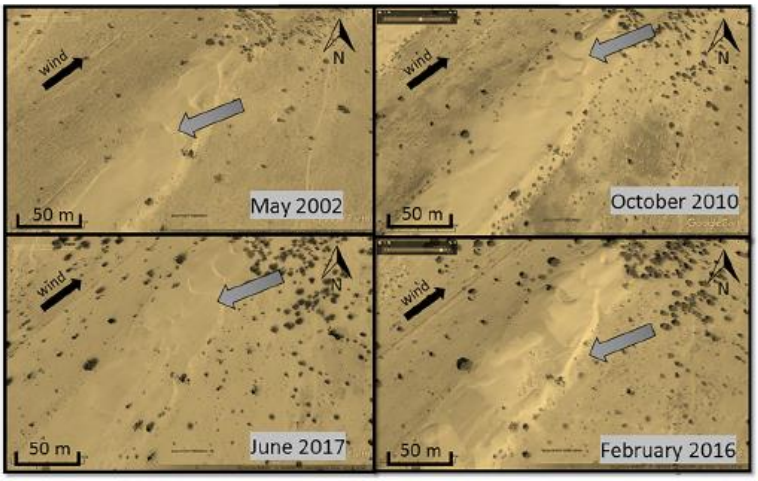


Figure 9. Meso-scale ephemeral transverse accretionary dune forms forming on the top of a parabolic dune arm in Dechu. The grey arrows point at their forward propagation over the past 15 years (clockwise). Satellite imagery courtesy of 2018 Google Earth Pro© 2018. [Colour figure can be viewed at wileyonlinelibrary.com]

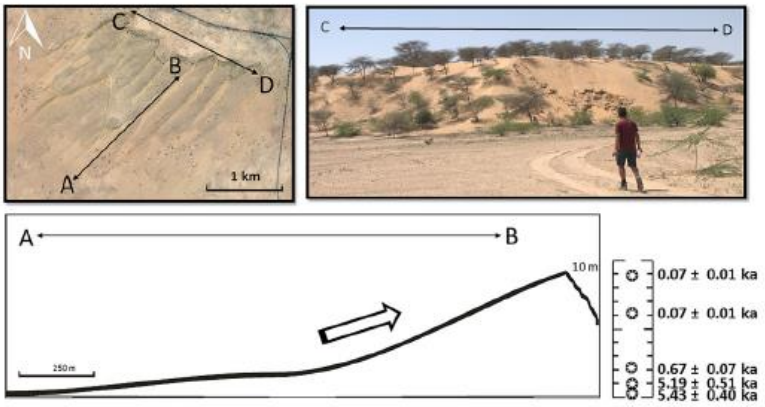


Figure 10. The NW-SE alignment of the transverse wall-like feature (C↔D) and their forepart appearance at Dechu (Thar 16/10). Note, the rapid ~4 m dune accumulation in last 70 years in the downwind direction. [Colour figure can be viewed at wileyonlinelibrary.com]

also suggests that these migratory superimposed features are depositing sand near the nose of the dunes. As a result, the sets of parabolic dunes are developing high transverse wall-like features (C↔D, Figure 10), which act as major zone of accumulation. The OSL ages show rapid net accumulation in recent times on the top half of these wall-like features, resting unconformably on the top of older, stabilised aeolian deposits. Such features are similar to the barchanoid-parabolic transitional dunes described recently by Yan and Baas (2017) using simulation results from the Extended-DECAL (Discrete Eco-geomorphic Aeolian Landscapes model of Nield and Baas (2008) and Baas and Nield (2010) and empirical data from fieldwork in Inner Mongolia, China. Although the transition of parabolic dunes to other dune types has been observed in various dune systems around the world (Pye and Tsoar, 1990), there have been very little investigation of them; the majority of which are based on aerial photographs (Yan and Baas, 2015). This study from a parabolic dunefield in the Thar presents OSL dating as a powerful chronometric tool to understand geomorphic transformations of dunes over longer time scales.

Conclusions

This study has presented a new history of desert dune accumulation in the eastern-central Thar Desert by applying OSL dating to a series of intensively sampled sections through dune sedimentary bodies. We demonstrate that the development of dunes in this region has been both more complex and more recent than previous investigations have suggested. The main

© 2019 John Wiley & Sons, Ltd.

parabolic dunefield present today is largely a function of late Pleistocene-early Holocene dune accumulation, which is significantly more recent than the previous chronologies presented by Singhvi and Kar (2004) and Dhir *et al.* (2010). Furthermore, there is a strong record of dune activity and disturbance in recent millennia and centuries, particularly during the last 70 years when a significantly expanded human presence in the landscape coincides with the widespread disturbance of dune surfaces and the development of superimposed transverse bedforms. These new bedforms seem to favour the formation of wall-like transverse features downwind.

The history of the Thar Desert dune landscape demonstrates the interplay of natural and anthropogenic processes in landscape development, and the susceptibility of this marginally arid region to land use pressures today. Other dune systems within this extensive desert region may reveal differing aeolian histories, but this study has shown that a strategic approach to sampling allows the scope for a more complex chronology to be identified and subsequently enhance our understanding of dune development.

Acknowledgements—The doctoral studies of the first author are funded by Clarendon Scholarship, University of Oxford. The authors thank the John Fell Fund, University of Oxford (Grant Number 132/062) for providing funding for fieldwork and laboratory analyses. The first author thanks Dr. Szilvia Bajkan for her assistance in the laboratory. He also thanks the Quaternary Research Association for supporting attendance at the 9th International Conference on Geomorphology in New Delhi (2017), where this work was initially presented. We thank the anonymous reviewers for their comments and suggestions.

References

Anton DJ, Vincent P. 1986. Parabolic dunes of the Jafurah desert, eastern province, Saudi Arabia. *Journal of Arid Environments* **11**.

Arnold LJ, Roberts RG. 2009. Stochastic modelling of multi-grain equivalent dose (De) distributions: implications for OSL dating of sediment mixtures. *Quaternary Geochronology* **4**(3): 204–230.

Atkinson OA, Thomas DS, Goudie AS, Bailey RM. 2011. Late Quaternary chronology of major dune ridge development in the northeast Rub'al-Khali, United Arab Emirates. *Quaternary Research* **76**(1): 93–105.

Baas AC, Nield JM. 2010. Ecogeomorphic state variables and phase-space construction for quantifying the evolution of vegetated aeolian landscapes. *Earth Surface Processes and Landforms: The Journal of the British Geomorphological Research Group* **35**(6): 717–731.

Bailey RM, Thomas DSG. 2014. A quantitative approach to understanding dated dune stratigraphies. *Earth Surface Processes and Landforms* **39**(5): 614–631.

Banerjee D, Murray AS, Bøtter-Jensen L, Lang A. 2001. Equivalent dose estimation using a single aliquot of polymineral fine grains. *Radiation Measurements* **33**(1): 73–94.

Bateman MD, Boulter CH, Carr AS, Frederick CD, Peter D, Wilder M. 2007. Detecting post-depositional sediment disturbance in sandy deposits using optical luminescence. *Quaternary Geochronology* **2**(1-4): 57–64.

Bell W. 1979. Attenuation factors for the absorbed radiation dose in quartz inclusions for thermoluminescence dating. *Ancient TL* **8**(2): 12.

Blott, S., 2000. GRADISTAT Version 4.0: A grain size distribution and statistics package for the analysis of unconsolidated sediments by sieving or laser granulometer. URL: http://www.kpal.co.uk/gradistat_abstract.htm

Bøtter-Jensen L, Andersen C, Duller GA, Murray AS. 2003. Developments in radiation, stimulation and observation facilities in luminescence measurements. *Radiation Measurements* **37**(4-5): 535–541.

Bryson AA, Barreis D. 1967. Possibilities of major climatic modifications and their implications: Northwest India, A case study. *Bulletin of the American Meteorological Society* **48**: 136–142.

Bullard J, Thomas D, Livingstone I, Wiggs G. 1997. Dunefield activity and interactions with climatic variability in the southwest Kalahari Desert. *Earth Surface Processes and Landforms* **22**(2): 165–174.

Chawla S, Dhir R, Singhvi A. 1992. Thermoluminescence chronology of sand profiles in the Thar Desert and their implications. *Quaternary Science Reviews* **11**(1-2): 25–32.

Dhir R, Singhvi A, Andrews J, Kar A, Sareen B, Tandon S, Kailath A, Thomas J. 2010. Multiple episodes of aggradation and calcrete formation in Late Quaternary aeolian sands, Central Thar Desert, Rajasthan, India. *Journal of Asian Earth Sciences* **37**(1): 10–16.

Dietze M, Kreutzer S, Burow C, Fuchs MC, Fischer M, Schmidt C. 2016. The abanico plot: visualising chronometric data with individual standard errors. *Quaternary Geochronology* **31**: 12–18.

Duller GAT. 2003. Distinguishing quartz and feldspar in single grain luminescence measurements. *Radiation Measurements* **37**(2): 161–165.

Duller GAT. 2008. Single-grain optical dating of Quaternary sediments: why aliquot size matters in luminescence dating. *Boreas* **37**(4): 589–612.

Durcan JA, Duller GAT. 2011. The fast ratio: a rapid measure for testing the dominance of the fast component in the initial OSL signal from quartz. *Radiation Measurements* **46**(10): 1065–1072.

Durcan JA, King GE, Duller GAT. 2015. DRAC: Dose Rate and Age Calculator for trapped charge dating. *Quaternary Geochronology* **28**: 54–61.

Durcan JA, Thomas DS, Gupta S, Pawar V, Singh RN, Petrie CA. 2017. Holocene landscape dynamics in the Ghaggar-Hakra palaeochannel region at the northern edge of the Thar Desert, northwest India. *Quaternary International*.

Fitzsimmons KE, Rhodes EJ, Magee JW, Barrows TT. 2007. The timing of linear dune activity in the Strzelecki and Tirari Deserts, Australia. *Quaternary Science Reviews* **26**(19-21): 2598–2616.

Fleitmann D, Burns SJ, Mudelsee M, Neff U, Kramers J, Mangini AAND, Matter A. 2003. Holocene forcing of the Indian monsoon recorded in a stalagmite from southern Oman. *Science* **300**(5626): 1737–1739.

Folk RL, Ward WC. 1957. Brazos River bar: a study in the significance of grain size parameters. *Journal of Sedimentary Research* **27**(1).

Galbraith RF, Roberts RG, Laslett GM, Yoshida H, Olley JM. 1999. Optical dating of single and multiple grains of quartz from Jinmium rock shelter, northern Australia: Part I, experimental design and statistical models. *Archaeometry* **41**(2): 339–364.

Giosan L, Clift PD, Macklin MG, Fuller DQ, Constantinescu S, Durcan JA, Stevens T, Duller GAT, Tabrez AR, Gangal K, Adhikari R, Alizai A, Filip F, Vanlaningham S, Syvitski JP. 2012. Fluvial landscapes of the Harappan civilization. *Proceedings of the National Academy of Sciences of the United States of America* **109**(26): E1688–E1694.

Guérin G, Mercier N, Adamiec G. 2011. Dose-rate conversion factors: update. *Ancient TL* **29**(1): 5–8.

Guérin G, Mercier N, Nathan R, Adamiec G, Lefrais Y. 2012. On the use of the infinite matrix assumption and associated concepts: a critical review. *Radiation Measurements* **47**(9): 778–785.

Gupta AK, Anderson DM, Overpeck JT. 2003. Abrupt changes in the Asian southwest monsoon during the Holocene and their links to the North Atlantic Ocean. *Nature* **421**(6921): 354.

Hack JT. 1941. Dunes of the western Navajo country. *Geographical Review* **31**(2): 240–263.

Heer AJ, Adamiec G, Moska P. 2012. How many grains are there on a single aliquot? *Ancient TL* **30**(1): 9–11.

Heiri O, Lotter AF, Lemcke G. 2001. Loss on ignition as a method for estimating organic and carbonate content in sediments: reproducibility and comparability of results. *Journal of Paleolimnology* **25**(1): 101–110.

Hugenholtz CH, Wolfe SA. 2005. Recent stabilization of active sand dunes on the Canadian prairies and relation to recent climate variations. *Geomorphology* **68**(1-2): 131–147.

HUgenholtz CH, Wolfe SA. 2006. Morphodynamics and climate controls of two aeolian blowouts on the northern Great Plains, Canada. *Earth Surface Processes and Landforms* **31**(12): 1540–1557.

Jacobs Z, Duller GAT, Wintle AG, Henshilwood CS. 2006. Extending the chronology of deposits at Blombos Cave, South Africa, back to 140 ka using optical dating of single and multiple grains of quartz. *Journal of Human Evolution* **51**(3): 255–273.

Juyal N, Chamyal L, Bhandari S, Bhushan R, Singhvi A. 2006. Continental record of the southwest monsoon during the last 130 ka:

© 2019 John Wiley & Sons, Ltd.

evidence from the southern margin of the Thar Desert, India. *Quaternary Science Reviews* **25**(19-20): 2632–2650.
Kar A. 1993. Aeolian processes and bedforms in the Thar Desert. *Journal of Arid Environments* **25**(1): 83–96.
Kar A. 2013. Quaternary geomorphic processes and landform development in the Thar Desert of Rajasthan. *Landforms Processes and Environment Management, pp.*: 225–256.
Kar A, Felix C, Rajaguru S, Singhvi A. 1998. Late Holocene growth and mobility of a transverse dune in the Thar Desert. *Journal of Arid Environments* **38**(2): 175–185.
Kar A, Mohrana P, Raina P, Kumar M, Soni M, Santra P, Arya AA, Dhinwa P. 2009. Desertification and its control measures. *Trends in Arid Zone Research in India*: 1–47.
Kar A, Singhvi A, Juyal N, Rajaguru S. 2004. Late Quaternary aeolian sedimentation history of the Thar Desert. *Geomorphology and Environment, pp.*: 105–122.
Kiss T, Sipos G, Kovács F. 2009. Human impact on fixed sand dunes revealed by morphometric analysis. *Earth Surface Processes and Landforms* **34**(5): 700–711.
Kreutzer, S., Dietze, M., Burow, C., Fuchs, M., Schmidt, C., Fischer, M. and Friedrich, J., 2017. Luminescence: Comprehensive Luminescence Dating Data Analysis. *R package version 0.7.3*,
Lancaster N, Wolfe S, Thomas D, Bristow C, Bubenzer O, Burrough S, Duller GAT, Halfen A, Hesse P, Roskin J. 2016. The INQUA dunes atlas chronologic database. *Quaternary International* **410**: 3–10.
Langford RP, Rose JM, White DE. 2009. Groundwater salinity as a control on development of eolian landscape: An example from the White Sands of New Mexico. *Geomorphology* **105**(1-2): 39–49.
Leighton CL, Bailey RM, Thomas DS. 2013. The utility of desert sand dunes as Quaternary chronostratigraphic archives: evidence from the northeast Rub'al Khali. *Quaternary Science Reviews* **78**: 303–318.
Moharana PC, Gaur MK, Chaudhary C, Chauhan JS, Rajpurohit RS. 2013. A system of geomorphological mapping for western Rajasthan with relevance for agricultural land use. *Annals of Arid Zone* **52**(3&4): 163–180.
Murray AS, Wintle AG. 2000. Luminescence dating of quartz using an improved single-aliquot regenerative-dose protocol. *Radiation Measurements* **32**(1): 57–73.
Murray AS, Wintle AG. 2003. The single aliquot regenerative dose protocol: potential for improvements in reliability. *Radiation Measurements* **37**(4-5): 377–381.
Nathan R, Thomas P, Jain M, Murray A, Rhodes E. 2003. Environmental dose rate heterogeneity of beta radiation and its implications for luminescence dating: Monte Carlo modelling and experimental validation. *Radiation Measurements* **37**(4-5): 305–313.
Nield JM, Baas AC. 2008. The influence of different environmental and climatic conditions on vegetated aeolian dune landscape development and response. *Global and Planetary Change* **64**(1-2): 76–92.
Olley JM, Pietsch T, Roberts RG. 2004. Optical dating of Holocene sediments from a variety of geomorphic settings using single grains of quartz. *Geomorphology* **60**(3-4): 337–358.
Piggott S. 1950. *Prehistoric India to 1000 B.C. (Penguin Books)*: Harmondsworth.
Prasad S, Enzel Y. 2006. Holocene paleoclimates of India. *Quaternary Research* **66**(3): 442–453.
Prescott JR, Hutton JT. 1994. Cosmic ray contributions to dose rates for luminescence and ESR dating: large depths and long-term time variations. *Radiation Measurements* **23**(2-3): 497–500.
Pye K, Tsoar H. 1990. *1990: Aeolian sand and sand dunes*. Unwin Hyman: London.
Rodell M, Velicogna I, Famiglietti JS. 2009. Satellite-based estimates of groundwater depletion in India. *Nature* **460**(7258): 999.
Roy P, Nagar Y, Juyal N, Smykatz-Kloss W, Singhvi A. 2009. Geochemical signatures of Late Holocene paleo-hydrological changes from Phulera and Pokharan saline playas near the eastern and western margins of the Thar Desert, India. *Journal of Asian Earth Sciences* **34**(3): 275–286.
Saini H, Mujtaba S. 2012. Depositional history and palaeoclimatic variations at the northeastern fringe of Thar Desert, Haryana Plains, India. *Quaternary International* **250**: 37–48.
Saini H, Tandon S, Mujtaba S, Pant N, Khorana R. 2009. Reconstruction of buried channel-floodplain systems of the northwestern Haryana Plains. *Current Science* **97**(11).
Shitaoka Y, Maemoku H, Nagatomo T. 2012. Quartz OSL dating of sand dunes in Ghaggar Basin, northwestern India. *Geochronometria* **39**(3): 221–226.
Singhvi A, Banerjee D, Rajaguru S, Kumar VK. 1994. Luminescence chronology of a fossil dune at Budha Pushkar, Thar Desert: Palaeoenvironmental and archaeological implications. *Current Science*: 770–773.
Singhvi A, Sharma Y, Agrawal D. 1982. Thermoluminescence dating of sand dunes in Rajasthan, India. *Nature* **295**(5847): 313.
Singhvi AK, Kar A. 2004. The aeolian sedimentation record of the Thar Desert. *Journal of Earth System Science* **113**(3): 371–401.
Stokes S. 1994. *Optical dating of selected Late Quaternary aeolian sediments from Western United States, D.* Phil Thesis, University of Oxford.
Stone A, Thomas D. 2008. Linear dune accumulation chronologies from the southwest Kalahari, Namibia: challenges of reconstructing late Quaternary palaeoenvironments from aeolian landforms. *Quaternary Science Reviews* **27**(17-18): 1667–1681.
Thomas J, Kar A, Kailath A, Juyal N, Rajaguru S, Singhvi A. 1999. Late Pleistocene-Holocene-history of aeolian accumulation in the Thar Desert, India. *ZEITSCHRIFT FUR GEOMORPHOLOGIE SUPPLEMENTBAND, pp.*: 181–194.
Von Rad U, Schaaf M, Michels KH, Schulz H, Berger WH, Sirocko F. 1999. A 5000-yr record of climate change in varved sediments from the oxygen minimum zone off Pakistan, Northeastern Arabian Sea. *Quaternary Research* **51**(1): 39–53.
Wadhawan S. 1998. Late Quaternary Evolution of Clustered Parabolic Megadunes in Thar Desert, India. *Quaternary Deserts and Climatic Change*: 185–195.
Wasson R, Rajaguru S, Misra V, Agrawal D, Dhir R, Singhvi A, Rao KK. 1983. Geomorphology, late Quaternary stratigraphy and palaeoclimatology of the Thar dunefield. *ZEITSCHRIFT FUR GEOMORPHOLOGIE SUPPLEMENTBAND* **45**: 117–151.
Wintle AG, Murray AS. 2006. A review of quartz optically stimulated luminescence characteristics and their relevance in single-aliquot regeneration dating protocols. *Radiation Measurements* **41**(4): 369–391.
Yan N, Baas AC. 2015. Parabolic dunes and their transformations under environmental and climatic changes: towards a conceptual framework for understanding and prediction. *Global and Planetary Change* **124**: 123–148.
Yan N, Baas AC. 2017. Environmental controls, morphodynamic processes, and ecogeomorphic interactions of barchan to parabolic dune transformations. *Geomorphology* **278**: 209–237.
Zhao H, LU, Y. and YIN, J. 2007. Optical dating of Holocene sand dune activities in the Horqin sand-fields in inner Mongolia, China, using the SAR protocol. *Quaternary Geochronology* **2**(1-4): 29–33.

© 2019 John Wiley & Sons, Ltd.

Appendix F: Paper 2 (Chapter 5) as included in journal *Geomorphology*.

Geomorphology 344 (2019) 90–98

Contents lists available at ScienceDirect

Geomorphology

journal homepage: www.elsevier.com/locate/geomorph

Analysis of late Quaternary linear dune development in the Thar Desert, India

Aayush Srivastava [a,*], Julie A. Durcan [a], David S.G. Thomas [a,b]

[a] School of Geography and the Environment, University of Oxford, Oxford OX1 3QY, United Kingdom
[b] School of Geography, Archaeology and Environmental Studies, University of the Witwatersrand, Johannesburg 2050, South Africa

ARTICLE INFO

Article history:
Received 17 March 2019
Received in revised form 20 July 2019
Accepted 21 July 2019
Available online 23 July 2019

Keywords:
Thar Desert
Optically stimulated luminescence (OSL) dating
Linear dunes
The Holocene
Geomorphological change

ABSTRACT

Linear dunes are the most widespread dune type worldwide and act as important geoproxies of late Quaternary environmental change in deserts. They are less common in the Thar Desert, India than other dune types, especially parabolic forms, and to date their development history is poorly understood. Here we investigate a linear dunefield in the northern Thar through analysis of a series of excavated full dune profile sites and the application of optically stimulated luminescence (OSL) dating to provide chronometric control. Results show that linear dunes have been present since at least ~58 ka and were active throughout much of the Holocene. The early Holocene, a period marked by strong Indian summer monsoon winds (e.g., Gill et al., 2017), has been shown as the last major phase of dune accumulation recorded in all sites, with ages ranging from ~11.6–8.6 ka. Two spatially restricted records of dune accumulation have also been identified during the later part of Holocene: ~4–3 ka and ~2–1 ka, attributed to localised reworking within the dunes. The suite of luminescence ages generated from the study region confirms the principle recognised in other dunefields (e.g., the south-western Kalahari; Stone and Thomas, 2008) and theoretically (Bailey and Thomas, 2014) that age records from individual dunes are unlikely to capture the developmental history of dunefields.

© 2019 Elsevier B.V. All rights reserved.

1. Introduction

A range of dune forms are present in the Thar Desert including parabolic, linear, transverse, star and network (e.g., Wasson et al., 1983; Kar, 1993; Moharana et al., 2013; Fig. 1A). The organisation and orientation of these dunes reflects the role of dominant south-west monsoon winds, which have governed aeolian dynamics regionally during the late Quaternary. The presence of superimposed forms, for example young meso-scale dunes on older, bigger parabolic dunes (Srivastava et al., 2019) attests to a more complex history of dune dynamics in the Thar.

Linear dunes, which are the most common desert dune type worldwide, including palaeo-dunes in semi-arid and arid landscapes (Lancaster, 1982; Tsoar, 1989) are relatively uncommon in the Thar. These dunes cover an area of approximately 11,200 km^2, representing around 7.5% of all aeolian landforms in the Thar, where parabolic dunes are the most commonly observed dune type (Wasson et al., 1983; Kar, 1993; Moharana et al., 2013). Thar linear dunes occur mostly in the border zone between India and Pakistan in Jaisalmer district in the western part of the desert (Kar, 1987). Other studies have mapped smaller areas of linear dunes in the northern Thar near Bikaner (Saxena and Singh, 1976; Kumar et al., 1993) and the central Thar near Jodhpur (Verstappen, 1968; Kar, 1993) (Fig. 1A). Many of these smaller dunefields, however, have since been flattened to make way for the expansion of irrigated agriculture, removing landforms and prohibiting their analysis.

Linear dunes in the Thar have often been considered as an 'old system' (e.g., Pandey et al., 1964; Kar, 1993; Singhvi and Kar, 2004; Kar, 2014) with natural vegetation forming an integral part of the dune bodies. The length of these dunes varies across the Thar from >10 km in Jaisalmer to 1–2 km in Bikaner and includes dunes forms which vary from Y-junctions to clusters of 5–8 linear dunes joining at acute angles which gradually merge with surrounding parabolic or transverse dunefields (Kar, 1987, 1993, 2014). The Y-junction pattern is similar to that of vegetated linear dunes in the north-western Negev (Tsoar and Møller, 1986; Tsoar et al., 2008) and south-western Kalahari (Thomas and Shaw, 1991; Bullard et al., 1995).

Linear dunes have the potential to offer long-term records of past aeolian episodes because of their accumulatory nature (Thomas, 1992; Livingstone and Thomas, 1993; Munyikwa, 2005; Telfer et al., 2010), and thus are considered important geoproxy records (Telfer and Hesse, 2013; Thomas, 2013). The accumulation histories of linear dunes reconstructed using luminescence dating have been frequently and consistently used for palaeoenvironmental reconstructions in dryland environments, notably in southern Africa (e.g., Stokes et al., 1997;

* Corresponding author.
E-mail address: aayush.srivastava@ouce.ox.ac.uk (A. Srivastava).

https://doi.org/10.1016/j.geomorph.2019.07.013
0169-555X/© 2019 Elsevier B.V. All rights reserved.

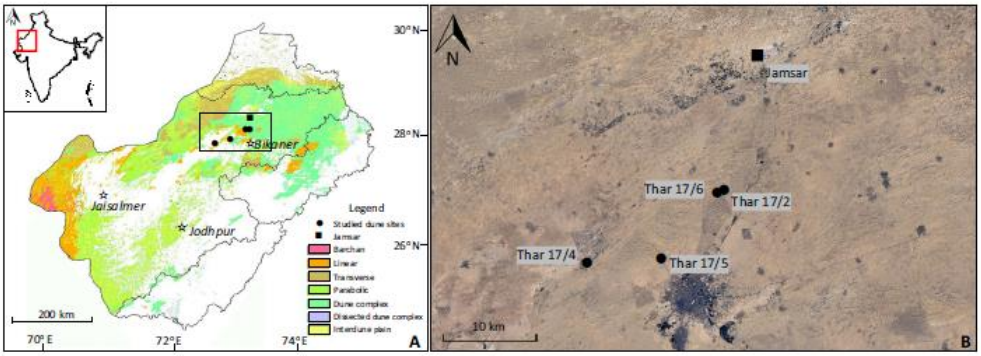


Fig. 1. A. Distribution of different dune types in the Thar Desert, India (after Moharana et al., 2013). B. Sampled linear dune sites (closed circles): Thar 17/2 (28.13728 N, 73.34283 E), Thar 17/4 (28.03315 N, 73.20950 E), Thar 17/5 (28.06017 N, 73.26852 E) and Thar 17/6 (28.13641 N, 73.33286 E).

O'Connor and Thomas, 1999; Telfer and Thomas, 2007; Stone and Thomas, 2008), Australia (e.g., Lomax et al., 2003; Fitzsimmons et al., 2007), Israel (Roskin et al., 2011a, 2011b) and the Arabian Peninsula (e.g., Glennie and Singhvi, 2002; Atkinson et al., 2013; Leighton et al., 2013). As a result, almost a third of the luminescence ages from drylands listed in the INQUA dune database are from linear dunes (Lancaster et al., 2016). In contrast, there are no ages in the database from linear dunes in the Thar Desert because the majority of chronometric studies to date have focussed on parabolic dunes (Thomas et al., 1999; Kar et al., 2001; Singhvi and Kar, 2004; Dhir et al., 2010; Srivastava et al., 2019). The aim of this work, therefore, is to apply a spatially intensive sampling strategy and modern luminescence dating techniques to develop a linear dunefield chronology from the Thar, and integrate it into existing knowledge of the geomorphic evolution of the Thar dunes and regional palaeoenvironmental interpretations arising from such results.

2. Study sites and methods

2.1. Study sites

The focus of this study is a ~500 km^2 area of the linear dunefield in the Bikaner area of the northern Thar (Fig. 1B). This area was selected because of its central location, accessibility, and representativeness, based on Google Earth assessment of the linear dunes in the Thar. The Bikaner dunefield today comprises a semiarid to arid landscape with a mean annual precipitation of 200–300 mm and an interannual rainfall coefficient of variation of 47%. The dunes here are colonised to a varying degree by natural vegetation such as *Lasiurus sindicus, Capparis decidua, Calligonum polygonoides* etc. Dunes range in height from 5 m to 20 m above the interdune areas and are <10 km in crestline length. The orientation of these dunes is in the SW direction controlled by the dominant Indian summer monsoon winds (Fig. 2A).

To identify the timing of periods of linear dune accumulation, field sampling for luminescence dating was conducted at four sites across the dunefield (Fig. 1B): Jaisalmer Bypass (Thar 17/2 and Thar 17/6), Nal (Thar 17/4) and Bajrang Dohra (Thar 17/5) sites. The two Jaisalmer Bypass sites, Thar 17/2 and Thar 17/6, are located <500 m apart near the northern edge of the dunefield. The other two sites, Thar 17/4 and Thar 17/5 fall in the central and south-central part of the dunefield. These were sampled to explore spatial and temporal variability in dune accumulation histories, with the number of sites analysed reflecting accessibility, the logistics of excavating exposures, and the number of samples generated that could effectively be dated while ensuring each sample location was represented by enough samples to capture accumulation histories. The sampled linear dunes are 9–12 m in height relative to the adjacent interdune area and aligned in the dominant direction of monsoon winds. At all four sites, the dune axis was targeted for sampling to obtain dune core sediment presumed to have preserve the maximum thickness of sediments within the dune bodies, and to be least affected by lateral dune movement. Sampled sections were excavated on the crest of these dunes using hydraulic excavators until a hard, calcrete rich layer, suggesting the base of the dune, was reached. The base of the dune was reached at sites Thar 17/2, 17/4 and 17/5, but not at Thar 17/6, where risk of sediment collapse prevented sampling. The dunes were composed of homogeneous, usually structureless sand with some fine laminations preserved in the top part of sampled profiles. Sediment faces in the excavated pits were cleaned prior to

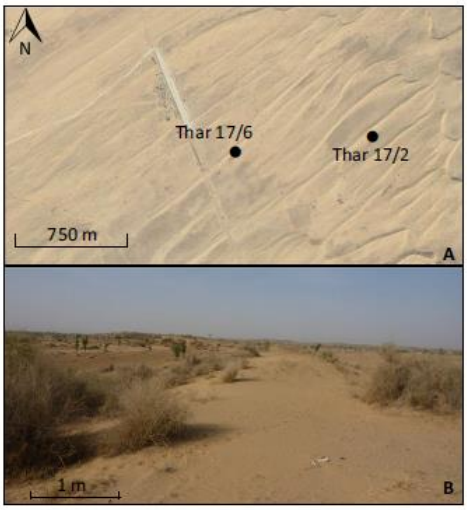


Fig. 2. A. Linear dune pattern in the Bikaner dunefield and location of two studied sites. B. Landscape at site Thar 17/2. The photo is taken from the linear dune crest facing in NE direction.

sampling for optically stimulated luminescence (OSL) dating. All samples were taken at least 0.5 m below the modern dune surfaces and 0.5 m above the hard, calcrete layer, by hammering black light-tight tubes into the cleaned sediment face. Sampling was performed at a 1 m interval unless field examination revealed changes in stratigraphy or sedimentology, in which case additional sampling was carried out to bracket such features.

2.2. Sedimentological analyses

Grain size analyses were conducted using a Malvern Mastersizer Hydro 2000 laser analyser with wet dispersion. Statistics were calculated using Gradistat (Blott and Pye, 2001) following the method of Folk and Ward (1957). Colour analysis was conducted on oven-dried samples using a Munsell colour chart. Organic and carbonate content were determined using sequential loss on ignition at 550 °C and 950 °C (Heiri et al., 2001) and expressed as a percentage of the sample weight.

2.3. Sediment preparation for luminescence dating

Samples were opened and prepared in subdued orange light conditions in the Oxford Luminescence Dating Laboratory. Prior to preparation of sediments for OSL dating, light-exposed sediments from the sample tube ends were removed and reserved for dose rate and sedimentological measurements. Sediments for luminescence dating were treated with hydrochloric acid and hydrogen peroxide to remove carbonate and organic matter, and sieved to isolate the 180–210 μm grain size fraction. Quartz mineral grains were removed from the bulk sample using sodium polytungstate density separation, which was followed by chemical etching using hydrofluoric acid to remove the alpha-irradiated outer surface of the quartz grains and fluorosilicic acid to remove persistent feldspar contamination. After chemical etching, hydrochloric acid was used to remove any fluoride precipitate, prior to re-sieving. Fully prepared dry sediment was mounted onto aluminium discs as a 2 mm (small aliquot) monolayer consisting of ~70 grains (Heer et al., 2012) using Silkospray silicon oil.

2.4. Equivalent dose determination

Equivalent dose (D_e) measurements were made using Risø DA-15 TL/OSL readers (for full reader specification see Srivastava et al., 2019) and a post-infrared blue single aliquot regenerative (SAR) dose protocol (Banerjee et al., 2001). Following pre-heat plateau and dose recovery tests, a pre-heat of 240 °C for 10 s and a cut-heat of 160 °C for 0 s were selected for use. The protocol comprised an infrared light (870 nm) stimulation at 50 °C for 100 s prior to measurement of the blue-light stimulated ultra-violet luminescence signals at 125 °C for 40 s. Dose recovery tests on samples Thar 17/2/4, 17/4/8, 17/5/1, 17/6/2, and 17/6/6, provided ratios of 0.94 ± 0.04, 0.95 ± 0.04, 1.00 ± 0.06, 1.00 ± 0.07, and 0.96 ± 0.05, respectively, indicating the suitability of the applied protocol. To ascertain the average number of luminescing signals, single grain analyses of samples on samples Thar 17/2/4, Thar 17/4/2, Thar 17/4/8, Thar 17/5/6, Thar 17/6/6 and Thar 17/6/9 was undertaken, and showed that between 2.4 and 5.0% of the measured 500 grains gave a discernible luminescence signal after a 50 Gy dose.

Luminescence signals were included in final D_e calculation when the following rejection criteria were satisfied: 1) recuperation less than 5% (where sample D_e was greater than 1.5 Gy) or 0.25 Gy (for D_es less than 1.5 Gy); 2) recycling ratio within 10% of unity, including uncertainties (Murray and Wintle, 2003); and 3) test dose signals 3σ greater than the background. Final D_e determinations for each sample were based upon at least 20 accepted aliquots and were calculated in the R Luminescence package (Kreutzer et al., 2017) using the central age model (CAM) (Galbraith et al., 1999).

2.5. Dose rate determination

Radionuclide concentrations (^{232}Th, ^{238}U and ^{40}K) were measured using inductively coupled plasma mass spectrometry at the Scottish University Environmental Research Centre, East Kilbride. Infinite-matrix dose rates were calculated using the conversion factors of Guérin et al. (2011) and were adjusted for attenuation by grain size and chemical etching using the datasets of Guérin et al. (2012) and Bell (1979) respectively, as well as a moisture content of 5 ± 2%. Following Prescott and Hutton (1994), cosmic dose rates were determined from sample longitude, latitude, altitude, and depth. All dose rate calculations were made using the DRAC (v1.2) software of Durcan et al. (2015).

3. Results

3.1. Sedimentology

Sedimentological data are provided in Table 1. The samples are consistent in colour within each dune. The majority of samples are unimodal (Fig. 3A), predominantly composed of medium to fine sand, with silt and clay components varying between 0 - 23.5% and 0–1.2% respectively (Fig. 3B). Mean grain sizes are within the range of ~105–220 μm, comparable with linear dune sediments, for example in north-eastern Rub' al Khali in Arabia (Leighton et al., 2013) and the north-western Negev (Roskin et al., 2011a). Most samples are well to moderately well sorted with symmetrical and mesokurtic distributions (Table 1). The organic content by weight is less than 2%, while carbonate content by weight increases with depth in a section, varying between ~1 and ~5%. These organic and carbonate values are consistent with other recently reported values from Thar parabolic dune sands (Srivastava et al., 2019).

3.2. Luminescence dating

In general, measured luminescence signals from small aliquots are bright enough to be discernible from the background (Fig. 4A) and are dominated by the quartz fast component in the initial part of the OSL signal (fast ratio > 20; Durcan and Duller, 2011). Single grain analyses confirm the low levels of luminescence sensitivity to dose (2–3 luminescing grains per disc), which ensures that any heterogeneity in D_e distributions should be identified. The heterogeneity or over-dispersion (σ_d), in D_e distributions for the majority samples in this study ranges between 20% and 45% (Table 2), with slightly higher values (~45%) observed for two of the younger samples. These σ_d values are in line with values calculated from other single aliquots of dune samples in the central Thar (σ_d = 20–40%; Srivastava et al., 2019), single grains of dune samples from the northern Thar margin (σ_d = 30–50%; Durcan et al., 2019) and are comparable to linear dunes studies elsewhere (e.g., the Negev, σ_d = 10–60%; Roskin et al., 2011a). Overdispersion can be caused by a combination of intrinsic factors, such as natural variability of quartz (Thomsen et al., 2012 and references therein), as well as extrinsic sources, such as heterogeneous bleaching (e.g., Olley et al., 2004), post-depositional mixing of sediments (e.g., Bateman et al., 2003, 2007; Kristensen et al., 2015), and dosimetric variability (e.g., Nathan et al., 2003; Mayya et al., 2006); and instrumental sources which have a small contribution (e.g., Thomsen et al., 2005; Cunningham et al., 2011). As discussed, the observed σ_d values for this suite of data is relatively low, and in line with other published values from aeolian, dryland contexts. σ_d values from dose recovery tests were <5%, and therefore we hypothesise external factors as the source of the observed variability. σ_d due to incomplete bleaching is unlikely, given the deposition by aeolian processes (Duller, 2004; Singhvi and Porat, 2008), and samples were carefully collected from visibly undisturbed strata, which should minimise D_e variability as a result of post-depositional mixing. We, therefore, hypothesise mild

Table 1
Sedimentology of samples showing Munsell colour, grain size statistics (in microns), organic and carbonate content.

Sample	Munsell Colour	Mean (μm)	Coarse Sand (500–1000 μm) (%)	Medium Sand (250–500 μm) (%)	Fine Sand (125–250 μm) (%)	Very fine Sand (63–125 μm) (%)	Silt (2–63 μm) (%)	Clay (<2 μm) (%)	Sorting*	Skewness**	Kurtosis***	Organic Content (%)	Carbonate Content (%)
Thar 17/2/1	10 YR 5/4	183.0	0.0	20.0	64.7	15.3	0.0	0.0	1.439 (MWS)	−0.001 (S)	0.952 (M)	0.62	1.80
Thar 17/2/2	10 YR 5/4	178.5	0.0	17.0	66.7	12.3	4.0	0.0	1.447 (MWS)	−0.086 (S)	1.072 (M)	0.76	2.31
Thar 17/2/4	10 YR 5/4	188.8	0.0	23.0	63.0	11.6	2.4	0.0	1.459 (MWS)	−0.037 (S)	0.994 (M)	0.87	2.80
Thar 17/2/6	10 YR 5/4	179.9	0.0	15.8	70.8	13.4	0.0	0.0	1.382 (WS)	0.000 (S)	0.956 (M)	0.72	2.10
Thar 17/2/8	10 YR 5/4	168.3	0.0	8.5	75.9	15.6	0.0	0.0	1.336 (WS)	0.001 (S)	0.965 (M)	0.60	3.88
Thar 17/2/10	10YR 5/4	106.8	0.8	20.1	37.1	17.4	23.4	1.2	3.114 (PS)	−0.470 (VFS)	1.226 (L)	1.36	3.94
Thar 17/4/1	10 YR 6/4	191.1	0.3	25.3	59.6	11.7	3.1	0.0	1.500 (MWS)	−0.051 (S)	1.013 (M)	0.58	1.70
Thar 17/4/2	10 YR 6/4	180.2	0.1	22.8	56.9	15.8	4.4	0.0	1.569 (MWS)	−0.088 (S)	1.063 (M)	0.87	2.24
Thar 17/4/6	10 YR 6/4	154.3	1.2	22.8	43.8	18.2	12.9	1.1	2.399 (PS)	−0.356 (VFS)	1.747 (VL)	0.71	2.60
Thar 17/4/8	10 YR 6/4	149.0	1.3	19.8	42.8	23.7	11.6	0.8	2.192 (PS)	−0.258 (FS)	1.463 (L)	0.98	5.06
Thar 17/5/1	10 YR 6/4	208.3	0.3	31.1	60.4	8.2	0.0	0.0	1.441 (MWS)	−0.006 (S)	0.952 (M)	0.88	1.90
Thar 17/5/2	10 YR 6/4	176.6	0.6	25.9	49.1	14.8	8.5	1.2	2.134 (PS)	−0.322 (VFS)	1.877 (VL)	0.87	1.96
Thar 17/5/4	10 YR 6/4	192.4	0.1	23.7	64.5	11.7	0.0	0.0	1.429 (MWS)	0.006 (S)	0.952 (M)	0.51	2.10
Thar 17/5/6	10 YR 6/4	219.0	0.9	35.5	57.4	6.2	0.0	0.0	1.446 (MWS)	0.009 (S)	0.952 (M)	0.48	2.48
Thar 17/5/8	10 YR 6/4	140.4	3.1	20.5	40.1	19.9	15.8	0.8	2.584 (PS)	−0.343 (VFS)	1.567 (VL)	1.65	3.85
Thar 17/6/2	10 YR 5/4	187.5	0.0	21.4	65.5	13.1	0.0	0.0	1.425 (MWS)	0.002 (S)	0.946 (M)	0.60	1.09
Thar 17/6/4	10 YR 5/4	175.7	0.2	22.5	54.5	15.3	6.9	0.6	1.932 (MS)	−0.295 (FS)	1.838 (VL)	0.59	2.20
Thar 17/6/6	10 YR 5/4	191.7	0.1	23.5	64.4	12.0	0.0	0.0	1.431 (MWS)	0.007 (S)	0.951 (M)	0.56	3.21
Thar 17/6/9	10 YR 5/4	214.6	0.1	32.0	63.2	4.7	0.0	0.0	1.381 (WS)	−0.003 (S)	0.956 (M)	0.52	2.78

* MWS = moderately well sorted, WS = well sorted, MS = moderately sorted, PS = poorly sorted.
** FS = finely skewed, VFS = very finely skewed, S = symmetrical.
*** L = leptokurtic, VL = very leptokurtic, M = mesokurtic.

microdosimetric variability as a source of variability in D_e distributions. It has been demonstrated empirically and through modelling that microdosimetric variability may contribute significantly to variations in D_es for well-bleached samples (up to ~45–50%; see Mayya et al., 2006; Cunningham et al., 2012; Guerin et al., 2015; Jankowski and Jacobs, 2018). In this context of relatively low σ_d values, which are in line with other published studies, and given that the D_e distributions tend to be symmetrical around a central value (e.g., Fig. 4B), the CAM (Galbraith et al., 1999) has been used for final D_e calculation. This follows the rationale of other dryland-based studies, such as Parton et al. (2015) and Durcan et al. (2019).

3.2.1. Calculation of minimum ages

One of the factors which limits the upper dateable range of OSL dating is signal saturation. A quartz OSL signal can be considered saturated if either the natural signal does not intercept the dose response curve (DRC) or if the natural signal interpolates onto the flat, asymptotic part of the DRC (e.g., Fig. 5). Interpolation of the natural signal from the asymptote of the saturated DRC results in a large and asymmetric uncertainty in D_e (Murray et al., 2002; Murray and Funder, 2003) and therefore should be avoided where possible. Wintle and Murray (2006) suggest that a prudent upper dating limit for saturated signals is the $2D_0$ parameter, which represents ~85% of the upper saturation point obtained from the DRC. D_0 is derived from the fitting of the DRC with a single saturating exponential function, $I=I_0\ (1-\exp^{-D/D0})$ where I is the OSL intensity after a dose (D), I_0 is the saturation intensity and D_0 is the dose level characteristic of the DRC (Wintle and Murray, 2006).

In this study, a signal was considered saturated if there was no interpolation on the DRC or if the calculated D_e was greater than $2D_0$. A

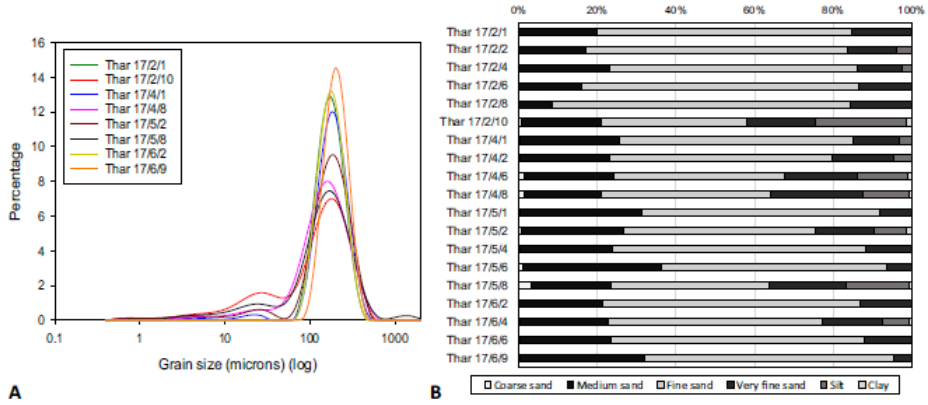


Fig. 3. A. Grain size distribution by volume for selected samples from each sampled dune. B. The percentage distribution of different grain sizes for all the samples. Clay <2 μm; silt = 2–63 μm; very fine sand = 63–125 μm; fine sand = 125–250 μm, medium sand = 250–500 μm; and coarse sand = 500–1000 μm (Blott and Pye, 2001 and references therein).

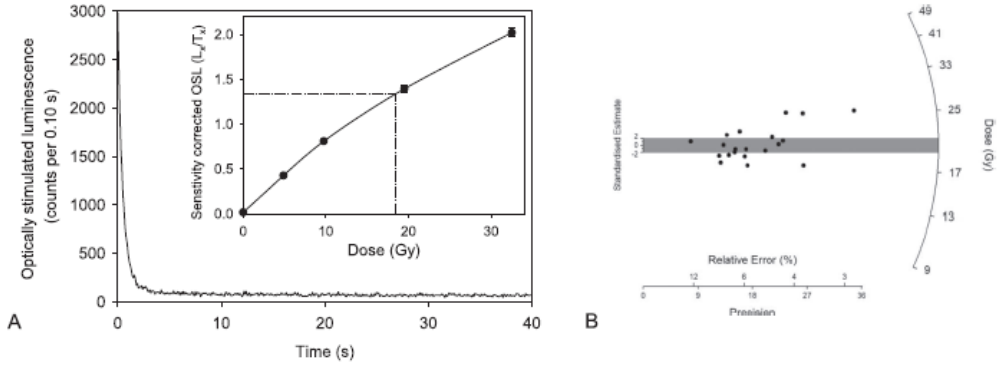


Fig. 4. A. An example OSL signal from sample Thar 17/2/6, and the dose response curve from the same aliquot (inset) B. Radial plot of individual D_es for Thar 17/2/6 (σ_E = 23%).

sample was considered saturated when more than 50% of measured accepted aliquots were saturated, and a minimum age was calculated using the mean $2D_0$ values of all accepted aliquots. These minimum ages are reported to the nearest integer and without an uncertainty, reflecting that the 'true' D_e is in excess of quoted minimum. Two samples are considered saturated (Table 2): Thar 17/2/10 (15/27 aliquots saturated) and Thar 17/5/8 (14/24) and yielded minimum ages of >58 ka and >48 ka respectively.

3.2.2. Luminescence ages

A summary of the luminescence dating results is provided in Table 2 along with stratigraphic sections (Fig. 6A) and age-depth profiles (Fig. 6B). At all four sites, OSL ages (including uncertainties) are in stratigraphic order and 17 of the 19 samples date to the Holocene, 10 of which date to the early part of the Holocene. Site Thar 17/2 depicts a Pleistocene feature with the oldest age at 9 m depth having a minimum age of >58 ka. At 7 and 3 m depths, sample ages are within uncertainties: 8.62 ± 0.64 ka (Thar 17/2/8) and 8.81 ± 0.71 ka (Thar 17/2/4) old respectively. Sample Thar 17/2/1 shows that the uppermost 0.8 m of dune sediments accumulated in the last ~500 years and is immediately underlain by a 4.07 ± 0.44 ka old sample at 0.9 m (Thar 17/2/2). The five samples from Thar 17/5 dune show a similar dune accumulation pattern to Thar 17/2 where the basal dune unit is atleast ~48 ka old (Thar 17/5/8) and is overlain by 2 m dune which accumulated between 9.38 ± 0.82 ka (Thar 17/5/6) and 9.27 ± 0.64 ka (Thar 17/5/4). The top 1.6 m of sediments at Thar 17/5 recorded dune activity in the last ~150 years (Thar 17/5/1). The site 17/4 preserves only Holocene accumulation with the oldest sample at 11 m dating to 11.61 ± 0.82 ka (Thar 17/4/8). 7 m of dune sand accumulation occurred between 10.52 ± 0.99 ka (Thar 17/4/6) and 8.79 ± 0.67 ka (Thar 17/4/2). The uppermost sample, taken 0.5 m below the dune surface, dates to 3.01 ± 0.24 ka (Thar 17/4/1). At site Thar 17/6, between 9.5 and 6 m down section, sample ages are within uncertainties- 9.39 ± 0.69 ka (Thar 17/6/9) and 9.38 ± 0.71 ka (Thar 17/6/6) old. The top 2 m dune is recent, dating from 0.34 ± 0.03 ka (Thar 17/6/2).

4. Discussion

Previous chronometric investigations of dunes in the northern Thar Desert have been limited, and have focussed chiefly on transverse and parabolic dunes (Kar et al., 1998; Thomas et al., 1999). These studies often relied on sampling pre-existing exposures and used older and now mostly redundant multiple aliquot luminescence dating techniques (Duller, 2004). The ages from these studies provided evidence

Table 2
Summary OSL data. Equivalent doses (D_e), dose rates ($\dot{D}$), and ages are shown to two decimal places, with all calculations made prior to rounding. Minimum D_es and ages are calculated for samples Thar 17/2/10 and Thar 17/5/8 due to signal saturation and are quoted to the nearest integer, without uncertainties. All ages are relative to the year 2018.

Sample	Depth (m)	Discs accepted (measured)	Over-dispersion (%)	D_e (Gy)	Beta $\dot{D}$ ($Gy.ka^{-1}$)	Gamma $\dot{D}$ ($Gy.ka^{-1}$)	Cosmic $\dot{D}$ ($Gy.ka^{-1}$)	Envir $\dot{D}$ ($Gy.ka^{-1}$)	Age (ka)
Thar 17/2/1	0.8	26 (38)	34.3 ± 4.8	1.22 ± 0.08	1.24 ± 0.11	0.68 ± 0.05	0.19 ± 0.02	2.10 ± 0.12	0.58 ± 0.05
Thar 17/2/2	0.9	22 (36)	36.6 ± 6.1	8.36 ± 0.78	1.17 ± 0.10	0.71 ± 0.05	0.18 ± 0.02	2.06 ± 0.11	4.07 ± 0.44
Thar 17/2/4	3.0	25 (46)	28.0 ± 4.0	19.74 ± 1.18	1.25 ± 0.11	0.85 ± 0.05	0.14 ± 0.01	2.24 ± 0.12	8.81 ± 0.71
Thar 17/2/6	5.0	21 (43)	22.3 ± 3.7	19.82 ± 1.04	1.24 ± 0.10	0.86 ± 0.06	0.11 ± 0.01	2.21 ± 0.12	8.97 ± 0.67
Thar 17/2/8	7.0	21 (27)	24.3 ± 3.8	19.64 ± 1.05	1.25 ± 0.10	0.94 ± 0.06	0.09 ± 0.01	2.28 ± 0.12	8.62 ± 0.64
Thar 17/2/10	9.0	27 (30)	–	>125	1.26 ± 0.11	0.82 ± 0.05	0.08 ± 0.01	2.15 ± 0.12	>58
Thar 17/4/1	0.5	21 (32)	28.4 ± 4.4	8.24 ± 0.51	1.44 ± 0.11	1.10 ± 0.07	0.21 ± 0.02	2.74 ± 0.14	3.01 ± 0.24
Thar 17/4/2	2.0	24 (35)	27.0 ± 3.9	20.39 ± 1.13	1.27 ± 0.10	0.89 ± 0.06	0.16 ± 0.02	2.32 ± 0.12	8.79 ± 0.67
Thar 17/4/6	9.0	24 (48)	37.0 ± 5.5	24.97 ± 1.94	1.35 ± 0.11	0.95 ± 0.06	0.08 ± 0.01	2.37 ± 0.13	10.52 ± 0.99
Thar 17/4/8	11.0	30 (43)	24.8 ± 3.3	25.23 ± 1.15	1.26 ± 0.10	0.85 ± 0.06	0.06 ± 0.01	2.17 ± 0.12	11.61 ± 0.82
Thar 17/5/1	1.4	22 (28)	44.3 ± 8.0	0.32 ± 0.03	1.28 ± 0.11	0.72 ± 0.05	0.17 ± 0.02	2.17 ± 0.13	0.15 ± 0.02
Thar 17/5/2	1.6	20 (36)	42.8 ± 6.8	2.51 ± 0.24	1.36 ± 0.11	1.04 ± 0.07	0.17 ± 0.02	2.56 ± 0.13	0.98 ± 0.10
Thar 17/5/4	3.7	23 (46)	19.2 ± 2.9	19.53 ± 0.79	1.23 ± 0.11	0.74 ± 0.05	0.13 ± 0.01	2.11 ± 0.12	9.27 ± 0.64
Thar 17/5/6	5.7	20 (46)	27.9 ± 4.8	18.75 ± 1.23	1.21 ± 0.11	0.68 ± 0.05	0.11 ± 0.01	2.00 ± 0.12	9.38 ± 0.82
Thar 17/5/8	8.7	24 (33)	–	>127	1.44 ± 0.11	1.13 ± 0.08	0.08 ± 0.01	2.65 ± 0.13	>48
Thar 17/6/2	2.0	22 (34)	33.0 ± 5.3	0.84 ± 0.06	1.34 ± 0.11	0.95 ± 0.06	0.16 ± 0.02	2.44 ± 0.13	0.34 ± 0.03
Thar 17/6/4	4.0	20 (35)	29.4 ± 5.0	3.72 ± 0.26	1.30 ± 0.11	0.83 ± 0.06	0.13 ± 0.01	2.26 ± 0.12	1.65 ± 0.15
Thar 17/6/6	6.0	24 (34)	30.4 ± 4.5	20.08 ± 1.07	1.22 ± 0.10	0.82 ± 0.05	0.10 ± 0.01	2.14 ± 0.12	9.38 ± 0.71
Thar 17/6/9	9.5	20 (46)	21.6 ± 3.9	22.10 ± 1.15	1.33 ± 0.11	0.96 ± 0.06	0.07 ± 0.01	2.35 ± 0.12	9.39 ± 0.69

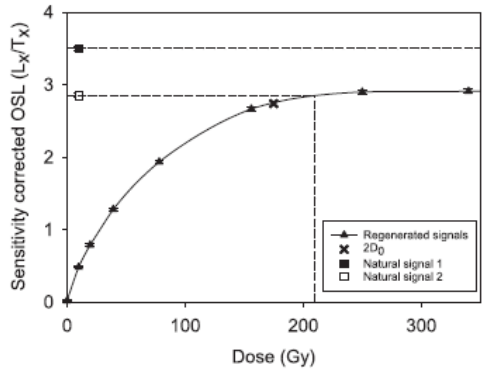


Fig. 5. The two types of OSL signal considered saturated in this study. i) where natural signal does not intercept the dose response curve (natural signal 1 square symbol) and ii) when the interpolated D_e exceeds $2D_0$ (natural signal 2 open square symbol).

of mid to late- Holocene dune activity (Kar et al., 1998; Thomas et al., 1999; Singhvi and Kar, 2004). The oldest ages in our new suite of data are from full depth profiles of sites Thar 17/5 and Thar 17/2. Though these two ages of >48 ka (Thar 17/5/8) and > 58 ka (Thar 17/2/10) are minimum age estimates, they are still considerably older than the records in previously published chronologies (Thomas et al., 1999; Singhvi and Kar, 2004), and provide the first reported occurrence of pre-Holocene dune activity in the northern Thar. This is important considering previous studies from southern, central and eastern Thar have presented dune records dating to >50 ka and attested to the antiquity of the desert (Chougaonkar et al., 1999; Dhir et al., 2010; Singhvi et al., 2010) while records from the northern Thar dunes were limited to the Holocene.

A significant component of our new dataset is evidence of early Holocene dune accumulation, and importantly this is recorded at all four sites, spanning 11.61 ± 0.82 ka to 8.62 ± 0.64 ka (Fig. 6B). Thick sediment accumulations are recorded during this period: 2 m and 3.5 m of sediment occurred at ~9.4 ka at sites Thar 17/5 and Thar 17/6 respectively. At site Thar 17/2, a 4 m thick dune accumulation dates to slightly later (~8.8 ka), and at Thar 17/4, the lowermost 7 m dune sand accumulated between 11.61 ± 0.82 ka and 8.79 ± 0.67 ka. At this site, this translates to an estimated accumulation rate of ~2.5 $m.ka^{-1}$. Regionally, comparable early Holocene net accumulation rates have been reported from NE-SW trending linear dune studies in the monsoon dominated northeast Rub 'al-Khali Desert (Atkinson et al., 2011, 2012). The early Holocene has been identified as a period marked by strong monsoonal winds compared to the late Holocene, evidenced by the enhanced

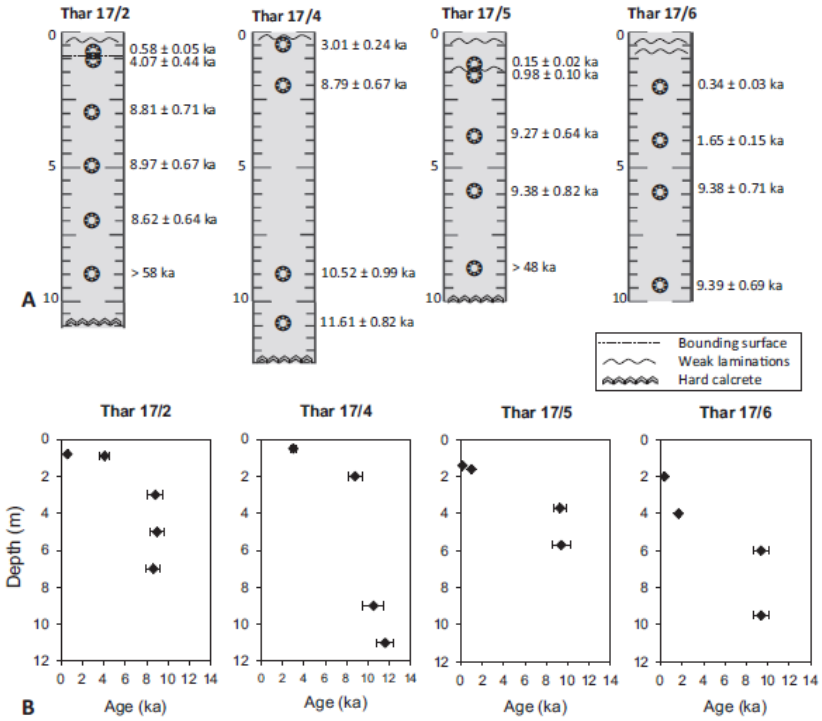


Fig 6. A. Stratigraphic sections and OSL ages for the sampled sites investigated in this study. Sample depth is in metres. Note the sections comprised largely homogeneous and structureless sand with very few laminations or other sedimentological features. B. Age-depth profiles for all four sites. The minimum ages for samples Thar 17/2/10 (>58 ka) and 17/5/8 (>48 ka) are not displayed.

upwelling off the coast of Oman (Gupta et al., 2003; Fig. 7) and a large wind stress curl across the western Arabian Sea (Gill et al., 2017; Fig. 7). Within the Thar Desert, the parabolic dunefield ~200 km south of the study area (Srivastava et al., 2019) and dunes associated with the Ghaggar-Hakra palaeochannel along the northern desert margin (Durcan et al., 2019) also recorded early Holocene accumulation. The data presented here demonstrate that the last major widespread dune accumulation in the Thar was not limited to the late glacial period (~17–~11 ka), but that major aeolian dynamism persisted into the early Holocene until ~8.6 ka.

In our study, only two dates identify mid to late-Holocene dune accumulation (4.07 ± 0.44 ka at Thar 17/2/2 and 3.01 ± 0.24 ka at Thar 17/4/1) (Table 2), both of which were sampled from within 1 m of the dune crest. The mid to late- Holocene dune activity, which resulted in thinner sediment accumulations compared to the early Holocene, suggests that dune activity in the region was less pervasive in terms of dune accumulation during the later part of the Holocene, with thicker units reflecting periods of more intensive dune activity (Telfer et al., 2010). Two sites (Thar 17/5 and 17/6) record seemingly more localised dune accumulation between 1.65 ± 0.15–0.98 ± 0.11 ka, which could be spatially restricted in nature or the result of localised reworking within the dune system. Unlike the early Holocene, the age depth profiles are more variable between the four studied sites during the mid- and late-Holocene (Fig. 6B) suggesting that individual dune profiles do not capture temporally comprehensive accumulation phases even in a spatially intensive dunefield. Telfer et al. (2010) and Bailey and Thomas (2014), through their modelling work, have suggested that preservation potential is unlikely to be equal spatially and temporally within a dune system, due to the interaction of exogenous and endogenous (stochastic) influences on accumulation. Stone and Thomas (2008), in their study of linear dunes in south-western Kalahari, also showed that only some accumulation phases are consistently recorded between dunes and individual dune profiles do not offer a temporal record even for a small region. Here, the younger phases of dune accumulation are preserved in pockets in three studied dunes, while absent in Thar 17/4, where the uppermost sample (0.5 m from the crest) yielded an age of 3.01 ± 0.24 ka. The absence of any common accumulation phases dating to the late Holocene could be due to differential preservation between the dunes or phases being missed in sampling. However, sampling at shallow depth of 0.5 m at Thar 16/4 should have minimised sampling bias towards younger phases. Likewise, at Thar 17/2 there is a jump from 0.58 ± 0.05 ka (Thar 17/2/1) to 4.07 ± 0.44 ka (Thar 17/2/2) over just 0.1 m, where a bounding surface exists, suggesting that missing an accumulation phase through sampling is not likely to be the major cause.

Although the INQUA Dunes Atlas chronologic database does not include any dated linear dune sites in the Thar, there are records from at least one dune site from Jamsar in the Bikaner region (Fig. 1B). Thomas et al. (1999) described the sampled feature as a linear dune site while later reviews designated it as a parabolic dune (Singhvi and Kar, 2004; Lancaster et al., 2016). Jamsar, which appears to be a linear dune site from Google Earth analysis, was a 3.9 m exposed dune section on the margins of an ephemeral lake studied by Thomas et al. (1999) and the authors reported 6 luminescence ages suggesting dune activity between 5.3 ± 0.7 ka and 4.7 ± 0.9 ka, and within the last 2000 years (Fig. 7). These ages were calculated using the multiple aliquot additive dose (MAAD) protocol that was widely used in the early decades of luminescence dating applications to sediments. It must be noted that earlier protocols did not explicitly check for changes in luminescence sensitivity, therefore, potentially adding an element of unreliability to them (Duller, 2004). Duller and Augustinus (2006) demonstrated the importance of checking the validity of luminescence dating results

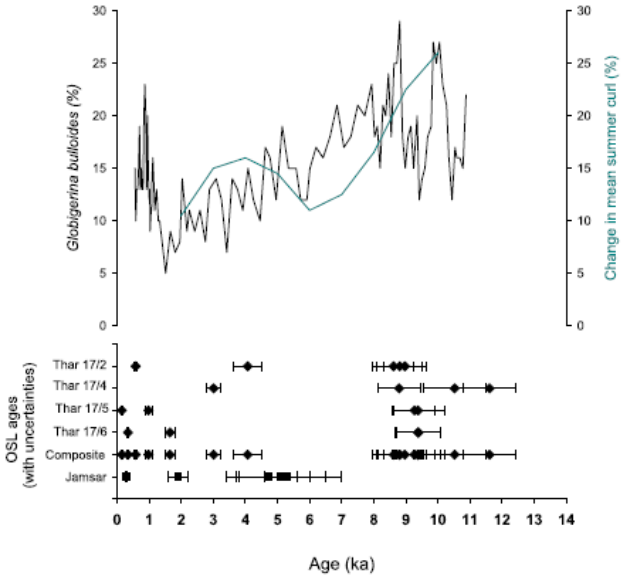


Fig. 7. Thar linear dune OSL ages plotted against reconstructions of *G. bulloides* percentage (Gupta et al., 2003) and percentage change in wind stress curl (blue) (Gill et al., 2017). The diamonds represent the ages determined in this study using post IR blue SAR protocol, while the squares are the MAAD OSL ages calculated by Thomas et al. (1999).

obtained using older protocols by dating the same samples from a stabilised linear dune in Tasmania and showed that MAAD protocol methods overestimated D_e values by up to 84% compared against SAR. Singhvi et al. (2010) presented SAR and MAAD ages for four dune samples from the Thar where MAAD ages overestimated the SAR ages by 15–53%. It is, therefore, possible that previously published ages from Jamsar dune feature (Thomas et al., 1999) are likely maximum ages for sediment accumulation.

The ages from the last millennium have been calculated at the crestal parts of three of the four studied dune sites (Fig. 6A). The site Thar 17/2 recorded 0.8 m of dune accumulation in last ~500 years, Thar 17/5 recorded 1.4 m of accumulation in last ~150 years and Thar 17/6 recorded 2 m of accumulation in the last ~350 years. These thicker units reflect the preservation bias towards younger sediments (Bailey and Thomas, 2014) and the absence of any late Holocene feature at site Thar 17/4 further confirms that individual dune profiles only provide partial information about the past changes. The parabolic dunes in the vicinity of the study area have also witnessed dune accumulation in the last millennium but those are significantly widespread with higher accumulation rates (Srivastava et al., 2019). This difference in dune accumulation rates could be attributed to parabolic dunes being more sensitive to natural and anthropogenic disturbances (e.g., Hugenholtz and Wolfe, 2005; Girardi and Davis, 2010), and the changing landscape in the Thar (Srivastava et al., 2019 and references therein). Nevertheless, the modern ages not only suggest that the Thar linear dunes remained active in later parts of the Holocene but also questions whether these dunes can be grouped under an 'old system' as previously implied (e.g., Pandey et al., 1964; Kar, 1993; Singhvi and Kar, 2004). Similar active and partially-active linear dunes have also been reported from the Negev (Roskin et al., 2011a), the Kalahari (Telfer and Thomas, 2007), the Strzelecki (Lomax et al., 2003) and the Tirari Deserts (Fitzsimmons et al., 2007).

5. Conclusions

This study presents a suite of OSL ages from intensively sampled linear dunes in the Thar Desert, India. The dataset show variability in dune activity between sites in terms of timing and nature of dune accumulation. In general, the record is characterised by consistent and rapid dune accumulation in the early Holocene, and multiple, distinct phases during the mid and late Holocene. The early Holocene period is the most active dune accumulation period which correlates with other Thar dunes records (Srivastava et al., 2019) and wider regional geoproxy evidence. The OSL ages show that the linear dunes in the Thar have remained active, accumulating sediment during the Holocene. The accumulation of up to 2 m of dune sediment in recent times rules out the earlier notion of classifying linear dunes as belonging to an 'old' Thar Desert system. The suite of ages also presents the first reported records of pre-Holocene dune activity in the northern Thar, albeit as minimum ages, and affirms findings from other desert dunefields that linear dunes preserve a relatively longer chronology. As dune records are increasingly being incorporated to wider palaeoenvironmental studies, our study emphasises on the importance of intensive dunefield sampling, rather than focusing on single dune profiles which do not capture temporally comprehensive accumulation phases, as done in the majority of previous studies in the Thar.

Acknowledgments

The doctoral studies of the first author are funded by the Clarendon Scholarship, University of Oxford. The authors thank the John Fell Fund, University of Oxford (Grant Number 132/062) for providing funding for fieldwork and lab analyses. The first author also thanks the International Society for Aeolian Research for supporting attendance at the 10th International Conference on Aeolian Research in Bordeaux (2018), where this work was initially presented. The authors thank the anonymous reviewers for their comments and suggestions.

References

Atkinson, O.A., Thomas, D.S.G., Goudie, A.S., Bailey, R.M., 2011. Late Quaternary chronology of major dune ridge development in the northeast Rub'al-Khali, United Arab Emirates. Quat. Res. 76, 93–105.
Atkinson, O.A., Thomas, D.S.G., Goudie, A.S., Parker, A.G., 2012. Holocene development of multiple dune generations in the northeast Rub'al-Khali, United Arab Emirates. The Holocene 22, 179–189.
Atkinson, O.A., Thomas, D.S.G., Parker, A.G., Goudie, A.S., 2013. Late Quaternary humidity and aridity dynamics in the northeast Rub'al-Khali, United Arab Emirates: implications for early human dispersal and occupation of eastern Arabia. Quat. Int. 300, 292–301.
Bailey, R.M., Thomas, D.S.G., 2014. A quantitative approach to understanding dated dune stratigraphies. Earth Surf. Process. Landf. 39, 614–631.
Banerjee, D., Murray, A.S., Botter-Jensen, L., Lang, A., 2001. Equivalent dose estimation using a single aliquot of polymineral fine grains. Radiat. Meas. 33, 73–94.
Bateman, M.D., Frederick, C.D., Jaiswal, M.K., Singhvi, A.K., 2003. Investigations into the potential effects of pedoturbation on luminescence dating. Quat. Sci. Rev. 22, 1169–1176.
Bateman, M.D., Boulter, C.H., Carr, A.S., Frederick, C.D., Peter, D., Wilder, M., 2007. Detecting post-depositional sediment disturbance in sandy deposits using optical luminescence. Quat. Geochronol. 2, 57–64.
Bell, W.T., 1979. Attenuation factors for the absorbed radiation dose in quartz inclusions for thermoluminescence dating. Ancient TL 8, 12.
Blott, S.J., Pye, K., 2001. GRADISTAT: a grain size distribution and statistics package for the analysis of unconsolidated sediments. Earth Surf. Process. Landf. 26, 1237–1248.
Bullard, J.E., Thomas, D.S.G., Livingstone, I., Wiggs, G.F.S., 1995. Analysis of linear sand dune morphological variability, southwestern Kalahari Desert. Geomorphology 11, 189–203.
Chougaonkar, M.P., Raghav, M.S., Rajaguru, S.N., Kar, A., Singhvi, A.K., Nambi, K.S.V., 1999. Luminescence dating results of dune profiles from margins of Thar desert and their implications. Man Environ 24, 21–26.
Cunningham, A.C., Wallinga, J., Minderhoud, P.S., 2011. Expectations of scatter in equivalent-dose distributions when using multi-grain aliquots for OSL dating. Geochronometria 38, 424.
Cunningham, A.C., DeVries, D.J., Schaart, D.R., 2012. Experimental and computational simulation of beta-dose heterogeneity in sediment. Radiat. Meas. 47, 1060–1067.
Dhir, R.P., Singhvi, A.K., Andrews, J.E., Kar, A., Sareen, B.K., Tandon, S.K., Kailath, A., Thomas, J.V., 2010. Multiple episodes of aggradation and calcrete formation in Late Quaternary aeolian sands, Central Thar Desert, Rajasthan, India. J. Asian Earth Sci. 37, 10–16.
Duller, G.A.T., 2004. Luminescence dating of Quaternary sediments: recent advances. J. Quat. Sci. 19, 183–192.
Duller, G.A.T., Augustinus, P.C., 2006. Reassessment of the record of linear dune activity in Tasmania using optical dating. Quat. Sci. Rev. 25, 2608–2618.
Durcan, J.A., Duller, G.A.T., 2011. The fast ratio: a rapid measure for testing the dominance of the fast component in the initial OSL signal from quartz. Radiat. Meas. 46, 1065–1072.
Durcan, J.A., King, G.E., Duller, G.A.T., 2015. DRAC: Dose Rate and Age Calculator for trapped charge dating. Quat. Geochronol. 28, 54–61.
Durcan, J.A., Thomas, D.S.G., Gupta, S., Pawar, V., Singh, R.N., Petrie, C.A., 2019. Holocene landscape dynamics in the Ghaggar-Hakra palaeochannel region at the northern edge of the Thar Desert, northwest India. Quat. Int. 501, 317–327. https://doi.org/10.1016/j.quaint.2017.10.012.
Fitzsimmons, K.E., Rhodes, E.J., Magee, J.W., Barrows, T.T., 2007. The timing of linear dune activity in the Strzelecki and Tirari Deserts, Australia. Quat. Sci. Rev. 26, 2598–2616.
Folk, R.L., Ward, W.C., 1957. Brazos River bar, Texas- a study in the significance of grain size parameters. J. Sediment. Res. 27, 3–26.
Galbraith, R.F., Roberts, R.G., Laslett, G.M., Yoshida, H., Olley, J.M., 1999. Optical dating of single and multiple grains of quartz from Jinmium rock shelter, northern Australia: part I, experimental design and statistical models. Archaeometry 41, 339–364.
Gill, E.C., Rajagopalan, B., Molnar, P.H., Kushnir, Y., Marchitto, T.M., 2017. Reconstruction of Indian summer monsoon winds and precipitation over the past 10,000 years using equatorial pacific SST proxy records. Paleoceanography 32, 195–216.
Girardi, J.D., Davis, D.M., 2010. Parabolic dune reactivation and migration at Napeague, NY, USA: Insights from aerial and GPR imagery. Geomorphology 114, 530–541.
Glennie, K.W., Singhvi, A.K., 2002. Event stratigraphy, paleoenvironment and chronology of SE Arabian deserts. Quat. Sci. Rev. 21, 853–869.
Guérin, G., Mercier, N., Adamiec, G., 2011. Dose-rate conversion factors: update. Ancient TL 29, 5–8.
Guérin, G., Mercier, N., Nathan, R., Adamiec, G., Lefrais, Y., 2012. On the use of the infinite matrix assumption and associated concepts: a critical review. Radiat. Meas. 47, 778–785.
Guerin, G., Jain, M., Thomsen, K.J., Murray, A.S., Mercier, N., 2015. Modelling dose rate to single grains of quartz in well-sorted sand samples: the dispersion arising from the presence of potassium feldspars and implications for single grain OSL dating. Quat. Geochronol. 27, 52–65.
Gupta, A.K., Anderson, D.M., Overpeck, J.T., 2003. Abrupt changes in the Asian southwest monsoon during the Holocene and their links to the North Atlantic Ocean. Nature 421, 354–357.
Heer, A.J., Adamiec, G., Moska, P., 2012. How many grains are there on a single aliquot. Ancient TL 30, 9–16.

Heiri, O., Lotter, A.F., Lemcke, G., 2001. Loss on ignition as a method for estimating organic and carbonate content in sediments: reproducibility and comparability of results. J. Paleolimnol. 25, 101–110.
Hugenholtz, C.H., Wolfe, S.A., 2005. Recent stabilization of active sand dunes on the Canadian prairies and relation to recent climate variations. Geomorphology 68, 131–147.
Jankowski, N.R., Jacobs, Z., 2018. Beta dose variability and its spatial contextualisation in samples used for optical dating: an empirical approach to examining beta microdosimetry. Quat. Geochronol. 44, 23–37.
Kar, A., 1987. Origin and transformation of longitudinal sand dunes in the Indian desert. Z. Geomorphol. 31, 311–337.
Kar, A., 1993. Aeolian processes and bedforms in the Thar Desert. J. Arid Environ. 25, 83–96.
Kar, A., 2014. The Thar or the Great Indian Sand Desert. Landscapes and Landforms of India. Springer, Dordrecht, pp. 79–90.
Kar, A., Felix, C., Rajaguru, S.N., Singhvi, A.K., 1998. Late Holocene growth and mobility of a transverse dune in the Thar Desert. J. Arid Environ. 38, 175–185.
Kar, A., Singhvi, A.K., Rajaguru, S.N., Juyal, N., Thomas, J.V., Banerjee, D., Dhir, R.P., 2001. Reconstruction of the late Quaternary environment of the lower Luni plains, Thar Desert, India. Journal of Quaternary Science: Published for the Quaternary Research Association 16, 61–68.
Kreutzer, S., Dietze, M., Burow, C., Fuchs, M.C., Schmidt, C., Fischer, M., Friedrich, J., 2017. Luminescence: Comprehensive luminescence dating data analysis. R Package Version 0.7.3.
Kristensen, J.A., Thomsen, K.J., Murray, A.S., Buylaert, J.P., Jain, M., Breuning-Madsen, H., 2015. Quantification of termite bioturbation in a savannah ecosystem: application of OSL dating. Quat. Geochronol. 30, 334–341.
Kumar, M., Goossens, E., Goossens, R., 1993. Assessment of sand dune change detection in Rajasthan Thar Desert, India. Int. J. Remote Sens. 14, 1689–1703.
Lancaster, N., 1982. Linear dunes. Prog. Phys. Geogr. 6, 475–504.
Lancaster, N., Wolfe, S., Thomas, D.S.G., Bristow, C., Bubenzer, O., Burrough, S.L., Duller, G., Halfen, A., Hesse, P.P., Roskin, J., Singhvi, A.K., 2016. The INQUA dunes atlas chronologic database. Quat. Int. 410, 3–10.
Leighton, C.L., Bailey, R.M., Thomas, D.S.G., 2013. The utility of desert sand dunes as Quaternary chronostratigraphic archives: evidence from the northeast Rub'al Khali. Quat. Sci. Rev. 78, 303–318.
Livingstone, I., Thomas, D.S.G., 1993. Modes of linear dune activity and their palaeoenvironmental significance: an evaluation with reference to southern African examples. Geol. Soc. Lond., Spec. Publ. 72, 91–101.
Lomax, J., Hilgers, A., Wopfner, H., Grün, R., Twidale, C.R., Radtke, U., 2003. The onset of dune formation in the Strzelecki Desert, South Australia. Quat. Sci. Rev. 22, 1067–1076.
Mayya, Y.S., Morthekai, P., Murari, M.K., Singhvi, A.K., 2006. Towards quantifying beta microdosimetric effects in single-grain quartz dose distribution. Radiat. Meas. 41, 1032–1039.
Moharana, P.C., Gaur, M.C., Choudhary, C., Chauhan, J.S., Rajpurohit, R.S., 2013. A system of geomorphological mapping for western Rajasthan with relevance for agricultural land use. Ann. Arid Zone 52, 163–180.
Munyikwa, K., 2005. The role of dune morphogenetic history in the interpretation of linear dune luminescence chronologies: a review of linear dune dynamics. Prog. Phys. Geogr. 29, 317–336.
Murray, A.S., Funder, S., 2003. Optically stimulated luminescence dating of a Danish Eemian coastal marine deposit: a test of accuracy. Quat. Sci. Rev. 22, 1177–1183.
Murray, A.S., Wintle, A.G., 2003. The single aliquot regenerative dose protocol: potential for improvements in reliability. Radiat. Meas. 37, 377–381.
Murray, A.S., Wintle, A.G., Wallinga, J., 2002. Dose estimation using quartz OSL in the non-linear region of the growth curve. Radiat. Prot. Dosim. 101, 371–374.
Nathan, R.P., Thomas, P.J., Jain, M., Murray, A.S., Rhodes, E.J., 2003. Environmental dose rate heterogeneity of beta radiation and its implications for luminescence dating: Monte Carlo modelling and experimental validation. Radiat. Meas. 37, 305–313.
O'Connor, P.W., Thomas, D.S.G., 1999. The timing and environmental significance of late Quaternary linear dune development in western Zambia. Quat. Res. 52, 44–55.
Olley, J.M., Pietsch, T., Roberts, R.G., 2004. Optical dating of Holocene sediments from a variety of geomorphic settings using single grains of quartz. Geomorphology 60, 337–358.
Pandey, S., Singh, S., Ghose, B., 1964. Orientation, distribution and origin of sand dunes in the central Luni basin. In Proceedings, Symposium on Problems of Indian Arid Zone, 84-91.
Parton, A., Farrant, A.R., Leng, M.J., Telfer, M.W., Groucutt, H.S., Petraglia, M.D., Parker, A.G., 2015. Alluvial fan records from southeast Arabia reveal multiple windows for human dispersal. Geology 43, 295–298.
Prescott, J.R., Hutton, J.T., 1994. Cosmic ray contributions to dose rates for luminescence and ESR dating: large depths and long-term time variations. Radiat. Meas. 23, 497–500.
Roskin, J., Porat, N., Tsoar, H., Blumberg, D.G., Zander, A.M., 2011a. Age, origin and climatic controls on vegetated linear dunes in the northwestern Negev Desert Israel. Quat. Sci. Rev. 30, 1649–1674.
Roskin, J., Tsoar, H., Porat, N., Blumberg, D.G., 2011b. Palaeoclimate interpretations of Late Pleistocene vegetated linear dune mobilization episodes: evidence from the northwestern Negev dunefield, Israel. Quat. Sci. Rev. 30, 3364–3380.
Saxena, S.K., Singh, S., 1976. Some Observations on the Sand Dunes and Vegetation of Bikaner District in Western Rajasthan. India, Annals of Arid Zone.
Singhvi, A.K., Kar, A., 2004. The aeolian sedimentation record of the Thar Desert. Journal of Earth System Science 113, 371–401.
Singhvi, A.K., Porat, N., 2008. Impact of luminescence dating on geomorphological and palaeoclimate research in drylands. Boreas 37, 536–558.
Singhvi, A.K., Williams, M.A.J., Rajaguru, S.N., Misra, V.N., Chawla, S., Stokes, Chauhan, N., Francis, T., Ganjoo, R., Humphreys, G.S., 2010. A ~200 ka record of climatic change and dune activity in the Thar Desert, India. Quat. Sci. Rev. 29, 3095–3105.
Srivastava, A., Thomas, D.S.G., Durcan, J.A., 2019. Holocene dune activity in the Thar Desert, India. Earth Surf. Process. Landf. 44, 1407–1418.
Stokes, S., Thomas, D.S.G., Shaw, P.A., 1997. New chronological evidence for the nature and timing of linear dune development in the Southwest Kalahari Desert. Geomorphology 20, 81–93.
Stone, A.E.C., Thomas, D.S.G., 2008. Linear dune accumulation chronologies from the southwest Kalahari, Namibia: challenges of reconstructing late Quaternary palaeoenvironments from aeolian landforms. Quat. Sci. Rev. 27, 1667–1681.
Telfer, M.W., Hesse, P.P., 2013. Palaeoenvironmental reconstructions from linear dunefields: recent progress, current challenges and future directions. Quat. Sci. Rev. 78, 1–21.
Telfer, M.W., Thomas, D.S.G., 2007. Late Quaternary linear dune accumulation and chronostratigraphy of the southwestern Kalahari: implications for aeolian palaeoclimatic reconstructions and predictions of future dynamics. Quat. Sci. Rev. 26, 2617–2630.
Telfer, M.W., Bailey, R.M., Burrough, S.L., Stone, A.E.S., Thomas, D.S.G., Wiggs, G.F.S., 2010. Understanding linear dune chronologies: insights from a simple accumulation model. Geomorphology 120, 195–208.
Thomas, D.S.G., 1992. Desert dune activity: concepts and significance. J. Arid Environ. 22, 31–38.
Thomas, D.S.G., 2013. Reconstructing paleoenvironments and palaeoclimates in drylands: what can landform analysis contribute? Earth Surf. Process. Landf. 38, 3–16.
Thomas, D.S.G., Shaw, P.A., 1991. The Kalahari Environment. Cambridge University Press.
Thomas, J.V., Kar, A., Kailath, A.J., Juyal, N., Rajaguru, S.N., Singhvi, A.K., 1999. Late Pleistocene–Holocene-history of aeolian accumulation in the Thar Desert, India. Zeitschrift für Geomorphologie Supplementband 181–194.
Thomsen, K.J., Murray, A.S., Bøtter-Jensen, L., 2005. Sources of variability in OSL dose measurements using single grains of quartz. Radiat. Meas. 39, 47–61.
Thomsen, K.J., Murray, A.S., Jain, M., 2012. The dose dependency of the over-dispersion of quartz OSL single grain dose distributions. Radiat. Meas. 47, 732–739.
Tsoar, H., 1989. Linear dunes-forms and formation. Prog. Phys. Geogr. 13, 507–528.
Tsoar, H., Møller, J.T., 1986. The role of vegetation in the formation of linear sand dunes. Aeol. Geomorph. 75–95.
Tsoar, H., Blumberg, D.G., Wenkart, R., 2008. Formation and geomorphology of the North-Western Negev sand dunes. Arid dune ecosystems. Springer, Berlin, Heidelberg, pp. 25–48.
Verstappen, H.T., 1968. On the origin of longitudinal seif dunes. Zeitschrift für Geomorphologie NF 12, 200–220.
Wasson, R.J., Rajaguru, S.N., Misra, V.N., Agrawal, D.P., Dhir, R.P., Singhvi, A.K., Rao, K.K., 1983. Geomorphology, Late Quaternary Stratigraphy and Palaeoclimatology of the Thar Dunefield.
Wintle, A.G., Murray, A.S., 2006. A review of quartz optically stimulated luminescence characteristics and their relevance in single-aliquot regeneration dating protocols. Radiat. Meas. 41, 369–391.

Appendix G: Supplementary Information for Paper 3 (Chapter 6).

G.1. Sampled sites

Ten new optically stimulated luminescence (OSL) ages from three sites are presented in the paper. The first site, IND 14/5 (29.32592 N, 73.88269 E), is a natural exposure of a ~ 26 m high source-bordering dune (Figure G.1), close to the settlement of Suratgarh and adjacent to the Ghaggar-Hakra palaeochannel. 6 samples were collected for OSL dating from this site at depths of 2 m, 3 m, 10 m, 11 m, 25 m and 26 m (Figure G.1). The site complements the aeolian-fluvial sequences in the region dated by Durcan *et al*. (2019) which reveal that the Ghaggar-Hakra was a highly dynamic geomorphic system, particularly in middle to late Holocene. The other two sites, Thar 16/2 (26.57924 N, 72.81612 E; Fig S1A) and Thar 16/8 (26.65793 N, 72.60611 E; Fig S1C) are from the central Thar area, close to the city of Jodhpur. At both sites, noses of parabolic dunes were excavated and then samples for OSL dating were retrieved from artificially created sections.

At each site, samples were retrieved by hammering opaque tubes into cleaned sediment faces and carefully closed with opaque lids. Sediment from potentially light exposed ends were removed and used for sedimentological analyses. Except for the section of site IND 14/5 which displayed cross bedding structures at the top (Figure G.1), the three sampled dunes were composed of homogenous, usually structureless sand with occasional weak laminations ensuring lack of post-depositional disturbance. Grain size analysis of these samples showed that all ten samples were predominantly fine sand, with mean

grain size varying between 150-250 μm (Figure G.2). The dune sediments are homogenous in colour within each dune (Table G.3), and the organic and carbonate contents are along the lines of published values from the Thar (Durcan *et al*., 2019; Srivastava *et al*., 2019a; 2019b). Samples Thar 16/2/1 and Thar 16/2/3 have slightly higher carbonate contents, due to their proximity to underlying pedogenic calcretes. During sampling it was ensured that the calcrete layer was away from sampling location to avoid dosimetry related issues (e.g. Nathan *et al*. 2003, Mayya *et al*., 2006).

G.2. Luminescence dating

Samples were opened and prepared under subdued orange light conditions at the Oxford Luminescence Dating Laboratory. Samples were treated with hydrochloric acid and hydrogen peroxide to remove carbonate and organic materials. After sieving, sodium polytungstate was used for density separation in order to isolate quart mineral grains. To remove the alpha-irradiated outer edge of the quartz grains, hydrofluoric acid was used, and samples were rinsed in hydrochloric acid and re-sieved. Small aliquots of sample (~2 mm in diameter) were used for measurement of the equivalent dose (D_e), which was measured using a post-infrared blue single aliquot regenerative dose (SAR) protocol (Banerjee *et al*., 2001). Table G.1 details the SAR protocol used. For environmental dose rate determination, dose rates were calculated from radionuclide concentrations measured using inductively coupled plasma mass spectrometry, with infinite matrix dose rates adjusted for grain size, etching and moisture (detailed in Srivastava *et al*., 2019a; 2019b). Final equivalent doses (D_es), dose rates, and ages are provided in Table 6.1.

Table G.1. The post -IR blue SAR protocol used in the study.

Step	Treatment	Observe
1	Beta irradiation (zero for natural)	
2	Pre-heat at 240°C for 10 s	
3	IR stimulation at 50°C for 100 s	
4	OSL stimulation at 125°C for 40 s	L_x
5	Test dose	
6	Cut-heat at 160°C for 10 s	
7	IR stimulation at 50°C for 100 s	
8	OSL stimulation at 125°C for 40 s	T_x

The calculated luminescence ages vary between 7.28 ± 0.52 and 11.83 ± 0.93 ka and are detailed in Table 6.1. Prior to the calculation of ages, individual D_es were screened using standard rejection criteria, including checks for recuperation and the recycling ratio, and the dominance of the fast component in the initial part of the signal was checked using the fast ratio (Durcan and Duller, 2011). Dose recovery test results for samples IND14/5/1, Thar16/8/1, and IND14/5/3 showed that laboratory administered doses could be recovered to within +/-10%, confirming the suitability of chosen protocol (Table G.1). Overdispersion in D_e values ranged between ~12-30 % across the suite of samples, in line with values calculated in previous Thar dating studies (e.g. Srivastava *et al*. 2019a; 2019b), and therefore the central age model of Galbraith *et al*. (1999) was used for final D_e calculation.

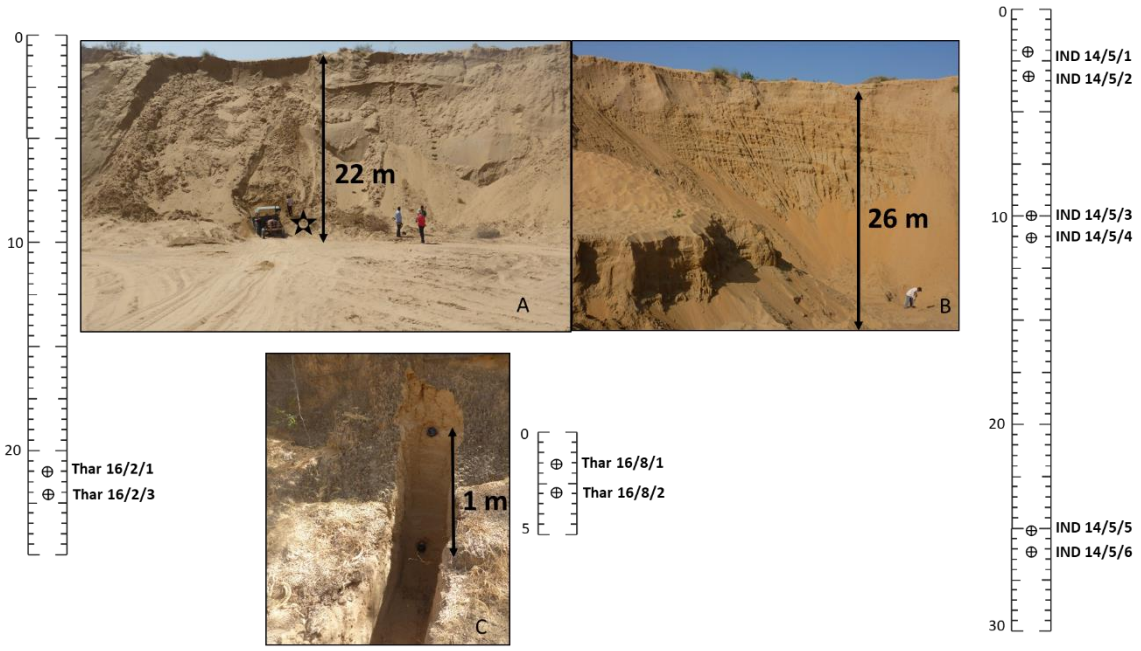


Figure G.1. (A) View of sampled sections at three dunes sites of (A) Thar 16/2, (B) IND 14/5 and (C) Thar 16/8 included in the paper, with the location of retrieved samples marked in the schematic logs alongside.

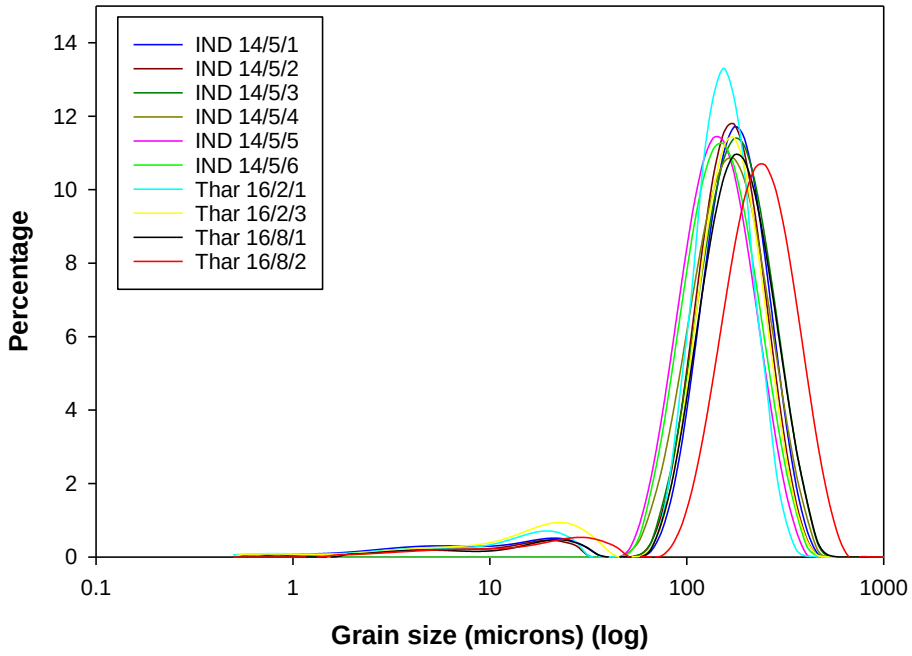


Figure G.2. Grain size distribution data measured using a Malvern Mastersizer Hydro 2000 laser analyser with wet dispersion.

Table G.2. Luminescence ages included in *AI* analysis in this study. The ages in black refer to the ages included in the first version of the INQUA dune atlas chronologic database (Lancaster *et al.*, 2016; https://www.dri.edu/inquaduneatlas), while the maroon ages are from the recently published studies including this thesis.

Sample code	Depth (m_	Age (a)	Error (a)	Reference
INDL00001	0.6	200	40	Singhvi and Kar (2004)
INDL00002	0.9	500	50	Singhvi and Kar (2004)
INDL00003	1.2	3640	510	Singhvi and Kar (2004)
INDL00004	1.5	4500	480	Singhvi and Kar (2004)
INDL00005	2	5080	680	Singhvi and Kar (2004)
INDL00006	0.8	400	180	Singhvi and Kar (2004)
INDL00007	1.0	450	510	Singhvi and Kar (2004)
INDL00008	1.9	830	330	Singhvi and Kar (2004)
INDL00009	2.5	5350	690	Singhvi and Kar (2004)
INDL00010	2.9	7540	750	Singhvi and Kar (2004)
INDL00011	3.25	7600	920	Singhvi and Kar (2004)
INDL00012	3.7	12590	1610	Singhvi and Kar (2004)
INDL00013	3.9	9830	1200	Singhvi and Kar (2004)
INDL00014	1.0	470	170	Singhvi and Kar (2004)
INDL00015	1.2	350	590	Singhvi and Kar (2004)
INDL00016	1.4	5300	700	Singhvi and Kar (2004)
INDL00050	0.5	60	10	Singhvi and Kar (2004)
INDL00051	6.5	13700	2900	Singhvi and Kar (2004)
INDL00052	6.9	17500	1900	Singhvi and Kar (2004)
INDL00053	7.5	26980	2500	Singhvi and Kar (2004)
INDL00054	8.1	27500	2700	Singhvi and Kar (2004)
INDL00055	8.9	58300	5600	Singhvi and Kar (2004)
INDL00056	10.1	100800	10400	Singhvi and Kar (2004)
INDL00057	12.1	107700	7800	Singhvi and Kar (2004)
INDL00059	13.5	73700	7800	Singhvi and Kar (2004)
INDL00060	13.6	81070	10600	Singhvi and Kar (2004)
INDL00063	16.1	82210	10990	Singhvi and Kar (2004)
INDL00064	18.0	151290	30400	Singhvi and Kar (2004)
INDL00071	0.8	300	30	Singhvi and Kar (2004)
INDL00072	1.3	1900	300	Singhvi and Kar (2004)
INDL00073	2.0	4700	900	Singhvi and Kar (2004)
INDL00074	2.2	5200	1800	Singhvi and Kar (2004)

INDL00075	3.65	5100	1400	Singhvi and Kar (2004)
INDL00076	3.9	5300	700	Singhvi and Kar (2004)
INDL00077	1.4	5400	1300	Singhvi and Kar (2004)
INDL00078	2.22	7900	1100	Singhvi and Kar (2004)
INDL00079	0.5	16000	2400	Singhvi and Kar (2004)
INDL00080	1.09	16000	2200	Singhvi and Kar (2004)
INDL00081	3.53	34000	4700	Singhvi and Kar (2004)
INDL00082	4.42	59000	7100	Singhvi and Kar (2004)
INDL00083	5.02	66000	12100	Singhvi and Kar (2004)
INDL00084	6.42	75000	12200	Singhvi and Kar (2004)
INDL00085	0.7	11000	1500	Singhvi and Kar (2004)
INDL00086	1.7	31000	3000	Singhvi and Kar (2004)
INDL00087	2.2	32000	3800	Singhvi and Kar (2004)
INDL00088	3.2	35000	4700	Singhvi and Kar (2004)
INDL00141	100	19000	9800	Singhvi and Kar (2004)
INDL00125	250	19000	7600	Singhvi and Kar (2004)
INDL00142	155	21000	8600	Singhvi and Kar (2004)
INDL00127	600	31000	5300	Singhvi and Kar (2004)
INDL00143	800	41000	5200	Singhvi and Kar (2004)
INDL00145	1160	42000	12600	Singhvi and Kar (2004)
INDL00132	1	31100	800	Singhvi and Kar (2004)
INDL00133	1.6	8100	3100	Singhvi and Kar (2004)
INDL00135	7.4	9500	4000	Singhvi and Kar (2004)
INDL00136	9	9500	1100	Singhvi and Kar (2004)
INDL00137	10	11700	4000	Singhvi and Kar (2004)
INDL00138	12.5	25800	5500	Singhvi and Kar (2004)
INDL00139	12.5	52400	218000	Singhvi and Kar (2004)
INDL00140	14.5	86300	28500	Singhvi and Kar (2004)
INDL00099	0.2	6000	1000	Singhvi and Kar (2004)
INDL00100	0.8	8000	1000	Singhvi and Kar (2004)
INDL00101	1.3	10000	3000	Singhvi and Kar (2004)
INDL00102	2.3	11000	3000	Singhvi and Kar (2004)
INDL00103	3.5	12000	3000	Singhvi and Kar (2004)
INDL00104	5	21000	2000	Singhvi and Kar (2004)
INDL00105	6.2	19000	5000	Singhvi and Kar (2004)
INDL00118	3.3	18000	2000	Singhvi and Kar (2004)
INDL00120	3.9	22000	4000	Singhvi and Kar (2004)
INDL00121	6	25000	3000	Singhvi and Kar (2004)
INDL00122	0.6	19000	5000	Singhvi and Kar (2004)
INDL00123	1.5	22000	5000	Singhvi and Kar (2004)
INDL00107	4.5	16000	3000	Singhvi and Kar (2004)
INDL00108	6	25000	6000	Singhvi and Kar (2004)
INDL00179	0.5	1690	280	Durcan *et al.* (2019)
INDL00180	1.0	2650	240	Durcan *et al.* (2019)
INDL00181	2.2	2890	360	Durcan *et al.* (2019)
INDL00182	1.0	230	40	Durcan *et al.* (2019)

INDL00183	0.5	8930	1140	Durcan *et al.* (2019)
INDL00184	3.3	8890	880	Durcan *et al.* (2019)
INDL00185	0.5	120	40	Durcan *et al.* (2019)
INDL00186	2.0	7060	850	Durcan *et al.* (2019)
INDL00187	3.0	6490	660	Durcan *et al.* (2019)
INDL00188	4.9	7130	610	Durcan *et al.* (2019)
INDL00189	0.6	2200	190	Durcan *et al.* (2019)
INDL00190	1.4	4540	430	Durcan *et al.* (2019)
INDL00191	2.4	5760	350	Durcan *et al.* (2019)
INDL00192	2.0	15300	1100	Shitaoka *et al.* (2012)
INDL00193	2.5	12100	700	Shitaoka *et al.* (2012)
INDL00194	1.0	12900	1100	Shitaoka *et al.* (2012)
INDL00195	1.6	13800	1000	Shitaoka *et al.* (2012)
INDL00196	0.5	5200	600	Shitaoka *et al.* (2012)
INDL00197	2.2	13100	800	Shitaoka *et al.* (2012)
INDL00198	3.0	14400	1100	Shitaoka *et al.* (2012)
INDL00199	2.0	4900	300	Shitaoka *et al.* (2012)
INDL00200	3.0	13200	700	Shitaoka *et al.* (2012)
INDL00201	2.0	11000	900	Shitaoka *et al.* (2012)
INDL00202	2.0	10300	600	Shitaoka *et al.* (2012)
INDL00203	1.0	5000	300	Shitaoka *et al.* (2012)
INDL00204	1.5	5100	300	Shitaoka *et al.* (2012)
Thar 16/1/1	0.5	450	60	This thesis
Thar 16/1/2	0.7	390	30	This thesis
Thar 16/1/4	6.0	550	50	This thesis
Thar 16/1/5	14.0	1070	90	This thesis
Thar 16/1/6	20.0	6860	490	This thesis
Thar 16/1/7	21.0	8300	690	This thesis
Thar 16/1/8	22.0	9600	740	This thesis
Thar 16/1/9	23.0	13850	1110	This thesis
Thar 16/3/1	11.0	680	80	This thesis
Thar 16/3/2	19.0	5690	500	This thesis
Thar 16/4/1	0.3	200	30	This thesis
Thar16/4/2	1.0	160	30	This thesis
Thar 16/4/4	2.0	840	80	This thesis
Thar 16/4/6	5.0	2090	180	This thesis
Thar 16/4/7	6.0	1920	160	This thesis
Thar 16/4/8	7.0	10140	690	This thesis
Thar 16/4/10	9.0	12250	820	This thesis
Thar 16/6/1	0.5	70	10	This thesis
Thar 16/6/5	5.0	70	10	This thesis
Thar 16/9/1	1.5	70	10	This thesis
Thar 16/9/2	2.5	60	10	This thesis
Thar 16/9/4	4.5	140	20	This thesis
Thar 16/9/5	5.5	130	10	This thesis
Thar 16/9/8	8.5	3520	340	This thesis

Thar 16/10/1	1.0	70	10	This thesis
Thar 16/10/4	3.7	70	10	This thesis
Thar 16/10/8	8.2	670	70	This thesis
Thar 16/10/9	9.2	5190	510	This thesis
Thar 16/10/10	10.2	5430	400	This thesis
Thar 18/1/2	1.0	50	10	This thesis
Thar18/1/4	2.0	150	30	This thesis
Thar 17/2/1	0.8	580	50	This thesis
Thar 17/2/2	0.9	4070	440	This thesis
Thar 17/2/4	3.0	8810	710	This thesis
Thar 17/2/6	5.0	8970	670	This thesis
Thar 17/2/8	7.0	8620	640	This thesis
Thar 17/2/10	9.0	> 58		This thesis
Thar 17/4/1	0.5	3010	240	This thesis
Thar 17/4/2	2.0	8790	670	This thesis
Thar 17/4/6	9.0	10520	990	This thesis
Thar 17/4/8	11.0	11610	820	This thesis
Thar 17/5/1	1.35	150	20	This thesis
Thar 17/5/2	1.6	980	100	This thesis
Thar 17/5/4	3.7	9270	640	This thesis
Thar 17/5/6	5.7	9380	820	This thesis
Thar 17/5/8	8.7	> 48		This thesis
Thar 17/6/2	2.0	340	30	This thesis
Thar 17/6/4	4.0	1650	150	This thesis
Thar 17/6/6	6.0	9380	710	This thesis
Thar 17/6/9	9.5	9390	690	This thesis
IND 14/5/1	2.0	7280	520	This thesis
IND 14/5/2	3.0	8860	660	This thesis
IND 14/5/3	10.0	10510	730	This thesis
IND 14/5/4	11.0	10510	640	This thesis
IND 14/5/5	25.0	10050	760	This thesis
IND 14/5/6	26.0	10330	970	This thesis
Thar 16/2/1	21.0	9530	870	This thesis
Thar 16/2/3	22.0	11830	930	This thesis
Thar 16/8/1	2.0	10010	700	This thesis
Thar 16/8/2	3.0	10040	850	This thesis

Table G.3. Sedimentology of new samples included in Chapter 6 (Paper 3) showing Munsell colour, grain size statistics (in microns), organic and carbonate content.

Sample	Munsell colour	Mean (μm)	Sand (%)				Silt (%)	Clay (%)	Sorting*	Skewness**	Kurtosis***	Organic content(%)	Carbonate content (%)
			Coarse	Medium	Fine	Very fine							
IND 14/5/1	10 YR 5/4	175.6	0.0	20.5	58.4	12.7	7.6	0.8	2.016 (PS)	-0.351 (VFS)	2.288 (VL)	1.45	2.80
IND 14/5/2	10 YR 5/4	169.4	0.0	17.3	59.7	16.7	5.8	0.5	1.860 (MS)	-0.305 (VFS)	1.975 (VL)	1.98	3.24
IND 14/5/3	10 YR 5/4	188.2	0.2	25.0	58.5	16.4	0.1	0.0	1.500 (MWS)	-0.014 (S)	0.943 (M)	1.25	3.12
IND 14/5/4	10 YR 5/4	174.0	0.1	20.4	56.8	22.3	0.5	0.0	1.536 (MWS)	-0.019 (S)	0.946 (M)	1.36	2.85
IND 14/5/5	10 YR 5/4	151.5	0.0	11.0	56.6	31.6	0.8	0.0	1.500 (MWS)	-0.004 (S)	0.944 (M)	1.58	2.12
IND 14/5/6	10 YR 5/4	158.4	0.0	13.8	57.0	28.7	0.5	0.0	1.510 (MWS)	-0.005 (S)	0.944 (M)	1.70	3.68
Thar 16/2/1	10 YR 7/4	153.1	0.0	8.7	63.4	19.0	7.9	1.0	1.890 (MS)	-0.361 (VFS)	2.407 (VL)	1.03	4.39
Thar 16/2/3	10 YR 7/4	160.8	0.0	16.1	57.5	14.7	10.9	0.8	2.020 (PS)	-0.368 (VFS)	2.144 (VL)	1.13	4.53
Thar 16/8/1	10 YR 5/4	183.4	0.2	24.5	55.8	14.0	5.5	0.0	1.823 (MS)	-0.260 (FS)	1.714 (VL)	0.87	3.33
Thar 16/8/2	10 YR 5/4	234.8	3.3	43.4	42.2	4.0	7.0	0.1	1.930 (MS)	-0.304 (VFS)	1.86 (VL)	0.84	2.65

* MWS= moderately well sorted, WS= well sorted, MS= moderately sorted, PS= poorly sorted.

** FS= finely skewed, VFS= very finely skewed, S= symmetrical.

*** L= leptokurtic, VL= very leptokurtic, M= mesokurtic